3D *in vitro*-based Alternative Approaches to Ecotoxicity Assessment

Dissertation

zur Erlangung des Grades

des Doktors der Naturwissenschaften

der Naturwissenschaftlich-Technischen Fakultäten

der Universität des Saarlandes

von

Chang Gyun Park

Saarbrücken

2022

Tag des Kolloquiums: 27.01.2023

Dekan:	Prof. Dr. Ludger Santen
Berichterstatter:	Prof. Dr. Andreas Manz,
	Prof. Dr. Alexandra K. Kiemer,
	Dr. Young Jun Kim
Vorsitz:	Prof. Dr. Marc Schneider
Akad. Mitarbeiter:	Dr. Maria Lopatniuk

Die vorliegende Arbeit wurde von Oktober 2018 bis September 2022 unter Anleitung von Herrn Prof. Dr. Andreas Manz und Herrn Dr. Young Jun Kim am KIST Europe Forschungsgesellschaft mbH angefertigt.

Summary

Given bioethics and the 3Rs (replacement, reduction, and refinement) principle, reliable test platforms are required due to the increased presence of endocrine-disrupting chemicals (EDCs) in the ecosystem. However, typical fish cell cultures show numerous limitations compared to primary cells. Therefore, there is a demand to develop novel systems for reproductive toxicity assessments as alternatives to animal testing. In this thesis, a zebrafish liver (ZFL) cell line was applied to three-dimensional (3D) cell culture techniques including *in silico* systems.

The 3D structure of the zebrafish estrogen receptor was generated to evaluate modes of action upon estrogenic chemical exposure. The integration of the *in silico* model and *in vitro* platforms provided valuable tools for screening EDCs. Besides, 3D ZFL spheroids exhibited increased gene expressions in liver functions and vitellogenin levels compared to monolayer cells. The use of hydrogels and nanofibers regulated intercellular organization and physiological function and compensated for the shortcomings in the spheroid culture. These findings suggest the engineering of novel 3D platforms shows promise as alternative tools that are useful for further eco-environmental assessment. Therefore, the current studies have yielded robust alternative platforms to animal and primary cells for identifying potential EDCs. These approaches can contribute to reducing the experimental use of animals under the 3Rs principle.

Zusammenfassung

Angesichts der Bioethik, dem 3R-Prinzip (Replacement, Reduction, und Refinement) und des Bestehens endokrin aktive Substanzen (EASs) im Ökosystem sind Testplattformen notwendig. Typische Fischzellkulturen weisen im Vergleich zu Primärzellen Limitierungen auf. Daher besteht Bedarf an der Entwicklung neuartiger Systeme für Reproduktionstoxizitätsbewertungen als Alternative zu Tierversuchen. In dieser Doktorarbeit wurde eine Zebrafischleber-Zelllinie auf 3D-Zellkulturtechniken, samt *in-silico* Systeme eingesetzt.

Die 3D-Struktur des Zebrafisch-Östrogenrezeptors wurde generiert, um Wirkungsweisen unter dem Einfluß von östrogenen Chemikalien auszuwerten. Die Integration des *in silico* Modells und *in vitro* Plattformen ergaben wertvolle Werkzeuge für das Screening von EASs. 3D Sphäroide zeigten im Vergleich zu Monoschichtzellen eine erhöhte leberspezifische Genexpression und Vtg Konzentrationen. Die Nutzung von Hydrogelen und Nanofasern regulierte die interzelluläre Organisation und physiologische Funktion und kompensierte die Mängel in der Sphäroidkultur. Diese Resultate deuten darauf hin, dass die Entwicklung neuartiger 3D-Plattformen ein vielversprechender Ansatz ist und für weitere Öko-Umweltbewertungen lohnend sind. Die vorgelegte Arbeit zeigt, dass die erzeugte, robuste, alternative Plattformen zu tierischen und primären Zellen es ermöglicht EASs zu identifizieren. Diese Ansätze können dazu beitragen die experimentelle Nutzung von Tieren nach dem 3R-Prinzip zu reduzieren.

Graphical Abstract

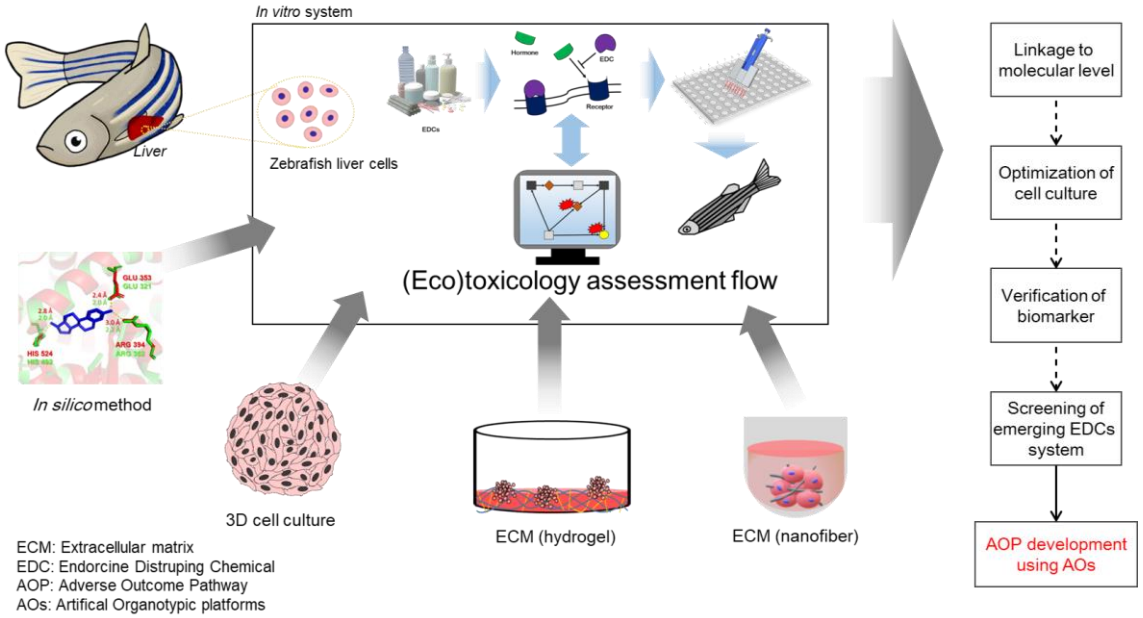

ECM: Extracellular matrix
EDC: Endorcine Distruping Chemical
AOP: Adverse Outcome Pathway
AOs: Artifical Organotypic platforms

Acknowledgments

I sincerely appreciate Prof. Dr. Andreas Manz and Dr. Young Jun Kim for their many supports and scientific discussions during my time on this thesis. Also, I would like to thank Dr. Changseon Ryu, Dr. Indong Jun, Dr. Youngsam Kim, Dr. Juyong Yoon, and Dr. Baeckkyoung Sung for their works, discussions, and advice on the published papers.

Furthermore, I appreciate Prof. Dr. Hyunjoon Kong and Prof. Dr. Heungsoo Shin for providing the biomaterials related to the published papers.

I am grateful to Mr. Hyunki Cho, Dr. Hyung-Seop Han, Ms. Kathryn M. Sullivan, Ms. Yu-Mi Park, Dr. Jonathan S. O'Connor, Dr. Matthias Altmeyer, Mr. Carsten Brill, Dr. Younghun Seo, Mr. Karim Md Adnan, Ms. Nancy Singh, and Prof. Dr. Leon Abelmann, who helped performing my experiments and advises for me. And I would like to thank Ms. Jana C. Steffens for improving and helping my thesis work.

Lastly, I would like to thank all KIST members and the university who helped me and gave good discussions.

Vorveröffentlichungen aus dieser Dissertation

Teile dieser Arbeit wurden vorab mit Genehmigung der Naturwissenschaftlich-Technischen Fakultäten, vertreten durch den Mentor der Arbeit, in folgenden Beiträgen veröffentlicht oder sind derzeit in Vorbereitung der Veröffentlichung.

Publications

Bereits veröffentlichte Publikationen (mit offenem Zugang):

1. Park, C.G.; Singh N.; Ryu, C.S.; Esterhuizen, M.; Kim, Y.J. Species differences in response to binding interactions of BPA and its analogs with the modeled estrogen receptor 1 and in vitro reporter gene assay in human and zebrafish. *Environmental Toxicology and Chemistry* **2022**, 10.1002/etc.5433

2. Park, C.G.; Jun, I.; Lee, S.; Ryu, C.S.; Lee, S.A.; Park, J.; Han, H.S.; Park, H.; Manz, A.; Shin, H.; Kim, Y.J. Integration of bioinspired fibrous strands with 3D spheroids for environmental hazard monitoring. *Small* **2022**, *18*(22), e2200757. https://doi.org/10.1002/smll.202200757

3. Park, C.G.; Ryu, C.S.; Sung, B.; Manz, A.; Kong, H.; Kim, Y.J. Transcriptomic and physiological analysis of endocrine disrupting chemicals Impacts on 3D zebrafish liver cell culture system. *Aquat. Toxicol.* **2022**, *245*, 106105. https://doi.org/10.1016/j.aquatox.2022.106105

4. Sullivan, K.M.; Park, C.G.; Ito, J.D.; Kandel, M.; Popescu, G.; Kim, Y.J.; Kong, H. Matrix softness-mediated 3D zebrafish hepatocyte modulates response to endocrine disrupting chemicals. *Environmental science & technology* **2020**, *54*(21), 13797–13806. https://doi.org/10.1021/acs.est.0c01988

Publikationen in Vorbereitung der Veröffentlichung:

Weitere Publikationen, die nicht Teil dieser Arbeit sind:

1. Park, C.G.; Jung, K.C.; Kim, D-H.; Kim, Y.J. Monohaloacetonitriles induce cytotoxicity and exhibit different mode of action in endocrine disruption. *Science of The Total Environment*, **2021**, *761*, 143316. https://doi.org/10.1016/j.scitotenv.2020.143316

2. Park, C.G.; Sung, B.; Ryu, C.S.; Kim, Y.J. Mono-(2-ethylhexyl) phthalate induces oxidative stress and lipid accumulation in zebrafish liver cells. *Comparative biochemistry and physiology. Toxicology & pharmacology: CBP* **2020**, *230*, 108704. https://doi.org/10.1016/j.cbpc.2020.108704

3. Kim, D.H.; Park, C.G.; Kim, S.H.; Kim, Y.J. The effects of mono-(2-Ethylhexyl) phthalate (MEHP) on human estrogen receptor (hER) and androgen receptor (hAR) by YES/YAS *in*

vitro assay. *Molecules* **2019**, *24*(8), 1558. https://doi.org/10.3390/molecules24081558

4. Park, J.; Park, C.G.; Lee, Y.; Ryu, C.S.; Park, J.; Kim, Y.J. Acute adverse effects of metallic nanomaterials on cardiac and behavioral changes in daphnia magna. *Environments* **2022**, *9*(2), 26. https://doi.org/10.3390/environments9020026

5. Park, C.B.; Kim, G.E.; Kim, Y.J.; On, J.; Park, C.G.; Kwon, Y.S.; Pyo, H.; Yeom, D.H.; Cho, S.H. Reproductive dysfunction linked to alteration of endocrine activities in zebrafish exposed to mono-(2-ethylhexyl) phthalate (MEHP). *Environmental pollution* **2020**, *265*, 114362. https://doi.org/10.1016/j.envpol.2020.114362

6. Kim, D.H.; Park, C.G.; Kim, Y.J. Characterizing the potential estrogenic and androgenic activities of two disinfection byproducts, mono-haloacetic acids and haloacetamides, using *in vitro* bioassays. *Chemosphere* **2020**, *242*, 125198. https://doi.org/10.1016/j.chemosphere.2019.125198

7. Kim, B.S.; Leong, J.; Yu, S.J.; Cho, Y.; Park, C.G.; Kim, D.H.; Ko, E.; Im, S.G.; Lee, J.; Kim, Y.J.; Kong, H. Stimulus-responsive anti-oxidizing drug crystals and their ecological implication. *Small* **2019**, *15*(21), e1900765. https://doi.org/10.1002/smll.201900765

Conference Contributions (Posters and Oral Presentations)

1. Poster presentation, *3D-culture & Organoid & Tox screening Europe Conference 2019*. Rotterdam, Netherlands, **2019**.

2. Poster presentation, *SETAC Europe 30th Annual Meeting*, Online, **2020**.

Table of Contents

Chapter 1. Introduction

1.1 Endocrin-disrupting chemicals (EDCs)

1.1.1 EDCs and its generation

Over the past few decades, the effects of environmental pollution have become a serious problem globally. Environmental pollutants are compounds that result from natural causes and human activities, leading adverse effects in the environment and human health [1]. Among the environmental pollutants, endocrine-disrupting chemicals (EDCs) have continuously aroused issues due to their direct/indirect impacts on wildlife population dynamics. EDCs are defined as "an exogenous (non-natural) chemical, or a mixture of chemicals, that interferes with any aspect of hormone action." by the Endocrine Society [2]. They change the hormonal balance through various mechanisms, such as mimicking hormones, altering the development of hormone receptors, and disrupting hormone synthesis or breakdown. Thus, EDCs interfere with hormone systems and cause adverse effects in humans and other organisms [2].

Many EDCs are released from the manufacture and utilization of human-made articles. The articles are mainly generated for human convenience and welfare. Representative sources and EDCs are presented in Figure 1.1. Plasticizers are a substance that is utilized to make materials more flexible and soft with increasing plasticity and decreasing viscosity. The majority is applied in cables, films, and consumer products. EDCs like phthalates, organochlorines, and polyfluoroalkyl compounds are mainly released from various plasticizers [3]. Pesticides are biological agents or materials that control pests and many of them are identified into chemical families. They include organochlorines, organophosphates, carbamates, and pyrethroids [4]. Flame retardants are added to manufactured materials such as plastics, surface finishes, and coatings to prevent the start or development of fires. Organophosphates, organohalogens, and brominated chemicals are released from various flame retardants [5]. Food additives are added to foods to conserve flavor or increase taste, appearance, and other qualities. Also, they are used for foods indirectly in manufacturing processes such as packaging, storage, or transport. Organotins and dioxins are known as EDCs in the group [6]. Surfactants generate self-assembled molecular clusters in a solution and adsorb to the interface between a solution and a different phase. They are deposited in numerous ways on land and into water systems, whether as part of an intended process or as industrial and household waste. Alkylphenols are considered as major EDCs [7]. Some of common EDCs are generated from different sources, however, the diversity of EDCs is continuously increasing.

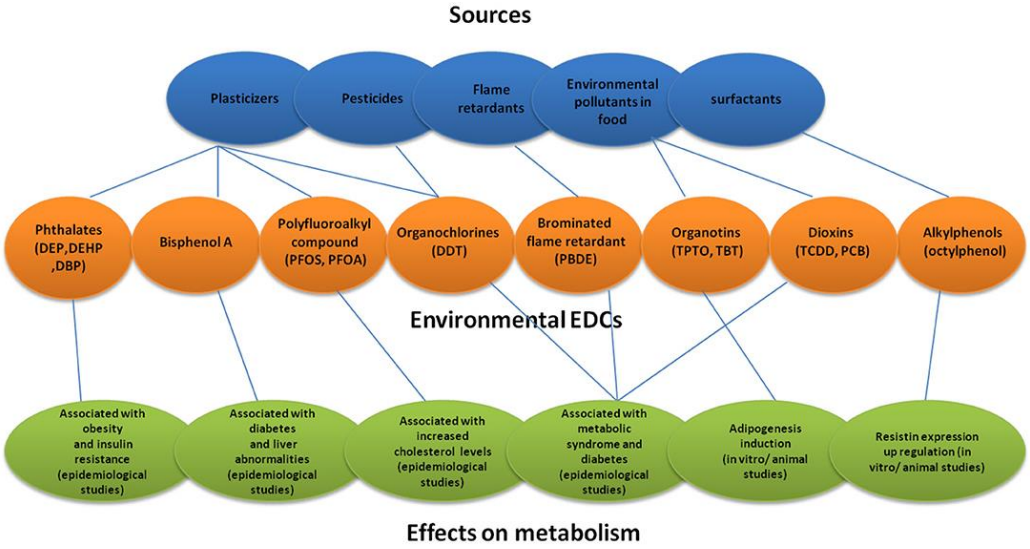

Figure 1.1. Representative source of EDCs and their adverse effects. DEP, Diethyl phthalate; DEHP, Diethylhexyl phthalate; DBP, Dibutyl phthalate; PFOS, Perfluorooctanote; DDT, Dichlorodiphenyltrichloro ethane; PBDE, Polybrominated diphenyl ether; TPTO, bis (triphenyltin) oxide; TBT, Tributyltin. The figure adapted from *Kumar et al. Frontiers in Public Health, **2020**, 8, 553850.*

1.1.2 The key characteristics of EDCs in hormone systems

The generated EDCs are easily exposed to humans and animals in various ways. The exposed EDCs interfere with hormone systems, ending in adverse health outcomes. Recently, Merrill et al (2020) reported common features of EDCs in hormone action and regulation. The features specify actions that interrupt hormone systems [8]. The major key characteristics (KCs) are indicated in Figure 1.2. KC1 denotes the interaction and activation with hormone receptors. Hormones usually play upon binding to a specific receptor or receptors, however, inappropriate receptor interaction or activation by EDCs can cause adverse effects on development and health [9,10]. KC2 denotes EDCs function as an antagonist with hormone receptors. They can block or inhibit the effects of endogenous hormones by functioning as receptor antagonists [10,11]. KC3 denotes an alteration of hormone receptor expression. As hormone functions are regulated by the receptors, expression patterns of the receptors control their response to hormone signals. Thus, EDCs can also modulate hormone receptor internalization, degradation, and expression [12]. KC4 denotes an alteration of signal transduction in hormone-responsive cells. The binding between a hormone and its receptor initiates specific intracellular responses that rely on the receptor and tissue-specific properties of the target cell. Signal transduction mediated through hormone receptors can be changed by some EDCs [13]. KC5 denotes epigenetic modifications in hormone-producing or -responsive cells. Hormones employ perpetual effects by modifying epigenetic processes such as chromatin modifications, DNA methylation and non-coding RNA expression during development and differentiation. In the same ways, some of EDCs can act like hormones to employ these epigenetic alterations [14]. KC6 represents an alteration of hormone synthesis by regulating both intracellular and distant endocrine feedback mechanisms [15]. KC7 denotes a change of hormone transport across cell membranes. Steroid hormones like progestins, androgens, and oestrogens are transferred passively through membranes due to their lipophilicity. Others are transported selectively to obtain entrance and/or to

secrete the cell. These processes may also be interrupted by some EDCs [16]. KC8 denotes an alteration of hormone distribution or circulating levels. Hormones normally circulate in blood and are transported with/without conjugations. EDCs can change bioavailability of hormones by disrupting the distribution or displacing their binding proteins [15]. KC9 denotes a change of hormone metabolism or clearance. EDCs impact on the hormone concentration and its activity by altering the rates of inactivation, the metabolic degradation or clearance of hormones [15,17]. Lastly, KC10 denotes a change of the fate of hormone-producing or responsive cells. EDCs can impact on tissue organization and structure by disrupting or promoting cell differentiation, proliferation, migration or death [18,19]. In light of these KCs, EDCs have the functional properties of agents that impact on hormone actions and these result in the major mechanisms for endocrine disorders.

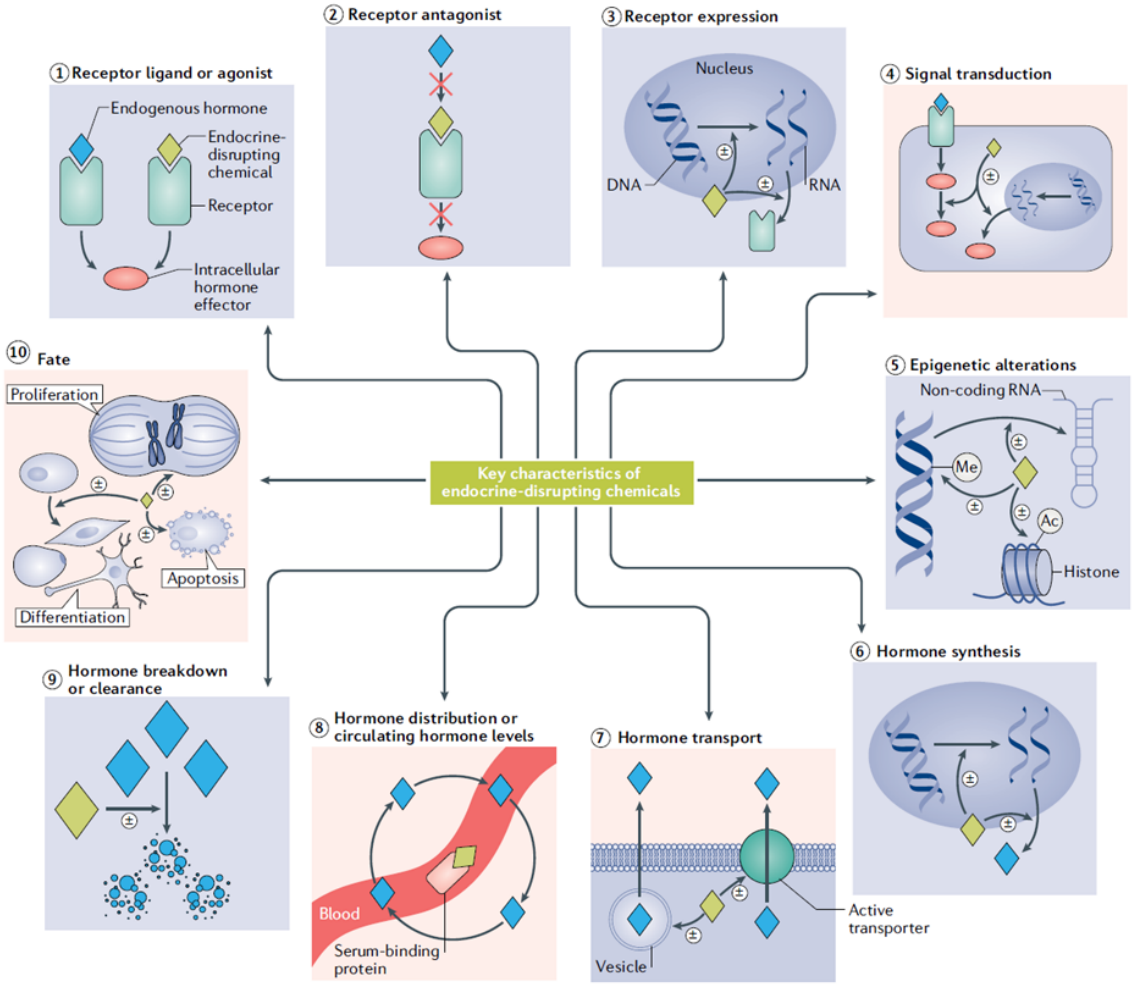

Figure 1.2. Key characteristics (KCs) of endocrine-disrupting chemicals (EDCs). Each arrow indicates specific KCs. The symbol of "±" presents an EDC can increase or decrease processes and effects. Ac, acetyl group; Me, methyl group. The figure adapted from *Merrill et al. Nature Reviews Endocrinology, **2020**, 16, 45-57.*

1.1.3 Adverse effects of EDCs

Due to their characteristics, EDCs can modulate the biological pathways and phenotypic changes through altered molecular/cellular processes and eventually cause adverse health outcomes, including diabetes, obesity, and disorders of blood pressure, cancer, thyroid homeostasis, and reproduction in humans and animals [20]. Phthalates such as di-(2-ethylhexyl) phthalate (DEHP) induce cancers, obesity, metabolic and inflammatory diseases, and developmental disorder [21,22]. Bisphenol A (BPA) and its analogs cause cancers, genetic and connective tissue disorders, and also reproductive, neurological, and cardiovascular diseases [23,24]. Alkylphenols such as nonylphenol result in cancers, inflammatory disease, skeletal & muscular, developmental, and genetic disorders [25]. Polychlorinated biphenyls (PCBs) cause cancers, obesity, metabolic, inflammatory, and reproductive diseases [26]. Other EDCs also have been reported to interfere with hormone systems and induce many adverse disorders. Moreover, EDCs have been presenting endocrine disorders in other organisms such as aquatic organisms. EDCs can significantly have a great influence on fish species. Because fishes are susceptible to exposure and accumulation of chemicals in water, and they have certain properties like rapid growth, reproduction, and population [27]. Phthalates and benzyl butyl phthalate (BBP) disrupt thyroid development, steroid biosynthesis, and metabolism [28,29]. BPA and its analogs induce reproductive effects including reductions in egg production, gonadosomatic index (GSI), egg fertility, and alterations in sexual behavior and maturation [30]. Alkylphenols like nonylphenol and octylphenol have reproductive effects like reduced egg production, skewed sex ratio, reduced GSI, intersex gonads, sexual maturation, and alteration of steroids [31,32]. Dichloro-diphenyl-trichloroethane (DDT) alters ATPase activity, thyroid hormone levels, sexual maturation and characteristics, and embryo mortality [32]. Adverse effects of EDCs have been reported steadily across species, and the diversity and exposure of EDCs are continuously increasing. Figure 1.3 shows a massive production and release of EDCs into the environment through numerous ways, and the numbers have increased over the years [33]. Previous studies support these facts with reporting the detection of EDCs in the environment [34,35]. Therefore, there is a need to manage the production and release of toxic chemicals. Although regulations like REACH (Registration, Evaluation, Authorization, and Restriction of Chemicals) have been implemented, it still requires the development of robust restrictions. Furthermore, precise and reliable toxicity assessment systems are also required to predict and evaluate the effects of chemicals. Mis-assessment and -judgment about chemicals can result in severe incidents of environmental and human health problems. Thus, minimizing the exposure of EDCs and damages generated from EDCs is needed through precise assessments.

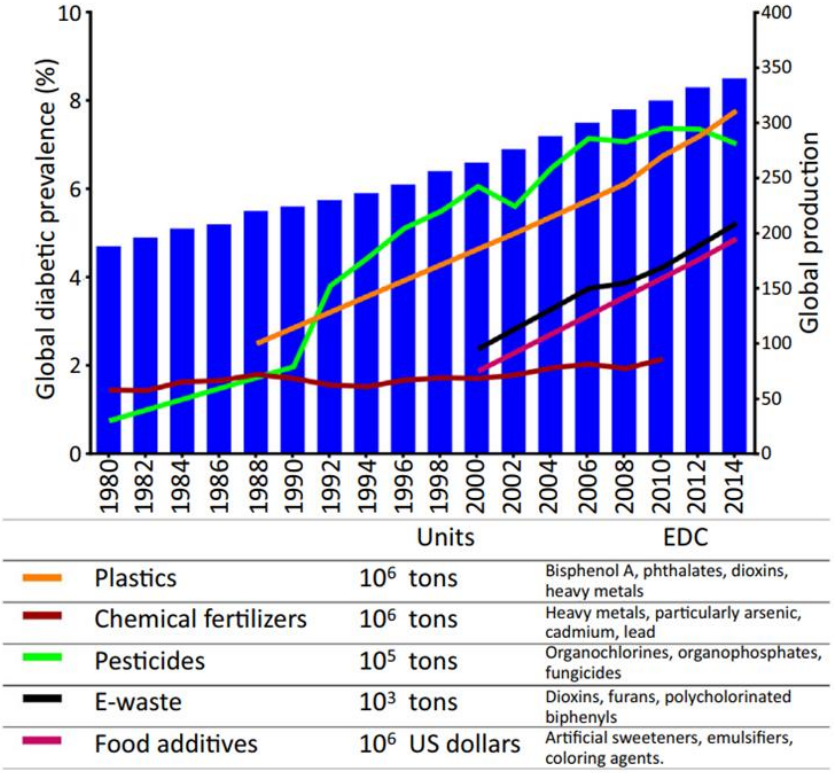

Figure 1.3. Sources of endocrine-disrupting chemicals (EDCs), the production of EDCs from the sources, and growth of diabetes incidence in the period 1980–2014. The relationship between sources of EDCs and global diabetes prevalence. The figure adapted from *Velmurugan et al. Trends Endocrinol Metab*, ***2017***, *28, 612-625.*

1.2 Zebrafish and its vitellogenesis

1.2.1 Zebrafish characteristics

The zebrafish (*Danio rerio*) is a freshwater fish that belongs to the minnow family (Cyprinidae) and is widely spread across regions of India, Bangladesh, Nepal, Myanmar, and Pakistan. They generally prefer environments like still or slow moving, slightly alkaline (pH ~ 8.0), water of a relatively high clarity (~>35 cm). Depending on husbandry conditions, the zebrafish can grow up to 4–5 cm in length and its lifespan in captivity is around two to three years [36]. The average generation time is three months. As asynchronous spawners, zebrafish can regularly spawn under proper conditions. Thus, females can spawn two or three times a week. Once eggs are released, the embryonic development can start with the first few cell divisions, even without sperm. Fertilized eggs become transparent and the embryo develops quickly, generating major organs within 36 hours post fertilization (hpf). The embryo starts as a yolk with a single enormous cell on top, but then the yolk shrinks over time because the fish uses it for nutrients during the first few days. After a few months, the adult fish reaches reproductive maturity [37]. Zebrafish has their own characteristics such as conserved vertebrate biology, small size, rapid development as well as optical transparency and tractability. These characteristics make zebrafish as a useful research model (Figure 1.4) [38-40].

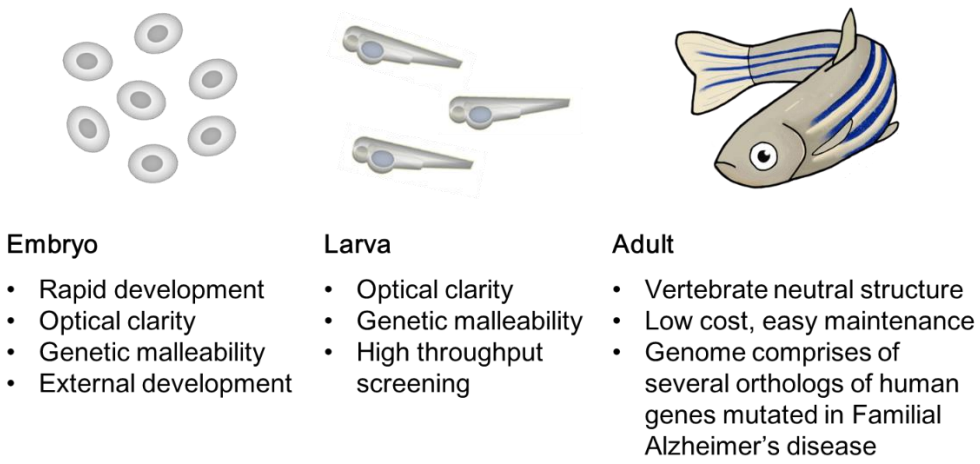

Figure 1.4 Advantages of using zebrafish as a research model. The figure adapted from *Saleem and Kannan. Cell Death Discovery*, ***2018***, *4, 45.*

The optical transparency provides the observation of organ development and phenotypic changes. It also makes it simple to generate transgenic models, gene expressions, and cell-specific reporter assays for real-time *in vivo* research of toxic mechanisms [41]. Phenotypic changes and/or toxic effects have been monitored after the exposure to xenobiotics by simply dissolving a chemical in water. Moreover, the zebrafish genome has been fully sequenced and reveals high homologues with human genes [42]. Zebrafish have 26,206 protein-coding genes, which is more than other sequenced vertebrates, and a higher number of species-specific genes than mouse, chicken, and human [43]. The comparison of protein-coding genes between zebrafish and human is indicated in Table 1.1. The table shows that human genes are associated with many zebrafish genes. Above all, 71.4% of protein-coding genes (14,623 genes) in human possess at least one zebrafish orthologue, and 68.8% of protein-coding genes (18,029 genes) in zebrafish possess at least one human orthologue. Among the orthologous genes, 46.5% of human genes possess a one-to-one relationship with zebrafish genes (9,528 genes). Furthermore, human genes are also associated with many zebrafish genes in the one-human-to-many-zebrafish category (the average: 1:2.28 ratio). This sequence homology provides an opportunity to study zebrafish for human genetic diseases. The application of genetic screens resulted in phenotypic characterization with a collection of mutations. These mutations can induce defects in a variety of organ systems with pathologies similar to human disease. Such studies notably contribute to understanding vertebrates of basic biology and development [43]. Furthermore, screenings in zebrafish also contribute to understanding the factors, which modulate the organ systems, body axes, and the specification and differentiation of cell types [39]. Although there are some differences related to anatomy and physiology, most organs have the same functions as their human counterparts and show well-conserved physiology [42]. Thereby, zebrafish has been utilized in many fields, including oncology, developmental biology, toxicology, reproductive studies, teratology, genetics and environmental sciences [39].

Table 1.1 Comparison of human and zebrafish protein-coding genes and their orthology relationships

Relationship type	Human	Core relationship	Zebrafish	Ratio
One to one	-	9,528	-	-
One to many	3,105	-	7,078	1:2.28
Many to one	1,247	-	489	2.55:1
Many to many	743	233	934	1:1.26
Orthologous total	14,623	13,355	18,029	1:1.28
Unique	5,856	-	8,177	-
Coding-gene total	20,479	-	26,206	-

Note. The table adapted from "The zebrafish reference genome sequence and its relationship to the human genome" *Howe et al. Nature, **2013**, 496(7446), 498-503*.

1.2.2 Endocrine system in zebrafish

As an excellent *in vivo* model with many advantages, zebrafish also show well-conserved hormone systems. Generally, the hypothalamic-pituitary axis primarily controls the activity of the endocrine system in vertebrates. There are some differences between humans and zebrafish, still the endocrine system is well-conserved with the structure and function [38]. Zebrafish have no hypothalamic−pituitary portal system and the neurosecretory fibers go in for the pituitary and secret their hormones directly to the adenohypophyseal cells [44]. Besides, zebrafish are absent a characteristic adrenal gland, however, zebrafish have a comparable interrenal gland. The development of the endocrine system is mostly completed within 5 days post fertilization (dpf) [38]. Gene expressions related to the pituitary hormone begins at 2 dpf, and the major steroidogenic gene expression of the interrenal organ also starts at 2 dpf [45]. Aromatase gene expression, that codes for the enzyme catalyzing the biosynthesis of estrogens from precursor androgens, can be measured from 1 dpf [46]. Moreover, estrogen receptors can be detected from 1 dpf and thyroxin production of the thyroid gland begins from 3 dpf [47,48].

These features result in many studies of endocrine toxicity from the embryo stage for screening EDCs on hormone systems. The studies on endocrine toxicity mainly have been focused on the estrogen, androgen, thyroid, and steroidogenesis (EATS) pathways. Specific biomarkers can be detected to evaluate the endocrine activity of xenobiotics (Figure 1.5) [49]. One of the representative examples is the measurement of vitellogenin (Vtg) levels. Vtg is an egg-yolk protein precursor induced in the liver and simulated by estrogens or estrogenic compounds [50]. Likewise, other markers such as thyroidal or steroidal hormones can be detected for screening the endocrine disruption of xenobiotics [51,52]. The analysis of gene expression is also considered as a useful approach to specify the pathways related to biological effects of EDCs in zebrafish and its embryo. For example, fadrozole caused a downregulation of brain aromatase and Vtg transcript abundances in 4 dpf. This event resulted in an adverse effect of the disrupted sex ratio during sexual differentiation, showing an adverse outcome pathway (AOP) for aromatase inhibition [53]. Meanwhile, multiple reporter models have been constructed for the endocrine toxicity of xenobiotics. The transgenic zebrafish lines have been developed for screening estrogen-responsive substances, thyroid, and glucocorticoid pathways [38]. These approaches are rapid and cost-effective methods for endocrine toxicity, and are available in real-time in *vivo* research.

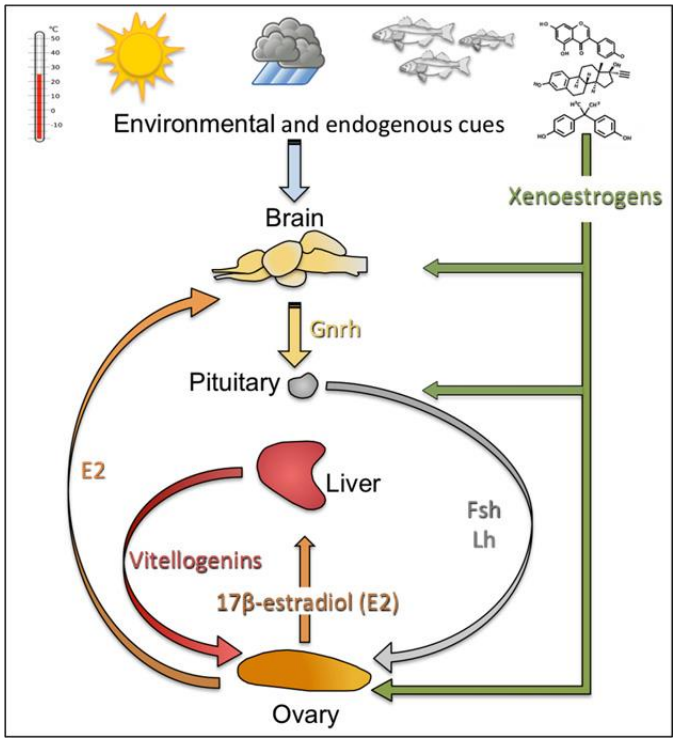

Figure 1.5. Regulations of vitellogenesis in teleost fish through the brain-pituitary-gonad (BPG) axis. Environmental factors presented at the top indicate (from left to right) water temperature, day length, rainy weather, fishes, and xenoestrogens in the environment. Xenoestrogens can impact the BPG axis at several levels. Fsh, follicle stimulating hormone; Gnrh, gonadotropin-releasing hormone; Lh, luteinizing hormone; E2, 17b-estradiol. The figure adapted from *Sullivan and Yilmaz. Encyclopedia of Reproduction (Second Edition), **2018**, 6, 266-277.*

1.2.3 Vitellogenesis in zebrafish

Vitellogenesis in fish is defined as the phase of oocyte growth characterized by the production of egg yolk precursor proteins (Vtgs) in the liver and its secretion and deposition as yok proteins in the ooplasm [54]. Thus, the formation of Vtgs is closely related to their reproduction and lifespan. Vtgs are massive proteins (300 – 600 kDa) and are mainly composed in homodimers of two identical polypeptides, which contain protein domains of phosphate, carbohydrate and lipid components. Vtgs are the main nutrients of amino acids for developing embryos and larvae. Moreover, the components take over the important function as carriers of minerals, vitamins, and hormones [55]. The complete structures of Vtg are serially lined with five yolk protein domains, which are amino terminus (N)-lipovitellin heavy chain (LvH), phosvitin (Pv), lipovitellin light chain (LvL), b'-component (b'-c), and C-terminal peptide (Ct)-carboxy terminus-(C) [55]. Once they are cleaved from the Vtg, LvH and LvL function as the main sources of nutrients during the development. Pv binds to iron, zinc, calcium, and magnesium via ionic interactions [56]. The production of Vtgs depends on the interaction of the estrogenic hormones with the classical nuclear estrogen receptors (Esrs), which are known as the three subtypes; Esr1, Esr2a, and Esr2b [57]. Once an estrogenic hormone introduces into liver cells and binds to cytosolic Esrs, conformational changes begin and recruit several co-regulatory proteins to activate Vtg gene transcription (Figure 1.6). Subsequently, the Esr is translocated into the cell nucleus dimerizing with another Esr, and the dimerized structure becomes an activated transcription factor, that binds

to specific DNA sequence motifs. It is called estrogen response elements (EREs), which are placed in the promoter region encoding genes of Vtgs. Then, ribosomes translate the mRNAs encoding Vtgs into their respective polypeptides, and they are folded into configuration and dimerized to be Vtgs. Once all of the processes are complete, the induced Vtgs exist in cisternae of the trans-Golgi and are transferred into secretory vesicles. The vesicles containing Vtgs combine with the cell membrane and secret Vtgs to the circulation for transit to the ovary [55].

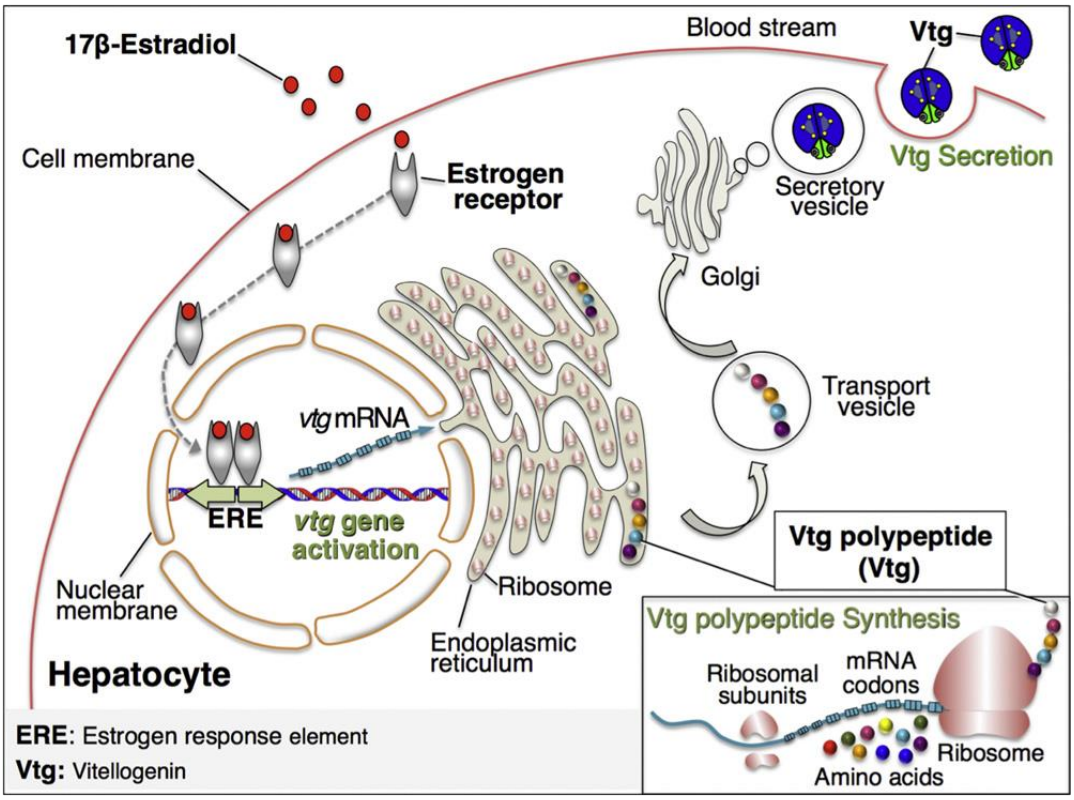

Figure 1.6. The synthesis of vitellogenin regulated by 17β-estradiol. The figure adapted from *Sullivan and Yilmaz. Encyclopedia of Reproduction (Second Edition),* ***2018****, 6, 266-277.*

Then, Vtgs egress porous capillaries in the follicle theca and enter the intercellular spaces of granulosa cells to come to the oocyte surface, where they bind to Vtg receptors. The complexes congregate into clathrin-coated pits and are endocytosed, forming endocytotic vesicles. The endocytosed Vtgs are dissociated with Vtg receptors by vesicle acidification and the receptors are reused to the oocyte surface again. The endosomes (vesicles) combine with lysosomes including inactive cathepsin D (CatD) and vacuolar ATPases activate CatD. The CatD cleaves Vtgs into its product yolk proteins [54]. Therefore, vitellogenesis is considered as an essential process for egg production and embryonic development. This process can be regulated by external conditions such as water conditions, weather, and xenobiotics. Especially, xenobiotics present in the environment, can disrupt the brain pituitary-gonad axis, and estrogenic chemicals play directly on the liver to produce vitellogenesis in males and juveniles [38]. On the other way, anti-estrogenic chemicals can inhibit vitellogenesis in females [58]. Vitellogenesis is highly reactive to estrogens and estrogenic chemicals. Therefore, the Vtgs have been considered as a key biomarker for endocrine disturbances in aquatic

organisms. According to OECD Test Guidelines 229, 230, 234, and 240 for *in vivo* reproductive screening assays (Table 1.2), Vtg levels are measured as an endpoint to predict the potential reproductive effects of chemicals on fish [59-62].

Table 1.2 Principal features of the OECD Test Guidelines (TGs) involving vitellogenin measurement in fish species.

OECD TG	Title	Date	Species involved	Exposure duration	Biological endpoint
229	Fish short term reproduction assay	2012	- Fathead minnow - Japanese medaka - Zebrafish	21 days	- Survival - Behaviour - Fecundity - Vitellogenin - optionally gonadal histopathology - Secondary sex characteristics
230	Fish assay	2009	- Fathead minnow - Japanese medaka - Zebrafish	21 days	- Survival - Behaviour - Vitellogenin - Secondary sex characteristics
234	Fish sexual development test	2011	- Fathead minnow - Japanese medaka - Zebrafish - Three-spined stickleback	60 days post hatch	- Hatching success - Survival - Gross-morphology - Vitellogenin - Gonadal histology - Sex ratio
240	Medaka Extended One Generation Reproduction Test (MEOGRT)	2015	- Japanese medaka - Small fish species (e.g., Zebrafish)	19 weeks	- Fecundity - Fertility - Hatching success - Survival - Gross-morphology - Vitellogenin - Secondary sex characteristics - Histopathology

1.3 Alternatives to animal testing

1.3.1 Three Rs principle

Animals have been globally used for various purposes such as pets, sports, foods, and as transportation for human beings themselves. Among the purposes, the use for research is considered as one of the major uses. Diverse animals are being utilized in research areas for a long time [63]. They are mainly applied for drug testing, toxicological screenings, surgical experiments, and developing vaccines as well as antibiotics [64]. Due to these purposes, millions of animals are sacrificed worldwide every year. For instance, 3.06 million procedures of experiments were carried out in Great Britain using animals in 2021 [65]. In the European Union, 10.7 million animals were used for research in 2017 [66]. In the USA, the available data from 2019 shows that, nearly 100 million mice and rats were sacrificed for research, and almost 1 million animals

excluding mice, rats, fishes, and birds, were held captive and used for research [67]. Despite many efforts to reduce the use of animals, massive populations of experimental animals are still observed worldwide. In addition, the stress, pain, and death inflicted on animals during experiments have been rising issues for a long time. The main issue is that the use of animals for experimentation is unethical, and animals should be guaranteed rights against stress and pain [68]. Thus, diverse regulations and acts have been implemented to control unethical uses and reduce stress, pain, and the use of animals. Many guidelines have been provided by organizations like Organisation for Economic Co-operation and Development (OECD), National Institute of Health (NIH), and Committee for Purpose of Control and Supervision on Experiments on Animal (CPCSEA) [68].

The 3Rs principle stands for replacement, reduction, and refinement of laboratory animal experiments [69]. The concept was first mentioned by Charles Hume and William Russell in 1957 and the 3Rs principle was launched by Russell and Burch in 1959 [70]. This principle prompts animal 'replacement' to alternative methodologies and lower organisms. Various alternatives like computer models, *in vitro* models, and cell cultures have been introduced and applied for the 'reduction' of the use of animals, and well-designed studies with statistical support can contribute to the reduction of the use of animals [71]. The animal experiment should be planned carefully for alleviation or minimization of pain and distress. Animal welfare is also included as the 'refinement'. The improvement of the cage environment for animals can reduce their stress. Hence, researchers must care for the animal facility to minimize their pain, distress, and discomfort during their life. Animals under harsh environments may have an imbalance or disrupted hormonal levels and may cause fluctuation and huge deviations in results. Due to this, experiments are needed to replicate for the reproducibility that requires the many numbers of animals [69]. The refinement of animals is important for improving their welfare and the quality of research. In light of these points, alternative approaches based on a strategy of 3Rs would result in the reduction of animals used in scientific procedures.

1.3.2 Adverse outcome pathway as an alternative approaches

Alternative approaches offer the opportunity to evaluate diverse research fields like toxicology, developmental biology, genetics, and environmental sciences and to structure adverse outcome pathways (AOPs) that represent biological events causing adverse effects [72]. AOPs link in a linear way with scientifically demonstrated key events (KE) from a molecular initiating event (MIE) for a chemical or drug to an adverse outcome (AO) (Figure 1.7). It occurs at a molecular level of biological organization relevant to risk assessment, and the connection between key events is set out key event relationships (KER) that explain the connected relationships between the key events [72].

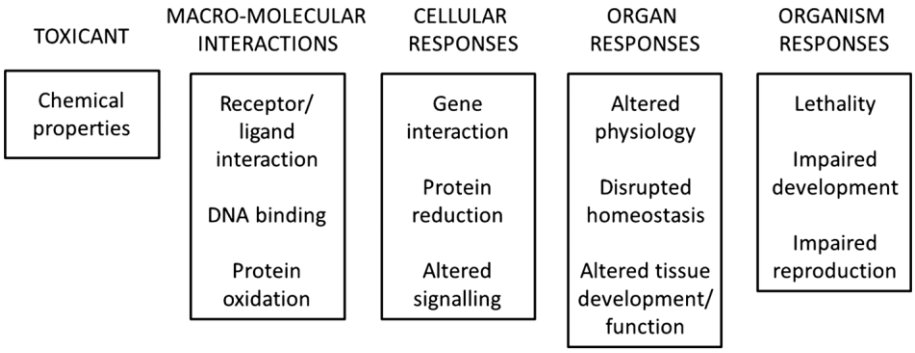

Figure 1.7. Schematic concept of the adverse outcome pathways with examples of different pathways (adapted from an OECD figure, found at http://www.oecd.org/chemicalsafety/testing/adverse-outcome-pathways-molecular-screening-and-toxicogenomics.htm). The figure adapted from *Burden et al. J. Appl. Toxicol, **2015**, 35, 971-975.*

Once AOPs developed, they can be approached in two different ways, which are the ‘‘top-down’ and ‘bottom-up’ approaches. The ‘top-down’ approach explains a measured AO through an MIE and KEs, and the approach relies on *in vivo* methods. The ‘bottom-up’ approach predicts the AO after evaluation of an MIE and downstream KEs, and the approach utilizes non-animal methods [72]. These targeted approaches would allow a change in the practical safety assessment away from the typical manner of observing endpoints, towards the application of biological data obtained from *in silico* and *in vitro* methods to predict a chemical risk. As AOPs explain the series of KEs that result in adversity at different levels, high throughput approaches of *in vitro* and *in silico* methods can be used to predict toxic potential. Thus, AOPs can take a role as a bridge between systems toxicology and non-animal tests, which could enhance the discipline of non-animal-based risk and safety assessment [72]. AOPs also offer the chance to extrapolate effects between species through the understanding of conserved MIEs, KEs, and KER. Therefore, AOPs offer a possibility to develop new and more accurate processes of risk and safety assessment for toxicants, drugs, and other chemicals. AOPs not only contribute to making a regulatory decisions but also significantly improve animal welfare with a reduced reliance on animal testing.

The alternative methods have advantages such as cost, time, and resources compared to animal experiments. The methods are mainly divided into three categories, i.e. cells and tissue cultures, computer models, and alternative organisms. The alternative approach using computer models, can help to interpret the basic principles of biology. Various software programs and computer models are used to predict the toxic and biological effects of chemicals [73]. The programs like molecular docking and molecular dynamic simulation, can be utilized to predict the binding interaction and site. Besides it is possible to create a compound for the specific binding site and interaction using software programs [73]. Another example is based on the Structure Activity Relationship (SAR) computer programs. It forecasts the biological activity of a chemical candidate based on the existed chemical moieties. Quantitative -Structure Activity-Relationship (QSAR) is a representative program, which is a computational modeling method for displaying relationships between biological activities and structural properties of chemicals [74]. Consequently, these applications of computer models can reduce the experimental use of animals.

The *in vitro* models of cell and tissue cultures are also an important alternative to animal testing. The

cultures are conducted outside of the body in a laboratory environment. Various cells and tissues like brain, kidney, liver, and brain can be cultured and kept outside of their body, lasting for a few days to even a few years. Cells generally are cultured as a monolayer on the surface of plates or flasks, and cellular components such as cellular enzymes also can be applied to the cultures. *In vitro* models enable studies of cellular mechanisms and responses in a controlled system. The models consequently provide preliminary information and interpretation for *in vivo* results. For instance, hepatocyte cell cultures provide information on drug metabolism and chemical elimination. These modes help to eliminate unsuitable chemicals in the early stages [75]. The use of stem cells can reduce the number of live animals and embryos on the experiment of developmental toxicity [76,77]. They have been provided superior scientific information in humans, exhibiting unique abilities like differentiation, infinite proliferation, and self-renewal [76]. Recently, various types of culture methods like 3D cultures and co-cultures have been applied to form the tissue-like environment [78,79]. Organ-on-a-chip systems offer a condition of several tissue/organ models on a single device and interlink these within a body-like environment [79]. Thus, the methodologies are utilized actively for understanding cellular mechanisms and screening the biological activities of chemicals and drugs.

The ethical issues of animal testing have brought strict regulations which prohibit on the use of higher vertebrates. Thus, the alternative organisms have been used widely instead of higher vertebrates, they are largely divided into lower vertebrates, invertebrates, and microorganisms. Lower vertebrates (fishes, amphibians, and reptiles) have genetic relatedness to the higher vertebrates and relatively fewer ethical issues in the research [80]. Invertebrate organisms also are an attractive option as an alternative to animal testing. They have been applied to various studies due to their properties, which are small size, simple anatomy, and a rapid life cycle [80]. However, the undeveloped organ system of invertebrates reveals some limitations in human-related studies. Still, they are used in experiments within a short period at less expensive costs. Lastly, microorganisms like *Saccharomyces cerevisiae* are an important and popular model organisms because of their advantages such as easy handling, replicating, mutant isolation, and rapid growth. Furthermore, they have highly versatile DNA transformation and well-defined genetic systems [81]. Another advantage of yeasts is the presence of similar cellular structure and life cycle like multi-cellular eukaryotes [82]. Therefore, yeasts have been used for a wide range of biological studies. Collectively, various methods and approaches can contribute to replace and reduce the experimental use of animals in line with the 3Rs principle.

1.3.3 Current limitations and future direction

Considerable advances have been observed in the current technologies to identify chemical toxicity, effect, and potential adverse reactions. However, the application of animal testing is still required, and the alternative methods are not representative enough to replace animal testing. In the approaches based on *in silico* systems, a relatively smaller scale of tests and limited sampling conditions might cause inadequate sampling and results compared to actual data [80]. One of the representative limitations of cell and tissue cultures is difficult to set up *in vivo* relevant *in vitro* systems. For instance, isolated primary hepatocytes appear to alterations in gene expressions and cell physiology compared to their original physiological environment [83]. Other limitations are difficulties to represent actual interactions between different cells; metabolism of xenobiotics; simulating the experiment of long-term exposures; extrapolation of exposure concentrations; extrapolation from the

information *in vitro* to adverse effects *in vivo*. Furthermore, organs may possess possibilities to relieve stress situations due to their organization and complex architecture [84]. As indicated above, the platforms are still far from the complete replacement of animal testing by alternative methods in the future.

However, the replacement of animal testing can be achievable when (i) we have complemented the current limitations of typical *in vitro* systems by applying innovative culture systems like the 3D culture, co-culture, and cell-ECM culture. The systems can improve cell functionality and physiology by forming tissue-like environments and eventually contribute to reducing the gap between *in vitro* and *in vivo* systems. Then, based on the systems, (ii) we need to understand relevant mechanisms like toxicity and interactions from initial key events to adverse outcomes, and (iii) to construct alternative methods which cover the relevant mechanisms. Therefore, we need to make more efforts to overcome the current limitations, and integrated approaches are necessary to realize the complete replacement of animal testing.

1.4 Bibliography

1. Suzuki, T.; Hidaka, T.; Kumagai, Y.; Yamamoto, M. Environmental pollutants and the immune response. *Nature Immunology* **2020**, *21*, 1486-1495, doi:10.1038/s41590-020-0802-6.
2. Diamanti-Kandarakis, E.; Bourguignon, J.-P.; Giudice, L.C.; Hauser, R.; Prins, G.S.; Soto, A.M.; Zoeller, R.T.; Gore, A.C. Endocrine-disrupting chemicals: an Endocrine Society scientific statement. *Endocr Rev* **2009**, *30*, 293-342, doi:10.1210/er.2009-0002.
3. Walters, P.; Cadogan, D.F.; Howick, C.J. Plasticizers. In *Ullmann's Encyclopedia of Industrial Chemistry*, **2020**, https://doi.org/10.1002/14356007.a20_439.pub2pp. 1-27.
4. Jayaraj, R.; Megha, P.; Sreedev, P. Organochlorine pesticides, their toxic effects on living organisms and their fate in the environment. *Interdiscip Toxicol* **2016**, *9*, 90-100, doi:10.1515/intox-2016-0012.
5. Lazar, S.T.; Kolibaba, T.J.; Grunlan, J.C. Flame-retardant surface treatments. *Nature Reviews Materials* **2020**, *5*, 259-275, doi:10.1038/s41578-019-0164-6.
6. Connolly, L.; Ropstad, E.; Verhaegen, S. In vitro bioassays for the study of endocrine-disrupting food additives and contaminants. *TrAC Trends in Analytical Chemistry* **2011**, *30*, 227-238, doi:https://doi.org/10.1016/j.trac.2010.10.009.
7. Nakama, Y. Chapter 15 - Surfactants. In *Cosmetic Science and Technology*, Sakamoto, K., Lochhead, R.Y., Maibach, H.I., Yamashita, Y., Eds. Elsevier: Amsterdam, **2017**, https://doi.org/10.1016/B978-0-12-802005-0.00015-Xpp. 231-244.
8. La Merrill, M.A.; Vandenberg, L.N.; Smith, M.T.; Goodson, W.; Browne, P.; Patisaul, H.B.; Guyton, K.Z.; Kortenkamp, A.; Cogliano, V.J.; Woodruff, T.J., et al. Consensus on the key characteristics of endocrine-disrupting chemicals as a basis for hazard identification. *Nature Reviews Endocrinology* **2020**, *16*, 45-57, doi:10.1038/s41574-019-0273-8.
9. Lee, H.-R.; Jeung, E.-B.; Cho, M.-H.; Kim, T.-H.; Leung, P.C.K.; Choi, K.-C. Molecular mechanism(s) of endocrine-disrupting chemicals and their potent oestrogenicity in diverse cells and tissues that express oestrogen receptors. *J Cell Mol Med* **2013**, *17*, 1-11, doi:10.1111/j.1582-4934.2012.01649.x.
10. Keminer, O.; Teigeler, M.; Kohler, M.; Wenzel, A.; Arning, J.; Kaßner, F.; Windshügel, B.; Eilebrecht, E. A tiered high-throughput screening approach for evaluation of estrogen and androgen receptor modulation by environmentally relevant bisphenol A substitutes. *The Science of the total environment* **2020**, *717*, 134743, doi:10.1016/j.scitotenv.2019.134743.
11. Gore, A.C.; Chappell, V.A.; Fenton, S.E.; Flaws, J.A.; Nadal, A.; Prins, G.S.; Toppari, J.; Zoeller, R.T. EDC-2: The endocrine society's second scientific statement on endocrine-disrupting chemicals. *Endocr Rev* **2015**, *36*, E1-E150, doi:10.1210/er.2015-1010.
12. Charlton, S.J. Agonist efficacy and receptor desensitization: from partial truths to a fuller picture. *British journal of pharmacology* **2009**, *158*, 165-168, doi:10.1111/j.1476-5381.2009.00352.x.
13. Routledge, E.J.; White, R.; Parker, M.G.; Sumpter, J.P. Differential effects of xenoestrogens on coactivator recruitment by estrogen receptor (ER) alpha and ER beta. *The Journal of biological chemistry* **2000**, *275*, 35986-35993, doi:10.1074/jbc.M006777200.
14. Walker, C.L. Minireview: epigenomic plasticity and vulnerability to EDC exposures. *Molecular*

endocrinology (Baltimore, Md.) **2016**, *30*, 848-855, doi:10.1210/me.2016-1086.
15. Jameson, J.L.; De Groot, J.L. Preface. In *Endocrinology: Adult and Pediatric (Seventh Edition)*, Jameson, J.L., De Groot, L.J., de Kretser, D.M., Giudice, L.C., Grossman, A.B., Melmed, S., Potts, J.T., Weir, G.C., Eds. W.B. Saunders: Philadelphia, **2016**, https://doi.org/10.1016/B978-0-323-18907-1.05001-0p. xvii.
16. Bernal, J.; Guadaño-Ferraz, A.; Morte, B. Thyroid hormone transporters--functions and clinical implications. *Nature reviews. Endocrinology* **2015**, *11*, 406-417, doi:10.1038/nrendo.2015.66.
17. Brucker-Davis, F. Effects of environmental synthetic chemicals on thyroid function. *Thyroid* **1998**, *8*, 827-856, doi:10.1089/thy.1998.8.827.
18. Toivanen, R.; Shen, M.M. Prostate organogenesis: tissue induction, hormonal regulation and cell type specification. *Development* **2017**, *144*, 1382-1398, doi:10.1242/dev.148270.
19. Bansal, R.; Zoeller, R.T. Polychlorinated biphenyls (aroclor 1254) do not uniformly produce agonist actions on thyroid hormone responses in the developing rat brain. *Endocrinology* **2008**, *149*, 4001-4008, doi:10.1210/en.2007-1774.
20. Yang, O.; Kim, H.L.; Weon, J.I.; Seo, Y.R. Endocrine-disrupting chemicals: review of toxicological mechanisms using molecular pathway analysis. *Journal of cancer prevention* **2015**, *20*, 12-24, doi:10.15430/jcp.2015.20.1.12.
21. Eales, J.; Bethel, A.; Galloway, T.; Hopkinson, P.; Morrissey, K.; Short, R.E.; Garside, R. Human health impacts of exposure to phthalate plasticizers: An overview of reviews. *Environment International* **2022**, *158*, 106903, doi:https://doi.org/10.1016/j.envint.2021.106903.
22. Wang, Y.; Qian, H. Phthalates and their impacts on human health. *Healthcare (Basel)* **2021**, *9*, 603, doi:10.3390/healthcare9050603.
23. Ma, Y.; Liu, H.; Wu, J.; Yuan, L.; Wang, Y.; Du, X.; Wang, R.; Marwa, P.W.; Petlulu, P.; Chen, X., et al. The adverse health effects of bisphenol A and related toxicity mechanisms. *Environmental Research* **2019**, *176*, 108575, doi:https://doi.org/10.1016/j.envres.2019.108575.
24. Erkekoğlu, P.; Yirün, A.; Balcı Özyurt, A. Toxic effects of bisphenols: a special focus on bisphenol a and its regulations. In: Erkekoğlu, P. , editor. Bisphenols [Internet]. London: IntechOpen; **2022**, Available from: https://www.intechopen.com/chapters/80501 doi: 10.5772/intechopen.102714
25. Cevdet, U.; Mesude, I.; Inci, T. Alkylphenols in the environment and their adverse effects on living organisms. *Kocatepe Vet. J.* **2009**, *2*, 49-58.
26. Carpenter, D.O. Polychlorinated biphenyls (PCBs): routes of exposure and effects on human health. *Reviews on environmental health* **2006**, *21*, 1-23, doi:10.1515/reveh.2006.21.1.1.
27. Schartl, M. Beyond the zebrafish: diverse fish species for modeling human disease. *Dis Model Mech* **2014**, *7*, 181-192, doi:10.1242/dmm.012245.
28. Oehlmann, J.; Schulte-Oehlmann, U.; Kloas, W.; Jagnytsch, O.; Lutz, I.; Kusk, K.O.; Wollenberger, L.; Santos, E.M.; Paull, G.C.; Van Look, K.J., et al. A critical analysis of the biological impacts of plasticizers on wildlife. *Philosophical transactions of the Royal Society of London. Series B, Biological sciences* **2009**, *364*, 2047-2062, doi:10.1098/rstb.2008.0242.
29. Zhai, W.; Huang, Z.; Chen, L.; Feng, C.; Li, B.; Li, T. Thyroid endocrine disruption in zebrafish larvae after exposure to mono-(2-ethylhexyl) phthalate (MEHP). *PLoS One* **2014**, *9*, e92465-e92465, doi:10.1371/journal.pone.0092465.
30. Faheem, M.; Bhandari, R.K. Detrimental effects of bisphenol compounds on physiology and reproduction in fish: A Literature Review. *Environmental Toxicology and Pharmacology* **2021**, *81*, 103497, doi:https://doi.org/10.1016/j.etap.2020.103497.
31. Ibor, O.R.; Adeogun, A.O.; Fagbohun, O.A.; Arukwe, A. Gonado-histopathological changes, intersex and endocrine disruptor responses in relation to contaminant burden in Tilapia species from Ogun River, Nigeria. *Chemosphere* **2016**, *164*, 248-262, doi:https://doi.org/10.1016/j.chemosphere.2016.08.087.
32. Kar, S.; Sangem, P.; Anusha, N.; Senthilkumaran, B. Endocrine disruptors in teleosts: Evaluating environmental risks and biomarkers. *Aquaculture and Fisheries* **2021**, *6*, 1-26, doi:https://doi.org/10.1016/j.aaf.2020.07.013.
33. Velmurugan, G.; Ramprasath, T.; Gilles, M.; Swaminathan, K.; Ramasamy, S. Gut Microbiota, Endocrine-disrupting chemicals, and the diabetes epidemic. *Trends in endocrinology and metabolism: TEM* **2017**, *28*, 612-625, doi:10.1016/j.tem.2017.05.001.
34. Kumar, M.; Sarma, D.K.; Shubham, S.; Kumawat, M.; Verma, V.; Prakash, A.; Tiwari, R. Environmental endocrine-disrupting chemical exposure: role in non-communicable diseases. *Frontiers in Public Health* **2020**, *8*, doi:10.3389/fpubh.2020.553850.
35. Zhou, X.; Yang, Z.; Luo, Z.; Li, H.; Chen, G. Endocrine disrupting chemicals in wild freshwater fishes: Species, tissues, sizes and human health risks. *Environmental pollution (Barking, Essex : 1987)* **2019**, *244*, 462-468, doi:10.1016/j.envpol.2018.10.026.

36. Lawrence, C. The husbandry of zebrafish (Danio rerio): a review. *Aquaculture* **2007**, *269*, 1-20, doi:https://doi.org/10.1016/j.aquaculture.2007.04.077.
37. Kimmel, C.B.; Ballard, W.W.; Kimmel, S.R.; Ullmann, B.; Schilling, T.F. Stages of embryonic development of the zebrafish. *Developmental dynamics : an official publication of the American Association of Anatomists* **1995**, *203*, 253-310, doi:10.1002/aja.1002030302.
38. Segner, H. Zebrafish (Danio rerio) as a model organism for investigating endocrine disruption. *Comparative biochemistry and physiology. Toxicology & pharmacology : CBP* **2009**, *149*, 187-195, doi:10.1016/j.cbpc.2008.10.099.
39. Khan, F.R.; Alhewairini, S. Zebrafish (Danio rerio) as a model organism. In: Streba, L. , Gheonea, D. I. , Schenker, M. , editors. Current Trends in Cancer Management [Internet]. London: IntechOpen; **2018**, Available from: https://www.intechopen.com/chapters/64178 doi: 10.5772/intechopen.81517
40. Saleem, S.; Kannan, R.R. Zebrafish: an emerging real-time model system to study Alzheimer's disease and neurospecific drug discovery. *Cell Death Discovery* **2018**, *4*, 45, doi:10.1038/s41420-018-0109-7.
41. Cassar, S.; Adatto, I.; Freeman, J.L.; Gamse, J.T.; Iturria, I.; Lawrence, C.; Muriana, A.; Peterson, R.T.; Van Cruchten, S.; Zon, L.I. Use of zebrafish in drug discovery toxicology. *Chemical Research in Toxicology* **2020**, *33*, 95-118, doi:10.1021/acs.chemrestox.9b00335.
42. MacRae, C.A.; Peterson, R.T. Zebrafish as tools for drug discovery. *Nature Reviews Drug Discovery* **2015**, *14*, 721-731, doi:10.1038/nrd4627.
43. Howe, K.; Clark, M.D.; Torroja, C.F.; Torrance, J.; Berthelot, C.; Muffato, M.; Collins, J.E.; Humphray, S.; McLaren, K.; Matthews, L., et al. The zebrafish reference genome sequence and its relationship to the human genome. *Nature* **2013**, *496*, 498-503, doi:10.1038/nature12111.
44. Zohar, Y.; Muñoz-Cueto, J.A.; Elizur, A.; Kah, O. Neuroendocrinology of reproduction in teleost fish. *General and comparative endocrinology* **2010**, *165*, 438-455, doi:10.1016/j.ygcen.2009.04.017.
45. To, T.T.; Hahner, S.; Nica, G.; Rohr, K.B.; Hammerschmidt, M.; Winkler, C.; Allolio, B. Pituitary-interrenal interaction in zebrafish interrenal organ development. *Molecular endocrinology (Baltimore, Md.)* **2007**, *21*, 472-485, doi:10.1210/me.2006-0216.
46. Lassiter, C.S.; Linney, E. Embryonic expression and steroid regulation of brain aromatase cyp19a1b in zebrafish (Danio rerio). *Zebrafish* **2007**, *4*, 49-57, doi:10.1089/zeb.2006.9995.
47. Mouriec, K.; Lareyre, J.J.; Tong, S.K.; Le Page, Y.; Vaillant, C.; Pellegrini, E.; Pakdel, F.; Chung, B.C.; Kah, O.; Anglade, I. Early regulation of brain aromatase (cyp19a1b) by estrogen receptors during zebrafish development. *Developmental dynamics : an official publication of the American Association of Anatomists* **2009**, *238*, 2641-2651, doi:10.1002/dvdy.22069.
48. Porazzi, P.; Calebiro, D.; Benato, F.; Tiso, N.; Persani, L. Thyroid gland development and function in the zebrafish model. *Molecular and Cellular Endocrinology* **2009**, *312*, 14, doi:10.1016/j.mce.2009.05.011.
49. Brion, F.; De Gussem, V.; Buchinger, S.; Hollert, H.; Carere, M.; Porcher, J.M.; Piccini, B.; Féray, C.; Dulio, V.; Könemann, S., et al. Monitoring estrogenic activities of waste and surface waters using a novel in vivo zebrafish embryonic (EASZY) assay: Comparison with in vitro cell-based assays and determination of effect-based trigger values. *Environment international* **2019**, *130*, 104896, doi:10.1016/j.envint.2019.06.006.
50. Yilmaz, O.; Patinote, A.; Nguyen, T.; Bobe, J. Multiple vitellogenins in zebrafish (Danio rerio): quantitative inventory of genes, transcripts and proteins, and relation to egg quality. *Fish physiology and biochemistry* **2018**, *44*, 1509-1525, doi:10.1007/s10695-018-0524-y.
51. Yu, L.-Q.; Zhao, G.-F.; Feng, M.; Wen, W.; Li, K.; Zhang, P.-W.; Peng, X.; Huo, W.-J.; Zhou, H.-D. Chronic exposure to pentachlorophenol alters thyroid hormones and thyroid hormone pathway mRNAs in zebrafish. *Environmental toxicology and chemistry* **2014**, *33*, 170-176, doi:https://doi.org/10.1002/etc.2408.
52. Nyakubaya, V.T.; Durney, B.C.; Ellington, M.C.; Kantes, A.D.; Reed, P.A.; Walter, S.E.; Stueckle, J.R.; Holland, L.A. Quantification of circulating steroids in individual zebrafish using stacking to achieve nanomolar detection limits with capillary electrophoresis and UV-visible absorbance detection. *Anal Bioanal Chem* **2015**, *407*, 6985-6993, doi:10.1007/s00216-015-8785-0.
53. Muth-Köhne, E.; Westphal-Settele, K.; Brückner, J.; Konradi, S.; Schiller, V.; Schäfers, C.; Teigeler, M.; Fenske, M. Linking the response of endocrine regulated genes to adverse effects on sex differentiation improves comprehension of aromatase inhibition in a Fish Sexual Development Test. *Aquat Toxicol* **2016**, *176*, 116-127, doi:10.1016/j.aquatox.2016.04.018.
54. Hara, A.; Hiramatsu, N.; Fujita, T. Vitellogenesis and choriogenesis in fishes. *Fisheries Science* **2016**, *82*, 187-202, doi:10.1007/s12562-015-0957-5.
55. Sullivan, C.; Yilmaz, O. Vitellogenesis and Yolk Proteins, Fish. In *Encyclopedia of Reproduction*, Skinner M.K., Eds, Elsevier: Amsterdam, **2018**, 10.1016/B978-0-12-809633-8.20567-0.

56. Lubzens, E.; Bobe, J.; Young, G.; Sullivan, C.V. Maternal investment in fish oocytes and eggs: The molecular cargo and its contributions to fertility and early development. *Aquaculture* **2017**, *472*, 107-143, doi:https://doi.org/10.1016/j.aquaculture.2016.10.029.
57. Babin, P.J.; Carnevali, O.; Lubzens, E.; Schneider, W.J. Molecular aspects of oocyte vitellogenesis in fish. In *The Fish Oocyte: From Basic Studies to Biotechnological Applications*, Babin, P.J., Cerdà, J., Lubzens, E., Eds. Springer Netherlands: Dordrecht, **2007**, 10.1007/978-1-4020-6235-3_2pp. 39-76.
58. Dang, Z. Interpretation of fish biomarker data for identification, classification, risk assessment and testing of endocrine disrupting chemicals. *Environment international* **2016**, *92-93*, 422-441, doi:10.1016/j.envint.2016.04.003.
59. OECD. Test No. 229: fish short term reproduction assay. **2012**, doi:https://doi.org/10.1787/9789264185265-en.
60. OECD. Test No. 230: 21-day fish assay. **2009**, doi:https://doi.org/10.1787/9789264076228-en.
61. OECD. Test No. 230: fish sexual development test. **2011**, doi:https://doi.org/10.1787/9789264076228-en.
62. OECD. Test No. 240: medaka extended one generation reproduction test (MEOGRT). **2015**, https://doi.org/10.1787/9789264122369-en.
63. National Research Council (US) and Institute of Medicine (US) Committee on the Use of Laboratory Animals in Biomedical and Behavioral Research. Use of laboratory animals in biomedical and behavioral research. Washington (DC): National Academies Press (US), **1988**, doi:10.17226/1098
64. Festing, S.; Wilkinson, R. The ethics of animal research. Talking Point on the use of animals in scientific research. *EMBO reports* **2007**, *8*, 526-530, doi:10.1038/sj.embor.7400993.
65. Government, U.K. Annual statistics of scientific procedures on living animals great britain. **2021**, Availabe online: https://assets.publishing.service.gov.uk/government/uploads/system/uploads/attachment_data/file/1085383/annual-statistics-scientific-procedures-living-animals-2021_v8.pdf.
66. Commission, E. Summary report on the statistics on the use of animals for scientific purposes in the member states of the european union and norway in 2018. **2018**, Availabe online: https://ec.europa.eu/environment/chemicals/lab_animals/pdf/SWD_%20part_A_and_B.pdf.
67. Animal and Plant Health Inspection Service, U.S.D.o.A. Annual report animal usage by fiscal year: total number of animals research facilities used in regulated activities (Column B). **2022**, Availabe online: https://www.aphis.usda.gov/aphis/ourfocus/animalwelfare/sa_obtain_research_facility_annual_report/ct_research_facility_annual_summary_reports.
68. Rollin, B.E. Toxicology and new social ethics for animals. *Toxicologic pathology* **2003**, *31 Suppl*, 128-131, doi:10.1080/01926230390175011.
69. Rusche, B. The 3Rs and animal welfare - conflict or the way forward? *Altex* **2003**, *20*, 63-76.
70. Russell, W.M.S.B., R. L. The principles of humane experimental technique. London: Methuen & Co. Limited, **1959**, Vol. 1, pp. 500-500.
71. Hubrecht, R.C.; Carter, E. The 3Rs and Humane Experimental Technique: Implementing Change. *Animals : an open access journal from MDPI* **2019**, *9*, doi:10.3390/ani9100754.
72. Burden, N.; Sewell, F.; Andersen, M.E.; Boobis, A.; Chipman, J.K.; Cronin, M.T.; Hutchinson, T.H.; Kimber, I.; Whelan, M. Adverse Outcome Pathways can drive non-animal approaches for safety assessment. *Journal of applied toxicology : JAT* **2015**, *35*, 971-975, doi:10.1002/jat.3165.
73. Lang, A.; Volkamer, A.; Behm, L.; Röblitz, S.; Ehrig, R.; Schneider, M.; Geris, L.; Wichard, J.; Buttgereit, F. In silico methods – Computational alternatives to animal testing. *ALTEX - Alternatives to animal experimentation* **2018**, *35*, 126-128, doi:10.14573/altex.1712031.
74. Knight, A.; Bailey, J.; Balcombe, J. Animal carcinogenicity studies: 3. Alternatives to the bioassay. *Alternatives to laboratory animals : ATLA* **2006**, *34*, 39-48, doi:10.1177/026119290603400119.
75. Kimber, I.; Pichowski, J.S.; Betts, C.J.; Cumberbatch, M.; Basketter, D.A.; Dearman, R.J. Alternative approaches to the identification and characterization of chemical allergens. *Toxicology in vitro : an international journal published in association with BIBRA* **2001**, *15*, 307-312, doi:10.1016/s0887-2333(01)00027-3.
76. Kim, T.W.; Che, J.H.; Yun, J.W. Use of stem cells as alternative methods to animal experimentation in predictive toxicology. *Regulatory toxicology and pharmacology : RTP* **2019**, *105*, 15-29, doi:10.1016/j.yrtph.2019.03.016.
77. Stummann, T.C.; Bremer, S. Embryonic stem cells in safety pharmacology and toxicology. *Advances in experimental medicine and biology* **2012**, *745*, 14-25, doi:10.1007/978-1-4614-3055-1_2.
78. Ma, X.; Liu, J.; Zhu, W.; Tang, M.; Lawrence, N.; Yu, C.; Gou, M.; Chen, S. 3D bioprinting of functional tissue models for personalized drug screening and in vitro disease modeling. *Advanced*

drug delivery reviews **2018**, *132*, 235-251, doi:10.1016/j.addr.2018.06.011.
79. Bédard, P.; Gauvin, S.; Ferland, K.; Caneparo, C.; Pellerin, È.; Chabaud, S.; Bolduc, S. Innovative human three-dimensional tissue-engineered models as an alternative to animal testing. *Bioengineering (Basel, Switzerland)* **2020**, *7*, doi:10.3390/bioengineering7030115.
80. Doke, S.K.; Dhawale, S.C. Alternatives to animal testing: A review. *Saudi Pharmaceutical Journal* **2015**, *23*, 223-229, doi:https://doi.org/10.1016/j.jsps.2013.11.002.
81. Botstein, D.; Chervitz, S.A.; Cherry, J.M. Yeast as a model organism. *Science (New York, N.Y.)* **1997**, *277*, 1259-1260, doi:10.1126/science.277.5330.1259.
82. Madeo, F.; Engelhardt, S.; Herker, E.; Lehmann, N.; Maldener, C.; Proksch, A.; Wissing, S.; Fröhlich, K.U. Apoptosis in yeast: a new model system with applications in cell biology and medicine. *Current genetics* **2002**, *41*, 208-216, doi:10.1007/s00294-002-0310-2.
83. Godoy, P.; Hewitt, N.J.; Albrecht, U.; Andersen, M.E.; Ansari, N.; Bhattacharya, S.; Bode, J.G.; Bolleyn, J.; Borner, C.; Böttger, J., et al. Recent advances in 2D and 3D in vitro systems using primary hepatocytes, alternative hepatocyte sources and non-parenchymal liver cells and their use in investigating mechanisms of hepatotoxicity, cell signaling and ADME. *Archives of toxicology* **2013**, *87*, 1315-1530, doi:10.1007/s00204-013-1078-5.
84. Taylor, K. Recent developments in alternatives to animal testing. In *Animal Experimentation: Working Towards a Paradigm Change*, Leiden, The Netherlands: Brill, **2019**, doi: https://doi.org/10.1163/9789004391192_0252019.

Chapter 2. Aim and Structure of the Thesis

Motivation

As stated in the title, this thesis aims to 3D *in vitro*-based alternative approaches to ecotoxicity assessment. In the context of this thesis, precise and reliable alternatives to animal testing are necessary as increasing the presence of EDCs in the ecosystem, considering the bioethics and the 3Rs. *In silico* and *in vitro* approaches have been introduced and tested as alternatives to animal testing. However, typical monolayer fish cell cultures show numerous limitations on endogenous and exogenous metabolic functions compared to freshly isolated primary cells. There is a need to develop novel test systems for robust reproductive toxicity assessment. Thus, I addressed the research question "Can *in vitro*/*in silico* systems replace animal testing for environmental hazard monitoring combined with AOP?". For the above purpose, the 3D structure of zebrafish estrogen receptor was generated to understand modes of action as a molecular initiating event upon estrogenic chemical exposure. In addition, the zebrafish liver cell line was selected and applied to various 3D cell culture techniques to develop novel *in vitro* platforms. The platforms were optimized for the assessment of chemicals and tested to understand key events that can lead to adverse outcomes.

Structure of the Thesis

After the introduction, the thesis is composed of five main chapters. Combined *in silico* and *in vitro* approaches for identifying EDCs are introduced in the first chapter. The study of the chapter has been published in the journal of *Environmental Toxicology & Chemistry*. In the second chapter, the 3D spheroid culture of ZFL cells is introduced. The study has been published in *Aquatic Toxicology*. In the subsequent chapter, the cluster culture of ZFL cells is conducted on collagen-based hydrogels. The study has been published in *Environmental Science & Technology*. The next chapter deals with hybrid-spheroid culture with nanofibers, and the study has been published in *Small*. Finally, the thesis is concluded with a conclusion. The published papers as their original formatting can be found in the appendix.

Chapter 3. Combined *in silico* and *in vitro* approaches for identifying EDCs

Contributions

As published in: **Chang Gyun Park**, Nancy Singh, Chang Seon Ryu, Ju Yong Yoon, Maranda Esterhuizen, and Young Jun Kim, "Species differences in response to binding interactions of BPA and its analogs with the modeled estrogen receptor 1 and *in vitro* reporter gene assay in human and zebrafish" *Environmental Toxicology and Chemistry* **2022**, 10.1002/etc.5433

Authorship contributions

Chang Gyun Park: writing - original draft, data curation, formal analysis, writing - review & editing
Nancy Singh: data curation, formal analysis, resources, methodology, writing - review & editing
Chang Seon Ryu: writing - original draft, data curation, formal analysis, writing - review & editing
Ju Yong Yoon: formal analysis, methodology, writing - review & editing.
Maranda Esterhuizen: conceptualization, investigation, methodology, writing - review & editing.
Young Jun Kim: writing - original draft, conceptualization, funding acquisition, investigation, methodology, writing - review & editing.

Relation to the thesis

This study develops a 3D homology model for the ligand-binding domain structure of zebrafish estrogen receptor 1 (zEsr1-LBD). This is the first time that binding patterns of BPA and its analogs with zebrafish estrogen receptor 1 have been investigated by using molecular dynamics simulations and binding free energy calculations with a combined *in vitro* reporter assay. The study was conducted with the docking of bisphenol A and its analogs on the human and the modeled zebrafish receptors to identify potential endocrine disruptors. Then, the results were compared to those of the *in vitro* reporter gene assays. The findings of this study will support the development of cross-species testing between humans and zebrafish for endocrine disruptors and aid in minimizing their impacts.

In this chapter, the main relationship with the thesis is the approach of combined *in silico* and *in vitro* systems for predicting EDCs. The 3D structure of zEsr1-LBD was generated using homology modeling, and the model was docked and simulated with EDCs. The results showed moderate or high correlations with the results of *in vitro* reporter gene assays. Therefore, the generated model can be useful for screening the estrogenic activities of EDCs. Also, the combined approaches are able to evaluate modes of action as a molecular initiating event upon estrogenic chemical exposure. Eventually, these approaches can contribute to reducing the experimental use of animals.

3.1 Abstract

Adverse impacts associated with the interactions of numerous endocrine-disruptor chemicals (EDCs) with estrogen receptor 1 play a pivotal role in reproductive dysfunction. The predictive studies on these interactions thus are crucial in the risk assessment of EDCs but heavily rely on the accuracy of specific protein structure in three-dimensional (3D). As the 3D structure of zebrafish estrogen receptor 1 (zEsr1) is not available, the 3D structure of zEsr1 ligand-binding domain (zEsr1-LBD) was generated using MODELLER, and its quality was assessed by PROCHECK, ERRAT, ProSA, and Verify-3D tools. After the generated model was verified as reliable, bisphenol A (BPA) and its analogs were docked on the zEsr1-LBD and human estrogen receptor 1 ligand-binding domain (hESR1-LBD) using Discovery Studio and Autodock Vina programs. Besides, molecular dynamics followed by molecular docking were simulated using the NAMD program and compared to those of the *in vitro* reporter gene assays. Some chemicals were bound with an orientation similar to that of 17β-estradiol (E2) in both models and *in silico* binding energies showed moderate or high correlations with *in vitro* results ($0.33 \leq r^2 \leq 0.71$). Notably, hydrogen bond occupancy during molecular dynamics simulations exhibited a high correlation with *in vitro* results ($r^2 \geq 0.81$) in both complexes. These results showed that the combined *in silico* and *in vitro* approaches can be provided the valuable tools for identifying EDCs in different species, facilitating the assessment of EDC-induced reproductive toxicity.

Keywords: *In silico* methods; Homology modeling; Estrogen receptor 1; Zebrafish; BPA and its analogs; *In vitro* assay

3.2 Introduction

Estrogen-induced actions promote various physiological processes, such as growth, homeostasis, and reproduction [1-5]. Additionally, estrogens regulate pubertal development and function of the female reproductive system [2], bone density [3], immune system [5], and lipid and glucose metabolism [4]. Most of these processes are mediated by estrogen receptors (ESRs), which can be divided into two subtypes: estrogen receptor 1 (ESR1) and estrogen receptor 2 (ESR2). Both receptors have been observed in non-mammalian vertebrates and mammals [6]. ESR1 is predominantly expressed in various tissues and organs, such as the liver, bones, glands, uterus, ovaries, testes, and prostate [7,8], and plays more important roles than ESR2 in the mammary glands and uterus, maintenance of skeletal homeostasis, and regulation of lipid and glucose metabolism [9,10]. ESRs are structurally composed of N-terminal, DNA-binding, and ligand-binding domains [11]. The LBD includes the ligand-binding pocket, which can activate ESRs by interacting with ligands, such as 17β-estradiol (E2). Owing to this interaction, many exogenous chemicals, which mimic estrogens, can alter the functions of the endocrine system and cause various adverse effects [12]. Therefore, concern regarding the possible threats posed by endocrine-disrupting chemicals (EDCs) in wildlife and humans is increasing [13,14].

Bisphenol A (BPA) has been reported to adversely affect the reproductive and developmental systems of humans, fish, and amphibians [15-17], and is a precursor to plastics, epoxy resins, and thermal

paper [18]. Although substitutes have recently been manufactured to replace BPA, some exert endocrine effects similar to those of BPA [19-22]. As a large number of comprehensive studies are required to evaluate potential endocrine disruption caused by BPA substitutes, molecular docking is a promising tool for predicting and screening potential EDCs, and has been conducted to predict the types of interactions, binding affinity, and orientations of the docked ligands at the binding site of the target receptor [23-26]. However, since most static docking protocols lack receptor flexibility, the reliability of the complexes might be uncertain [27]. Hence, molecular dynamics (MD) simulation has been applied to understand the dynamic behavior of complexation and provide significant complementary with molecular docking. MD simulation can offer fundamental molecular mechanisms and conformational changes [27,28]. Although most docking studies have been conducted on BPA and its analogs for human ESRs, docking and MD simulations for aquatic organisms remain limited as there are currently no available crystal structures [25,29].

Therefore, this study aimed to generate the structure of a zEsr1-LBD using homology modeling. Zebrafish (*Danio rerio*) have been utilized as a model organism for toxicity testing by the Organization for Economic Co-operation and Development (OECD) guidelines. Furthermore, zebrafish exhibit rapid development and growth, and signaling pathways highly similar to those in humans [30,31]. The zEsr1-LBD was generated using the MODELLER program and the structural quality was then verified using PROCHECK, ERRAT, ProSA, and Verify-3D tools. Consequently, the generated zEsr1-LBD model was used to investigate its interactions with E2, BPA, 4,4′-(9-Fluorenyliden)-diphenol (BPFL), tetramethyl bisphenol A (TMBPA), and 4-phenylphenol. BPFL, TMBPA, and 4-phenylphenol are classified as alternative substances of BPA, and these analogs are introduced mainly for the usage in thermal paper, polymer, polycarbonate, and fire retardant [22]. As these applications cause exposure of chemicals into the environment, the analogs have been detected in nature with environmental relevance [32-34]. These chemicals have been reported to have endocrine disruptor potential by exhibiting anti- or estrogenic activities in humans [22]. In addition, BPFL showed anti-estrogenic effect in mice and zebrafish and hormetic effects on regulating hypothalamic-pituitary-thyroid axis in zebrafish [35-37]. However, there is still a lack of studies on their estrogenic disruptive activities and their modes of action in aquatic species. Thereby, the complex geometry and putative chemical-receptor binding energies of BPA and its analogs were then calculated and validated by conducting *in vitro* assays. The correlations between the *in silico* and *in vitro* analyses confirmed that the newly generated zEsr1-LBD is useful for predicting and evaluating the estrogenic activities of EDCs.

3.3 Materials and Methods

3.3.1 Sequence alignment, template selection, and homology modeling

Sequence alignment was conducted to observe sequence identity between human ESRs (hESRs) and zebrafish Esrs (zEsrs). Multiple sequence alignment and Principal Components Analysis (PCA) were conducted, and a phylogenetic tree was generated using JalView [38]. The PCA and phylogenetic tree were constructed using amino acid sequences of estrogen receptors available from Uniprot. The sequence sources and UniProt IDs were as follows: human estrogen receptor 1 (hESR1, P03372), zebrafish estrogen receptor 1 (zEsr1, P57717),

human estrogen receptor 2 (hESR2, Q92731), zebrafish estrogen receptor 2a (zEsr2a, Q7ZU32), and zebrafish estrogen receptor 2b (zEsr2b, Q90WS9).

The crystal structure of hESR1 (PDB ID: 2YJA) was selected as hESR1-LBD, which is bounds to stapled peptides and E2 [39]. The LBD structure of zEsr1 was created using homology modeling. First, the LBD sequence of zEsr1 (P57717) was retrieved from the UniProt database to build the model. The query sequence was then used to search for an optimal template with the protein-basic local alignment search tool (BLASTp) [40]. The hESR1-LBD (2YJA) was selected as the optimal template after utilizing BLASTp. MODELLER 9.25 was used to create the homology model for zEsr1-LBD. The program is a homology or comparative modeling tool that conducts comparative protein structure modeling based on satisfaction of spatial restraints. Comparative modeling predicts the 3D structure of a given protein target sequence based primarily on its alignment with one or more proteins with known template structures to generate a zebrafish Esr1 model [41]. The LBD sequence of zEsr1 and template structure (2YJA) were used as the inputs in MODELLER v9.25 (https://salilab.org/modeller/9.25/release.html). When target-template alignment is conducted, the program automatically calculates a 3D model of the target using its automodel class [41]. MODELLER finally generates a 3D model containing all the main chain and sidechain non-hydrogen atoms as the output of the given target sequence. Ten models were generated, and one structure with the lowest DOPE score was selected as the zEsr1-LBD model for molecular docking [42].

3.3.2 Homology model validation

The structural qualities of zEsr1-LBD and hESR1-LBD were validated using ERRAT [43], PROCHECK [44], ProSA [45], and Verify 3D tools [46]. ERRAT analyzes the relative frequencies of non-covalent interactions between various types of atoms [43], while PROCHECK uses the Ramachandran plot for structural verification, which assesses the quality and accuracy of the stereochemical properties of a model [44]. The Protein Structure Analysis (ProSA) program is an established tool with a large user base that is frequently used to refine and validate experimental protein structures and for structural prediction and modeling [45]. The program Verify 3D measures the compatibility of a protein model with its own amino acid sequence [46].

3.3.3 Molecular Docking

The hESR1-LBD and generated zEsr1-LBD structures were used for molecular docking with BPA analogues including E2, BPA, BPFL, TMBPA, and 4-phenylphenol as the test ligands from the PubChem database (E2: 5757, BPA: 6623, BPFL: 76716, TMBPA: 79717, and 4-phenylphenol: 7103). All the chemicals were saved as a SDF file, and their geometries were optimized following the MM2 energy minimization method. The files were converted into PDB format using Discovery Studio Visualizer 2016 (Accelrys Software Inc., San Diego, CA, USA).

Molecular docking simulations were conducted using the CDOCKER module of Discovery Studio [47] and AutoDock Vina [48], which uses the CHARMM-based molecular dynamics method. CDOCKER

generates the conformation using high-temperature MD and then forwarding the conformations to the binding site for binding pose analysis. The CDOCKER interaction energy is taken as an estimate of the molecular binding affinity, with lower values suggesting more favorable binding between the protein and ligand [47]. Autodock Vina utilizes protein and ligand information, along with the grid box properties, in the docking configuration file, and assumes that the receptor is rigid and ligands are flexible during docking [48]. Root-mean-squared-deviation (RMSD) values below 1.0 Å were clustered and considered the results with the most favorable binding free energy. The grid size was set to 40 points each in the x, y, and z directions, with a grid spacing of 1.0 Å. The energetic map was determined using the distance-dependent function of the dielectric constant, and the default settings were applied to all the other parameters. All docked poses were determined using rankings based on binding energies. The pose with the lowest binding energy was extracted and aligned with the receptor structure for further analysis.

3.3.4 Molecular dynamics (MD) simulations

All simulations were performed using the nanoscale molecular dynamics (NAMD) 2.14 software with the CHARMM27 force field [28]. System preparations for MD simulations and analysis of the computed trajectories were performed using visual dynamics studio (VMD) v1.9 [49]. The CHARMM GUI web server was utilized to prepare the system for the MD simulations, including ligand parameter files. Coordinates for the missing hydrogen atoms and amino acids side chains were added with AutoPSF plugin from VMD and based on the CHARMM27 force field [27]. The system was solvated with TIP3P water using the solvate plugin from VMD with a spacing of 10 Å in all directions [50]. The MD simulations were considered Na^+ and Cl^- ions in explicit water for neutralizing the charges of the system. After the minimization of the solvated system, the system was equilibrated at a temperature of 310 K. The simulations were conducted in the isothermal-isobaric (NPT) ensemble with periodic boundary conditions. Electrostatic interactions were computed using the particle mesh Ewald method [51]. The van der Waals interactions were calculated at a cutoff and switching distances of 12 Å and 10 Å, respectively. The temperature and pressure were maintained constant using a Langevin thermostat and a Langevin barostat, respectively. All simulations were conducted for at least 20 ns using 2 fs time steps [52].

The RMSD of protein Cα atoms was calculated in each simulation. Moreover, the H-bonding occupancy was analyzed using the H-bond plugin. The cutoff distance and angle of occupancy were set to 3.5 Å and 120°, respectively. The simulation of binding free energy (ΔG_{bind}) was also calculated by MM/PBSA (Molecular Mechanics/Poisson-Boltzmann Surface Area) in the CaFE plugin. Each simulation extracted at least 5000 snapshots from the last 5 ns of the trajectories. The calculation of MM/PBSA was performed according to a methodology described previously [53].

3.3.5 Recombinant yeast assay

All the chemicals were purchased from Sigma-Aldrich (St. Louis, MO, USA) and dissolved in dimethyl sulfoxide (DMSO), the concentration of which did not exceed 1% (v/v) of the test chemicals. *Saccharomyces*

cerevisiae recombinant yeast was purchased from Xenometrix AG (XenoScreen YES; Allschwil, Switzerland) and was genetically integrated to express hESR1 (YES). The expression plasmid of the reporter gene *lac*-Z was also inserted into the yeast, which induces the β-galactosidase enzyme. Therefore, when an agonist bound to the hESR1 in the yeast, yeast was activated and expressed β-galactosidase, which converts chlorophenol red-β-D-galactopyranoside (CPRG) into chlorophenol red [54]. Based on this principle, the yeast could be used to evaluate the estrogenic activity of chemicals; for this, we used E2 as a reference chemical. The test yeast was exposed to half-logarithmic (3.16-fold) dilutions of E2 and other chemicals. The exposure ranges were 10^{-11} to 10^{-8} M for E2, 10^{-7} to 10^{-4} M for BPA and TMBPA, and 10^{-8} to 10^{-5} M for BPFL and 4-phenylphenol, respectively. The medium containing yeast and CPRG (200 µL) was exposed to the test chemicals (2 µL) in 96-well plates and incubated at 31 °C with shaking (100 rpm) for 48 h. E2 treatment resulted in the cleavage of CPRG into chlorophenol red by the induction of β-galactosidase. We analyzed optical density at 690 nm (OD_{690}) and 570 nm (OD_{570}) using a spectrophotometer (Tecan, Männedorf, Switzerland). Data analysis was conducted according to the yeast assay manufacturer's protocol [54].

3.3.6 Cell culture, transfection, and luciferase reporter assay

The human embryonic kidney 293 cell line (HEK293, CRL-1573; ATCC, Wesel, Germany) was utilized as a transfection host for the zEsr1 construct. The HEK293 cells were cultured in Dulbecco's modified Eagle's medium without phenol red (DMEM; Thermo Scientific, Karlsruhe, Germany), with 10% fetal bovine serum (Thermo Scientific) and 1% penicillin-streptomycin (Thermo Scientific), at 37 °C and 5% CO_2.

The HEK293 cells were transduced with the pGreenFire Lenti-reporter plasmid (pGF2-ERE-rFLuc-T2A-GFP-mPGK-Puro, TR455VA-P; System Biosciences, Palo Alto, CA, USA) that encodes GFP reporter and red-shifted luciferase, under the control of ERE response elements with the puromycin resistance, according to a previously described methodology [55]. Briefly, the cells were plated with 3×10^5 cells per well in a 6-well plate (Thermo Scientific) before transduction. After overnight culture, the old medium was aspirated and the virus-containing medium was treated with 5 µg/mL of polybrene for 8 h. Subsequently, the virus-containing medium was removed and the transduced cells were allowed to recover overnight before the addition of puromycin (10 µg/mL) for selection in the medium. In the second step, the transduced cells (HEK293-ERE) were transfected with the piggyBac transposon gene expression system. The zEsr1 expression vector was custom-cloned by vectorbuilder (pPB-Neo-CAG>zEsr1, VB210426-1022cns; Vectorbuilder Inc. Chicago, USA) and the pRP-mCherry-CAG>hyPBase plasmid (VB160216-10057; Vectorbuilder Inc) encodes the hyperactive version of piggyBac transposase. The cells were plated with 1 x 10^5 cells per well in a 6-well plate. After overnight culture, 1 µg of the vector and 0.75 µL of the lipofectamine 3000 reagent were mixed in 250 µL of Opti-MEM medium and incubated for 15 min for DNA-lipid complex formation. The complex was treated to the wells and incubated for 6 h. Afterward, the medium was removed and the cells were allowed to recover overnight before the addition of puromycin and neomycin (10 µg/mL and 2 µg/mL, respectively). Finally, the transfected cells (HEK293-ERE-zEsr1) were collected.

The HEK293-ERE-zEsr1 cells were used to assess the estrogenic activity of chemicals. E2 was used as a reference chemical and the cells were exposed to half-logarithmic (3.16-fold) dilutions of E2 and

other chemicals. The exposure ranges were 10^{-12}–10^{-9} M for E2 and 10^{-10}–10^{-5} M for other chemicals, respectively. The test chemicals were obtained with high purity (≥ 98%) from Sigma–Aldrich and were dissolved in dimethyl sulfoxide (DMSO), with a concentration not exceeding 0.5% (v/v). The cells were seeded at a rate of 1.0×10^4 cells per well on a 96-well plate. After overnight culture, the chemical solutions were treated with a ratio of 1:1 in each well containing the medium, and cultured for 24 h. The cells were lysed with passive lysis buffer (Promega, Mannheim, Germany), and the lysates were applied to evaluate Firefly luciferase activity using the Luciferase Reporter Assay System (Promega). Luminescence was measured as relative luminescence units with an integration time of 10 sec and a settling time of 1 sec using a microplate reader.

3.3.7 Statistical analysis

All data of the *in vitro* studies are presented as the mean of triplicate of three wells per concentration and are presented as the mean ± standard deviation. Graphs are prepared using SigmaPlot (Version 12.0, Systat Software Inc., San Jose, CA, USA). The correlation analysis was performed using Pearson correlation test in R version 3.5.1 through RStudio Version 1.2.5042.

3.4 Results and Discussion

3.4.1 Sequence alignment, template selection, and homology modeling

Sequence alignments of hESRs and zEsrs were obtained and are compared in Figure 3.1. The sequence identity between hESR1 and zEsr1 is 47% (Figure 3.1a). Notably, the sequence identity of LBD between hESR1 and zEsr1 increase to 62%, which indicates better conservation compared to other domains. The sequence similarity of the LBD regions between both sequences is 78%. The PCA results indicated clear separations between estrogen receptor 1 and estrogen receptor 2, regardless of the species (Figure 3.1b). The hESR1 and zEsr1 isoforms are closer to each other than the hESR2 and zEsr2 isoforms. The phylogenetic tree reveals the close inter-relationship of 1 and 2 isoforms of hESR and zEsr in terms of evolutionary distance metric. (Figure 3.1c). Sequence alignment is a pivotal step in generating a homology model, as sequence misalignment can result in homology model errors and the generation of different models [56,57]. Phylogenetic analysis confirmed that zEsr1 is derived from the estrogen receptor 1 ancestral subtype and that zEsr2 isoforms belong to the estrogen receptor 2 subgroup. Moreover, the LBD is highly conserved following the DNA binding domain [58]. Consequently, the LBD sequences of hESR1 and zEsr1 were considered well conserved within the same subtype.

A homology model of zEsr1-LBD was generated using MODELLER based on sequence alignment (Figure 3.2). The hESR1-LBD (PDB ID: 2YJA; Figure 3.2a) was selected as a template, with a query coverage, sequence identity, e-value, and bit score of 44%, 62.1%, 6e-109, and 327, respectively. Ten homology models were generated, and the optimal zEsr1-LBD model was selected according to the lowest discrete optimized protein energy (DOPE score: −32,888; Figure 3.2b). The x-ray crystal structure of hESR1-

LBD and the homology model of zEsr1-LBD are superimposed in Figure 3.2c. The backbone positional RMSD between the two structures was 0.162 Å, indicating that the zEsr1-LBD model has high similarity and structural comparability with the hESR1-LBD structure [59,60]. The ligand-binding cavities when both receptors were bound to E2 are superimposed in Figure 3.2d. Three residues at corresponding positions of the ligand-binding cavities of hESR1 and zEsr1 were involved in hydrogen bonding and each residue of the two receptors formed hydrogen bonding interactions with the identical atoms of E2. Moreover, the distances of each corresponding hydrogen bond are comparable between the two species. Taken together, these results confirmed the reliability of the generated zEsr1-LBD and binding similarity between the hESR1- and zEsr1-LBDs.

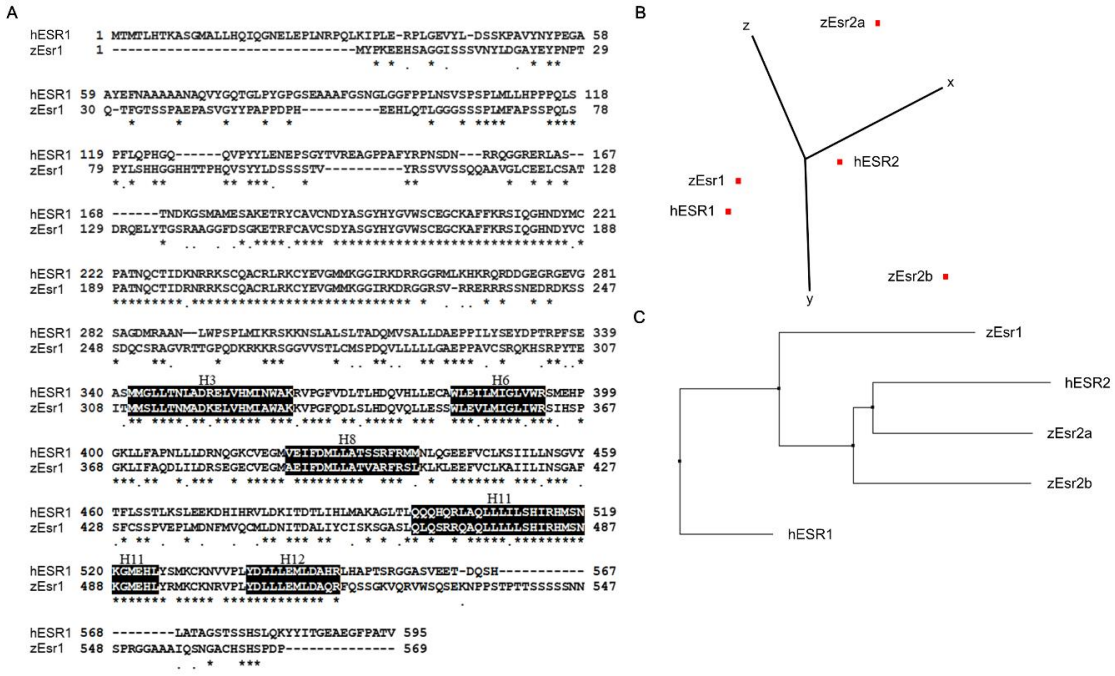

Figure 3.1. Sequence alignment comparison. (a) Sequence alignment between human estrogen receptor 1 (hESR1) and zebrafish estrogen receptor 1 (zEsr1). The conserved amino acids are marked with asterisks and similar properties between different amino acids are marked as dots. The helices surrounding the ligand-binding cavity are colored black in the E/F domain. Gaps are denoted with a hyphen. (b) Principal component analysis (PCA) of human and zebrafish estrogen receptors. (c) Phylogenetic analysis showing the relationships between human and zebrafish estrogen receptors.

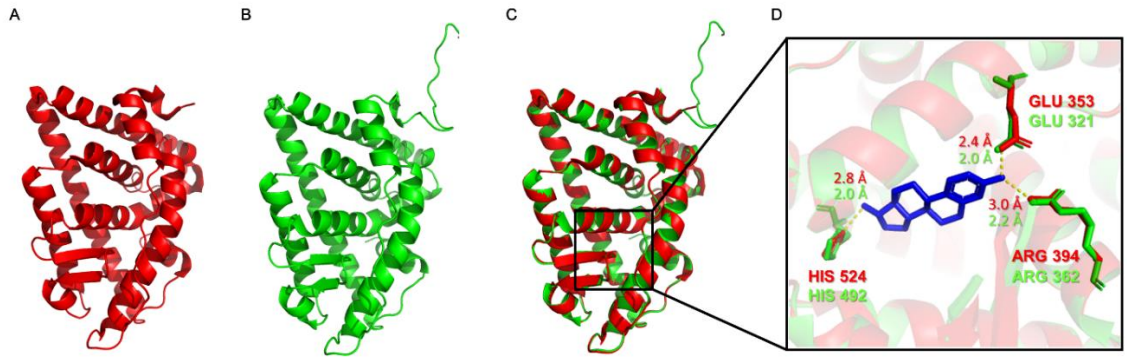

Figure 3.2. 3D ligand-binding domain structures of the hESR1 and modeled zEsr1. (a) Ligand-binding domain of human estrogen receptor 1 (hESR1-LBD; PDB:2YJA). (b) Ligand-binding domain of zebrafish estrogen receptor 1 (zEsr1-LBD) generated by homology modeling using MODELLER. (c) Superimposed images of hESR1-LBD (red) and zEsr1-LBD (green). (d) Hydrogen bond interactions of 17β-estradiol (E2) with both structures. Red and green residues indicate hESR1-LBD and zEsr1-LBD, respectively.

3.4.2 Model validation

The generated model, including the conformation-dependent backbone geometry, was validated using PROCHECK, ERRAT, ProSA, and Verify-3D (Supplementary Table 3.1 and Supplementary Figure 3.1). PROCHECK was used to obtain a Ramachandran plot [44] for evaluating the stereochemical properties of hESR1-LBD and zEsr1-LBD, which presents the phi (φ) and psi (ψ) distributions of backbone conformation angles for each residue in a protein structure consistent with a right-handed α-helix (Supplementary Figure 3.1a). A good-quality model is expected to occupy over 90% of the most favorable region in the Ramachandran plot [44,61]. For the plots of hESR1-LBD and zEsr1-LBD, amino acids occupied 96.6% and 97.5% of the most favorable region, respectively. None of the residues were present in the disallowed region in the plot generated for zEsr1-LBD, while 0.4% of the residues were present in the disallowed region of the plot for hESR1-LBD, indicating that both structures were good stereochemical models. ERRAT was used to assess the relative distributions of different atom types in the test structure and determine the overall quality factor for non-covalent bonded atomic interactions, scoring exceeding 90% which resulted in 97.0% and 90.8% for hESR1-LBD and zEsr1-LBD, respectively, indicating that the backbone conformation and non-covalent bonding interactions of hESR1-LBD and zEsr1-LBD were acceptable for high-quality structure models (Supplementary Figure 3.1b) [43,62].

The structures were also cross-validated using ProSA-web (z-score), which resulted in -6.80 and -6.76 for hESR1-LBD and zEsr1-LBD, respectively, and plotted within the range for entire proteins determined by the Nuclear Magnetic Resonance and x-ray-derived structures (Supplementary Figure 3.1c). The results suggest that the prediction accuracy of the 3D protein structure models is acceptable, when compared to the previous studies [45,60,61]. Finally, the Verify-3D server was used to predict the hESR1-LBD and zEsr1-LBD structures as profile-3D scores, which were presented as a table computed from the atomic coordinates of the structure (Supplementary Figure 3.1d). A 3D-1D score exceeding 0.2 for over 65% of a structure indicates high quality in a general manner, according to previous studies [46,62]. The verify-3D server predicted that 79.2% of the residues in hESR1-LBD had an average 3D-1D score of > 0.2, while

78.0% of the residues in zEsr1-LBD had an average 3D-1D score of > 0.2. Both structures are quite matched their amino sequences, with high scores. Overall, the modeled zEsr1-LBD was comparatively robust and could be applied for the subsequent evaluation of binding activities.

3.4.3 Molecular docking and MD simulations

The docking of chemicals on hESR1-LBD and zEsr1-LBD was successfully simulated and revealed multiple docking poses for each ligand binding site. The binding poses of the docked complexes are illustrated in Figure 3.3. Especially, the docked complexes of E2/hESR1-LBD and E2/zEsr1-LBD exhibited an identical pattern of interactions between ligand and receptor, consisting of three hydrogen bonds and nine hydrophobic interactions. The hydrogen bonds were Glu353, Arg394, and His524 for hESR1-LBD, and Glu321, Arg362, and His492 for zEsr1-LBD. However, the interactions with BPA differed between hESR1-LBD and zEsr1-LBD. The interactions of BPA with hESR1-LBD consisted of two hydrogen bonds and nine hydrophobic interactions, while three hydrogen bonds and ten hydrophobic interactions were observed in the BPA/zEsr1-LBD complex. Notably, two hydrogen bonds (Glu353 and His524 for hESR1-LBD, and Glu321 and His492 for zEsr1-LBD) were shared between both structures. The docked complex between BPFL and hESR1-LBD consisted of one hydrogen bond and five hydrophobic interactions. Ser512 hESR1-LBD a hydrogen bond with BPFL as a hydrogen bond. The docked complex with BPFL/zEsr1-LBD exhibited one hydrogen bond, two electrostatic interactions, and five hydrophobic interactions. TMBPA exhibited the same hydrogen bonds as BPA in hESR1-LBD. Two phenolic hydroxyl groups formed hydrogen bonds with polar residues of Glu353 and His524, respectively. TMBPA formed electrostatic interaction with the Met343 residue. Only one hydrogen bond (His492) was observed in the TMBPA/zEsr1-LBD complex. Additionally, 4-phenylphenol formed the same hydrogen bonds and hydrophobic interactions in both receptors. The van der Waals interactions of only three residues differed, and the hydrogen bonds were Glu353 and Arg394 for hESR1-LBD, and Glu321 and Arg362 for zEsr1-LBD.

Before analyzing the MD simulation results, each ligand-receptor complex was evaluated for dynamic stability based on the RMSD values of all atoms (Supplementary Figure 3.2 and Supplementary Figure 3.3). The RMSD values were between 0.8 and 2.2 Å in ligand/hESR1-LBD complexes, and between 1.6 and 4.5 Å in ligand/zEsr1-LBD complexes. All complexes favored to converge from 5 ns and reached a steady state after 10 ns equilibration. The hydrogen bond (H-bonding) occupancies between 10 and 15 ns in the MD trajectory analysis were analyzed with Glu353, Arg394, and His524 for hESR1-LBD and Glu321, Arg362, and His492 for zEsr1-LBD, respectively (Figure 3.4). These residues are interacted with E2 as major hydrogen bonds, as previously described [63,64]. In contrast of TMBPA, E2, BPA, BPFL and 4-phenylphenol exhibited similar patterns in the docked complexes with hESR1-LBD and zEsr1-LBD. Considering the sum of three H-bonding occupancies, E2/hESR1- and E2/zEsr1-LBDs ratio exhibited superiority when compared with those of other chemicals, in the order of E2 > BPA > 4-phenylphenol > TMBPA > BPFL. Similar to E2, BPA formed mainly hydrogen bonds with Glu353 and His524 in hESR1-LBD, and with Glu321 and His492 in zEsr1-LBD. None of the H-bonding occupancies with the residues was observed for BPFL. High occupancy with Glu353 was observed in the TMBPA/hESR1-LBD complex, whereas high occupancy with

His492 was observed in the TMBPA/zEsr1-LBD complex. Lastly, 4-phenylphenol exhibited similar H-bonding occupancy trends in both structures. Glu353 and Arg394 were observed in the hESR1-LBD complex, and Glu321 and Arg362 were observed in the zEsr1-LBD complex.

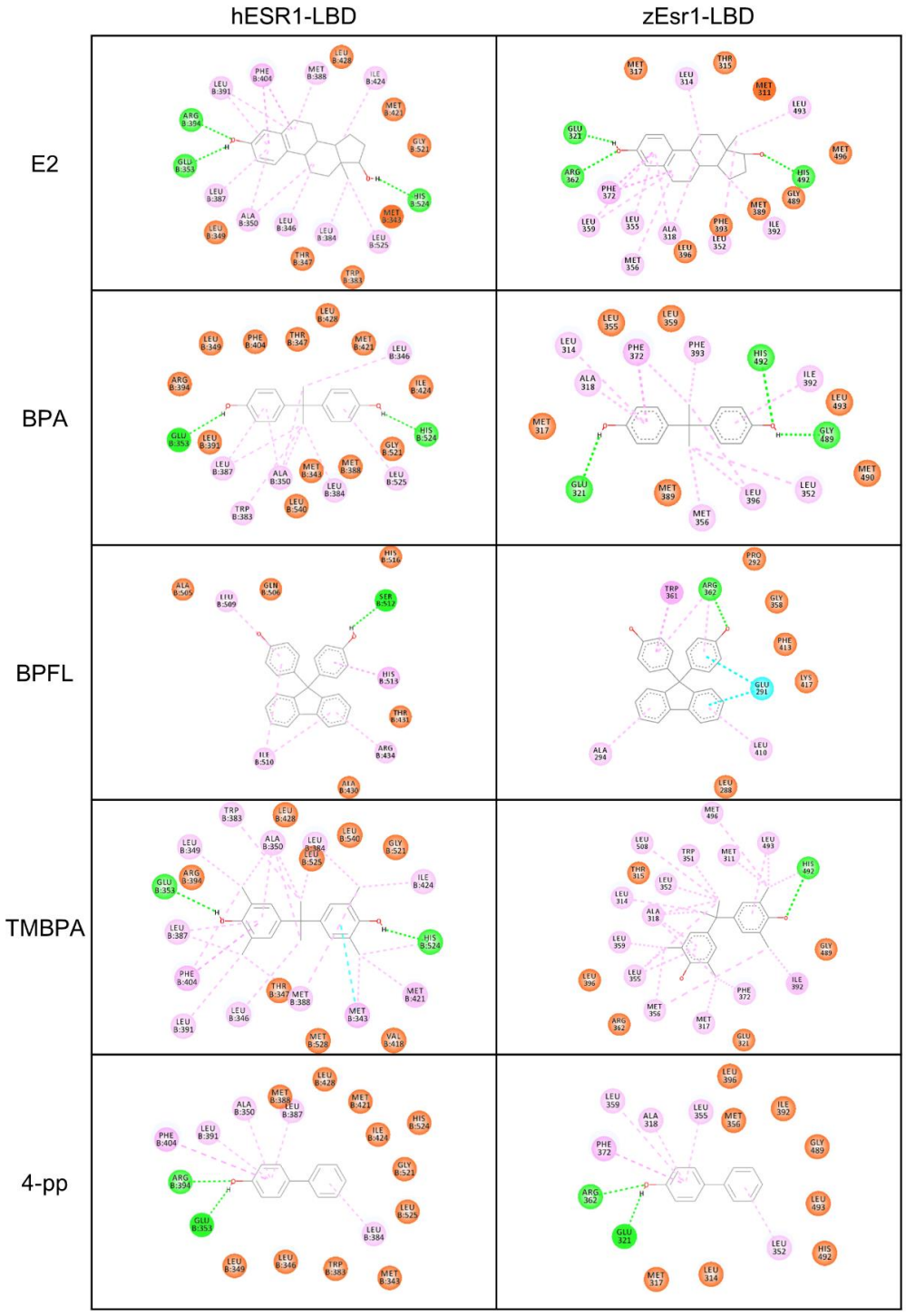

Figure 3.3. Interactions of the ligand-receptor complexes. 2D docking results for receptor-ligand complex indicating hydrogen bonding (green), hydrophobic interactions (pink), van der Waals interactions (orange), and electrostatic interactions (cyan).

Previous studies have attempted to determine the major amino acid residues involved in ligand recognition by hESR [65-67]. The 515-535 residue region has been identified as responsible for ligand recognition through an alanine-scanning mutagenesis assay [67]. Consequently, Gly521, His524, Leu525, and Met528 in helix 11 were identified as the key residues for ligand recognition [66]. The His524 residue has recently been recognized as a key player with a critical role in maintaining agonist conformation in hESR1-LBD [29,68]. Furthermore, the hydrogen bonds with Glu353 and Arg394 residues also have been reported to stabilize ligands embedded in the hESR1 cavity, thereby providing a stable recognition site [69-71]. In the present study, hydrogen bonds with the Glu353, Arg394, and His524 residues were observed in the E2/hESR1-LBD complex, and the interactions corresponded with previously reported docking results [64,68,72,73]. Collectively, the docking results of this work indicated that BPA and its analogs were located in hESR1-LBD forming diverse interactions. BPA, TMBPA, and 4-phenylphenol shared some similarity to E2 in hydrogen bonding interactions. BPA and TMBPA formed hydrogen bonds with Glu353 and His524, which were associated with the ligand recognition site. Although 4-polyphenol interacted with two other hydrogen bonds, Gly521, His524, Leu525, and Met528 in H11 formed van der Waals interactions. Two to four hydrogen bonds were observed in the BPA/hESR1-LBD complex: Glu353, Arg394, Gly521, and His524. Glu353 and His524 interactions have been commonly observed in previous studies [24,68,74-76]. Such differences regarding hydrogen bonds appear to be due to the different calculations and simulation methods used in different docking programs. Cao et al. (2017) docked TMBPA on hESR1-LBD and reported that TMBPA interacted as hydrogen bonds with Glu353 and His524 during MD simulations, which are consistent with our results. Several docking simulations have been conducted using zEsr1-LBD, and they have shown that E2 forms three hydrogen bonds corresponding to those (Glu321, Arg362, and His492) observed in the present study [63,77]. Mu et al. (2018) reported that BPA forms the same hydrogen bonds as E2, which are similar to those (Glu321 and His492) observed in our results . When considering the key residues for ligand recognition in hESR1-LBD, BPA, TMBPA, and 4-phenylphenol were fitted to zEsr1-LBD and interacted with the residues for ligand recognition. Considering the similarity of their ligand recognition patterns to E2, these interactions were assumed to contribute to agonism. Similar to in hESR1-LBD, the interactions of TMBPA and 4-phenylphenol with zEsr1-LBD indicated that BPA and its analogs exhibited similar binding modes, which may explain how they mimic endogenous hormones that disrupt zebrafish endocrine system.

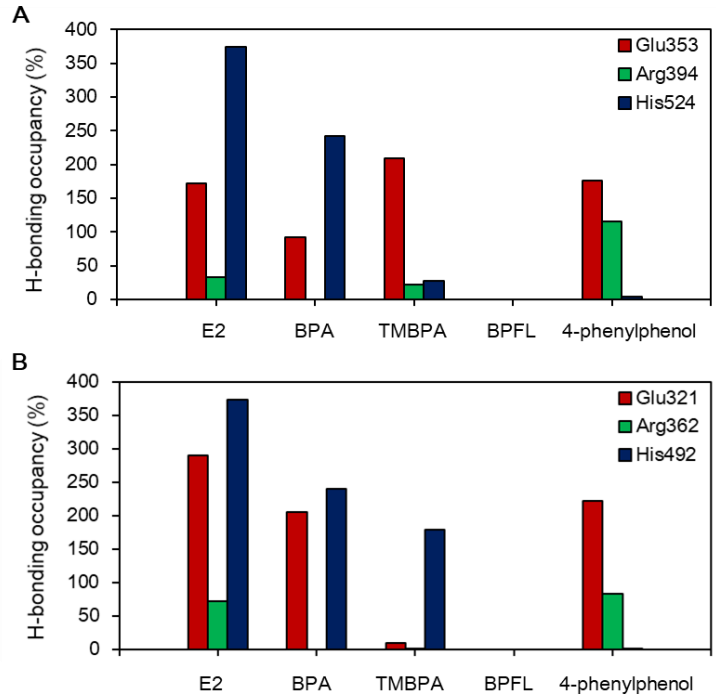

Figure 3.4. Occupancies of hydrogen bonds between ligands and (a) Glu353, Arg394, and His524 residues for ligand-binding domain of human estrogen receptor 1 (hESR1-LBD), and between ligands and (b) Glu321, Arg362, and His492 residues for ligand-binding domain of zebrafish estrogen receptor 1 (zEsr1-LBD) during MD simulations (10–15 ns).

3.4.4 Binding energy analysis

To assess the binding affinity of ligand-receptor complexes, binding energies were calculated with molecular docking and the MD simulations. The binding energies of each chemical are listed in Table 3.1 and Supplementary Table 3.2. Docking simulations were conducted using CHARMm-based (CDOCKER) and AutoDock Vina, and all chemicals were docked in hESR1-LBD and zEsr1-LBD. In the hESR1-LBD simulations, the E2/hESR1-LBD complex exhibited the lowest binding energy among the test chemicals in both docking programs, while the BPFL/hESR1-LBD complex exhibited the highest energy. The binding energies in hESR1-LBD were ranked as follows: E2 > TMBPA ≥ BPA > 4-phenylphenol > BPFL. In the zEsr1-LBD simulations, a similar pattern to hESR1-LBD was observed, with the lowest binding energy occurring for the E2/zEsr1-LBD complex, and the highest occurring for the BPFL/hESR1-LBD complex among the test chemicals. The binding energies were ranked as follows: E2 > BPA ≒ TMBPA > 4-phenylphenol > BPFL. The steady state of 10 and 15 ns MD simulations revealed the following order, TMBPA > E2 > BPA > 4-phenylphenol > BPFL, in which TMBPA revealed a lower binding free energy than E2 in the hESR1. For the zEsr1 complexes, the binding free energies were ranked as follows: E2 > BPA > TMBPA > 4-phenylphenol > BPFL. The binding energies differed according to the chemicals used. The docking programs exhibited similar binding energy patterns, and they corresponded with the results of previous studies [24,74,78]. BPA and its analogs were docked, and their binding energies with hESR1-LBD were compared. E2/hESR1-LBD exhibited lower binding energy than BPA and its substitutes. Cavaliere et al. reported the

same binding energy pattern for hESR1-LBD (E2 > TMBPA > BPA). Makarova et al. simulated E2 and BPA docking on simulated hESR1-LBD and zEsr1-LBD using AutoDock, and E2 exhibited lower binding energy than BPA. The binding energies were -11.5 and -7.73 kcal/mol for hESR1-LBD and -11.0 and -7.56 kcal/mol for zEsr1-LBD, respectively. The E2/hESR1-LBD manifested lower binding free energy than BPA/hESR1-LBD using MM/PBSA and MMGBSA methods [76]. Notably, the TMBPA/hESR1-LBD displayed a lower binding free energy than the E2 complex during MD simulation, which is not consistent with docking calculation. It can be explained by van der Waals and hydrophobic interactions (Supplementary Table 3.2). The calculated van der Waals (ΔG_{vdw}) and non-polar solvation (ΔG_{SA}) of TMBPA interactions revealed the lowest energies among the complexes. Previous reports have shown that the energies of the apolar (ΔG_{vdw} + ΔG_{SA}) and electrostatic (ΔG_{elec}) components dominantly contribute to the estimate of binding free energy in MM/PBSA [79,80]. Therefore, TMBPA resulted in a lower binding free energy than E2 in hESR1-LBD. Whereas, the TMBPA-zEsr1-LBD complex exhibited a higher binding free energy than E2 due to the electrostatic interactions. The electrostatic energy was markedly lower in zEsr1-LBD than in the hESR1-LBD complex. Collectively, each complex showed different binding energies and the patterns were confirmed by docking programs and MD simulation.

Table 3.1 Binding energies of molecular dockings and MD simulation

Docking program	Molecular docking				MD simulation (10 – 15 ns)	
	Discovery Studio Cdocker interaction energy (kcal/mol)		AutoDock Vina Binding free energy (kcal/mol)		MMPBSA Binding free energy, ΔG_{bind} (kcal/mol)	
Ligands/receptors	hESR1-LBD	zEsr1-LBD	hESR1-LBD	zEsr1-LBD	hESR1-LBD	zEsr1-LBD
Estradiol (E2)	-53.2 ± 0.00	-49.8 ± 0.00	-11.1 ± 0.00	-10.7 ± 0.00	-18.8 ± 2.76	-18.6 ± 2.55
Bisphenol A (BPA)	-38.2 ± 0.00	-38.0 ± 0.00	-8.13 ± 0.10	-8.36 ± 0.04	-17.8 ± 3.09	-17.3 ± 3.17
Bisphenol FL (BPFL)	-14.5 ± 0.00	-12.3 ± 0.00	-7.26 ± 0.05	-7.02 ± 0.12	-7.23 ± 2.61	-3.48 ± 4.67
Tetramethyl Bisphenol A (TMBPA)	-41.8 ± 0.00	-42.3 ± 0.00	-8.10 ± 0.08	-8.13 ± 0.12	-22.9 ± 3.46	-16.8 ± 3.79
4-phenylphenol	-30.4 ± 0.00	-29.7 ± 0.00	-7.80 ± 0.00	-7.60 ± 0.00	-13.1 ± 2.64	-12.3 ± 3.53

3.4.5 Comparison of *in silico* and *in vitro* experiments

The *in silico* and *in vitro* results were compared to evaluate their correlation, as shown in Figure 3.5. The human estrogenic activities of BPA and its analogs were evaluated by conducting an *in vitro* reporter gene assay (Figure 3.5a). The maximum concentration of each chemical with a non-toxic effect on the yeast strain was selected based on the results of the cytotoxicity test. E2 was used as the reference chemical and exhibited

a dose response depending on the concentration. BPA and its analogs also exhibited dose-response curves, excluding BPFL. The EC_{50} values for E2, BPA, TMBPA, and 4-phenylphenol were 1.25, 14,657, 10,216, and 4,594 nM, respectively. The maximal induction rates of BPA and its analogs were ranked in the following order: BPA > TMBPA > 4-phenylphenol > BPFL. Even though the EC_{50} value of BPA was higher than those of TMBPA and 4-phenylphenol, BPA exhibited the highest induction rate (90.7%) at the maximum concentration except E2. Similar results have been reported in other reporter gene studies [68,81-83]. TMBPA exhibited lower EC_{20} and EC_{50} values than BPA; however, the estrogenic activity at the maximum concentration of BPA was higher than that of TMBPA [68,81]. Two studies reported that the EC_{50} value of 4-phenylphenol is lower than that of BPA [82,83]. Conversely, Li et al. reported a higher EC_{50} value for 4-phenylphenol than for BPA. Such differences can be attributed to the different reporter systems, and the different host cells and their cytotoxicity and ligand-binding affinity. Our *in vitro* assay showed that BPFL and 4-phenylphenol appeared to be more cytotoxic (> 10 μM) than BPA and TMBPA (> 100 μM). Keminer et al. recently conducted a ligand-binding assay using a commercially available fluorescence polarization-based technique. BPA inhibited the fluorescent ligand by 61.2%, followed by 4-phenylphenol (53.1%), TMBPA (24.2%), and BPFL (-2.06%). Therefore, it seems that BPA exhibited the highest estrogenic activity compared to BPA analogs, despite the lower EC_{50} values of TMBPA and 4-phenylphenol.

In the present study, zebrafish estrogenic activities of BPA and its analogs were evaluated using an *in vitro* reporter gene assay (Figure 3.5b). The maximum concentrations of compounds with a non-toxic effect on the cells were selected based on the results of the cytotoxicity test. E2, BPA, and 4-phenylphenol exhibited dose-response curves. The EC_{50} values for E2, BPA, and 4-phenylphenol were 0.09, 583, and 9,787 nM, respectively. TMBPA induced weak estrogenic activity (16.6% as the maximal induction), which was different from the estrogenic activity in the human *in vitro* assay. The maximal induction rates of BPA and its analogs were ranked in the following order: BPA > 4-phenylphenol > TMBPA > BPFL. Each chemical exhibited different estrogenic activities in this reporter assay. None of the previous studies showed estrogenic activity with BPFL, TMBPA, and 4-phenylphenol in zEsr1, while estrogenic activity has been observed with BPA [84-86].

Lastly, the *in silico* and *in vitro* results were compared to evaluate their correlation. All the factors computed by *in silico* experiments revealed moderate or high correlations with *in vitro* results (Figure 3.5c and 3.5d). High correlation was observed between Cdocker and AutoDock Vina (r^2 = 0.84 for hESR1 and r^2 = 0.77 for zEsr1). Notably, the H-bonding occupancy exhibited high correlations with *in vitro* results (r^2 = 0.81 for hESR1 and r^2 = 0.87 for zEsr1). The result indicates that hydrogen bond interactions with certain residues have pivotal roles for ligand recognition and its activation. The interaction of modelled zEsr1 with TMBPA resulted in relatively poor correlations, especially compared to the correlations of hESR1, although the TMBPA complex in both receptors revealed comparable binding free energies compared with BPA and 4-phenylphenol interactions. The *in vitro* results of weak estrogenic activity of TMBPA can be explained by the MM/PBSA calculated lowest energies in van der Waals and non-polar solvation among the complexes. In addition, TMBPA formed a hydrogen bond with the His492 residue in the docking programs and the MD simulation. The residue is considered to be critical in ligand recognition and maintenance of the agonist conformation [25,60]. The results are inconsistent with previous reports and the present *in vitro* result. However, the inconsistency can be elucidated with other residues such as Glu353 and Arg394 in hESR1-LBD.

Considering the reported functions of Glu353 and Arg394 residues, and the results in H-bonding occupancy, we speculate that even though the His492 residue plays critical roles, other residues such as Glu321 and Arg362 are necessary as well for the complex stabilization and its activation. For these reasons, it seems TMBPA induced different estrogenic activities on human ESRα and zebrafish ESRα. Overall, the present study found a good agreement between the results from *in silico* and *in vitro* approaches using the hESR1-LBD and zEsr1-LBD structures. The structures can be useful for screening EDCs that have potential estrogenic disruptive activities. However, the current approach also reveals some limitations, which are needed to consider for better prediction. A relatively smaller scale of the test and limited sampling conditions in pose prediction and approximated scoring, might cause poor correlation of results with experimental *in vitro* data. Moreover, this structure only predicts estrogenic activity between the LBD and a ligand, thereby it is impossible to predict estrogenic activities related to other mechanisms or domains. In light of these limitations, more studies with diverse ligands are necessary to draw a solid conclusion, and detailed analyses of binding energy and interaction modes are required to predict estrogenic activity. Our future study will be the assessment of other EDCs and the investigation to reveal other mechanisms inducing (anti)estrogenic activities.

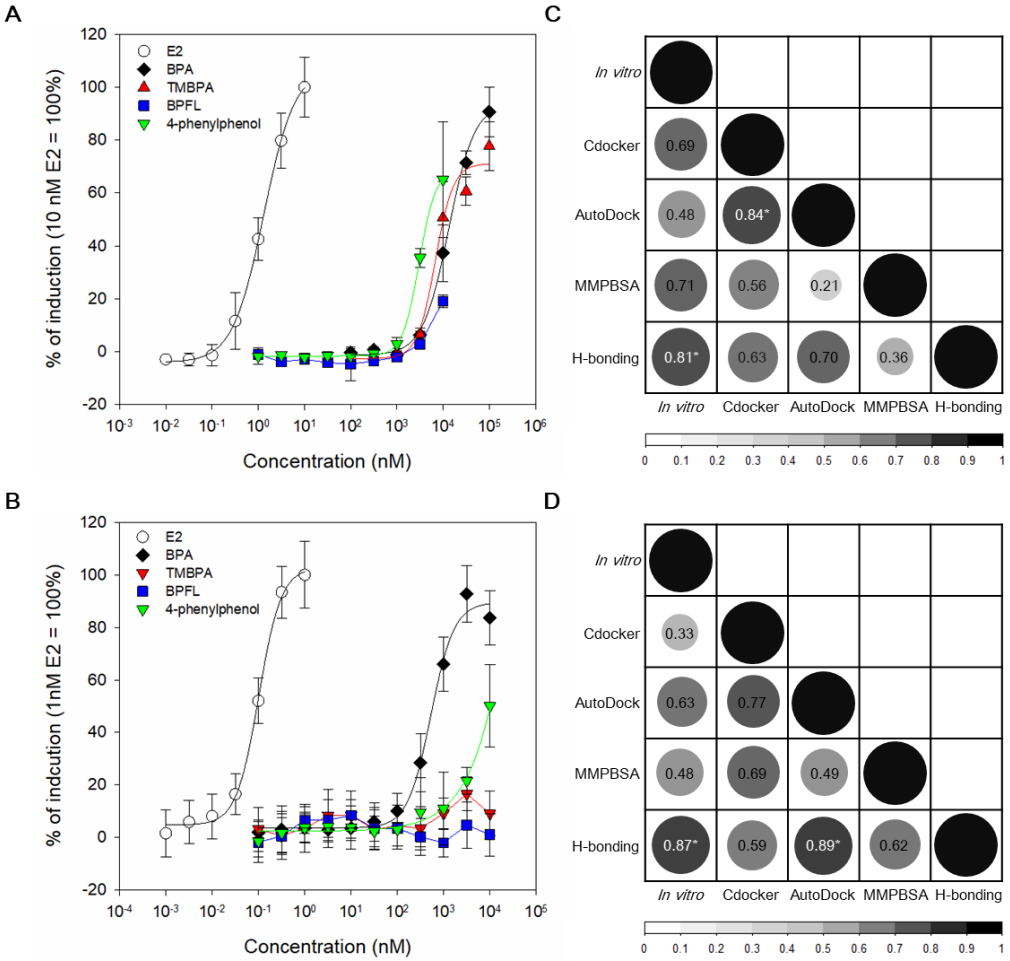

Figure 3.5. Comparisons of *in silico* and *in vitro* assays. (a–b) *In vitro* assays for estrogenic activity in (a) hESR1 and (b) zEsr1, respectively. The induction value at the maximum concentration of 17β-estradiol (E2;

10 nM for hESR1 and 1 nM for zEsr1) was set to 100%. (c-d) Correlation matrix plot. Pearson correlation coefficient (*r*) between *in silico* and *in vitro* results in (c) hESR1 and (d) zEsr1, respectively. Values are indicated as r^2. The color intensity and the size of rounds are proportional to r^2. An asterisk indicates significant correlation ($p < 0.05$). The applied *in vitro* data are the maximal induction ratios of each chemical. The binding energies computed by Discovery studio, Autodock Vina, and MMBPSA, were applied in the analysis. The H-bonding data are the sum of H-bonding occupancies of each complex during MD simulations.

3.5 Summary and Conclusion

As the 3D structure of zebrafish ESRα is not available, a homology-based 3D model of zEsr1-LBD was constructed and validated using PROCHECK, ERRAT, ProSA, and Verify-3D tools, which have suitable models to represent the 3D structure. After validation, BPA and its analogs were docked on zEsr1- and hESR1-LBDs. MD simulation was conducted to understand the dynamic behavior of each complex and provided noteworthy complementary with molecular docking. Several BPA and its analogs were bound to both models with an orientation as E2 in both structures. Additionally, the *in vitro* results demonstrated that the *in silico* and *in vitro* results were in good agreement with moderate to high correlations. Therefore, the combined *in silico* and *in vitro* approaches provide useful prediction models for identifying EDCs by taking into account the difference between the two species.

3.6 Acknowledgments

This research was supported by the National Research Council of Science & Technology (NST) grant by the Korea government (MSIP) (No. CAP-17-01-KIST Europe).

3.7 Bibliography

1. Barkhem, T.; Nilsson, S.; Gustafsson, J.A. Molecular mechanisms, physiological consequences and pharmacological implications of estrogen receptor action. *American Journal of Pharmacogenomics* **2004**, *4*, 19-28, doi:10.2165/00129785-200404010-00003.
2. Hewitt, S.C.; Winuthayanon, W.; Korach, K.S. What's new in estrogen receptor action in the female reproductive tract. *J Mol Endocrinol* **2016**, *56*, R55-71, doi:10.1530/JME-15-0254.
3. Khalid, A.B.; Krum, S.A. Estrogen receptors alpha and beta in bone. *Bone* **2016**, *87*, 130-135, doi:https://doi.org/10.1016/j.bone.2016.03.016.
4. Shen, M.; Shi, H. Sex hormones and their receptors regulate liver energy homeostasis. *International journal of endocrinology* **2015**, *2015*, 294278, doi:10.1155/2015/294278.
5. Kovats, S. Estrogen receptors regulate innate immune cells and signaling pathways. *Cellular immunology* **2015**, *294*, 63-69, doi:10.1016/j.cellimm.2015.01.018.
6. Hawkins, M.B.; Thornton, J.W.; Crews, D.; Skipper, J.K.; Dotte, A.; Thomas, P. Identification of a third distinct estrogen receptor and reclassification of estrogen receptors in teleosts. *Proceedings of the National Academy of Sciences of the United States of America* **2000**, *97*, 10751, doi:10.1073/pnas.97.20.10751.
7. Dahlman-Wright, K.; Cavailles, V.; Fuqua, S.A.; Jordan, V.C.; Katzenellenbogen, J.A.; Korach, K.S.; Maggi, A.; Muramatsu, M.; Parker, M.G.; Gustafsson, J.A. International union of pharmacology. LXIV. estrogen receptors. *Pharmacological reviews* **2006**, *58*, 773-781, doi:10.1124/pr.58.4.8.

8. Heldring, N.; Pike, A.; Andersson, S.; Matthews, J.; Cheng, G.; Hartman, J.; Tujague, M.; Ström, A.; Treuter, E.; Warner, M., et al. Estrogen receptors: how do they signal and what are their targets. *Physiological reviews* **2007**, *87*, 905-931, doi:10.1152/physrev.00026.2006.
9. Paterni, I.; Granchi, C.; Katzenellenbogen, J.A.; Minutolo, F. Estrogen receptors alpha (ERα) and beta (ERβ): subtype-selective ligands and clinical potential. *Steroids* **2014**, *90*, 13-29, doi:10.1016/j.steroids.2014.06.012.
10. Barros, R.P.; Gustafsson, J. Estrogen receptors and the metabolic network. *Cell metabolism* **2011**, *14*, 289-299, doi:10.1016/j.cmet.2011.08.005.
11. Kumar, R.; Zakharov, M.N.; Khan, S.H.; Miki, R.; Jang, H.; Toraldo, G.; Singh, R.; Bhasin, S.; Jasuja, R. The dynamic structure of the estrogen receptor. *Journal of amino acids* **2011**, *2011*, 812540, doi:10.4061/2011/812540.
12. Bardet, P.L.; Horard, B.; Robinson-Rechavi, M.; Laudet, V.; Vanacker, J.M. Characterization of oestrogen receptors in zebrafish (*Danio rerio*). *J Mol Endocrinol* **2002**, *28*, 153-163, doi:10.1677/jme.0.0280153.
13. Mills, L.J.; Chichester, C. Review of evidence: are endocrine-disrupting chemicals in the aquatic environment impacting fish populations? *Science of The Total Environment* **2005**, *343*, 1-34, doi:10.1016/j.scitotenv.2004.12.070.
14. Zhang, Y.; Zhou, J.L. Removal of estrone and 17β-estradiol from water by adsorption. *Water Research* **2005**, *39*, 3991-4003, doi:https://doi.org/10.1016/j.watres.2005.07.019.
15. Rochester, J.R. Bisphenol A and human health: a review of the literature. *Reproductive Toxicology* **2013**, *42*, 132-155, doi:10.1016/j.reprotox.2013.08.008.
16. Kang, J.H.; Asai, D.; Katayama, Y. Bisphenol A in the aquatic environment and its endocrine-disruptive effects on aquatic organisms. *Critical reviews in toxicology* **2007**, *37*, 607-625, doi:10.1080/10408440701493103.
17. Mathieu-Denoncourt, J.; Wallace, S.J.; de Solla, S.R.; Langlois, V.S. Plasticizer endocrine disruption: highlighting developmental and reproductive effects in mammals and non-mammalian aquatic species. *General and comparative endocrinology* **2015**, *219*, 74-88, doi:10.1016/j.ygcen.2014.11.003.
18. Geens, T.; Aerts, D.; Berthot, C.; Bourguignon, J.P.; Goeyens, L.; Lecomte, P.; Maghuin-Rogister, G.; Pironnet, A.M.; Pussemier, L.; Scippo, M.L., et al. A review of dietary and non-dietary exposure to bisphenol-A. *Food and Chemical Toxicology* **2012**, *50*, 3725-3740, doi:10.1016/j.fct.2012.07.059.
19. Rosenmai, A.K.; Dybdahl, M.; Pedersen, M.; Alice van Vugt-Lussenburg, B.M.; Wedebye, E.B.; Taxvig, C.; Vinggaard, A.M. Are structural analogues to bisphenol A safe alternatives? *Toxicological Sciences* **2014**, *139*, 35-47, doi:10.1093/toxsci/kfu030.
20. Chen, D.; Kannan, K.; Tan, H.; Zheng, Z.; Feng, Y.-L.; Wu, Y.; Widelka, M. Bisphenol analogues other than BPA: environmental occurrence, human exposure, and toxicity—a review. *Environmental Science & Technology* **2016**, *50*, 5438-5453, doi:10.1021/acs.est.5b05387.
21. Usman, A.; Ahmad, M. From BPA to its analogues: Is it a safe journey? *Chemosphere* **2016**, *158*, 131-142, doi:10.1016/j.chemosphere.2016.05.070.
22. Keminer, O.; Teigeler, M.; Kohler, M.; Wenzel, A.; Arning, J.; Kaßner, F.; Windshügel, B.; Eilebrecht, E. A tiered high-throughput screening approach for evaluation of estrogen and androgen receptor modulation by environmentally relevant bisphenol A substitutes. *Science of The Total Environment* **2020**, *717*, 134743, doi:10.1016/j.scitotenv.2019.134743.
23. Montes-Grajales, D.; Olivero-Verbel, J. Computer-aided identification of novel protein targets of bisphenol A. *Toxicology letters* **2013**, *222*, 312-320, doi:10.1016/j.toxlet.2013.08.010.
24. Cavaliere, F.; Lorenzetti, S.; Cozzini, P. Molecular modelling methods in food safety: Bisphenols as case study. *Food and Chemical Toxicology* **2020**, *137*, 111116, doi:10.1016/j.fct.2020.111116.
25. Babu, S.; Vellore, N.A.; Kasibotla, A.V.; Dwayne, H.J.; Stubblefield, M.A.; Uppu, R.M. Molecular docking of bisphenol A and its nitrated and chlorinated metabolites onto human estrogen-related receptor-gamma. *Biochemical and biophysical research communications* **2012**, *426*, 215-220, doi:10.1016/j.bbrc.2012.08.065.
26. Sliwoski, G.; Kothiwale, S.; Meiler, J.; Lowe, E.W., Jr. Computational methods in drug discovery. *Pharmacological reviews* **2013**, *66*, 334-395, doi:10.1124/pr.112.007336.
27. Kalé, L.; Skeel, R.; Bhandarkar, M.; Brunner, R.; Gursoy, A.; Krawetz, N.; Phillips, J.; Shinozaki, A.; Varadarajan, K.; Schulten, K. NAMD2: greater scalability for parallel molecular dynamics. *Journal of Computational Physics* **1999**, *151*, 283-312, doi:https://doi.org/10.1006/jcph.1999.6201.
28. Phillips, J.C.; Braun, R.; Wang, W.; Gumbart, J.; Tajkhorshid, E.; Villa, E.; Chipot, C.; Skeel, R.D.; Kalé, L.; Schulten, K. Scalable molecular dynamics with NAMD. *Journal of Computational Chemistry* **2005**, *26*, 1781-1802, doi:https://doi.org/10.1002/jcc.20289.
29. Zhang, J.; Li, T.; Wang, T.; Yuan, C.; Zhong, S.; Guan, T.; Li, Z.; Wang, Y.; Yu, H.; Luo, Q., et al.

Estrogenicity of halogenated bisphenol A: in vitro and in silico investigations. *Archives of toxicology* **2018**, *92*, 1215-1223, doi:10.1007/s00204-017-2127-2.

30. MacRae, C.A.; Peterson, R.T. Zebrafish as tools for drug discovery. *Nature Reviews Drug Discovery* **2015**, *14*, 721-731, doi:10.1038/nrd4627.
31. Kari, G.; Rodeck, U.; Dicker, A.P. Zebrafish: an emerging model system for human disease and drug discovery. *Clinical Pharmacology & Therapeutics* **2007**, *82*, 70-80, doi:10.1038/sj.clpt.6100223.
32. Chafi, S.; Azzouz, A.; Ballesteros, E. Occurrence and distribution of endocrine disrupting chemicals and pharmaceuticals in the river Bouregreg (Rabat, Morocco). *Chemosphere* **2022**, *287*, 132202, doi:https://doi.org/10.1016/j.chemosphere.2021.132202.
33. Jin, H.; Zhu, L. Occurrence and partitioning of bisphenol analogues in water and sediment from Liaohe River Basin and Taihu Lake, China. *Water Research* **2016**, *103*, 343-351, doi:10.1016/j.watres.2016.07.059.
34. Banaderakhshan, R.; Kemp, P.; Breul, L.; Steinbichl, P.; Hartmann, C.; Fürhacker, M. Bisphenol A and its alternatives in Austrian thermal paper receipts, and the migration from reusable plastic drinking bottles into water and artificial saliva using UHPLC-MS/MS. *Chemosphere* **2022**, *286*, 131842, doi:https://doi.org/10.1016/j.chemosphere.2021.131842.
35. Jin, M.; Dang, J.; Paudel, Y.N.; Wang, X.; Wang, B.; Wang, L.; Li, P.; Sun, C.; Liu, K. The possible hormetic effects of fluorene-9-bisphenol on regulating hypothalamic-pituitary-thyroid axis in zebrafish. *Science of The Total Environment* **2021**, *776*, 145963, doi:https://doi.org/10.1016/j.scitotenv.2021.145963.
36. Zhang, Z.; Hu, Y.; Guo, J.; Yu, T.; Sun, L.; Xiao, X.; Zhu, D.; Nakanishi, T.; Hiromori, Y.; Li, J., et al. Fluorene-9-bisphenol is anti-oestrogenic and may cause adverse pregnancy outcomes in mice. *Nature Communications* **2017**, *8*, 14585, doi:10.1038/ncomms14585.
37. Mi, P.; Zhang, Q.-P.; Zhang, S.-H.; Wang, C.; Zhang, S.-Z.; Fang, Y.-C.; Gao, J.-Z.; Feng, D.-F.; Chen, D.-Y.; Feng, X.-Z. The effects of fluorene-9-bisphenol on female zebrafish (*Danio rerio*) reproductive and exploratory behaviors. *Chemosphere* **2019**, *228*, 398-411, doi:https://doi.org/10.1016/j.chemosphere.2019.04.170.
38. Procter, J.B.; Carstairs, G.M.; Soares, B.; Mourão, K.; Ofoegbu, T.C.; Barton, D.; Lui, L.; Menard, A.; Sherstnev, N.; Roldan-Martinez, D., et al. Alignment of biological sequences with Jalview. *Methods in Molecular Biology* **2021**, *2231*, 203-224, doi:10.1007/978-1-0716-1036-7_13.
39. Phillips, C.; Roberts, L.R.; Schade, M.; Bazin, R.; Bent, A.; Davies, N.L.; Moore, R.; Pannifer, A.D.; Pickford, A.R.; Prior, S.H., et al. Design and structure of stapled peptides binding to estrogen receptors. *Journal of the American Chemical Society* **2011**, *133*, 9696-9699, doi:10.1021/ja202946k.
40. Altschul, S.F.; Gish, W.; Miller, W.; Myers, E.W.; Lipman, D.J. Basic local alignment search tool. *Journal of molecular biology* **1990**, *215*, 403-410, doi:10.1016/s0022-2836(05)80360-2.
41. Webb, B.; Sali, A. Comparative protein structure modeling using MODELLER. *Current protocols in bioinformatics* **2016**, *54*, 5.6.1-5.6.37, doi:10.1002/cpbi.3.
42. Shen, M.Y.; Sali, A. Statistical potential for assessment and prediction of protein structures. *Protein Science* **2006**, *15*, 2507-2524, doi:10.1110/ps.062416606.
43. Colovos, C.; Yeates, T.O. Verification of protein structures: patterns of nonbonded atomic interactions. *Protein Science* **1993**, *2*, 1511-1519, doi:10.1002/pro.5560020916.
44. Morris, A.L.; MacArthur, M.W.; Hutchinson, E.G.; Thornton, J.M. Stereochemical quality of protein structure coordinates. *Proteins* **1992**, *12*, 345-364, doi:10.1002/prot.340120407.
45. Wiederstein, M.; Sippl, M.J. ProSA-web: interactive web service for the recognition of errors in three-dimensional structures of proteins. *Nucleic acids research* **2007**, *35*, W407-410, doi:10.1093/nar/gkm290.
46. Lüthy, R.; Bowie, J.U.; Eisenberg, D. Assessment of protein models with three-dimensional profiles. *Nature* **1992**, *356*, 83-85, doi:10.1038/356083a0.
47. Wu, G.; Robertson, D.H.; Brooks Iii, C.L.; Vieth, M. Detailed analysis of grid-based molecular docking: A case study of CDOCKER—A CHARMm-based MD docking algorithm. *Journal of Computational Chemistry* **2003**, *24*, 1549-1562, doi:https://doi.org/10.1002/jcc.10306.
48. Trott, O.; Olson, A.J. AutoDock Vina: improving the speed and accuracy of docking with a new scoring function, efficient optimization, and multithreading. *Journal of computational chemistry* **2010**, *31*, 455-461, doi:10.1002/jcc.21334.
49. Humphrey, W.; Dalke, A.; Schulten, K. VMD: visual molecular dynamics. *Journal of molecular graphics* **1996**, *14*, 33-38, doi:10.1016/0263-7855(96)00018-5.
50. Jorgensen, W.L.; Chandrasekhar, J.; Madura, J.D.; Impey, R.W.; Klein, M.L. Comparison of simple potential functions for simulating liquid water. *The Journal of Chemical Physics* **1983**, *79*, 926-935, doi:10.1063/1.445869.
51. Cheatham, T.E., III; Miller, J.L.; Fox, T.; Darden, T.A.; Kollman, P.A. Molecular dynamics

simulations on solvated biomolecular systems: the particle mesh Ewald method leads to stable trajectories of DNA, RNA, and Proteins. *Journal of the American Chemical Society* **1995**, *117*, 4193-4194, doi:10.1021/ja00119a045.

52. Feller, S.E.; Zhang, Y.; Pastor, R.W.; Brooks, B.R. Constant pressure molecular dynamics simulation: The Langevin piston method. *The Journal of Chemical Physics* **1995**, *103*, 4613-4621, doi:10.1063/1.470648.
53. Hou, T.; Wang, J.; Li, Y.; Wang, W. Assessing the performance of the MM/PBSA and MM/GBSA methods. 1. The accuracy of binding free energy calculations based on molecular dynamics simulations. *Journal of chemical information and modeling* **2011**, *51*, 69-82, doi:10.1021/ci100275a.
54. Xenometrix. XenoScreen YES/YAS instructions for use. Availabe online: https://www.aniara.com/mm5/PDFs/IFU/IFU_AN05-233-Y.pdf.
55. Elegheert, J.; Behiels, E.; Bishop, B.; Scott, S.; Woolley, R.E.; Griffiths, S.C.; Byrne, E.F.X.; Chang, V.T.; Stuart, D.I.; Jones, E.Y., et al. Lentiviral transduction of mammalian cells for fast, scalable and high-level production of soluble and membrane proteins. *Nature Protocols* **2018**, *13*, 2991-3017, doi:10.1038/s41596-018-0075-9.
56. Chang, C.; Swaan, P.W. Computational approaches to modeling drug transporters. *European Journal of Pharmaceutical Sciences* **2006**, *27*, 411-424, doi:10.1016/j.ejps.2005.09.013.
57. Venclovas, C. Comparative modeling in CASP5: progress is evident, but alignment errors remain a significant hindrance. *Proteins* **2003**, *53*, 380-388, doi:10.1002/prot.10591.
58. Menuet, A.; Pellegrini, E.; Anglade, I.; Blaise, O.; Laudet, V.; Kah, O.; Pakdel, F. Molecular characterization of three estrogen receptor forms in zebrafish: binding characteristics, transactivation properties, and tissue distributions. *Biology of reproduction* **2002**, *66*, 1881-1892, doi:10.1095/biolreprod66.6.1881.
59. Martí-Renom, M.A.; Stuart, A.C.; Fiser, A.; Sánchez, R.; Melo, F.; Sali, A. Comparative protein structure modeling of genes and genomes. *Annual review of biophysics and biomolecular structure* **2000**, *29*, 291-325, doi:10.1146/annurev.biophys.29.1.291.
60. Shehadi, I.A.; Rashdan, H.R.M.; Abdelmonsef, A.H. Homology modeling and virtual screening studies of antigen MLAA-42 protein: identification of novel drug candidates against leukemia—an in silico approach. *Computational and Mathematical Methods in Medicine* **2020**, *2020*, 8196147, doi:10.1155/2020/8196147.
61. Otero, J.M.; Papadakis, M.A.; Udatha, D.B.; Nielsen, J.; Panagiotou, G. Yeast biological networks unfold the interplay of antioxidants, genome and phenotype, and reveal a novel regulator of the oxidative stress response. *PloS one* **2010**, *5*, e13606, doi:10.1371/journal.pone.0013606.
62. Shamsara, J. Homology modeling of 5-alpha-reductase 2 using available experimental data. *Interdisciplinary sciences, computational life sciences* **2019**, *11*, 475-484, doi:10.1007/s12539-017-0280-1.
63. Asnake, S.; Modig, C.; Olsson, P.-E. Species differences in ligand interaction and activation of estrogen receptors in fish and human. *The Journal of Steroid Biochemistry and Molecular Biology* **2019**, *195*, 105450, doi:https://doi.org/10.1016/j.jsbmb.2019.105450.
64. Kalaiarasi, C.; Manjula, S.; Kumaradhas, P. Combined quantum mechanics/molecular mechanics (QM/MM) methods to understand the charge density distribution of estrogens in the active site of estrogen receptors. *RSC Advances* **2019**, *9*, 40758-40771, doi:10.1039/C9RA08607B.
65. Danielian, P.S.; White, R.; Hoare, S.A.; Fawell, S.E.; Parker, M.G. Identification of residues in the estrogen receptor that confer differential sensitivity to estrogen and hydroxytamoxifen. *Molecular Endocrinology* **1993**, *7*, 232-240, doi:10.1210/mend.7.2.8469236.
66. Ekena, K.; Weis, K.E.; Katzenellenbogen, J.A.; Katzenellenbogen, B.S. Identification of amino acids in the hormone binding domain of the human estrogen receptor important in estrogen binding. *Journal of Biological Chemistry* **1996**, *271*, 20053-20059, doi:10.1074/jbc.271.33.20053.
67. Pakdel, F.; Katzenellenbogen, B.S. Human estrogen receptor mutants with altered estrogen and antiestrogen ligand discrimination. *Journal of Biological Chemistry* **1992**, *267*, 3429-3437.
68. Cao, H.; Wang, F.; Liang, Y.; Wang, H.; Zhang, A.; Song, M. Experimental and computational insights on the recognition mechanism between the estrogen receptor α with bisphenol compounds. *Archives of toxicology* **2017**, *91*, 3897-3912, doi:10.1007/s00204-017-2011-0.
69. Mu, Y.; Peng, S.; Zhang, A.; Wang, L. Role of pocket flexibility in the modulation of estrogen receptor alpha by key residue arginine 394. *Environmental toxicology and chemistry* **2011**, *30*, 330-336, doi:10.1002/etc.389.
70. Lee, S.; Barron, M.G. Structure-based understanding of binding affinity and mode of estrogen receptor α agonists and antagonists. *PloS one* **2017**, *12*, e0169607-e0169607, doi:10.1371/journal.pone.0169607.
71. Miller, C. A brief on the structure and function of estrogen receptor alpha (BCMB8010 Enzyme

Project). 2015; https://doi.org/10.13140/RG.2.1.4082.5044.
72. Park, C.G.; Jung, K.C.; Kim, D.-H.; Kim, Y.J. Monohaloacetonitriles induce cytotoxicity and exhibit different mode of action in endocrine disruption. *Science of The Total Environment* **2021**, *761*, 143316, doi:https://doi.org/10.1016/j.scitotenv.2020.143316.
73. Wang, T.; Wang, Y.; Zhuang, X.; Luan, F.; Zhao, C.; Cordeiro, M.N.D.S. Interaction of coumarin phytoestrogens with ERα and ERβ: a molecular dynamics simulation study. *Molecules* **2020**, *25*, 1165, doi:10.3390/molecules25051165.
74. Jeong, J.; Kim, H.; Choi, J. In silico molecular docking and In vivo validation with *Caenorhabditis elegans* to discover molecular initiating events in adverse outcome pathway framework: case study on endocrine-disrupting chemicals with estrogen and androgen receptors. *International journal of molecular sciences* **2019**, *20*, 1209, doi:10.3390/ijms20051209.
75. Delfosse, V.; Grimaldi, M.; Pons, J.L.; Boulahtouf, A.; le Maire, A.; Cavailles, V.; Labesse, G.; Bourguet, W.; Balaguer, P. Structural and mechanistic insights into bisphenols action provide guidelines for risk assessment and discovery of bisphenol A substitutes. *Proceedings of the National Academy of Sciences of the United States of America* **2012**, *109*, 14930-14935, doi:10.1073/pnas.1203574109.
76. Li, L.; Wang, Q.; Zhang, Y.; Niu, Y.; Yao, X.; Liu, H. The molecular mechanism of bisphenol A (BPA) as an endocrine disruptor by interacting with nuclear receptors: insights from molecular dynamics (MD) simulations. *PloS one* **2015**, *10*, e0120330-e0120330, doi:10.1371/journal.pone.0120330.
77. Costache, A.D.; Pullela, P.K.; Kasha, P.; Tomasiewicz, H.; Sem, D.S. Homology-modeled ligand-binding domains of zebrafish estrogen receptors alpha, beta1, and beta2: from in silico to in vivo studies of estrogen interactions in *Danio rerio* as a model system. *Molecular Endocrinology* **2005**, *19*, 2979-2990, doi:10.1210/me.2004-0435.
78. Makarova, K.; Siudem, P.; Zawada, K.; Kurkowiak, J. Screening of toxic effects of bisphenol A and products of Its degradation: Zebrafish (*Danio rerio*) embryo test and molecular docking. *Zebrafish* **2016**, *13*, 466-474, doi:10.1089/zeb.2016.1261.
79. Tan, J.J.; Chen, W.Z.; Wang, C.X. Investigating interactions between HIV-1 gp41 and inhibitors by molecular dynamics simulation and MM–PBSA/GBSA calculations. *Journal of Molecular Structure* **2006**, *766*, 77-82, doi:https://doi.org/10.1016/j.theochem.2006.02.022.
80. Verma, S.; Grover, S.; Tyagi, C.; Goyal, S.; Jamal, S.; Singh, A.; Grover, A. Hydrophobic Interactions Are a Key to MDM2 Inhibition by Polyphenols as Revealed by Molecular Dynamics Simulations and MM/PBSA Free Energy Calculations. *PloS one* **2016**, *11*, e0149014-e0149014, doi:10.1371/journal.pone.0149014.
81. Pelch, K.E.; Li, Y.; Perera, L.; Thayer, K.A.; Korach, K.S. Characterization of estrogenic and androgenic activities for bisphenol A-like chemicals (BPs): in vitro estrogen and androgen receptors transcriptional activation, gene regulation, and binding profiles. *Toxicological Sciences* **2019**, *172*, 23-37, doi:10.1093/toxsci/kfz173.
82. Bergmann, A.J.; Simon, E.; Schifferli, A.; Schönborn, A.; Vermeirssen, E.L.M. Estrogenic activity of food contact materials—evaluation of 20 chemicals using a yeast estrogen screen on HPTLC or 96-well plates. *Analytical and Bioanalytical Chemistry* **2020**, *412*, 4527-4536, doi:10.1007/s00216-020-02701-w.
83. Sun, H.; Xu, X.-L.; Qu, J.-H.; Hong, X.; Wang, Y.-B.; Xu, L.-C.; Wang, X.-R. 4-Alkylphenols and related chemicals show similar effect on the function of human and rat estrogen receptor α in reporter gene assay. *Chemosphere* **2008**, *71*, 582-588, doi:https://doi.org/10.1016/j.chemosphere.2007.09.031.
84. Le Fol, V.; Ait-Aissa, S.; Sonavane, M.; Porcher, J.-M.; Balaguer, P.; Cravedi, J.-P.; Zalko, D.; Brion, F. In vitro and in vivo estrogenic activity of BPA, BPF and BPS in zebrafish-specific assays. *Ecotoxicology and Environmental Safety* **2017**, *142*, 150-156, doi:10.1016/j.ecoenv.2017.04.009.
85. Cosnefroy, A.; Brion, F.; Maillot-Maréchal, E.; Porcher, J.M.; Pakdel, F.; Balaguer, P.; Aït-Aïssa, S. Selective activation of zebrafish estrogen receptor subtypes by chemicals by using stable reporter gene assay developed in a zebrafish liver cell line. *Toxicological Sciences* **2012**, *125*, 439-449, doi:10.1093/toxsci/kfr297.
86. Pinto, C.; Hao, R.; Grimaldi, M.; Thrikawala, S.; Boulahtouf, A.; Aït-Aïssa, S.; Brion, F.; Gustafsson, J.; Balaguer, P.; Bondesson, M. Differential activity of BPA, BPAF and BPC on zebrafish estrogen receptors in vitro and in vivo. *Toxicology and applied pharmacology* **2019**, *380*, 114709, doi:10.1016/j.taap.2019.114709.

3.8 Supporting Information

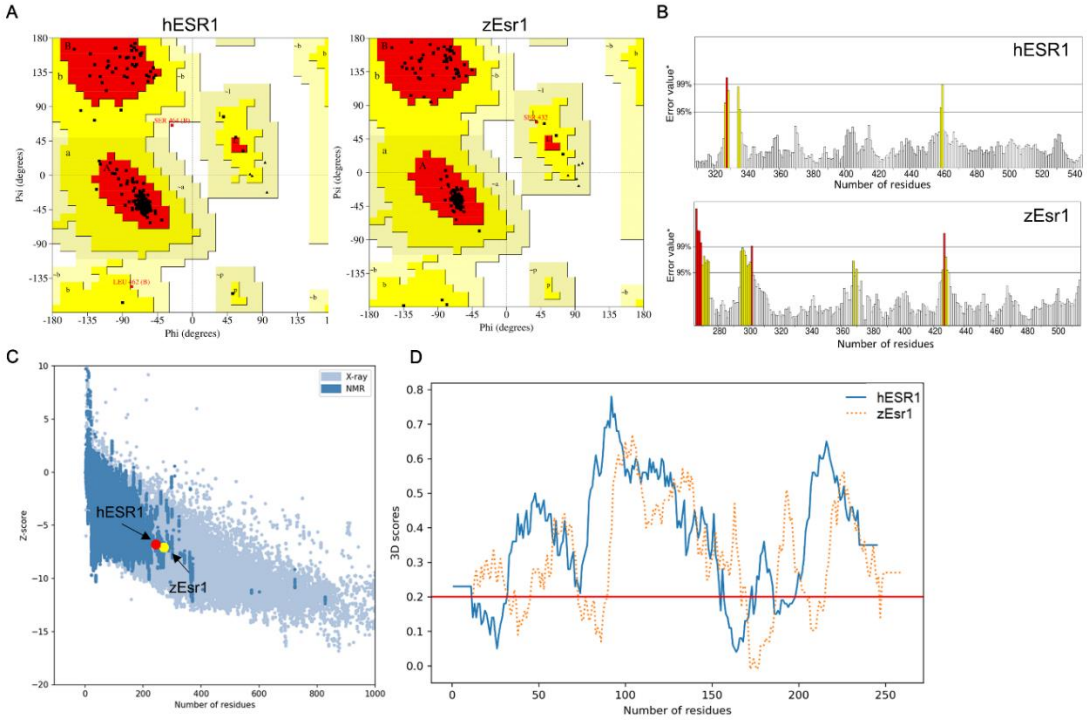

Supplementary Figure 3.1. Validations of hESR1-LBD and zEsr1-LBD structures. (a) Ramachandran plot hESR1-LBD (left) and zEsr1-LBD (right) after refinement. The red, yellow, and white regions represent the favoured, allowed, and the disallowed regions respectively. (b) ERRAT plots for overall model quality (c) PROSA map. The red color indicates hESR1-LBD; yellow indicates zEsr1-LBD in relation to all protein chains in PDB determined by X-ray crystallography (light blue) or NMR spectroscopy (dark blue). (d) 3D profile energy plots. Score over 0.2 indicates high quality of model.

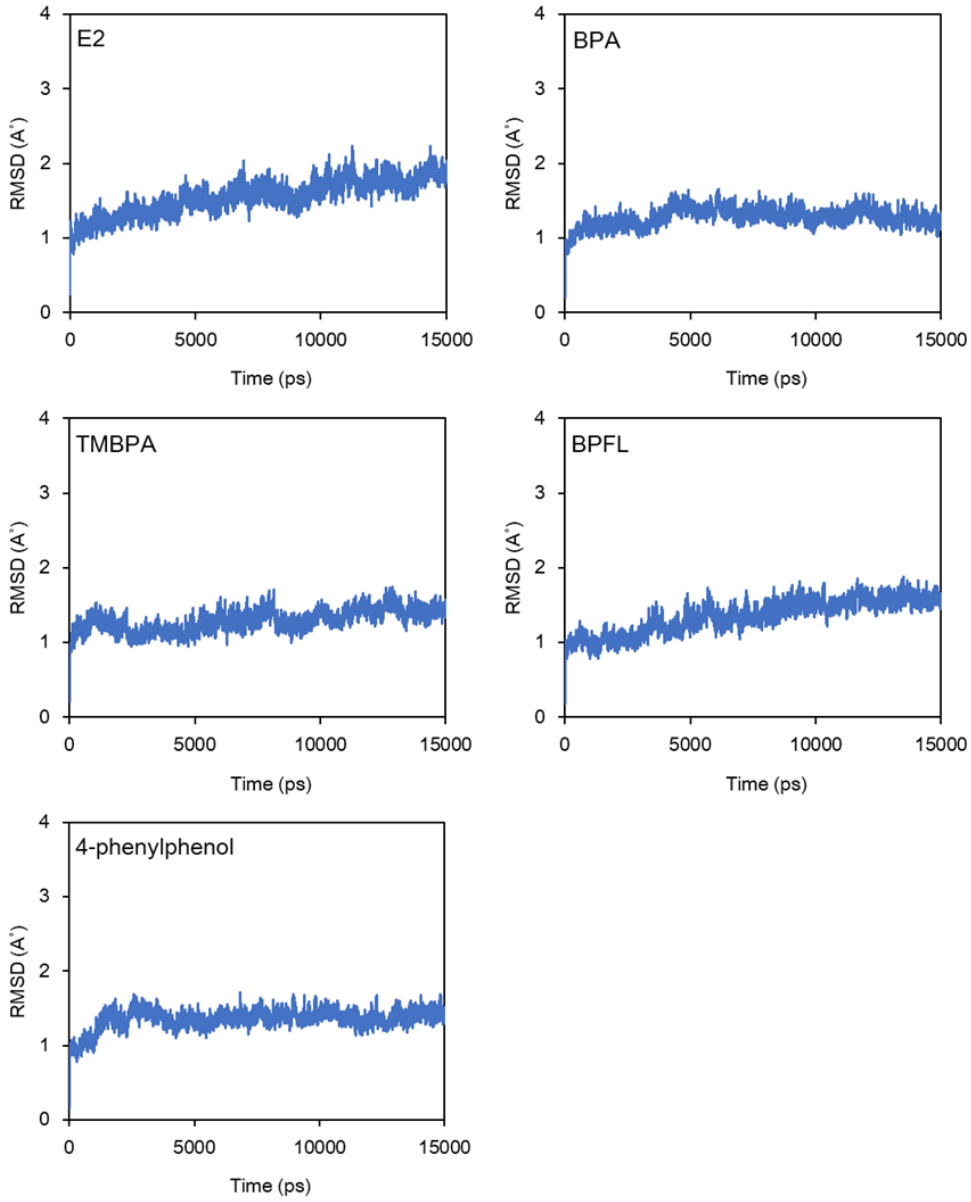

Supplementary Figure 3.2. Time dependence of the RSMD in ligand/hESR1-LBD complexes.

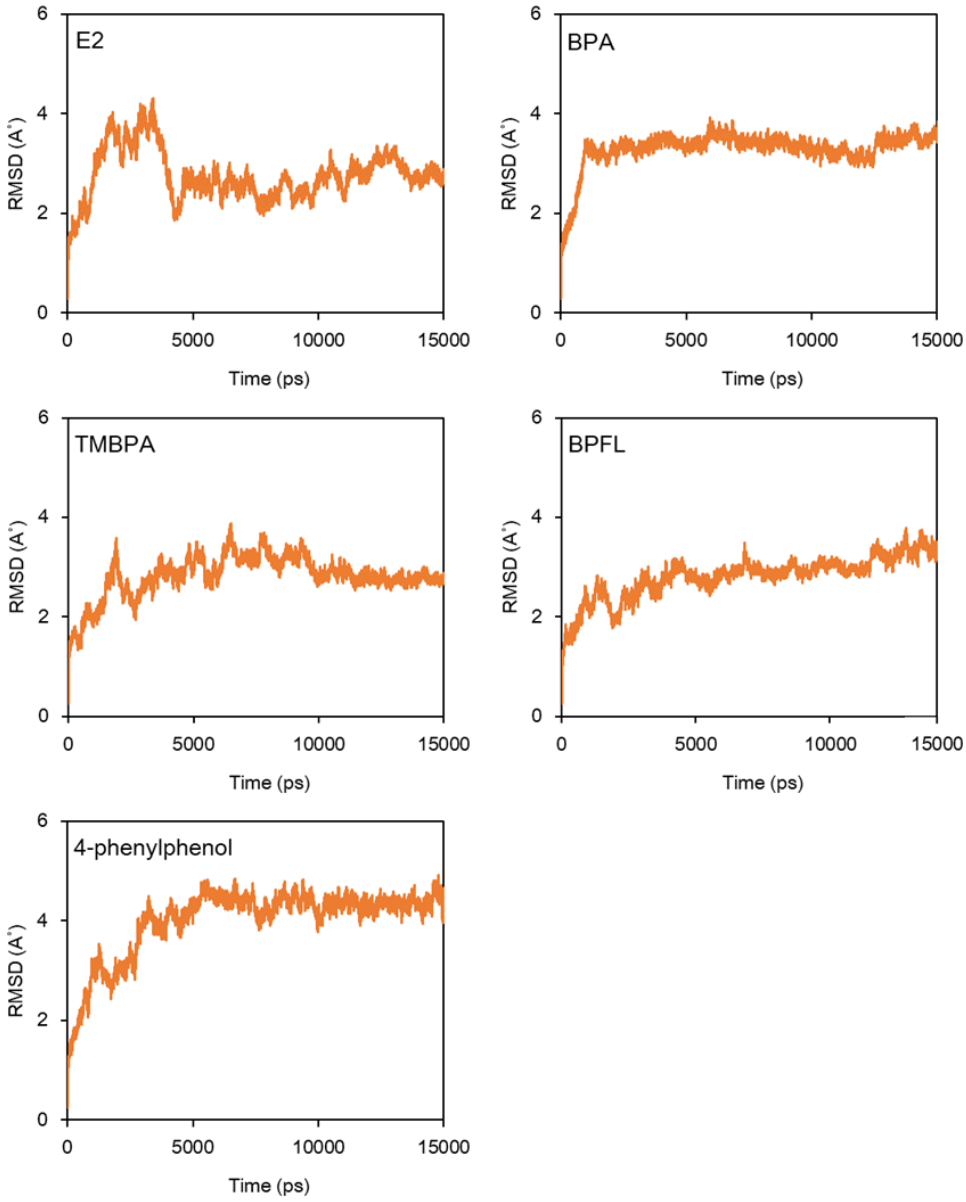

Supplementary Figure 3.3. Time dependence of the RSMD in ligand/zEsr1-LBD complexes.

Supplementary Table 3.1. Validations of hESR1-LBD and zEsr1-LBD structures

Validation programs		hESR1-LBD	zEsr1-LBD	Standard
Procheck (Ramachandran Plot)	Most Favoured regions	96.6%	97.5%	Good quality of models expected to have over 90% most favored regions
	Additionally allowed regions	2.60%	2.10%	
	Generously allowed regions	0.40%	0.40%	
	Disallowed Regions	0.40%	0.00%	
ERRAT	Overall model quality	97.0%	90.8%	For low resolutions native structures is around 90%
PROSA		-6.80	-6.76	Checks if z-score is within the range of score typically found for native proteins of similar size
Verify-3D		79.2%	78.0%	Good models more than 65% of the amino acids have scored >=0.2 in the 3D/1D profile

Supplementary Table 3.2. Average MMPBSA free engeries of docking complexes calculated from MD simulations (10-15ns).

Receptor	Ligands	Van der Waals (ΔG_{vdw})	Electrostatic (ΔG_{elec})	Polar Solvation (ΔG_{PB})	Non-polar solvation (ΔG_{SA})	Total Binding Free Energy (ΔG_{bind})
hESR1-LBD	E2	-38.01 ± 2.11	-14.43 ± 6.58	38.41 ± 5.54	-4.72 ± 0.08	-18.76 ± 2.76
	BPA	-33.98 ± 2.11	-19.48 ± 7.79	40.05 ± 6.75	-4.43 ± 0.06	-17.84 ± 3.09
	TMBPA	-43.20 ± 2.28	-14.19 ± 3.41	39.74 ± 3.43	-5.27 ± 0.08	-22.92 ± 3.46
	BPFL	-23.26 ± 4.23	-5.84 ± 3.93	25.44 ± 5.27	-3.57 ± 0.26	-7.23 ± 2.61
	4-phenylphenol	-26.23 ± 1.83	-15.09 ± 3.20	32.07 ± 2.03	-3.88 ± 0.07	-13.14 ± 2.64
zEsr1-LBD	E2	-37.96 ± 2.78	-20.62 ± 3.26	44.59 ± 2.68	-4.63 ± 0.06	-18.63 ± 2.55
	BPA	-32.29 ± 2.24	-24.53 ± 6.34	43.85 ± 3.84	-4.36 ± 0.06	-17.33 ± 3.17
	TMBPA	-40.83 ± 6.10	-6.99 ± 3.93	36.23 ± 7.42	-5.20 ± 0.61	-16.79 ± 3.79
	BPFL	-10.27 ± 6.51	-1.34 ± 3.64	10.34 ± 7.54	-2.20 ± 0.79	-3.48 ± 4.67
	4-phenylphenol	-26.01 ± 2.21	-10.95 ± 4.55	28.53 ± 2.83	-3.87 ± 0.08	-12.31 ± 3.53

Chapter 4. 3D spheroid culture of zebrafish liver cell

Contributions

As published in: **Chang Gyun Park**, Chang Seon Ryu, Baeckkyoung Sung, Andreas Manz, Hyunjoon Kong, and Young Jun Kim, "Transcriptomic and physiological analysis of endocrine disrupting chemicals Impacts on 3D zebrafish liver cell culture system" *Aquat. Toxicol.* **2022**, *245*, 106105. https://doi.org/10.1016/j.aquatox.2022.106105

Authorship contributions

Chang Gyun Park: writing - original draft, data curation, formal analysis, writing - review & editing
Chang Seon Ryu: writing - original draft, data curation, formal analysis, writing - review & editing
Baeckkyoung Sung: data curation, formal analysis, writing - review & editing.
Andreas Manz: investigation, methodology, resources, writing - review & editing.
Hyunjoon Kong: conceptualization, investigation, methodology, writing - review & editing.
Young Jun Kim: writing - original draft, conceptualization, funding acquisition, investigation, methodology, writing - review & editing.

Relation to the thesis

The importance of recognizing endocrine-disrupting chemicals on toxicological impact is evident through numerous publications on their prevalence. However, as *in vivo* studies often miss important intermediate molecular and cell dynamic events, there are increasing efforts to assemble *in vitro* test models that can replicate specific organs' morphology and physiological function. Aligned with the 3Rs policy, it would be ideal for building the *in vitro* platform with zebrafish cell lines instead of isolating primary cells by sacrificing fishes whenever needed. Unfortunately, studies report that cell lines cultured in a monolayered form do not reproduce the sensitivity of organs to endocrine disruptors.

To address such unmet needs, this study tested if cell culture in a 3D spherical form would enhance cellular sensitivity and physiological function. The zebrafish liver (ZFL) cell line was selected as a model system. The spheroid's size was optimized to make them viable for 28 days. Throughout a comparative study with a monolayered cell for 28 days, 3D ZFL spheroids were confirmed to significantly enhanced hepatic function. More interestingly, 3D ZFL spheroids treated with 17β-estradiol (E2) and endocrine-disrupting chemicals were activated to synthesize a higher level of vitellogenin than monolayer cells. RNA-seq analysis also confirmed that 3D ZFL spheroids hold the increased transcriptional activities of genes related to reproductive toxicities, compared with monolayer cells. These results provide an advanced *in vitro* tissue platform that allows long-term assessment of reproductive toxicity on the ecological system at molecular and cellular levels.

4.1 Abstract

In recent decades, extensive efforts have focused on developing *in vitro* platforms mimicking fish livers to better understand the acute or chronic effects of toxicants on lower aquatic vertebrates. Fish liver cell lines have emerged as a promising culture system for these *in vitro* platforms because they complement the currently limited *in vitro* tools that mostly consist of mammalian cell lines and adhere to the 3Rs: replacement, reduction, and refinement of live animal tests. However, monolayer cell lines have lower transcriptional and physiological responses upon exposure to toxic chemicals than freshly isolated primary cells. To overcome this challenge, we utilized a three-dimensional (3D) spheroid-based *in vitro* platform, in which hepatocyte cells had self-organized into spheroid forms via E-cadherin bonds. This platform exhibited augmented transcriptomic and phenotypic regulation of liver cells in comparison to monolayer cells. We examined the organoid platform using the zebrafish liver (ZFL) cell line as a model system. ZFL cells spontaneously clustered into 3D spheroids with long-term viability by optimizing cell seeding density on a non-adherent substrate. Interestingly, 3D ZFL spheroids treated with estrogenic chemicals were activated to synthesize a higher level of vitellogenin (Vtg) than monolayer cells. Whole-transcriptome sequencing analysis confirmed that 3D ZFL spheroids had greater transcriptional regulation of genes related to reproductive toxicological response and liver functions, such as the urea cycle, estrogen receptors, and vitellogenin, compared to monolayer cells. These results may contribute to the engineering of novel 3D *in vitro* platforms for screening harmful chemicals and improving understanding of the underlying liver toxicity mechanisms at the molecular and cellular levels.

Keywords: 3D spheroid culture, 17β-estradiol, *in vitro* platforms, vitellogenin, zebrafish liver cell

4.2 Introduction

Hepatic and reproductive toxicity in fish has been extensively evaluated within the adverse outcome pathway framework during assessments of environmental disturbances caused by various contaminants [1]. Many of these contaminants are endocrine-disrupting chemicals (EDCs), which can mimic the modes-of-action of sex hormones [2]. These EDCs have adverse effects on wildlife population dynamics [2]. For example, EDCs inhibit the biosynthesis of enzymes including steroidogenic cytochrome p450, steroid hydroxylase, and hydroxysteroid dehydrogenases. Some EDCs can also interact with nuclear receptors such as estrogen receptors (ERs), androgen receptors, peroxisome proliferator-activated receptors, and other physiologically critical nuclear receptors, including retinoid X receptors [3,4]. In particular, the binding of estrogenic EDCs to ERs triggers the transcription of vitellogenin (Vtg), a precursor of the egg yolk proteins [5]. Vtg is present not only in females but also in males that express Vtg in response to exposure with xenoestrogens [6]. Therefore, Vtg is a critical biomarker of endocrine disturbances in aquatic organisms [6].

Zebrafish (*Danio rerio*) have been used as a model vertebrate organism globally and are part of several Organization for Economic Co-operation and Development (OECD) test guidelines because of their rapid growth, development, and high conservation of signaling pathways compared to those of humans [7,8].

Zebrafish are increasingly used in single-chemical toxicity testing [9-11]. High numbers of zebrafish are also required for long-term studies on toxin bioaccumulation and reproduction. Due to growing concerns about the welfare of laboratory animals in toxicity testing, the reduction, refinement, and replacement principles (3Rs) have been actively attempted in vertebrate animal studies, including those using fish. Among alternative approaches, *in vitro* cell-based systems represent a promising technology for the predictive assessment of *in vivo* toxicity, allowing for more controlled manipulation of cellular functions and biological processes. Both freshly isolated primary hepatocytes and the zebrafish liver (ZFL) cell line are commonly cultured on two-dimensional (2D) substrates to study liver response dynamics to EDCs at the molecular and cellular level [12-14]. In particular, the ZFL cell line offers continued cell proliferation and adheres to the 3Rs [15]. However, monolayer-cultured cells exhibit decreased hepatic polarity and detoxification processes than 3D cell cultures [16]. It is difficult to conduct long-term chronic toxicity assessments using monolayer-cultured cells due to cellular detachment [17]. Furthermore, ZFL cells have a limited capacity for synthesizing Vtg upon exposure to estrogen hormones under monolayer culture conditions [18,19]. Therefore, there is an urgent need to develop a novel *in vitro* system to enhance the physiological activity of ZFL cells for robust reproductive toxicity assessment. *In vivo*-like cell aggregates such as a three-dimensional (3D) cell cultures represent a promising approach to address this need because they show higher cell-to-cell interactions, metabolic activity, and the tissue-like environment than monolayer cell cultures. Therefore, 3D cell culture is increasingly being employed in various fields including toxicology, pharmacology, and biomedical applications [20-24].

In this study, we hypothesized that ZFL cells cultured in 3D spheroids would present genetic profiles and physiological functionality more similar to liver tissue due to enhanced E-cadherin-mediated intercellular adhesion. E-cadherin plays pivotal roles in the formation of hepatocyte spheroids, the maintenance of epithelial cell behavior, and the prevention of cell death [25-27]. The resulting ZFL spheroids are expected to exhibit enhanced liver-specific functions and tissue-like environments compared with monolayer cell cultures. To achieve this objective, we optimized the cell-seeding conditions under which ZFL spheroids remain viable and metabolically active over 28 days, and prepared a monolayer ZFL cell culture as the control. We conducted comparative analyses of Vtg synthesis, detoxification, and transcriptional regulation using these two systems based on immunofluorescence, enzyme-linked immunosorbent assay (ELISA), quantitative reverse-transcription polymerase chain reaction (RT-qPCR), and whole-transcriptome RNA sequencing (RNA-Seq) techniques. We anticipate that the results of this study will contribute to improving understanding of EDC-induced endocrine disorders and the ability to design toxicity tests that empower fit-for-purpose chemical regulation.

4.3 Materials and Methods

4.3.1 Formation of 3D ZFL spheroids

The ZFL cell line was purchased from ATCC (CRL2643, Wesel, Germany) and then cultured and maintained in complete growth medium within T-75 flasks at 28°C in a cell incubator (Thermo Scientific, Karlsruhe, Germany). The complete growth medium consisted of 50% Leibowitz-15 (ATCC), 35% Dulbecco's modified

Eagle's medium (DMEM; Thermo Scientific), and 15% Ham's F12 (Thermo Scientific), supplemented with 15 mM of HEPES (Sigma-Aldrich, Steinheim, Germany), 0.15 g/L sodium bicarbonate (Sigma-Aldrich), 1% penicillin–streptomycin (Sigma–Aldrich), 0.01 mg/mL bovine insulin (Sigma-Aldrich), 50 ng/mL mouse epidermal growth factor (Thermo Scientific), 5% heat-inactivated fetal bovine serum (FBS), and 0.5% trout serum (Caisson Laboratories, Smithfield, UT, USA). For the generation of 3D spheroids, cells in the T-75 flask were washed with phosphate buffered saline (PBS; pH 7.4, Thermo Scientific). Next, the cells were treated with 0.25% trypsin–EDTA (ATCC), suspended in complete growth medium, and spun at 125 × *g* for 5 min. The pelleted cells were re-suspended in the medium and counted using a hemocytometer after staining with 0.4% trypan blue (Sigma-Aldrich). Cells from the same batch were seeded into a 96-well flat-bottomed plate (Thermo Scientific) for monolayer cell culture, and ultra-low-attachment 96-well round-bottomed plates (Corning B.V. Life Sciences, Amsterdam, Netherlands) for 3D spheroid culture, respectively. The initial spheroid cell densities were 5,000, 10,000, 25,000, 50,000, and 100,000 cells/well. The 3D ZFL spheroids formed in ultra-low-attachment 96-well round-bottomed plates (Figure 4.1a). Seeded cells were cultured in an incubator at 28°C, and 50% of the complete growth medium was replaced every 2–3 days in both monolayer cells and 3D spheroid cultures. To analyze changes in size and shape, bright-field images of the 3D ZFL spheroids were obtained at 1, 3, 7, 14, 21, and 28 days of culture using an inverted light microscope (Olympus CKX41, Olympus, Tokyo, Japan) equipped with a digital camera (C5060-ADUS, Olympus, Tokyo, Japan).

4.3.2 ZFL cell viability measurement

To measure cell viability in 3D ZFL spheroids, the cells were seeded at different densities in ultra-low-attachment 96-well round-bottomed plates and measured at 1 and 28 days. Complete medium containing a 3D spheroid (100 μL) was transferred from the ultra-low-attachment plates to 96-well white opaque culture plates (Thermo Scientific). Next, each well was treated with 100 μL CellTiter-Glo 3D reagent (Promega, Mannheim, Germany), and luminescent signals were recorded after 30 min using a microplate reader (Tecan, Männedorf, Switzerland). Bioluminescence from viable cells among the spheroids on day 1 was correlated to the cell seeding density (Figure 4.2a). Each cell density group was replicated for eight spheroids and a mean value was calculated. The experiment was repeated three times from independent cultures (n = 3). Measured response values revealed a non-linear trend at higher cell seeding densities (≥ 25,000 cells/well) and fit a polynomial regression equation. The expected linear fit was calculated for accurate cell viability measurement [28]. Based on the linear fit equation, the fractions of viable cells were measured on days 1 and 28. Each cell density group was replicated for five spheroids and a mean value was calculated. The experiment was repeated three times from independent cultures (n = 3). For live and dead staining, each cell concentration was cultivated for 28 days, and then the medium was removed. Fluorescein diacetate (FDA; Sigma-Aldrich) and propidium iodide (PI; Sigma-Aldrich) were dissolved in culture medium without FBS and trout serum, and the solution was added to each well. After incubation in the dark for 10 min, the staining solution was removed, and the cells were washed with PBS. The stained cells were observed under an inverted fluorescence optical microscope (DMi8, Leica Microsystems, Wetzlar, Germany) equipped with a digital camera (DCF295, Leica Microsystems), N PLAN 40×/0.55 CORR objective lens (11506297, Leica Microsystems), a

fluorescence excitation light source CoolLED pE300-lite (CoolLED Ltd. Andover, UK), fluorescence filters [350/50 4',6-diamidino-2-phenylindole (DAPI) excitation filter and 460/40 emission, 480/40 excitation fluorescein isothiocyanate (FITC) filter and 527/30 emission, and 546/10 RHOD excitation filter and emission 585/40], and fluorescence overlay software (LAS AF v3.1.0, Leica Microsystems).

4.3.3 Chemical exposure

The test chemicals were dissolved in dimethyl sulfoxide (DMSO) and the concentration of which did not exceed 0.5% (v/v). We obtained high-purity (≥ 98%) 17β-estradiol (E2), 17α-ethynylestradiol (EE2), bisphenol A (BPA), and bisphenol S (BPS) from Sigma-Aldrich. The concentrations of the E2, EE2, BPA, and BPS working stocks were 0.0002, 0.002, 2, and 2 mM, respectively. From these stocks, diluted solutions were prepared through 100 × dilution with complete medium. Each diluted solution was treated to wells containing spheroid or monolayer cells and complete medium at a 1:1 ratio. After exposure for 24 or 48 h, the spheroid and monolayer cells were used for assays.

4.3.4 Immunofluorescence assay

Cells with nuclear non-histone, cytoskeleton, and nuclei were stained with Ki67, F-actin, and DAPI, respectively. To obtain fluorescence images, monolayer cells and 3D spheroids were fixed in 3.7% paraformaldehyde at room temperature (RT) for 15 min, washed with PBS, and permeabilized in PBS supplemented with 0.1% Triton X-100 at RT for 5 min. After permeabilization, the samples were washed three times with PBS and blocked with 3% bovine serum albumin (BSA; Sigma–Aldrich) at RT for 30 min. Next, the samples were incubated with primary antibodies at 4°C overnight. After being washed three times with 1% BSA, the samples were incubated with secondary antibodies for 2 h and rewashed three times with 1% BSA. Finally, the samples were embedded in mounting medium containing DAPI (Vector Laboratories, Burlingame, CA, USA). Table 4.1 lists the primary and secondary antibodies used in this experiment. F-actin staining was performed using phalloidin-iFluor (ab176753, Abcam). Images of the monolayer cells were obtained by using a fluorescence microscope (DMi8, Leica) and analyzed using the ImageJ software (NIH and LOCI). The 3D spheroids were imaged using a Lightsheet Z.1 microscope (Carl Zeiss Microscopy GmbH, Jena, Germany) with two-sided 10×/0.2 illumination optics and a 20×/1.0 detection optic equipped with a pco.edge 4.2 camera (PCO AG, Kelheim, Germany). The captured images were analyzed using the ZEN imaging software (Carl Zeiss). The relative intensity of Vtg was calculated using the ImageJ software. Fluorescence microscope images of the samples were measured at the same exposure time and laser power, and the corrected total cell fluorescence (CTCF) were calculated as follows [29]:

Whole-cell signal = Sum of pixel intensity values for one cell (1)

Background signal = Average intensity per pixel for a selected region adjacent to the cell (2)

CTCF = Whole-cell signal (Number of pixels in the cell = Area of the selected surface × Background signal) (3)

Images obtained from eight replicates of each condition were analyzed as mean relative intensity values. The experiment was repeated three times with independent cultures (n = 3).

4.3.5 Urea assay

Cellular synthesis of urea was measured to evaluate hepatic functionality. The urea cycle converts toxic ammonia to urea in the liver for excretion, thereby acting as a detoxification mechanism [30]. The urea content of cell pellets was analyzed using a urea assay kit (MAK006, Sigma-Aldrich). In the monolayer culture, 1 mL of ZFL cells (50,000 cells/mL) was seeded into each well of a 6-well flat-bottomed plate and cultured for 7 and 28 days. After trypsinization and cell counting, 1.0×10^6 cells were collected from three wells into a tube by centrifugation at 125 × g for 5 min. For the 3D spheroids, 100 μL (i.e., 5,000 cells at a density of 50,000 cell/mL) were seeded into each well of an ultra-low-attachment 96-well round-bottomed plate and cultured for 7 and 28 days. About 200 spheroids were collected into a tube and centrifuged at 125 × g for 5 min. Each tube of pooled monolayer cells and spheroids was considered a sample, and six replicate samples of each condition were prepared from independent cultures (n = 6). After washing with PBS and another centrifugation at 125 × g for 5 min, 100 μL of cold urea assay buffer was added to a tube and homogenized by vortexing for 2 min. The homogenates were centrifuged at 14,000 × g and 4°C for 10 min. The supernatants were used for urea quantification according to the manufacturer's instructions. This assay determined the urea concentration: a coupled enzyme reaction resulted in a colored product that was measured by reading the absorbance at 570 nm on a microplate reader (Tecan). The supernatants of each sample were normalized to total protein content, quantified using a bicinchoninic acid (BCA) protein assay.

4.3.6 ELISA

Vtg synthesis was measured using an ELISA kit (10004995, Cayman Chemical, Ann Arbor, MI, USA). Monolayer cells and 3D spheroids were cultivated for 7, 14, and 28 days, and collected in the same manner as for the urea assay. Each tube of pooled monolayer cells and spheroids was considered a sample, and three replicate samples of each condition were prepared from independent cultures (n = 3). After washing with PBS and another centrifugation at 125 × g for 5 min, 100 μL of passive lysis buffer (Promega) was added to a tube and homogenized by vortexing for 2 min. The homogenates were centrifuged at 14,000 × g and 4°C for 10 min. The supernatants were used for Vtg quantification according to the manufacturer's instructions (Cayman Chemical). The supernatants of each sample were normalized to total protein content and quantified using a BCA protein assay.

4.3.7 mRNA expression analysis

To extract total RNA samples from monolayer cell cultures, 1 mL of ZFL cells (50,000 cells/mL) were seeded

into each well of a 6-well flat-bottom plate and cultured for 7 days. The cells of three wells were collected in a tube and lysed with RLT buffer (Qiagen, Hilden, Germany) after washing with cold PBS. For 3D spheroids, 100 μL of cells (i.e., 5,000 cells at a density of 50,000 cell/mL) were seeded into each well of an ultra-low-attachment 96-well round-bottomed plate and cultured for 7 days. We collected 100 spheroids in a tube and centrifuged them at 125 × *g* for 5 min. After washing with cold PBS and another centrifugation at 125 × *g* for 5 min, 3D spheroids were lysed in the same manner as monolayer cells. Each tube of pooled monolayer cells and spheroids was considered a sample, and three replicate samples were prepared from independent cultures for each condition ($n = 3$). Total RNA of each sample was extracted using an RNeasy Plus mini kit (74136, Qiagen). Sample concentration and purity were determined spectrophotometrically using a NanoDrop 2000 spectrophotometer (Thermo Scientific). Reverse transcription was performed for samples with purity > 2.0 (OD_{260}/OD_{280} and OD_{260}/OD_{230}) using the High-Capacity RNA-to-cDNA kit (Applied Biosystems, Waltham, MA, USA) according to the manufacturer's instructions. Total RNA (1 μg) was used for reverse transcription. Next, qRT-PCR (7500 FAST Real-Time PCR System, Applied Biosystems) was conducted using the TaqMan Gene Expression Master Mix (Thermo Scientific) and PowerUp SYBR Green Master Mix (Applied Biosystems). Table 4.2 and Table 4.3 describe the probe assay identifications and reaction cycles. Relative mRNA expression was determined using the $2^{-\Delta\Delta CT}$ method [31].

4.3.8 RNA-Seq analysis

Total RNA samples of monolayer cells and 3D spheroids were extracted in the same manner as those subjected to mRNA expression analysis. Six total RNA samples (monolayer cells and 3D spheroids in triplicate) were sent to a Novogene for RNA-Seq (Novogene, Cambridge, UK). Total RNA samples were purified using poly-T oligo-attached magnetic beads after quality control checks. Paired-end sequencing (150 bp) was conducted using an Illumina NovaSeq 6000 system. Samples were sequenced at a sequencing depth of at least 48 million clean reads, and 15 G raw bases were generated per sample. Raw sequences were filtered for contaminant adapter sequences and reads with > 10% uncertain nucleotides or > 50% low-quality nucleotides (Qphred ≤ 5). Filtered reads were considered clean reads, and the reads of each sample were used for data analysis. Data analysis was conducted by Novogene. Paired-end clean reads were aligned to the reference genome (genome assembly: GRCz11_gca_000002035_4, Taxon ID: 7955) using HISAT2 to count the read numbers mapped to each gene, and the expected FPKM number was determined for each gene based on the gene length and read count mapped to the gene. Differential expression analyses of two conditions/groups (in triplicate for each condition) were conducted using the *DESeq2* R package, which identifies differential expression among genes using a model based on the negative binomial distribution. To control the false discovery rate, *P* values were adjusted (P_{adj}) using the Benjamini and Hochberg methods. Differentially expressed genes (DEGs) were evaluated at a level of $P_{adj} < 0.05$.

4.3.9 Statistical analyses

Statistical analyses were performed using the SPSS Statistics v21 software (SPSS, Inc, IBM, Chicago, IL,

USA). All data are expressed as means ± standard deviation (SD). Data were tested for normality using the Shapiro–Wilk test and for homogeneity of variance using Levene's test to determine whether to perform parametric or non-parametric statistical tests. Statistical differences among test groups were determined using Student's *t*-test or one-way analysis of variance (ANOVA) followed by post hoc Dunnett's T3 test (non-homogeneous variance) or Scheffe's test (homogeneous variances). Data for cell viability, urea synthesis, and Vtg intensity analyses were evaluated using Student's *t*-test. Data for Vtg synthesis and gene transcript abundance analyses were evaluated using one-way ANOVA. All statistical analyses for RNA-Seq were performed using the *DESeq2* R package; heatmaps were generated based on FPKM cluster analysis according to the log2(FPKM+1) value, and a volcano plot was created from DEG gene expression levels according to $-\log10(P_{adj})$. For principal component analysis (PCA), six samples from two groups were scaled to unit variance and calculated as PC1 (85.5%) and PC2 (6.05%).

Table 4.1 Antibody information

Antibodies	Source	Catalog	RRID
Anti-E-cadherin	Thermo	PA5-19479	AB_10988711
Anti-Ki67	GeneTex	GTX16667	AB_422351
Anti-Total ERK	Cell signaling	4696	AB_390780
Anti-Vitiellogenin	LifeSpan	LS-C76845-100	AB_1602614
Anti-Rabbit IgG Alexa Fluor 546	Thermo	A-11010	AB_2534077
Anti-Mouse IgG1 FITC	Thermo	31232	AB_429670
Goat Anti-Mouse IgG H&L (HRP)	Abcam	Ab6789	AB_955439
Goat Anti-Rabbit IgG H&L (HRP)	Abcam	Ab6721	AB_955447

Table 4.2 The information of assay identification and probes

Gene Name	Gene symbol	RefSeq Identification	Assay Identification	Source
Estrogen receptor 1	*esr1*	NM_152959.1	Dr03093579	Thermo
Estrogen receptor 2a	*esr2a*	NM_180966.2	Dr03074408	Thermo
Estrogen receptor 2b	*esr2b*	NM_174862.3	Dr03150586	Thermo
Vitellogenin 1	*vtg1*	NM_001044897.3	PPZ09938A	Qiagen
Vitellogenin 2	*vtg2*	NM_001044913.1	PPZ10052A	Qiagen
Vitellogenin 3	*vtg3*	NM_131265.1	PPZ00317A	Qiagen
Vitellogenin 4	*vtg4*	NM_001045294.2	Dr03191564	Thermo
Vitellogenin 5	*vtg5*	NM_001025189.2	PPZ00676A	Qiagen
Glucose-6-phosphate dehydrogenase	*g6pd*	XM_694076	PPZ12949A	Qiagen
Eukaryotic translation elongation factor 1 alpha 1, like 1	*eef1a1l1*	NM_131263.1	Dr03432748	Thermo

Table 4.3 Condition of reaction cycles

Mode	Cycles	Temperature (°C)	Duration (sec)	Step
SYBR green assay	Hold	95	20	AmpliTaq Fast DNA polymerase and Up activation
	40	95	3	Denature
		60	30	Anneal/Extend
TaqMan assay	Hold	50	120	UNG incubation
		95	120	Polymerase activation
	40	95	3	Denature
		60	30	Anneal/Extend

4.4 Results

4.4.1 Formation of 3D ZFL spheroids

The ultra-low-attachment plate inhibited cellular attachment, and cells gradually aggregated to form spheroids during cultivation (Figure 4.1b). Bright-field microscopy images revealed that the initial cell seeding densities influenced spheroid morphology. Morphological changes were evaluated by measuring the 2D surface area, diameter, solidity, and roundness of the spheroids over a period of 28 days (Supplementary Figure 4.1 and Supplementary Table 4.1). The surface area and diameter of spheroids decreased over time, whereas their roundness and solidity increased continuously over 28 days of cell culture (Supplementary Table 4.1). Initial cell densities > 25,000 cells/well resulted in more significant changes in spheroidal area and diameter. Notably, initial seeding densities of 5,000 and 10,000 cells/well resulted in high solidity values (> 0.9) on day 3. In monolayer cell culture, cells had a typical epithelial appearance (Supplementary Figure 4.2a). After cells were plated at a density of 5,000 cells/well, cell numbers increased over time, finally reaching confluency on day 7 (Supplementary Figure 4.2a). Cells continued to grow, but a delay in cell doubling time coincided with over-confluency at day 14 (Supplementary Figure 4.2b).

4.4.2 Long-term viability of 3D ZFL spheroids

Cell viability measurements using bioluminescence differed significantly between days 1 and 28 for cell seeding densities > 25,000 cells/well, indicating cell death during culture (Figure 4.2b). In contrast, no significant difference was observed in the fraction of viable cells for cell seeding densities of 5,000 and 10,000 cells/well between days 1 and 28. Cell viability was further assessed using a live/dead cell staining method (Figure 4.2c). Cell seeding densities of ≥ 50,000 cells/well showed red fluorescence in the spheroid cores, indicating cell death. In contrast, spheroids formed from cell seeding densities of 5,000 and 10,000 cells/well remained viable for 28 days. Therefore, we selected a seeding density of 5,000 cells/well as the optimal condition for subsequent experiments.

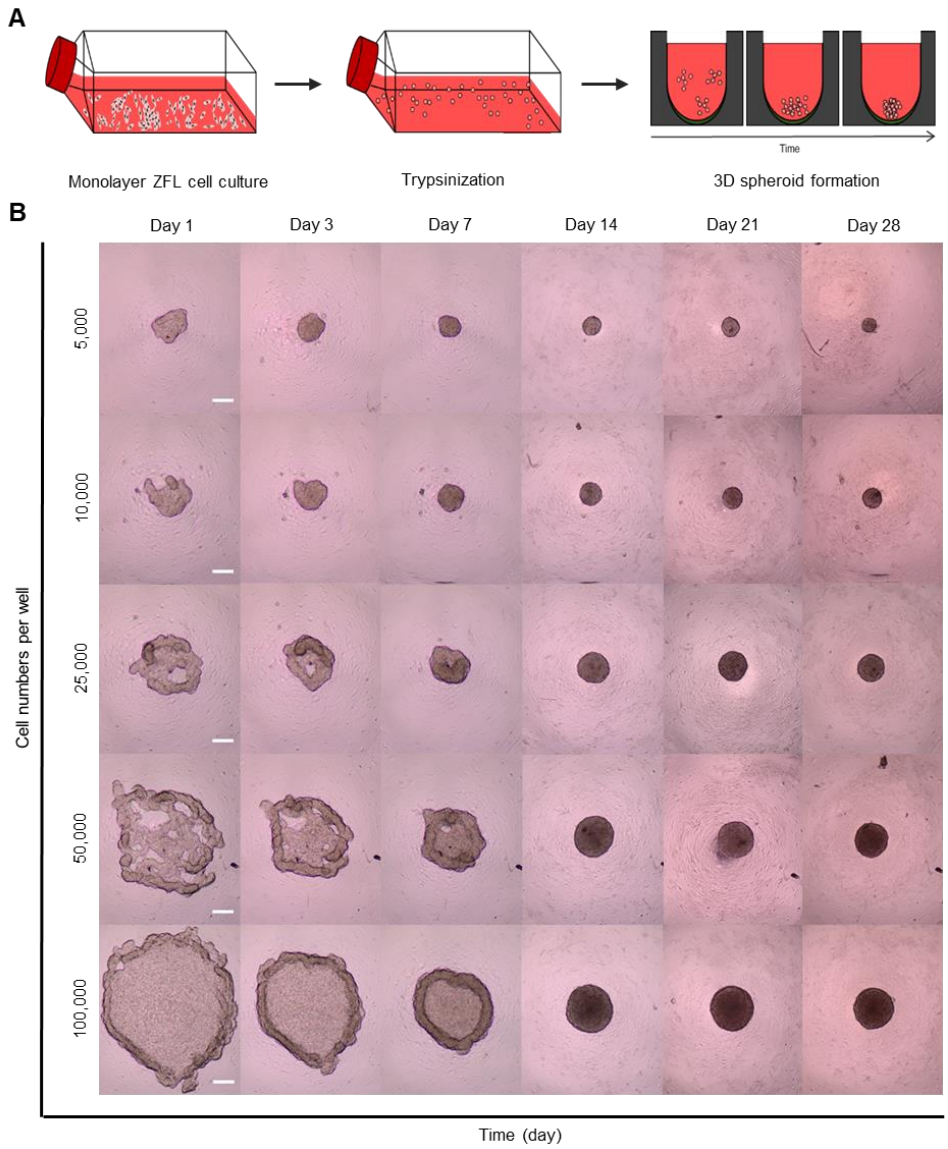

Figure 4.1. Process of three-dimensional (3D) spheroid formation and morphological changes. (a) Schematic of 3D spheroid formation. A monolayer culture of zebrafish liver (ZFL) cells was trypsinized for cell dissociation and collected by centrifugation at 125 × *g*. The collected cells were transferred to an ultra-low-attachment plate and cultured. (b) Representative bright-field images of 3D spheroids seeded at different cell densities over 28 days of culture. Cells were seeded into an ultra-low attachment plate, and bright-field images were captured at 1, 3, 7, 14, 21, and 28 days. White scale bar: 200 μm.

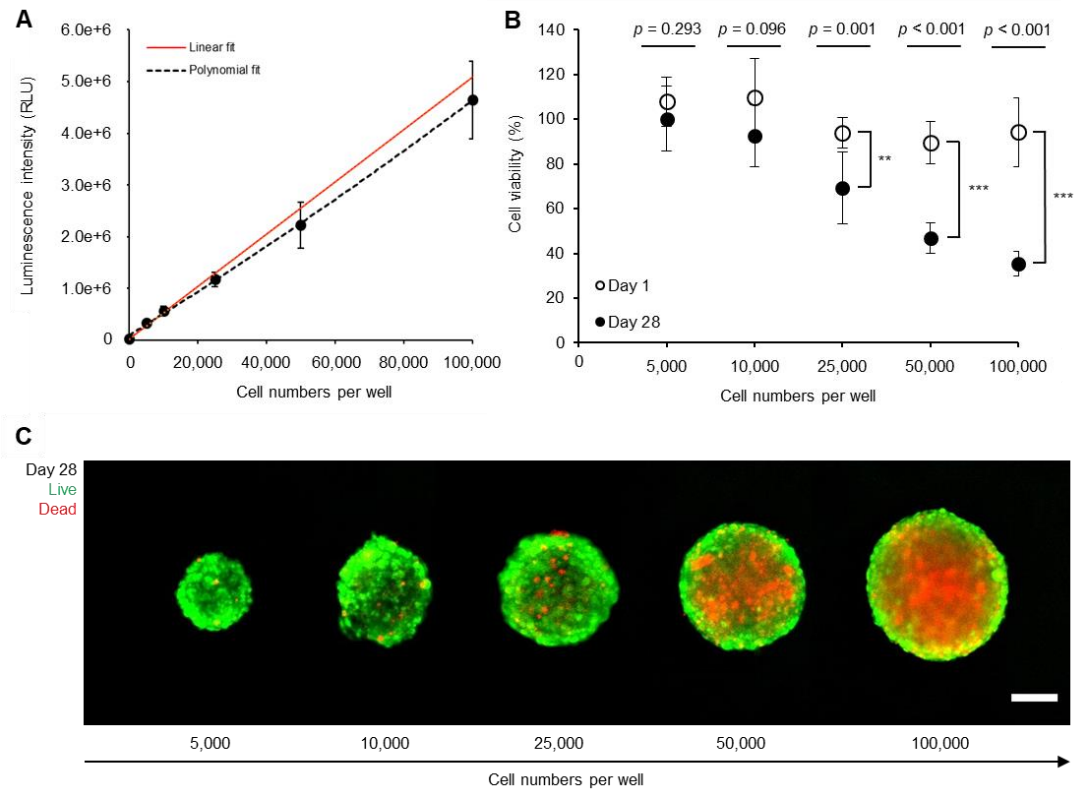

Figure 4.2. Cell viability in 3D spheroid cultures over 28 days of culture. (a) Cell viability of 3D spheroids cultured in an ultra-low-attachment plate. Different cell densities (5,000–100,000 cells/well) were seeded into an ultra-low-attachment plate and cultured for 24 h. The CellTiter-Glo 3D cell viability assay was used to measure luminescence intensity according to cell numbers. The polynomial fit indicates the measured relationship between luminescence and cell number, and the linear fit (red line) is the expected relationship. The graph presents means of three replicates of eight spheroids for each cell number condition. Data are means ± standard deviation (SD; $n = 3$). (b) Comparison of cell viability between days 1 and 28. Cell viability rates (%) were calculated based on the linear fit in (a). The graph presents means of three replicates of five spheroids for each cell number condition. Data are means ± SD ($n = 3$). Student's t-test was performed to compare means between days 1 and 28 of cell number groups (*$P < 0.05$; **$P < 0.01$; ***$P < 0.001$). (c) Images of live and dead 3D spheroids cultured for 28 days as a function of increasing cell number (5,000 cells from left, 100,000 cells to the right). White scale bar: 100 μm. Green and red fluorescence indicates live and dead cells, respectively.

4.4.3 Comparative studies of growth, cell–cell adhesion, and hepatic functionality

Phenotypic properties and physiological functions of 3D ZFL spheroids prepared at a seeding density of 5,000 cells/well were assessed by monitoring cell proliferation, cell-to-cell interaction, and urea synthesis (Figure 4.3). In general, Ki-67 is expressed only during active cell cycle phases with its effects on cell proliferation. Positive Ki67 expression was observed at the periphery of 3D spheroids on day 7, but became minimal by day 28. Monolayer cells also had decreased Ki67 expression throughout the 28-day culture period (Figure 4.3a). A separate analysis of cellular adhesion to neighboring cells revealed that cells in the 3D ZFL spheroids had more active cell-to-cell interactions induced by E-cadherin bonds responsible for hepatic junction formation in the liver. Immunofluorescence images revealed that E-cadherin expression increased over time in 3D spheroids compared to cell monolayers (Figure 4.3b). Western blot analysis of E-cadherin expression confirmed higher expression by cells constituting 3D spheroids than monolayer cells (Supplementary Figure

4.3a). However, according to our RNA-Seq results, 3D spheroids cultured for 7 days had significantly lower expression of genes related to cell proliferation and replication (e.g., *mki67* and *pcna*) than monolayer cells (Figure 4.3c). Genes related to cell-to-cell junctions such as *cdh1*, *cadm*, *cldn*, and *tjp* had enhanced expression within 3D spheroids (Figure 4.3d). Section 3.5 provides more detailed hepatic functional gene expression analysis results. The hepatic functionality of cells was evaluated by quantifying the cellular synthesis of urea (Figure 4.3e). Interestingly, 3D spheroids had significantly more urea synthesis activity than monolayer cells over 28 days. Additionally, 3D spheroids displayed a 2-fold increase in urea synthesis activity over time, whereas monolayer cells exhibited constant urea synthesis activity. Overall, the difference in the urea synthesis activity between 3D spheroids and monolayer cells became more prominent over the cell culture period.

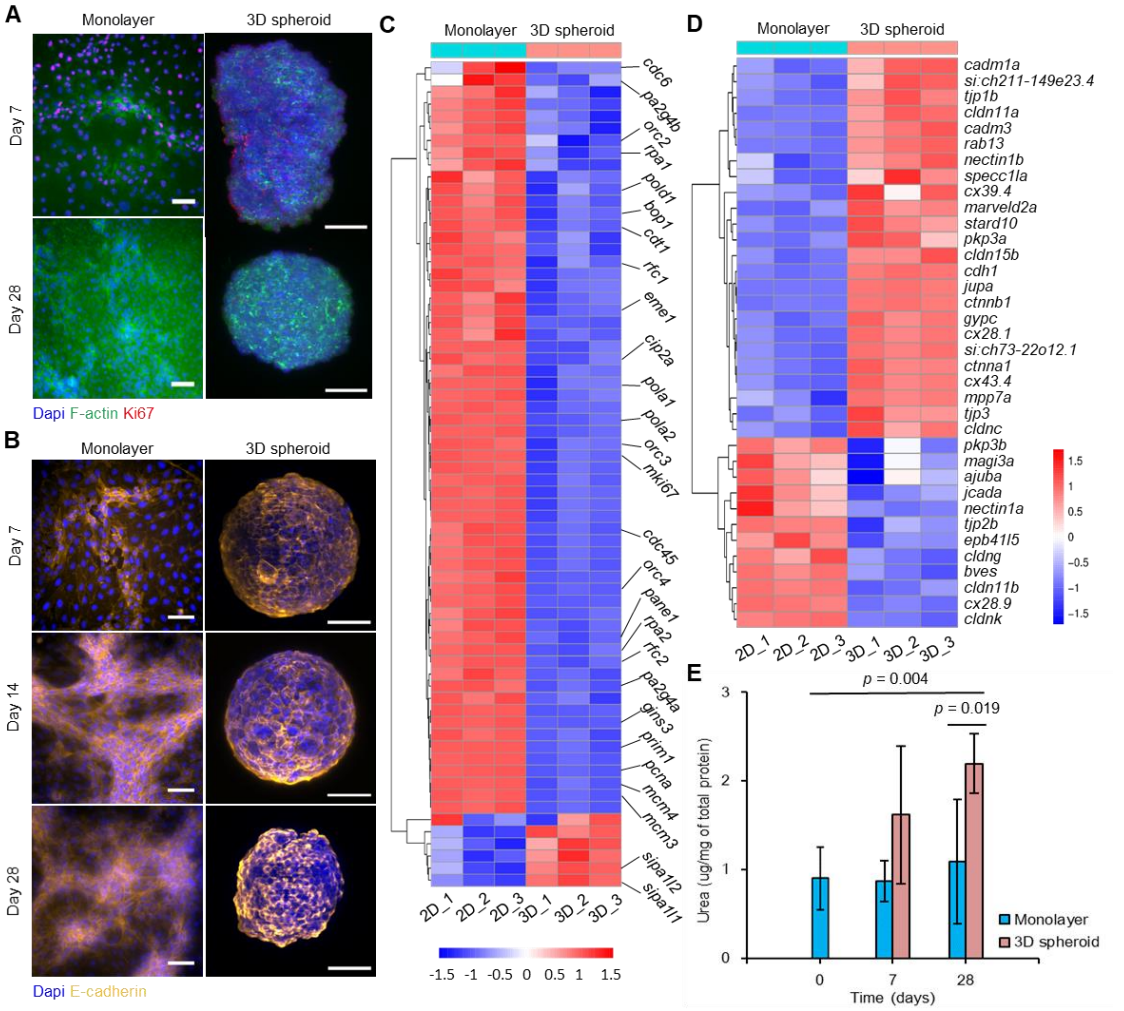

Figure 4.3. Evaluation of 3D spheroid properties and urea synthesis. (a–b) Immunofluorescence observations of monolayer cells and 3D spheroids using fluorescence optical and lightsheet microscopies. Cells seeded at a density of 5,000 cells/well were cultured for 7, 14, and 28 days. Scale bars: 50 µm. (a) Representative images of Ki67 (red), F-actin (green), and 4',6-diamidino-2-phenylindole (DAPI; blue) staining to investigate cell proliferation and cell structure. (b) Representative images of E-cadherin (orange) and DAPI (blue) staining to investigate cell–cell interaction. (c–d) RNA-seq analysis. Heatmaps of gene expression differences between monolayer and 3D spheroid cells at day 7. For monolayer cells, 50,000 cells/mL were seeded into each well of a 6-well flat-bottom plate; cells were collected from three wells into a tube. For 3D spheroids,

100 spheroids (5,000 cells/well) were collected into a tube. Each tube of pooled monolayer cells or spheroids was considered a sample, and three replicate samples were prepared for each condition from independent cultures (n = 3). (c) Heatmap of expression differences in genes related to cell proliferation and replication, (d) Heatmap of expression differences in genes related to cell–cell junctions. (e) Urea synthesis analysis. We collected 1.0×10^6 monolayer cells or 200 spheroids (5,000 cells/well) into a tube. Each tube was considered a sample, and six replicate samples were prepared for each condition from independent cultures (n = 6). Urea concentrations were normalized to total protein concentration. Error bars indicate means ± SD. Student's t-test was performed to compare means between groups. Significant differences were observed between monolayer cells (day 0) and 3D spheroids cultured for 28 days (P = 0.004) and between monolayer cells and 3D spheroids cultured for 28 days (P = 0.019).

4.4.4. Comparative analysis of Vtg synthesis

Immunostaining revealed that monolayer cells produced a limited amount of Vtg even after stimulation with exogenous E2 (Figure 4.4a). In contrast, 3D ZFL spheroids actively synthesized Vtg even without the addition of exogenous E2 (Figure 4.4b). Cellular Vtg synthesis levels continued to increase over 28 days in both the presence and absence of exogenous E2 (Figure 4.4c). The relative intensity of Vtg demonstrated that BPA and BPS, both of which are agonists to ERs, resulted in a significant increase in Vtg synthesis by 3D spheroids (1.6-fold with 10 µM BPA; 3.2-fold with 10 µM BPS; Figure 4.4D and Supplementary Figure 4.3c). The 3D spheroids also exhibited increased Vtg synthesis in response to 17α-ethynylestradiol (EE2), which is a synthetic hormone for ER activation (Supplementary Figure 4.3c). The transcript abundance of genes involved in Vtg synthesis was also compared between monolayer cells and 3D spheroids after 7 days of culture (Figure 4.4e). Each condition was treated with 1 nM E2 for 24 h to activate Vtg transcript abundance. E2 decreased e*sr2b* expression levels in 3D spheroids and increased e*sr2a* expression more significantly than monolayer cells (2.1- and 1.8-fold in the absence and presence of exogenous E2, respectively). We further examined the effects of E2 on transcript abundance among Vtg sub-family genes. *Vtg1* and *vtg5* are major precursors for ovulation and egg maturation. The abundance of *vtg1* transcripts was 2.9-fold higher in 3D spheroids than in monolayer cells following E2 exposure. Similarly, 3D spheroids had 5.3-fold higher *vtg5* transcript abundance than monolayer cells.

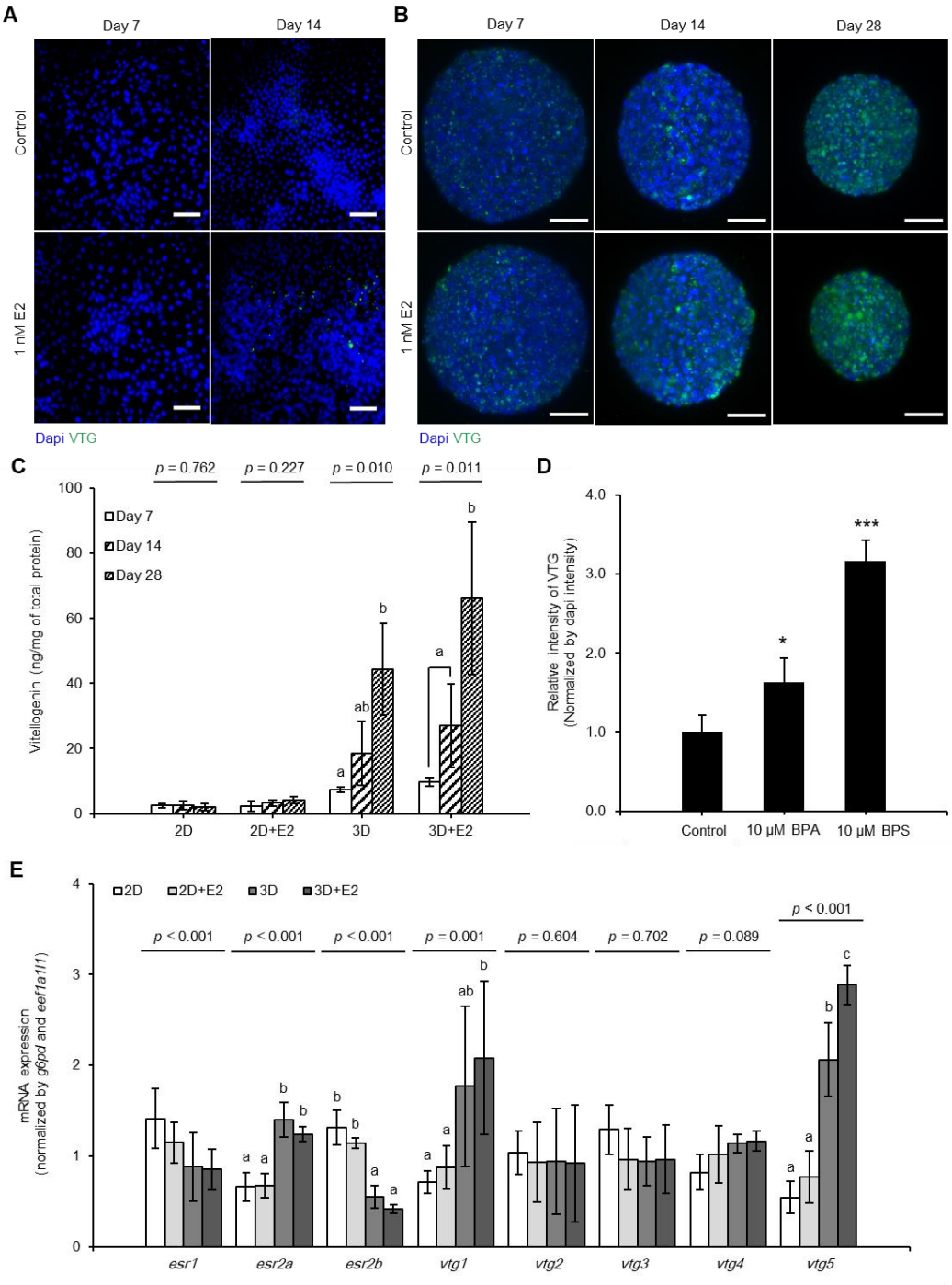

Figure 4.4. Analysis of Vtg synthesis in 3D spheroids. (a–b) Fluorescence images of monolayer cells and 3D spheroids stained with DAPI (blue) and Vtg (green). Cells seeded at a density of 5,000 cells/well were cultured for 7, 14, and 28 days. On days 7 and 28, cell cultures were treated with 1 nM 17β-estradiol (E2) for 24 h. Scale bar: 50 μm. (c) Quantification of Vtg synthesis in two-dimensional (2D) monolayer cells and 3D spheroids. Cells were treated with 1 nM E2 for 24 h. We collected 1.0×10^6 cells or 200 spheroids (5,000 cells/well) into a tube. Each tube was considered a sample, and three replicate samples were prepared for each condition from independent cultures (n = 3). Vtg was normalized to total protein concentration. Error bars indicate means ± SD. Comparisons of means between culture days in each group were performed using one-way analysis of variance (ANOVA; $P < 0.05$), followed by Dunnett's T3 test (non-homogeneous variance) or Scheffe's test (homogeneous variance). Different letters indicate significant differences. (d) Relative intensity of Vtg, normalized by DAPI intensity. The 3D spheroids (5,000 cells/well) were cultured for 7 days with charcoal stripped fetal bovine serum (FBS); subsequently, 10 μM of bisphenol A (BPA), and

bisphenol S (BPS) were treated for 48 h. Eight replicate spheroids of each group were measured and the mean relative intensity was calculated. Measurements were repeated three times from independent cultures. Error bars indicate means ± SD (n = 3). Student's t-test was performed to compare means between the control and chemical treatment groups (99.9% confidence interval; *P < 0.05; **P < 0.01; ***P < 0.001). (e) mRNA expression related to vitellogenesis in 2D and 3D measured by a TaqMan gene expression assay and SYBR Green gene expression assay, as described in the Methods section. For monolayer cells, 50,000 cells/mL were seeded into each well of a 6-well flat-bottomed plate, and cells were collected from three wells into a tube. For 3D spheroids, 100 spheroids (5,000 cells/well) were collected into a tube. Each tube was considered a sample, and three replicate samples were prepared for each condition from independent cultures (n = 3). Data were normalized to the transcript abundance of *eef1a1l1* (TaqMan assay) or *g6pd* (SYBR Green assay). After 7 days of culture, both groups were treated with 1 nM E2 for 24 h. Error bars indicate means ± SD. Comparisons of means between sample groups for each gene were performed using one-way ANOVA (P < 0.05), followed by Dunnett's T3 test for non-homogeneous variance or Scheffe's test for homogeneous variance.

4.4.5 Analysis of whole transcriptome sequence (RNA-Seq) related to hepatic function

We further analyzed differential gene expression in 3D spheroids using whole-transcriptome sequencing analysis (Figure 4.5). A heatmap of hierarchical clustering revealed distinct expression profiles between monolayer cells and 3D spheroids (Figure 4.5a). Principal component analysis (PCA) also revealed clear separation between monolayer cells and 3D spheroids sets (Figure 4.5b). The 3D spheroids exhibited significant upregulation of 4,324 genes and downregulation of 4,363 genes compared to monolayer cells (Figure 4.5c). Interestingly, 3D spheroids expressed greater transcript abundance of genes related to hepatic functions than monolayer cells (Figure 4.5d–h). Supplementary Tables 2–6 present detailed gene functions associated with the heatmap data. The 3D spheroids had more transcript abundance of genes related to the urea cycle, such as *acy1* (a marker of aminoacylase) and *oat* (a marker of ornithine aminotransferase), than monolayer cells. However, they expressed lower levels of some markers such as *ass1* (a marker of argininosuccinate synthase), *cad* (a pyrimidine biosynthesis marker), and *otc* (a marker of ornithine carbamoyltransferase) (Figure 4.5d). This trend is consistent with our urea synthesis results (Figure 4.3e). We observed significantly more *vtg3* and *vtg5* gene transcript abundance in spheroids compared to monolayer cells (Figure 4.5e). The 3D spheroids had greater expression of *cyp2* family genes such as *cyp2aa*s and *cyp2k*s (markers of endogenous and xenobiotics compound metabolism) than monolayer cells (Figure 4.5f). Moreover, the expression of other *cyp* genes increased, including *cyp1d1* (a marker of testosterone 6-beta-hydroxylase function), *cyp7a1* (a marker of a rate-limiting factor for synthesizing bile acids), and *cyp39a1* (a bile acid synthesis marker). In contrast, monolayer cells expressed more *cyp17a1* and *cyp2ad*s genes, which encode proteins involved with hydroxylase activity and metabolic functions, respectively, than 3D spheroids. The 3D ZFL spheroids had more transcript abundance of genes related to glucose and glycogen synthesis and metabolism activity than monolayer cells, as shown by higher levels of *pdk*s (a glucose homeostasis marker), *irs1* (an insulin receptor binding activity marker), and *gcgra* (a glucose metabolism marker) (Figure 4.5g).

Nuclear receptor genes *esr2a* and *esr2b* (estrogen receptor activity markers) were increased in 3D spheroids (Figure 4.5h). The 3D spheroids also had more transcript abundance of *ppar* genes than monolayer cells. These genes regulate energy homeostasis and metabolic function; *ppardb* regulates cholesterol storage, and *pparaa* regulates fatty acid metabolism. Other markers such as *arntl1b* (a photoperiodism regulation marker), *thrb* (thyroid hormone-mediated signaling pathway), *pgr* (steroid binding and steroid hormone

receptor activity), and *nr1i2* (*pxr*, responses to diverse xenobiotic and endogenous chemicals) were also enhanced in 3D spheroids. These markers play critical roles in regulating numerous biological processes such as cell proliferation, development, metabolism, and reproduction [32].

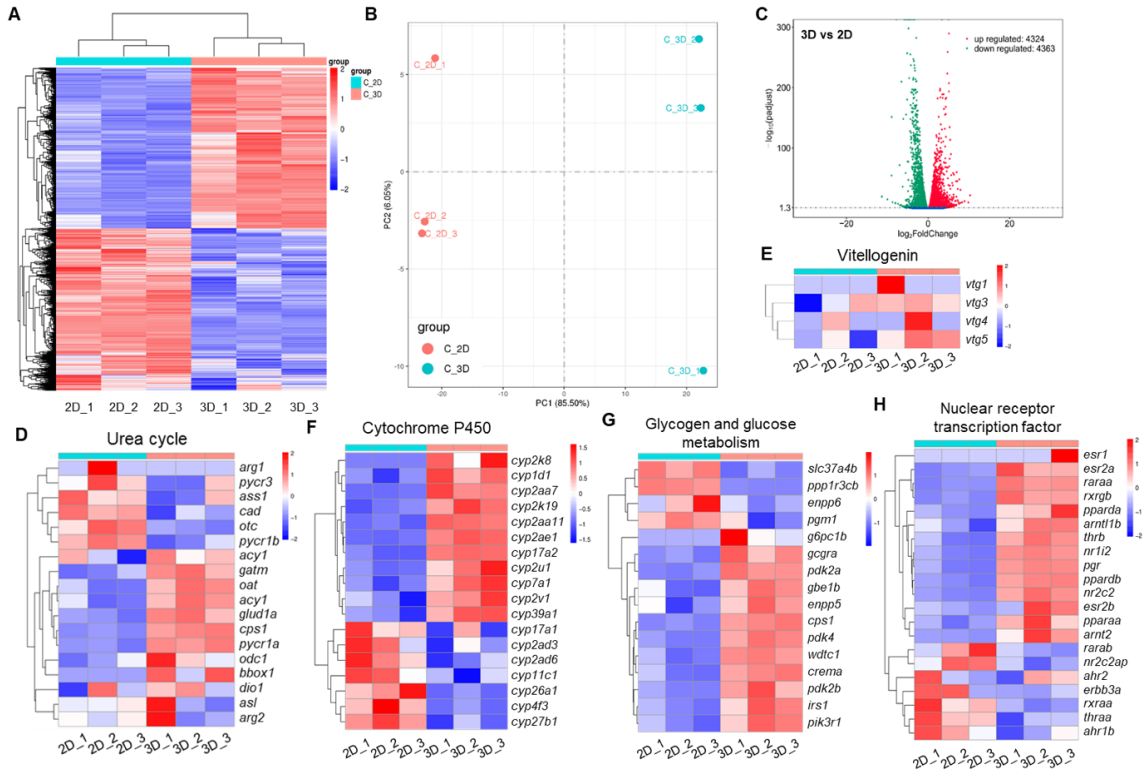

Figure 4.5. RNA sequencing (RNA-Seq) analysis of monolayer cells and 3D spheroids. (a–h) RNA-Seq analysis. Heatmaps of differences in expression between monolayer and 3D spheroid cells at day 7 (n = 3). Samples were prepared as described for mRNA expression. (a) Heatmap hierarchical clustering according to log2(FPKM+1) indicates differentially expressed genes (DEGs) between groups. Red and blue indicate genes with high and low expression levels, respectively. (b) The 2D principal component analysis (PCA) results for both groups. (c) Volcano plot analysis results. Plots indicate overall DEG distribution. (d–h) Heatmaps of differential expression between groups. (d) Urea cycle; (e) vitellogenin; (f) cytochrome P450 activity; (g) glycogen and glucose metabolism; (h) nuclear receptor and transcription factor.

4.5 Discussion

In this study, we systematically examined the extent to which 3D culture of the ZFL cell line provides improved and more realistic assessments of cell viability, detoxification activity, and sensitivity to reproductive toxicants. We successfully assembled 3D ZFL spheroids that remained viable and metabolically active for 28 days *in vitro* by tuning the initial cell seeding density to 5,000 cells/non-adherent wells. At optimized cell densities (5,000 cells and 10,000 cells/well), uniform spheroidal shapes were achieved during cultivation, without necrotic cores. The consistent maintenance of 3D spheroid morphology is a key factor in their viability, functionality, and application [22,28]. In contrast, at cell seeding densities ≥ 25,000 cells/well,

excess cells aggregated within the limited space of the concave well and rolled up the boundary of the cell layer, causing irregular cell aggregates > 500 μm in size. The resulting spheroids had an internal quiescent zone and necrotic core, probably due to limited diffusion of nutrients and oxygen [22,28]. These findings suggest that the optimized cell densities have reproducible and consistent viability and function. In contrast, monolayer cells reached 100% confluency after 7 days of culture, followed by over-confluency. A previous study reported that an over-confluent environment altered signaling and led to irreproducible behavior [33]. Therefore, monolayer cell culture and 3D ZFL spheroids at high cell density (≥ 25,000 cells/well) are inappropriate for long-term culture experiments.

Compared to monolayer cells, 3D ZFL spheroids had increased cell–cell interaction driven by E-cadherin and urea synthesis, and decreased cell proliferation and replication. These results are consistent with previous studies reporting that 3D spheroids display more realistic hepatic functions and properties [23,34]. In human cell lines, E-cadherin inhibition in primary hepatocytes prevented cell–cell attachment and spheroid formation, subsequently leading to cell death through a caspase-independent mechanism [27]. E-cadherin also plays a crucial role in cell–cell interactions related to contact formation and junction remodeling [35]. Several studies have reported that 3D spheroids exhibit enhanced cell–cell interactions and hepatic functions, such as albumin secretion and urea synthesis, compared to monolayer culture [23,34,36]. The results of whole-transcriptome sequencing analysis revealed distinct differences in cell–cell interaction and cell proliferation and replication between monolayer cells and 3D spheroids. One representative finding is the upregulation of *ctnnb* in 3D spheroids. The *ctnnb1* gene encodes β-catenin; this is a major participant in the Wnt signaling pathway, which is important in liver metabolism and the development and maintenance of liver functions [37]. However, the roles of other genes within the same category according to the heatmap have not yet been fully evaluated. *Cldn* genes encode claudin, a family of proteins important in tight junction formation and function. The functions of claudin proteins remain poorly understood, except for claudin-1 [38]. Additionally, 3D spheroids had increased the expression of genes relevant to primary hepatic functions including the urea cycle, hepatic cytochrome P450, glycogen and glucose metabolism, nuclear receptors, and transcriptional factors compared to 2D cultures. These expression patterns were previously reported in other 3D human hepatocyte spheroids [20], where they were found to be similar to those of *in vivo* liver samples through whole-proteome analysis. The 3D spheroid model of hepaRG cells was more similar to liver tissue-specific gene expression profiles than monolayer cell culture [39]. The *cyp2* family (e.g., *cyp2aas* and *cyp2ks*) can be markers of endogenous and xenobiotics compounds. In addition, *cyp7a1* and *cyp39a1* are used as bile acid synthesis markers. Nuclear receptors such as *pxr* and *ppar*, which have important regulatory functions in the liver, were also more abundant in 3D spheroids compared to monolayer cells, which may indicate enhanced hepatic functionality; however, the regulation of enzymatic activity and metabolites via these receptors should be confirmed in further studies, as well as differences in the responses of related pathways. Future studies should focus on the effects of receptor ligand upregulation on xenobiotic and lipid metabolism.

The 3D spheroid culture increased vitellogenesis over time, suggesting that the spheroid model can be further developed as a suitable model system for screening reproductive toxicity. According to OECD Test Guidelines 229, 230 and 240 for *in vivo* reproductive screening assays, Vtg levels are measured as an endpoint to predict the potential reproductive effects of chemicals on fish [40-42]. Compared to the test guidelines, our model is able to measure Vtg levels in chemical exposure up to 28 days without the need for live animal

testing. Another important finding is that 3D ZFL spheroids synthesize Vtg in response to ER signaling, as shown by antibody fluorescence staining and ELISA. The transcript abundance of *vtg5* gene in the 3D spheroids was further increased through exposure to exogenous E2, whereas monolayer cells did not respond to this stimulus. Interestingly, we found a correlation between the improved Vtg synthesis by 3D ZFL spheroids and ER gene transcriptional activity. Exogenous E2 induces *esr1* and *esr2a* expression, but downregulates *esr2b* expression, in the liver [43]. Esr2a and esr2b are essential for female zebrafish reproduction: esr2a plays a vital role in follicle cell proliferation and trans-differentiation, follicle growth, and chorion formation [44] and esr2a-knockout female medaka fish (Oryzias latipes) are completely infertile [45]. Our 3D ZFL spheroids had increased *esr2a* expression compared with monolayer cells, consistent with responses observed *in vivo* during increased vitellogenesis [46]. The increased Vtg expression was also correlated with the elevation of *esr1* expression by E2 induction [47]. A previous zebrafish embryo study reported that exogenous E2 also induced *vtg1*, *3*, and *5* [48]. Similarly, 3D ZFL spheroids expressed *vtg1* and *vtg5* more actively than monolayer cells. Therefore, we propose that 3D ZFL spheroids are more receptive than monolayer cells to ER signaling and vitellogenesis activation. The results of this study also indicate that 3D ZFL spheroids are sensitive to BPA and BPS, as demonstrated by the increased Vtg intensity during exposure. BPA and BPS have been shown to bind with ERs and stimulate Vtg synthesis [5,49,50]. Interestingly, BPS had greater Vtg intensity than BPA in the present study. This tendency can be interpreted according to relative estrogenic potency (REP). Previous studies have found that BPA has higher REP in esr1 than esr2s [5,50], whereas BPS has the highest REP in esr2a among ERs [49]. These findings confirm that the 3D ZFL spheroid model responds with Vtg synthesis upon exposure to EDCs with estrogenic potency.

4.6 Summary and Conclusion

In summary, the results of this study demonstrate that 3D ZFL spheroids are advantageous to retaining hepatic functions and vitellogenesis via phenotypic and whole-RNA-Seq analysis. Compared with monolayer cells, 3D spheroids exhibited increased intercellular interactions marked by E-cadherin, as well as increased urea and Vtg synthesis activity. Interestingly, these increases in phenotypic activity were correlated with increased expression of genetic markers of hepatic functions and Vtg. Together, these findings indicate that 3D cell culture is crucial to ZFL cell sensitization and activation for transcription, and ultimately to physiological function. Therefore, this study has yielded a robust alternative *in vitro* platform to animal and primary cells for accurate and rapid *in vitro* screening of estrogenic or anti-estrogenic substances.

4.7 Acknowledgments

This research was supported by a National Research Council of Science & Technology (NST) grant by the Korean Government (MSIP, No. CAP-17-01-KIST Europe) and the Korea Institute of Science and Technology Europe Basic Research Program (Project no. 12001).

4.8 Bibliography

1. Garcia-Reyero, N.; Murphy, C.A. *A Systems Biology Approach to Advancing Adverse Outcome Pathways for Risk Assessment*, 1 ed.; Garcia-Reyero, N., Murphy, C.A., Eds.; Springer, Cham: **2018**; https://doi.org/10.1007/978-3-319-66084-4pp. 422.
2. Mills, L.J.; Chichester, C. Review of evidence: are endocrine-disrupting chemicals in the aquatic environment impacting fish populations? *The Science of the total environment* **2005**, *343*, 1-34, doi:10.1016/j.scitotenv.2004.12.070.
3. Sanderson, J.T. The steroid hormone biosynthesis pathway as a target for endocrine-disrupting chemicals. *Toxicological sciences : an official journal of the Society of Toxicology* **2006**, *94*, 3-21, doi:10.1093/toxsci/kfl051.
4. Grimaldi, M.; Boulahtouf, A.; Delfosse, V.; Thouennon, E.; Bourguet, W.; Balaguer, P. Reporter cell lines for the characterization of the interactions between human nuclear receptors and endocrine disruptors. *Frontiers in endocrinology* **2015**, *6*, 62, doi:10.3389/fendo.2015.00062.
5. Cosnefroy, A.; Brion, F.; Maillot-Maréchal, E.; Porcher, J.M.; Pakdel, F.; Balaguer, P.; Aït-Aïssa, S. Selective activation of zebrafish estrogen receptor subtypes by chemicals by using stable reporter gene assay developed in a zebrafish liver cell line. *Toxicological sciences : an official journal of the Society of Toxicology* **2012**, *125*, 439-449, doi:10.1093/toxsci/kfr297.
6. Hara, A.; Hiramatsu, N.; Fujita, T. Vitellogenesis and choriogenesis in fishes. *Fisheries Science* **2016**, *82*, 187-202, doi:10.1007/s12562-015-0957-5.
7. MacRae, C.A.; Peterson, R.T. Zebrafish as tools for drug discovery. *Nature reviews. Drug discovery* **2015**, *14*, 721-731, doi:10.1038/nrd4627.
8. Kari, G.; Rodeck, U.; Dicker, A.P. Zebrafish: an emerging model system for human disease and drug discovery. *Clinical pharmacology and therapeutics* **2007**, *82*, 70-80, doi:10.1038/sj.clpt.6100223.
9. OECD. Test no. 210: fish, early-life stage toxicity test. *OECD Publishing* **1992**.
10. OECD. Test no. 212: fish, short-term toxicity test on embryo and sac-fry stages. *OECD Publishing* **1998**.
11. OECD. Test no. 215: fish, juvenile growth test. *OECD Publishing* **2000**.
12. Ghosh, C.; Zhou, Y.L.; Collodi, P. Derivation and characterization of a zebrafish liver cell line. *Cell Biology and Toxicology* **1994**, *10*, 167-176, doi:10.1007/bf00757560.
13. Chen, D.S.; Chan, K.M. Differentially expressed proteins in zebrafish liver cells exposed to copper. *Aquatic Toxicology* **2011**, *104*, 270-277, doi:https://doi.org/10.1016/j.aquatox.2011.05.004.
14. Park, C.G.; Sung, B.; Ryu, C.S.; Kim, Y.J. Mono-(2-ethylhexyl) phthalate induces oxidative stress and lipid accumulation in zebrafish liver cells. *Comparative Biochemistry and Physiology Part C: Toxicology & Pharmacology* **2020**, *230*, 108704, doi:https://doi.org/10.1016/j.cbpc.2020.108704.
15. EU. Directive 2010/63/EU of the European parliament and of the council of 22 September 2010 on the protection of animals used for scientific purposes. *Off J EU* **2010**, *276*, 33–79.
16. Godoy, P.; Hewitt, N.J.; Albrecht, U.; Andersen, M.E.; Ansari, N.; Bhattacharya, S.; Bode, J.G.; Bolleyn, J.; Borner, C.; Bottger, J., et al. Recent advances in 2D and 3D in vitro systems using primary hepatocytes, alternative hepatocyte sources and non-parenchymal liver cells and their use in investigating mechanisms of hepatotoxicity, cell signaling and ADME. *Archives of toxicology* **2013**, *87*, 1315-1530, doi:10.1007/s00204-013-1078-5.
17. Braunbeck, T.; Segner, H. Isolation and cultivation of teleost hepatocytes. In *The Hepatocyte Review*, Berry, M.N., Edwards, A.M., Eds. Springer Netherlands: Dordrecht, 2000; https://10.1007/978-94-017-3345-8_6pp. 49-71.
18. Wallace, R.A.; Selman, K. Major protein changes during vitellogenesis and maturation of Fundulus oocytes. *Developmental Biology* **1985**, *110*, 492-498, doi:https://doi.org/10.1016/0012-1606(85)90106-X.
19. Eide, M.; Rusten, M.; Male, R.; Jensen, K.H.; Goksoyr, A. A characterization of the ZFL cell line and primary hepatocytes as in vitro liver cell models for the zebrafish (Danio rerio). *Aquatic toxicology (Amsterdam, Netherlands)* **2014**, *147*, 7-17, doi:10.1016/j.aquatox.2013.11.023.
20. Bell, C.C.; Hendriks, D.F.; Moro, S.M.; Ellis, E.; Walsh, J.; Renblom, A.; Fredriksson Puigvert, L.; Dankers, A.C.; Jacobs, F.; Snoeys, J., et al. Characterization of primary human hepatocyte spheroids as a model system for drug-induced liver injury, liver function and disease. *Scientific reports* **2016**, *6*, 25187, doi:10.1038/srep25187.
21. dit Faute, M.A.; Laurent, L.; Ploton, D.; Poupon, M.F.; Jardillier, J.C.; Bobichon, H. Distinctive

alterations of invasiveness, drug resistance and cell-cell organization in 3D-cultures of MCF-7, a human breast cancer cell line, and its multidrug resistant variant. *Clinical & experimental metastasis* **2002**, *19*, 161-168, doi:10.1023/a:1014594825502.

22. Hirschhaeuser, F.; Menne, H.; Dittfeld, C.; West, J.; Mueller-Klieser, W.; Kunz-Schughart, L.A. Multicellular tumor spheroids: an underestimated tool is catching up again. *Journal of biotechnology* **2010**, *148*, 3-15, doi:10.1016/j.jbiotec.2010.01.012.
23. Ramaiahgari, S.C.; den Braver, M.W.; Herpers, B.; Terpstra, V.; Commandeur, J.N.; van de Water, B.; Price, L.S. A 3D in vitro model of differentiated HepG2 cell spheroids with improved liver-like properties for repeated dose high-throughput toxicity studies. *Archives of toxicology* **2014**, *88*, 1083-1095, doi:10.1007/s00204-014-1215-9.
24. Tung, Y.C.; Hsiao, A.Y.; Allen, S.G.; Torisawa, Y.S.; Ho, M.; Takayama, S. High-throughput 3D spheroid culture and drug testing using a 384 hanging drop array. *The Analyst* **2011**, *136*, 473-478, doi:10.1039/c0an00609b.
25. van Roy, F.; Berx, G. The cell-cell adhesion molecule E-cadherin. *Cellular and Molecular Life Sciences* **2008**, *65*, 3756-3788, doi:10.1007/s00018-008-8281-1.
26. Capra, J.; Eskelinen, S. Correlation between E-cadherin interactions, survivin expression, and apoptosis in MDCK and ts-Src MDCK cell culture models. *Laboratory investigation; a journal of technical methods and pathology* **2017**, *97*, 1453-1470, doi:10.1038/labinvest.2017.89.
27. Luebke-Wheeler, J.L.; Nedredal, G.; Yee, L.; Amiot, B.P.; Nyberg, S.L. E-cadherin protects primary hepatocyte spheroids from cell death by a caspase-independent mechanism. *Cell transplantation* **2009**, *18*, 1281-1287, doi:10.3727/096368909x474258.
28. Zanoni, M.; Piccinini, F.; Arienti, C.; Zamagni, A.; Santi, S.; Polico, R.; Bevilacqua, A.; Tesei, A. 3D tumor spheroid models for in vitro therapeutic screening: a systematic approach to enhance the biological relevance of data obtained. *Scientific reports* **2016**, *6*, 19103, doi:10.1038/srep19103.
29. Banerjee, A.; Sahana, A.; Lohar, S.; Hauli, I.; Mukhopadhyay, S.K.; Safin, D.A.; Babashkina, M.G.; Bolte, M.; Garcia, Y.; Das, D. A rhodamine derivative as a "lock" and SCN- as a "key": visible light excitable SCN- sensing in living cells. *Chemical communications (Cambridge, England)* **2013**, *49*, 2527-2529, doi:10.1039/c3cc40582f.
30. Atkinson, D.E. Functional Roles of Urea Synthesis in Vertebrates. *Physiological Zoology* **1992**, *65*, 243-267, doi:10.1086/physzool.65.2.30158252.
31. Schmittgen, T.D.; Livak, K.J. Analyzing real-time PCR data by the comparative C(T) method. *Nature protocols* **2008**, *3*, 1101-1108.
32. Sever, R.; Glass, C.K. Signaling by nuclear receptors. *Cold Spring Harb Perspect Biol* **2013**, *5*, a016709-a016709, doi:10.1101/cshperspect.a016709.
33. Han, J.; Farnsworth, R.L.; Tiwari, J.L.; Tian, J.; Lee, H.; Ikonomi, P.; Byrnes, A.P.; Goodman, J.L.; Puri, R.K. Quality prediction of cell substrate using gene expression profiling. *Genomics* **2006**, *87*, 552-559, doi:https://doi.org/10.1016/j.ygeno.2005.11.017.
34. Jung, H.-R.; Kang, H.M.; Ryu, J.-W.; Kim, D.-S.; Noh, K.H.; Kim, E.-S.; Lee, H.-J.; Chung, K.-S.; Cho, H.-S.; Kim, N.-S., et al. Cell spheroids with enhanced aggressiveness to mimic human liver cancer in vitro and in vivo. *Scientific reports* **2017**, *7*, 10499, doi:10.1038/s41598-017-10828-7.
35. Kim, S.A.; Tai, C.-Y.; Mok, L.-P.; Mosser, E.A.; Schuman, E.M. Calcium-dependent dynamics of cadherin interactions at cell–cell junctions. *Proceedings of the National Academy of Sciences* **2011**, *108*, 9857-9862, doi:10.1073/pnas.1019003108.
36. Chua, A.C.Y.; Ananthanarayanan, A.; Ong, J.J.Y.; Wong, J.Y.; Yip, A.; Singh, N.H.; Qu, Y.; Dembele, L.; McMillian, M.; Ubalee, R., et al. Hepatic spheroids used as an in vitro model to study malaria relapse. *Biomaterials* **2019**, *216*, 119221, doi:10.1016/j.biomaterials.2019.05.032.
37. Behari, J. The Wnt/β-catenin signaling pathway in liver biology and disease. *Expert review of gastroenterology & hepatology* **2010**, *4*, 745-756, doi:10.1586/egh.10.74.
38. Roehlen, N.; Roca Suarez, A.A.; El Saghire, H.; Saviano, A.; Schuster, C.; Lupberger, J.; Baumert, T.F. Tight Junction Proteins and the Biology of Hepatobiliary Disease. *International journal of molecular sciences* **2020**, *21*, doi:10.3390/ijms21030825.
39. Kim, D.-S.; Ryu, J.-W.; Son, M.-Y.; Oh, J.-H.; Chung, K.-S.; Lee, S.; Lee, J.-J.; Ahn, J.-H.; Min, J.-S.; Ahn, J., et al. A liver-specific gene expression panel predicts the differentiation status of in vitro hepatocyte models. *Hepatology* **2017**, *66*, 1662-1674, doi:10.1002/hep.29324.
40. OECD. Test no. 229: Fish Short Term Reproduction Assay. **2012**.
41. OECD. Test no. 230: 21-day Fish Assay: A Short-Term Screening for Oestrogenic and Androgenic

Activity, and Aromatase Inhibition. **2009**.
42. OECD. Test no. 240: Medaka Extended One Generation Reproduction Test (MEOGRT). **2015**.
43. Chandrasekar, G.; Archer, A.; Gustafsson, J.-Å.; Andersson Lendahl, M. Levels of 17β-estradiol receptors expressed in embryonic and adult zebrafish following in vivo treatment of natural or synthetic ligands. *PLOS ONE* **2010**, *5*, e9678, doi:10.1371/journal.pone.0009678.
44. Lu, H.; Cui, Y.; Jiang, L.; Ge, W. Functional analysis of nuclear estrogen receptors in zebrafish reproduction by genome editing approach. *Endocrinology* **2017**, *158*, 2292-2308, doi:10.1210/en.2017-00215.
45. Kayo, D.; Zempo, B.; Tomihara, S.; Oka, Y.; Kanda, S. Gene knockout analysis reveals essentiality of estrogen receptor beta1 (Esr2a) for female reproduction in medaka. *Scientific reports* **2019**, *9*, 8868, doi:10.1038/s41598-019-45373-y.
46. Tingaud-Sequeira, A.; Knoll-Gellida, A.; Andre, M.; Babin, P.J. Vitellogenin expression in white adipose tissue in female teleost fish. *Biology of reproduction* **2012**, *86*, 38, doi:10.1095/biolreprod.111.093757.
47. Menuet, A.; Le Page, Y.; Torres, O.; Kern, L.; Kah, O.; Pakdel, F. Analysis of the estrogen regulation of the zebrafish estrogen receptor (ER) reveals distinct effects of ERalpha, ERbeta1 and ERbeta2. *Journal of molecular endocrinology* **2004**, *32*, 975-986, doi:10.1677/jme.0.0320975.
48. Hao, R.; Bondesson, M.; Singh, A.V.; Riu, A.; McCollum, C.W.; Knudsen, T.B.; Gorelick, D.A.; Gustafsson, J.A. Identification of estrogen target genes during zebrafish embryonic development through transcriptomic analysis. *PLoS One* **2013**, *8*, e79020, doi:10.1371/journal.pone.0079020.
49. Le Fol, V.; Aït-Aïssa, S.; Sonavane, M.; Porcher, J.M.; Balaguer, P.; Cravedi, J.P.; Zalko, D.; Brion, F. In vitro and in vivo estrogenic activity of BPA, BPF and BPS in zebrafish-specific assays. *Ecotoxicology and environmental safety* **2017**, *142*, 150-156, doi:10.1016/j.ecoenv.2017.04.009.
50. Pinto, C.; Hao, R.; Grimaldi, M.; Thrikawala, S.; Boulahtouf, A.; Aït-Aïssa, S.; Brion, F.; Gustafsson, J.; Balaguer, P.; Bondesson, M. Differential activity of BPA, BPAF and BPC on zebrafish estrogen receptors in vitro and in vivo. *Toxicology and applied pharmacology* **2019**, *380*, 114709, doi:10.1016/j.taap.2019.114709.

4.9 Supporting Information

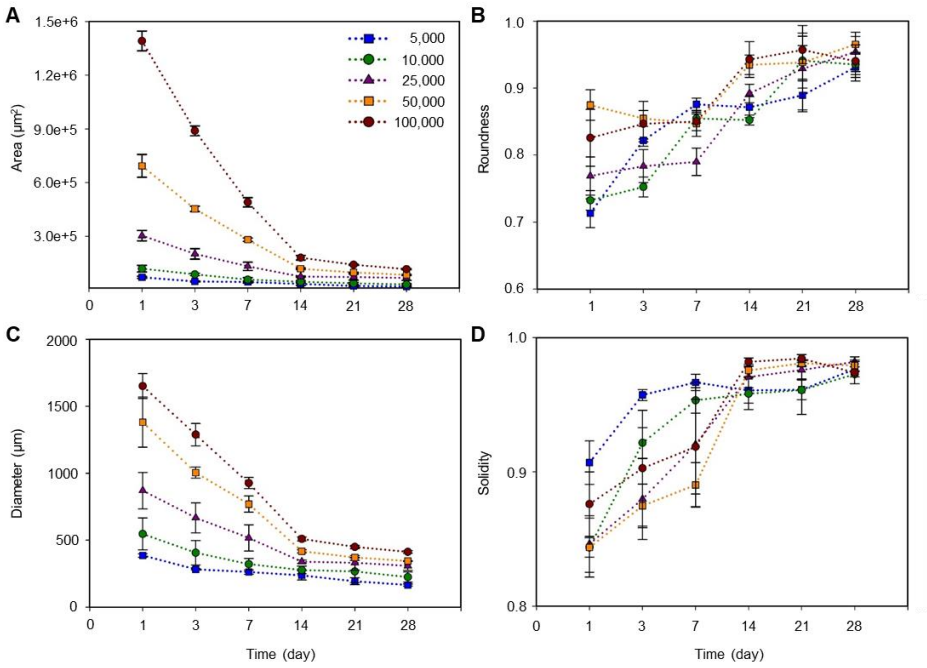

Supplementary Figure 4.1. Influence of culture time (days) on morphological parameters of 3D spheroids depending on cell numbers. (a) area, (b) roundness, (c) diameter, and (d) solidity of 3D spheroids depending on cell numbers. All parameters were analyzed by ImageJ software. The graph presents the means of five replicates of eight wells for each cell number condition, and error bars represent means ± SD (n = 5).

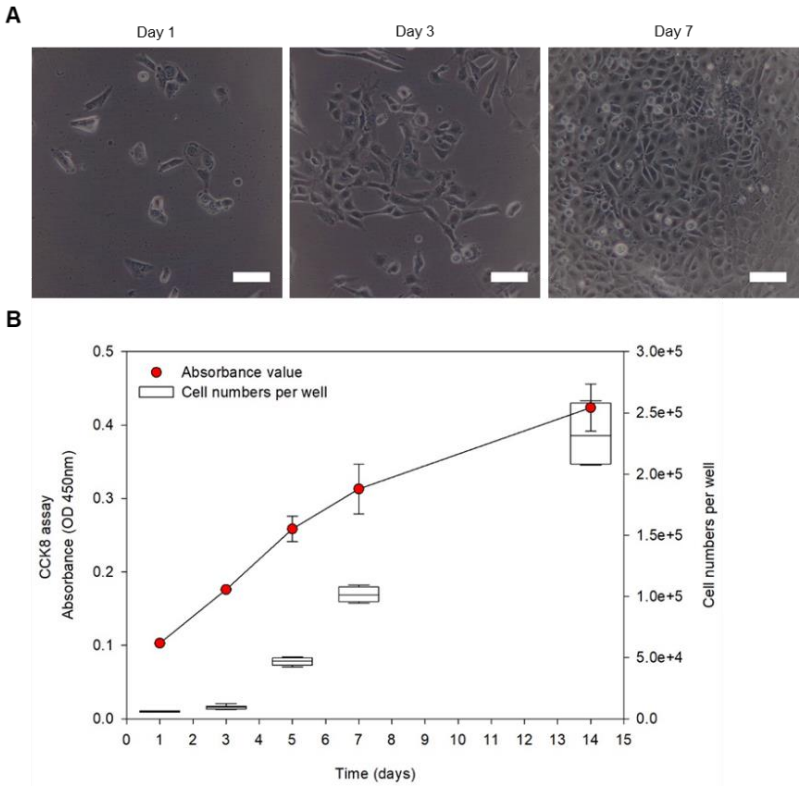

Supplementary Figure 4.2. Observations of the monolayer cell culture. The seeding density was 5,000 cells per well in a 96-well flat-bottom plate. (a) Bright-field images of monolayer cells for 7 day cultures. Scale bar: 20 μm. (b) Measurements of CCK8 assay and cell number for 14 days cultures. The graph presents the means of eight replicates of three wells for CCK8 assay and the means of five replicates of three wells for cell number. Data are expressed as mean ± SD (CCK8 assay; n = 8 and cell number; n = 5).

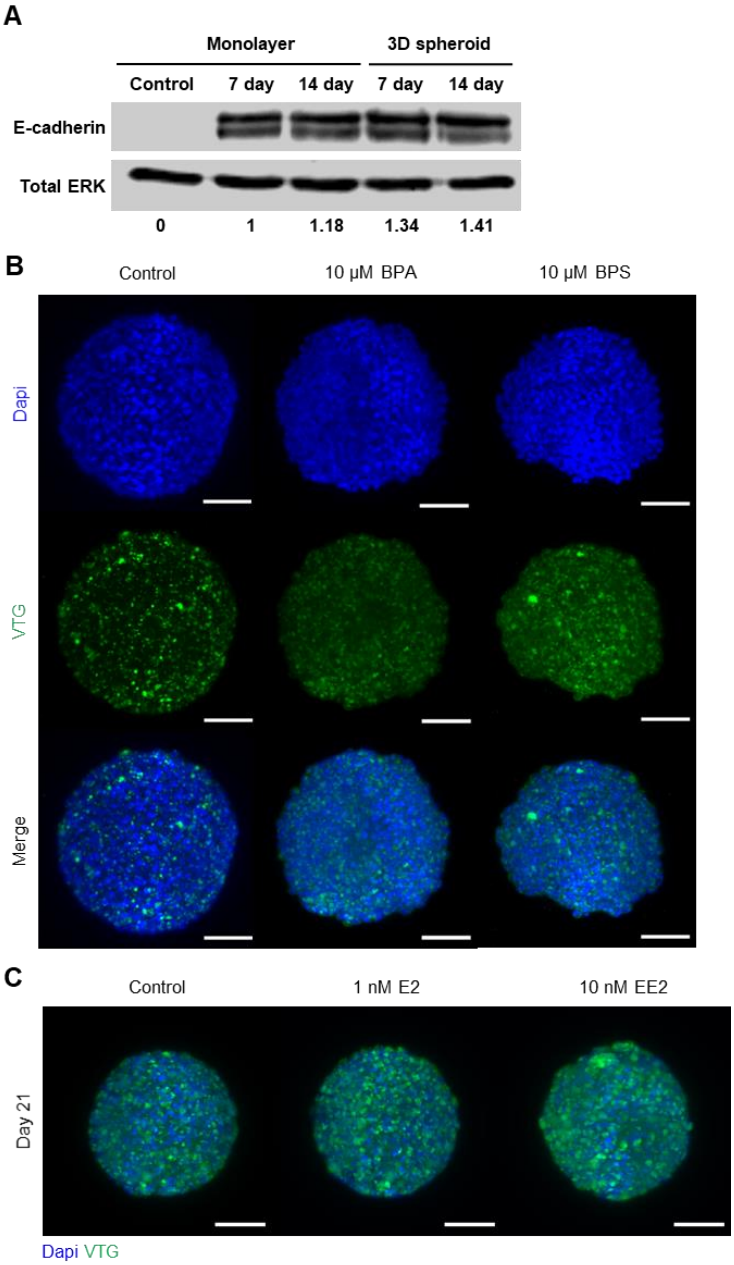

Supplementary Figure 4.3. E-cadherin protein expression and fluorescence images of vitellogenin. (a) Comparisons of E-cadherin expressions between monolayer cells and 3D spheroids. E-cadherin protein was visualized by western blot analysis. Monolayer cells and 3D spheroids were cultured for 7 and 14 days respectively. For monolayer cells, 50,000 cells/mL were seeded into each well of a 6-well flat-bottom plate; cells were collected from three wells into a tube. For 3D spheroids, 100 spheroids (5,000 cells/well) were collected into a tube. Each tube of pooled monolayer cells or spheroids was considered a sample and 15 μg of total protein from each sample was loaded and normalized by total ERK protein. (b–c) Representative fluorescence images of 3D spheroids stained with DAPI (blue) and Vtg (green) by a lightsheet microscopy.

Scale bars: 50 μm. (b) 3D spheroids (5,000 cells/well) were cultured for 7 days with charcoal stripped FBS. After that, 10 μM of BPA and BPS were treated for 48 h. (c) 3D spheroids (5,000 cells/well) were cultured for 21 days with charcoal stripped FBS. The 3D spheroids at 21 days were exposed to 1 nM of 17β-estradiol (E2) and 10 nM of 17α-ethynylestradiol (EE2) for 48 h respectively.

Supplementary Table 4.1. Statistical analysis for influence of cultivation days on area, roundness, diameter, and solidity of 3D spheroids according to cell numbers

Area (μm^2)		Cell numbers				
		5,000	10,000 *	25,000	50,000	100,000
Time (day)	1	70,308 ± 5,751 ^{a}	118,832 ± 18,419 ^{a}	303,448 ± 29,017 ^{a}	716,915 ± 70,465 ^{a}	1,391,460 ± 55,380 ^{a}
	3	47,188 ± 3,879 ^{b}	86,649 ± 7,017 ^{b}	200,977 ± 29,007 ^{b}	452,585 ± 14,720 ^{b}	889,340 ± 27,225 ^{b}
	7	43,683 ± 5,491 ^{b}	57,457 ± 11,436 ^{c}	131,659 ± 23,068 ^{bc}	280,507 ± 9,416 ^{c}	489,819 ± 25,884 ^{c}
	14	33,201 ± 8,436 ^{bc}	45,056 ± 6,691 ^{c}	74,201 ± 3,627 ^{cd}	118,396 ± 4,188 ^{d}	179,868 ± 12,646 ^{d}
	21	22,046 ± 4,067 ^{c}	36,741 ± 5,388 ^{c}	71,601 ± 17,027 ^{cd}	98,148 ± 2,741 ^{e}	144,362 ± 8,774 ^{e}
	28	18,739 ± 2,550 ^{c}	30,471 ± 4,714 ^{c}	66,603 ± 13,360 ^{d}	83,683 ± 2,999 ^{f}	115,589 ± 3,600 ^{f}
F-value		58.088	46.182	79.885	209.983	1441.411

Diameter (μm)		Cell numbers				
		5,000 *	10,000	25,000	50,000	100,000
Time (day)	1	366 ± 13 ^{a}	546 ± 60 ^{a}	870 ± 117 ^{a}	1,360 ± 158 ^{a}	1,651 ± 93 ^{a}
	3	262 ± 5 ^{b}	406 ± 35 ^{ab}	667 ± 92 ^{ab}	1,004 ± 42 ^{a}	1,288 ± 83 ^{b}
	7	222 ± 17 ^{bc}	321 ± 43 ^{b}	517 ± 29 ^{bc}	769 ± 60 ^{b}	926 ± 42 ^{c}
	14	207 ± 34 ^{cd}	277 ± 28 ^{b}	339 ± 13 ^{bc}	417 ± 12 ^{c}	510 ± 15 ^{d}
	21	153 ± 26 ^{de}	266 ± 84 ^{b}	331 ± 55 ^{c}	373 ± 5 ^{c}	449 ± 11 ^{e}
	28	125 ± 8 ^{e}	224 ± 37 ^{b}	308 ± 34 ^{c}	344 ± 3 ^{d}	413 ± 10 ^{f}
F-value		68.959	10.302	27.209	99.628	386.72

Roundness		Cell numbers				
		5,000 *	10,000 *	25,000 *	50,000 *	100,000 *
Time (day)	1	0.713 ± 0.043 ^{a}	0.732 ± 0.025 ^{a}	0.769 ± 0.028 ^{a}	0.831 ± 0.024 ^{a}	0.826 ± 0.042 ^{a}
	3	0.822 ± 0.004 ^{b}	0.752 ± 0.026 ^{ab}	0.784 ± 0.025 ^{a}	0.846 ± 0.057 ^{a}	0.847 ± 0.032 ^{a}
	7	0.876 ± 0.019 ^{bc}	0.855 ± 0.012 ^{b}	0.790 ± 0.020 ^{a}	0.847 ± 0.020 ^{a}	0.850 ± 0.014 ^{a}
	14	0.872 ± 0.031 ^{bc}	0.852 ± 0.013 ^{b}	0.892 ± 0.014 ^{b}	0.935 ± 0.015 ^{b}	0.943 ± 0.027 ^{b}
	21	0.889 ± 0.043 ^{bc}	0.941 ± 0.071 ^{bc}	0.929 ± 0.065 ^{b}	0.939 ± 0.021 ^{b}	0.937 ± 0.047 ^{b}
	28	0.931 ± 0.051 ^{c}	0.935 ± 0.034 ^{c}	0.954 ± 0.029 ^{b}	0.965 ± 0.012 ^{b}	0.940 ± 0.024 ^{b}
F-value		17.116	20.398	22.668	14.835	10.753

Solidity		Cell numbers				
		5,000	10,000	25,000	50,000	100,000 *
Time (day)	1	0.907 ± 0.032 ^{a}	0.844 ± 0.013 ^{a}	0.846 ± 0.021 ^{a}	0.832 ± 0.029 ^{a}	0.876 ± 0.024 ^{a}
	3	0.957 ± 0.007 ^{b}	0.922 ± 0.020 ^{b}	0.880 ± 0.030 ^{a}	0.875 ± 0.016 ^{a}	0.903 ± 0.043 ^{a}
	7	0.967 ± 0.012 ^{b}	0.953 ± 0.017 ^{b}	0.920 ± 0.046 ^{ab}	0.890 ± 0.017 ^{a}	0.919 ± 0.035 ^{a}
	14	0.960 ± 0.019 ^{b}	0.958 ± 0.020 ^{b}	0.971 ± 0.008 ^{b}	0.976 ± 0.005 ^{b}	0.982 ± 0.003 ^{b}
	21	0.961 ± 0.015 ^{b}	0.961 ± 0.032 ^{b}	0.976 ± 0.007 ^{b}	0.980 ± 0.003 ^{b}	0.983 ± 0.004 ^{b}
	28	0.978 ± 0.004 ^{b}	0.973 ± 0.005 ^{b}	0.982 ± 0.004 ^{b}	0.979 ± 0.004 ^{b}	0.974 ± 0.008 ^{b}
F-value		8.84	24.976	21.268	56.365	14.993

A comparison between the days was performed using a one-way ANOVA test ($p < 0.05$, Dunnett T3 test for non-homogeneity of variance and Scheffe test for homogeneity of variance (asterisk)). Different letters within the same cell numbers denote significant differences.

Supplementary Table 4.2. Gene function in the heat map of urea cycle

Number	Gene name (Zebrafish)	Main function (Predicted: referred from Zebrafish Information Network, ZFIN)	Synteny gene name (Human)	Reference
1	*arg1*	Predicted: Arginase and manganese ion binding activities; arginine catabolic process to ornithine	*arg1*	Caldovic et al., 2014; LeMoine and Walsh, 2013; ZFIN*
2	*pycr3*	Predicted: Pyrroline-5-carboxylate reductase activity; L-proline biosynthetic process	*pycr3*	ZFIN*
3	*ass1*	Predicted: Argininosuccinate synthase activity; arginine biosynthetic process; argininosuccinate metabolic process; and urea cycle	*ass1*	Caldovic et al., 2014; LeMoine and Walsh, 2013; ZFIN*
4	*cad*	Predicted: Aspartate carbamoyltransferase and dihydroorotase activities; pyrimidine nucleobase biosynthetic process; cranial nerve morphogenesis; and regulation of signal transduction	*cad*	ZFIN*
5	*otc*	Predicted: Ornithine carbamoyltransferase activity; arginine biosynthetic process via ornithine and citrulline biosynthetic process	*otc*	Caldovic et al., 2014; LeMoine and Walsh, 2013; ZFIN*
6	*pycr1b*	Predicted: Pyrroline-5-carboxylate reductase activity; brain development	*pycr1*	ZFIN*
7	*acy1*	Predicted: Aminoacylase activity; cellular amino acid metabolic process	*acy1*	Caldovic et al., 2014; ZFIN*
8	*gatm*	Predicted: Glycine amidinotransferase activity; creatine biosynthetic process	*gatm*	ZFIN*
9	*oat*	Predicted: Identical protein binding activity; ornithine-oxo-acid transaminase activity; pyridoxal phosphate binding activity; and arginine catabolic process to glutamate and arginine catabolic process to proline via ornithine	*oat*	ZFIN*
11	*glud1a*	Predicted: Glutamate dehydrogenase (NAD+) activity; glutamate catabolic process	*glud1*	ZFIN*
12	*cps1*	Carbamoyl-phosphate synthase (ammonia) activity; ammonium homeostasis and urea cycle	*cps1*	Caldovic et al., 2014; LeMoine and Walsh, 2013; ZFIN*
13	*pycr1a*	Predicted: Pyrroline-5-carboxylate reductase activity; L-proline biosynthetic process.	*pycr1*	ZFIN*

14	*odc1*	Predicted: Ornithine decarboxylase activity; eye photoreceptor cell development	*odc1*	ZFIN*
15	*bbox1*	Predicted: Gamma-butyrobetaine dioxygenase activity; carnitine biosynthetic process	*bbox1*	ZFIN*
16	*dio1*	Predicted: Thyroxine 5'-deiodinase activity; regulation of neural retina development	*dio1*	ZFIN*
17	*asl*	Predicted: Argininosuccinate lyase activity; arginine biosynthetic process via ornithine	*asl*	Caldovic et al., 2014; LeMoine and Walsh, 2013; ZFIN*
18	*arg2*	Predicted: Arginase activity and manganese ion binding activity; arginine catabolic process to ornithine	*arg2*	Caldovic et al., 2014; LeMoine and Walsh, 2013; ZFIN*

*ZFIN: Gene data for this paper were retrieved from the Zebrafish Information Network (ZFIN), University of Oregon, Eugene, OR 97403-5274; URL: http://zfin.org/

Supplementary Table 4.3. Gene function in the heat map of vitellogenin

Number	Gene name (Zebrafish)	Main function (Predicted: referred from Zebrafish Information Network)	Synteny gene name (Human)	Reference
1	*vtg1*	Exhibits antioxidant activity; cellular response to estrogen stimulus; response to estradiol; and response to xenobiotic stimulus	-	Sullivan and Yilmaz, 2018; ZFIN*
2	*vtg3*	Predicted: Lipid transporter activity; cellular response to estrogen stimulus	-	Sullivan and Yilmaz, 2018; ZFIN*
3	*vtg4*	Predicted: Lipid transporter activity; cellular response to estrogen stimulus and response to estradiol	-	Sullivan and Yilmaz, 2018; ZFIN*
4	*vtg5*	Predicted: Lipid transporter activity; cellular response to estrogen stimulus and response to estradiol	-	Sullivan and Yilmaz, 2018; ZFIN*

*ZFIN: Gene data for this paper were retrieved from the Zebrafish Information Network (ZFIN), University of Oregon, Eugene, OR 97403-5274; URL: http://zfin.org/

Supplementary Table 4.4. Gene function in the heat map of cytochrome P450

Number	Gene name (Zebrafish)	Main function (Predicted: referred from Zebrafish Information Network)	Synteny gene name (Human)	Reference
1	*cyp2k8*	Predicted: Metabolic functions targeting endogenous and xenobiotics compounds; heme binding activity; oxidoreductase activity, acting on paired donors, with incorporation or reduction of molecular oxygen, reduced flavin or flavoprotein as one donor, and incorporation of one atom of oxygen; and steroid hydroxylase activity	*cyp2w1*	Goldstone et al., 2010; Gomez et al., 2010; Guo et al., 2016; Saad et al., 2016; ZFIN*

2	*cyp1d1*	Metabolic functions targeting endogenous and xenobiotics compounds; testosterone 6-beta-hydroxylase activity	*cyp1d1*	Goldstone et al., 2009; Goldstone et al., 2010; Scornaienchi et al., 2010; ZFIN*
3	*cyp2aa7*	Predicted: Metabolic functions targeting endogenous and xenobiotics compounds; heme binding activity; oxidoreductase activity, acting on paired donors, with incorporation or reduction of molecular oxygen, reduced flavin or flavoprotein as one donor, and incorporation of one atom of oxygen; and steroid hydroxylase activity	-	Goldstone et al., 2010; Kubota et al., 2013; Kubota et al., 2015; ZFIN*
4	*cyp2k19*	Metabolic functions related to Metabolism/oxidoreductase Members of this xenobiotic CYP family	*cyp2w1*	Goldstone et al., 2010; Gomez et al., 2010; Guo et al., 2016; Saad et al., 2016; ZFIN*
5	*cyp2aa11*	Predicted: Metabolic functions targeting endogenous and xenobiotics compounds; heme binding activity; oxidoreductase activity, acting on paired donors, with incorporation or reduction of molecular oxygen, reduced flavin or flavoprotein as one donor, and incorporation of one atom of oxygen; and steroid hydroxylase activity	-	Goldstone et al., 2010; Kubota et al., 2013; Kubota et al., 2015; ZFIN*
6	*cyp2ae1*	Predicted: Metabolic functions targeting endogenous and xenobiotics compounds; heme binding activity; oxidoreductase activity, acting on paired donors, with incorporation or reduction of molecular oxygen, reduced flavin or flavoprotein as one donor, and incorporation of one atom of oxygen; and steroid hydroxylase activity	-	Goldstone et al., 2010; Saad et al., 2016; ZFIN*
7	*cyp17a2*	Steroid 17-alpha-monooxygenase activity; Progesterone metabolic process	*cyp17a1*	Goldstone et al., 2010; Zhou et al., 2007a; Zhou et al., 2007b; ZFIN*
8	*cyp2u1*	Predicted: Metabolic functions targeting endogenous and xenobiotics compounds; heme binding activity; oxidoreductase activity, acting on paired donors, with incorporation or reduction of molecular oxygen, reduced flavin or flavoprotein as one donor, and incorporation of one atom of oxygen; and steroid hydroxylase activity	*cyp2u1*	Chuang et al., 2004; Goldstone et al., 2010; ZFIN*
9	*cyp7a1*	Rate-limiting factor for synthesizing bile acids; steroid hydroxylase activity; bile acid biosynthetic process and cholesterol homeostasis	*cyp7a1*	Enya et al., 2018; Goldstone et

				al., 2010; ZFIN*
10	*cyp2v1*	Predicted: Metabolic functions targeting endogenous and xenobiotics compounds; heme binding activity; oxidoreductase activity, acting on paired donors, with incorporation or reduction of molecular oxygen, reduced flavin or flavoprotein as one donor, and incorporation of one atom of oxygen; and steroid hydroxylase activity	*cyp2j2*	Goldstone et al., 2010; ZFIN*
11	*cyp39a1*	Predicted: Oxysterol 7-alpha-hydroxylase and steroid 7-alpha-hydroxylase activities; bile acid biosynthetic process and cholesterol homeostasis	*cyp39a1*	Goldstone et al., 2010; Jelinek and Russell, 1990; ZFIN*
12	*cyp17a1*	17-alpha,20-alpha-dihydroxypregn-4-en-3-one dehydrogenase, 17-alpha-hydroxyprogesterone aldolase, and steroid 17-alpha-monooxygenase activities; androst-4-ene-3,17-dione biosynthetic process; female sex determination; and progesterone metabolic process.	*cyp17a1*	DeVore and Scott, 2012; Goldstone et al., 2010; ZFIN*; Zhai et al., 2017; Zhai et al., 2018
13	*cyp2ad3*	Predicted: Metabolic functions targeting endogenous and xenobiotics compounds; heme binding activity; oxidoreductase activity, acting on paired donors, with incorporation or reduction of molecular oxygen, reduced flavin or flavoprotein as one donor, and incorporation of one atom of oxygen; and steroid hydroxylase activity	*cyp2j2*	Goldstone et al., 2010; ZFIN*
14	*cyp2ad6*	Predicted: Metabolic functions targeting endogenous and xenobiotics compounds; heme binding activity; oxidoreductase activity, acting on paired donors, with incorporation or reduction of molecular oxygen, reduced flavin or flavoprotein as one donor, and incorporation of one atom of oxygen; and steroid hydroxylase activity	*cyp2j2*	Goldstone et al., 2010; ZFIN*
15	*cyp11c1*	Catalyze the formation of cortisol and 11-Ketotestosterone (11-KT) Prediced: heme binding, iron ion binding, and oxidoreductase activities	-	Goldstone et al., 2010; ZFIN*; Zhang et al., 2020; Zheng et al., 2020
16	*cyp26a1*	Controls retinoic acid (RA) homeostasis by metabolizing RA into bioinactive metabolites; animal organ development; cellular response to vitamin A	*cyp26a1/c1*	Emoto et al., 2005; Goldstone et al., 2010; Hu et al., 2008; Topletz et al., 2012; ZFIN*

17	*cyp4f3*	Predicted: heme binding, iron ion binding, and oxidoreductase activites; oxidation-reduction process.	*cyp4f*	Goldstone et al., 2010; Hardwick, 2008; Kalsotra and Strobel, 2006; ZFIN*
18	*cyp27b1*	Conversion of prohormone 25-hydroxyvitamin D3 (25D) to active 1,25-dihydroxyvitamin D3 (1,25D); hematopoietic stem cell proliferation	-	Chun et al., 2014; Goldstone et al., 2010; ZFIN*

*ZFIN: Gene data for this paper were retrieved from the Zebrafish Information Network (ZFIN), University of Oregon, Eugene, OR 97403-5274; URL: http://zfin.org/

Supplementary Table 4.5. Gene function in the heat map of glycogen and glucose metabolism

Number	Gene name (Zebrafish)	Main function (Predicted: referred from Zebrafish Information Network)	Synteny gene name (Human)	Reference
1	*slc37a4a*	Predicted: Symporter activity; transmembrane transport	*slc37a4*	Van Schaftingen and Gerin, 2002; ZFIN*
2	*ppp1r3cb*	Predicted: Glycogen binding and protein phosphatase 1 binding activities; glycogen biosynthetic process and regulation of glycogen biosynthetic process	*ppp1r3c*	ZFIN*
3	*enpp6*	Predicted: Glycerophosphocholine cholinephosphodiesterase and glycerophosphodiester phosphodiesterase activities; choline metabolic process and lipid metabolic process	*enpp6*	Massé et al, 2010; ZFIN*
4	*pgm1*	Predicted: Phosphoglucomutase activity; carbohydrate metabolic process	*pgm1*	ZFIN*
5	*g6pc1b*	Predicted: Glucose-6-phosphatase activity; gluconeogenesis and glucose 6-phosphate metabolic process	*g6pc*	ZFIN*
6	*gcgra*	Glucagon receptor activity and peptide hormone binding activities; regulation of glucose metabolic process.	*gcgr*	Li et al, 2015; ZFIN*
7	*pdk2a*	Predicted: Protein serine/threonine kinase activity; glucose homeostasis and negative regulation of pyruvate dehydrogenase activity	*pdk2*	ZFIN*
8	*gbe1b*	Predicted: 1,4-alpha-glucan branching enzyme activity; glycogen biosynthetic process	*gbe1*	ZFIN*
9	*enpp5*	Predicted: Catalytic activity	*enpp5*	ZFIN*
10	*cps1*	Carbamoyl-phosphate synthase (ammonia) activity; ammonium homeostasis and urea cycle.	*cps1*	Caldovic et al, 2014; ZFIN*

11	*pdk4*	Predicted: protein serine/threonine kinase activity; glucose homeostasis and negative regulation of pyruvate dehydrogenase activity	*pdk4*	ZFIN*
12	*wdtc1*	Predicted: negative regulation of fatty acid biosynthetic process	*wdtc1*	ZFIN*
13	*crema*	Predicted: DNA binding and DNA-binding transcription factor activities; regulation of transcription and DNA-templated	*crema*	ZFIN*
14	*pdk2b*	Predicted: Protein serine/threonine kinase activity; glucose homeostasis and negative regulation of pyruvate dehydrogenase activity.	*pdk2*	ZFIN*
15	*irs1*	Predicted: Insulin receptor binding and phosphatidylinositol 3-kinase binding activities.	*irs1*	ZFIN*
16	*pik3r1*	Predicted: 1-phosphatidylinositol-3-kinase regulator activity; in insulin receptor signaling pathway; phosphatidylinositol phosphorylation; and regulation of phosphatidylinositol 3-kinase activity	*pik3r1*	ZFIN*

*ZFIN: Gene data for this paper were retrieved from the Zebrafish Information Network (ZFIN), University of Oregon, Eugene, OR 97403-5274; URL: http://zfin.org/

Supplementary Table 4.6. Gene function in the heat map of nuclear receptors and transcription factors

Number	Gene name (Zebrafish)	Main function (Predicted: referred from Zebrafish Information Network)	Synteny gene name (Human)	Reference
1	*esr1*	Estrogen receptor, nuclear receptor, and steroid hormone binding activities; cellular response to estrogen stimulus; posterior lateral line neuromast primordium migration; and response to estradiol	*esr1*	Novac and Heinzel, 2004; Schaaf, 2017; ZFIN*
2	*esr2a*	Estrogen receptor, nuclear receptor, and steroid hormone binding activities; reponse to estrogen	*esr2*	Novac and Heinzel, 2004; Schaaf, 2017; ZFIN*
3	*raraa*	Nuclear receptor activity; hindbrain morphogenesis; liver development; and response to retinoic acid	*rara*	Novac and Heinzel, 2004; Schaaf, 2017; ZFIN*
4	*rxrgb*	Predicted: Nuclear receptor and retinoic acid-responsive element binding activities; positive regulation of transcription by RNA polymerase II; response to retinoic acid; and retinoic acid receptor signaling pathway	*rxrg*	Novac and Heinzel, 2004; Schaaf, 2017; ZFIN*
5	*pparda*	Sequence-specific DNA binding activity; neural crest cell development and response to activity	*ppard*	Novac and Heinzel, 2004; Schaaf, 2017; ZFIN*
6	*arnt1b*	Chromatin binding activity; contribution to DNA binding activity; photoperiodism and positive regulation of gene expression	*arnt*	Novac and Heinzel, 2004; Schaaf, 2017; ZFIN*

7	*thrb*	Nuclear receptor activity; regulation of transcription and DNA-templated; sensory organ development; and thyroid hormone mediated signaling pathway	*thrb*	Novac and Heinzel, 2004; Schaaf, 2017; ZFIN*
8	*nr1i2*	Nuclear receptor and steroid hormone receptor activities; regulation of transcription and DNA-templated; response to toxic substance; and transcription by RNA polymerase II	*nr1i2*	Novac and Heinzel, 2004; Schaaf, 2017; ZFIN*
9	*pgr*	Steroid binding and steroid hormone receptor activities; luteinizing hormone signaling pathway and ovulation.	*pgr*	Novac and Heinzel, 2004; Schaaf, 2017; ZFIN*
10	*ppardb*	Predicted: DNA-binding transcription factor activity; RNA polymerase II-specific and RNA polymerase II cis-regulatory region sequence-specific DNA binding activity; RNA polymerase II repressing transcription factor binding activity; negative regulation of cholesterol storage; positive regulation of fatty acid metabolic process; and regulation of transcription by RNA polymerase II	*ppard*	Novac and Heinzel, 2004; Schaaf, 2017; ZFIN*
11	*nr2c2*	Predicted: RNA polymerase II cis-regulatory region sequence-specific DNA binding and nuclear receptor activities; cell differentiation; positive regulation of embryonic development; and positive regulation of transcription by RNA polymerase II	*nr2c2*	Novac and Heinzel, 2004; Schaaf, 2017; ZFIN*
12	*esr2b*	Exhibits estrogen receptor, nuclear receptor, and steroid hormone binding activities; response to estrogen	*esr2*	Novac and Heinzel, 2004; Schaaf, 2017; ZFIN*
13	*pparaa*	Predicted: DNA-binding transcription factor activity; RNA polymerase II-specific and RNA polymerase II cis-regulatory region sequence-specific DNA binding activity; RNA polymerase II repressing transcription factor binding activity; negative regulation of cholesterol storage; positive regulation of fatty acid metabolic process; and regulation of transcription by RNA polymerase II	*ppara*	Novac and Heinzel, 2004; Schaaf, 2017; ZFIN*
14	*arnt2*	DNA-binding transcription factor activity; animal organ development; neuron differentiation; and response to hypoxia	*arnt2*	Novac and Heinzel, 2004; Schaaf, 2017; ZFIN*
15	*rarab*	Predicted: RNA polymerase II cis-regulatory region sequence-specific DNA binding activity and nuclear receptor activity; animal organ development and pectoral fin development	*rara*	Novac and Heinzel, 2004; Schaaf, 2017; ZFIN*
16	*nr2c2ap*	Unkown	*nr2c2ap*	Novac and Heinzel, 2004; Schaaf, 2017; ZFIN*
17	*ahr2*	Nuclear receptor and sequence-specific DNA binding activities; contribution to DNA	*ahr*	Novac and Heinzel, 2004;

		binding activity; including fin development; ovarian follicle development; and positive regulation of transcription by RNA polymerase II		Schaaf, 2017; ZFIN*
18	*erbb3a*	Predicted: neuregulin binding, neuregulin receptor, and transmembrane receptor protein tyrosine kinase activities; positive regulation of cell population proliferation; positive regulation of kinase activity; and transmembrane receptor protein tyrosine kinase signaling pathway	*erbb3*	Novac and Heinzel, 2004; Schaaf, 2017; ZFIN*
19	*rxraa*	Predicted: Nuclear receptor and retinoic acid-responsive element binding activities; regulation of transcription by RNA polymerase II; response to retinoic acid; and retinoic acid receptor signaling pathway	*rxra*	Novac and Heinzel, 2004; Schaaf, 2017; ZFIN*
20	*thraa*	Nuclear receptor activity; regulation of transcription by RNA polymerase II; thyroid hormone mediated signaling pathway; and ventricular system development.	*thra*	Novac and Heinzel, 2004; Schaaf, 2017; ZFIN*
21	*ahr1b*	DNA-binding transcription factor and RNA polymerase II-specific and ligand-activated transcription factor activities	*ahr*	Novac and Heinzel, 2004; Schaaf, 2017; ZFIN*

*ZFIN: Gene data for this paper were retrieved from the Zebrafish Information Network (ZFIN), University of Oregon, Eugene, OR 97403-5274; URL: http://zfin.org/

Supplementary Bibliography

Caldovic, L., Haskins, N., Mumo, A., Majumdar, H., Pinter, M., Tuchman, M., Krufka, A. Expression pattern and biochemical properties of zebrafish N-Acetylglutamate synthase. *PLoS ONE* **2014**, *9*, e85597. doi:10.1371/journal.pone.0085597

Chuang, S. S., Helvig, C., Taimi, M., Ramshaw, H. A., Collop, A. H., Amad, M., White, J. A., Petkovich, M., Jones, G., Korczak, B. CYP2U1, a novel human thymus- and brain-specific cytochrome P450, catalyzes omega- and (omega-1)-hydroxylation of fatty acids. *J Biol Chem* **2004**, *279*, 6305-14. doi: 10.1074/jbc.M311830200

Chun, R. F., Blatter, E., Elliott, S., Fitz-Gibbon, S., Rieger, S., Sagasti, A., Adams, J. S., Hewison, M. Cloning of a functional 25-hydroxyvitamin D-1α-hydroxylase in zebrafish (Danio rerio). *Cell Biochem Funct* **2014**, *32*, 675-82. doi: 10.1002/cbf.3071

DeVore, N. M., and Scott, E. E. Structures of cytochrome P450 17A1 with prostate cancer drugs abiraterone and TOK-001. *Nature* **2012**, *482*, 116-9. doi: 10.1038/nature10743

Emoto, Y., Wada, H., Okamoto, H., Kudo, A., Imai, Y. Retinoic acid-metabolizing enzyme Cyp26a1 is essential for determining territories of hindbrain and spinal cord in zebrafish. *Dev Biol* **2005**, *278*, 415-27. doi: 10.1016/j.ydbio.2004.11.023

Enya, S., Kawakami, K., Suzuki, Y., Kawaoka, S. A novel zebrafish intestinal tumor model reveals a role for cyp7a1-dependent tumor-liver crosstalk in causing adverse effects on the host. *Dis Model Mech* **2018**, *11*, dmm032383. doi: 10.1242/dmm.032383

Goldstone, J. V., Jönsson, M. E., Behrendt, L., Woodin, B. R., Jenny, M. J., Nelson, D. R., Stegeman, J.J. Cytochrome P450 1D1: a novel CYP1A-related gene that is not transcriptionally activated by PCB126 or TCDD. *Arch Biochem Biophys* **2009**, *482*, 7-16. doi: 10.1016/j.abb.2008.12.002

Goldstone, J. V., McArthur, A. G., Kubota, A., Zanette, J., Parente, T., Jönsson, M. E., Nelson, D. R., Stegeman, J.J. Identification and developmental expression of the full complement of Cytochrome P450 genes in Zebrafish. *BMC Genomics* **2010**, *11*, 643. https://doi.org/10.1186/1471-2164-11-643

Gomez, A., Nekvindova, J., Travica, S., Lee, M. Y., Johansson, I., Edler, D., Mkrtchian, S., Ingelman-Sundberg, M. Colorectal cancer-specific cytochrome P450 2W1: intracellular localization,

glycosylation, and catalytic activity. *Mol Pharmacol* **2010**, *78*, 1004-11. doi: 10.1124/mol.110.067652

Guo, J., Johansson, I., Mkrtchian, S., Ingelman-Sundberg, M. The CYP2W1 enzyme: regulation, properties and activation of prodrugs. *Drug Metab Rev* **2016**, *48*, 369-78. doi: 10.1080/03602532.2016.1188939

Hardwick, J. P. Cytochrome P450 omega hydroxylase (CYP4) function in fatty acid metabolism and metabolic diseases. *Biochem Pharmacol* **2008**, *75*, 2263-75. doi: 10.1016/j.bcp.2008.03.004

Hu, P., Tian, M., Bao, J., Xing, G., Gu, X., Gao, X., Linney, E., Zhao, Q. Retinoid regulation of the zebrafish cyp26a1 promoter. *Dev Dyn* **2008**, *237*, 3798-808. doi: 10.1002/dvdy.21801

Jelinek, D. F., and Russell, D. W. Structure of the rat gene encoding cholesterol 7 alpha-hydroxylase. *Biochemistry* **1990**, *29*, 7781-5. doi: 10.1021/bi00486a001

Kalsotra, A., and Strobel, H. W. Cytochrome P450 4F subfamily: at the crossroads of eicosanoid and drug metabolism. *Pharmacol Ther* **2006**, *112*, 589-611. doi: 10.1016/j.pharmthera.2006.03.008

Kubota, A., Bainy, A. C., Woodin, B. R., Goldstone, J. V., Stegeman, J. J. The cytochrome P450 2AA gene cluster in zebrafish (Danio rerio): expression of CYP2AA1 and CYP2AA2 and response to phenobarbital-type inducers. *Toxicol Appl Pharmacol* **2013**, *272*, 172-9. doi: 10.1016/j.taap.2013.05.017

Kubota, A., Goldstone, J. V., Lemaire, B., Takata, M., Woodin, B. R., Stegeman, J. J. Role of pregnane X receptor and aryl hydrocarbon receptor in transcriptional regulation of pxr, CYP2, and CYP3 genes in developing zebrafish. *Toxicol Sci* **2015**, *143*, 398-407. doi: 10.1093/toxsci/kfu240

Li, M., Dean, E. D., Zhao, L., Nicholson, W. E., Powers, A. C., Chen, W. Glucagon receptor inactivation leads to α-cell hyperplasia in zebrafish. *J Endocrinol* **2015**, *227*, 93-103. doi: 10.1530/JOE-15-0284

LeMoine, C. M., and Walsh, P. J. Ontogeny of ornithine-urea cycle gene expression in zebrafish (Danio rerio). *American journal of physiology. Regulatory, integrative and comparative physiology* **2013**, *304*, R991-R1000. 10.1152/ajpregu.00411.2012

Massé, K., Bhamra, S., Allsop, G., Dale, N., Jones, E. A. Ectophosphodiesterase/nucleotide phosphohydrolase (Enpp) nucleotidases: cloning, conservation and developmental restriction. *Int J Dev Biol* **2010**, *54*, 181-93. doi: 10.1387/ijdb.092879km

Novac, N., and Heinzel, T. Nuclear receptors: overview and classification. *Curr Drug Targets Inflamm Allergy.* **2004**, *3*, 335-46. doi: 10.2174/1568010042634541

Saad, M., Cavanaugh, K., Verbueken, E., Pype, C., Casteleyn, C., Van Ginneken, C., Van Cruchten, S. Xenobiotic metabolism in the zebrafish: a review of the spatiotemporal distribution, modulation and activity of Cytochrome P450 families 1 to 3. *J Toxicol Sci* **2016**, *41*, 1-11. doi: 10.2131/jts.41.1

Schaaf, M. J. M. Nuclear receptor research in zebrafish. *J Mol Endocrinol* **2017**, *59*, R65-R76. doi: 10.1530/JME-17-0031

Scornaienchi, M. L., Thornton, C., Willett, K. L., Wilson, J. Y. Functional differences in the cytochrome P450 1 family enzymes from zebrafish (Danio rerio) using heterologously expressed proteins. *Arch Biochem Biophys.* **2010**, *502*, 17-22. doi: 10.1016/j.abb.2010.06.018

Sullivan, C., and Yilmaz, O. Vitellogenesis and Yolk Proteins, Fish. **2018**, 10.1016/B978-0-12-809633-8.20567-0

Van Schaftingen, E., and Gerin, I. The glucose-6-phosphatase system. *Biochem J* **2002**, *362*, 513-32. doi: 10.1042/0264-6021:3620513

Topletz, A. R., Thatcher, J. E., Zelter, A., Lutz, J. D., Tay, S., Nelson, W. L., Isoherranen, N. Comparison of the function and expression of CYP26A1 and CYP26B1, the two retinoic acid hydroxylases. *Biochem Pharmacol* **2012**, *83*, 149-63. doi: 10.1016/j.bcp.2011.10.007

Zhai, G., Shu, T., Xia, Y., Jin, X., He, J., Yin, Z. Androgen signaling regulates the transcription of anti-Müllerian hormone via synergy with SRY-related protein SOX9A. *Science Bulletin* **2017**, *62*, 197-203. https://doi.org/10.1016/j.scib.2017.01.007

Zhai, G., Shu, T., Xia, Y., Lu, Y., Shang, G., Jin, X., He, J., Nie, P., Yin, Z. Characterization of sexual trait development in cyp17a1-deficient Zebrafish. *Endocrinology* **2018**, *159*, 3549-3562. https://doi.org/10.1210/en.2018-00551

Zhang, Q., Ye, D., Wang, H., Wang, Y., Hu, W., Sun, Y. Zebrafish cyp11c1 knockout reveals the roles of 11-ketotestosterone and cortisol in sexual development and reproduction. *Endocrinology* **2020**, *161*, bqaa048. https://doi.org/10.1210/endocr/bqaa048

Zheng, Q., Xiao, H., Shi, H., Wang, T., Sun, L., Tao, W., Kocher, T. D., Li, M., Wang, D. Loss of Cyp11c1 causes delayed spermatogenesis due to the absence of 11-ketotestosterone. *J Endocrinol* **2020**, *244*, 487-499. doi: 10.1530/JOE-19-0438

Zhou, L. Y., Wang, D. S., Kobayashi, T., Yano, A., Paul-Prasanth, B., Suzuki, A., Sakai, F., Nagahama, Y. A novel type of P450c17 lacking the lyase activity is responsible for C21-steroid biosynthesis in the fish ovary and head kidney. *Endocrinology* **2007a**, *148*, 4282-91. doi: 10.1210/en.2007-0487

Zhou, L. Y., Wang, D. S., Shibata, Y., Paul-Prasanth, B., Suzuki, A., Nagahama, Y. Characterization, expression and transcriptional regulation of P450c17-I and -II in the medaka, Oryzias latipes. *Biochem Biophys Res Commun.* **2007b**, *362*, 619-25. doi: 10.1016/j.bbrc.2007.08.044

Chapter 5. Zebrafish liver cell cluster culture on collagen-based hydrogels

Contributions

As published in: Kathryn M. Sullivan, **Chang Gyun Park**, John D Ito, Mikhail Eugene Kandel, Gabriel Popescu, Young Jun Kim, and Hyunjoon Kong, "Matrix softness-mediated 3D zebrafish hepatocyte modulates response to endocrine disrupting chemicals" *Environmental science & technology* **2020**, *54*(21), 13797–13806. https://doi.org/10.1021/acs.est.0c01988

Authorship contributions

Kathryn M. Sullivan: writing - original draft, data curation, formal analysis, writing - review & editing
Chang Gyun Park: writing - original draft, data curation, formal analysis, writing - review & editing
John D Ito: formal analysis, methodology, writing - review & editing.
Mikhail Eugene Kandel: formal analysis, writing - review & editing.
Gabriel Popescu: methodology, investigation, writing - review & editing.
Young Jun Kim: writing - original draft, conceptualization, funding acquisition, investigation, methodology, writing - review & editing.
Hyunjoon Kong: writing - original draft, conceptualization, funding acquisition, investigation, methodology, writing - review & editing.

Relation to the thesis

There are significant ethical and methodological concerns for using zebrafish as model organisms for testing EDCs, as well as aquatic environmental risks from EDC accumulation. The 3Rs are essential values in legislation and guidelines governing the ethical use of animals in experiments. Hence, there is an ethical obligation to minimize the pain, stress, and suffering of fish, although there is still debate about whether fish can experience pain or have consciousness. Methodological challenges include de-differentiation of primary zebrafish tissues for *ex vivo* cultures on conventional cell culture substrates. Therefore, the engineered *in vitro* zebrafish liver model not only mimics the natural zebrafish liver, but also complements alternatives to animal testing.

The main challenge for adapting *in vitro* tissue models is that the cells do not form into physiologically similar units which maintain the structural and functional characteristics of their target organs. This study addresses this challenge by creating a hydrogel system which provides repeatable and consistent hepatoid formation from a singularized cell line. The hydrogel drove cells to form a cell sheet with a canaliculi-like structure compared to its stiffer gel counterpart. The hepatoids cultured on the softer gel

exhibited the more active urea production and Vtg levels upon exposure to estrogenic compounds. By creating a stable zebrafish liver model *in vitro*, researchers can test EDCs and other water-borne chemicals in a reliable manner. Moreover, what can be used from this study is the hydrogel construct which can regulate phenotypes of human hepatocytes or other cell types and engineer human organoids. Therefore, this study is broadly applicable to toxicology testing where the use of live animal models is costly or ethically prohibited.

5.1 Abstract

Endocrine disrupting chemicals (EDCs) include synthetic compounds that mimic the structure or function of natural hormones. While most studies utilize live embryos or primary cells from adult fish, these cells rapidly lose functionality when cultured on plastic or glass substrates coated with extracellular matrix proteins. This study hypothesizes that the softness of a matrix with adhered fish cells can regulate the intercellular organization and physiological function of engineered hepatoids during EDC exposure. We scrutinized this hypothesis by culturing zebrafish hepatocytes (ZF-L) on collagen-based hydrogels with controlled elastic moduli by examining morphology, urea production, and intracellular oxidative stress of hepatoids exposed to 17β-estradiol (E2). Interestingly, the softer gel drove cells to form a cell sheet with a canaliculi-like structure compared to its stiffer gel counterpart. The hepatoids cultured on the softer gel exhibited the more active urea production upon exposure to E2 and displayed faster recovery of intracellular reactive oxygen species level confirmed by gradient light interference microscopy (GLIM), a live-cell imaging technique. These results are broadly useful to improve screening and understanding of potential EDC impacts on aquatic organisms and human health.

Keywords: Endocrine disrupting chemicals; Hydrogels; zebrafish hepatocytes; Zebrafish; 17β-estradiol

5.2 Introduction

For the last few decades, endocrine disrupting chemicals (EDCs) have been extensively used in various industrial and household products and medicine. It is well documented that the majority of endocrine disruption effects in field populations are due to exposure to natural and synthetic steroidal estrogens and their breakdown products such as E2 [1]. Certain industrial chemicals also have shown an estrogenic activity. For example, bisphenol A is a precursor of polycarbonate plastics and resins [2]. Another chemical, di(2-ethylhexyl) phthalate, is used as a plasticizer of food packaging and medical devices [3]. The subsequent increase in EDC levels in the river and potential drinking water prompted efforts to understand their impacts on the human endocrine system. EDCs may disrupt endocrine pathways through mimicking naturally occurring hormones or by blocking receptors. As they are transported into the liver for metabolic degradation, chronic exposure can result in non-alcoholic fatty liver disease which severely impacts metabolism, potentially leading to cirrhosis or cancer [4]. Thus, a platform must be developed to test chemical substitutes for their potentially adverse effects on liver morphology and function.

One common way to examine the potential toxicity of EDCs is through the examination of the zebrafish (*Danio rerio*), a standard testing fish species for biomonitoring due to their small size, easy cultivation, and transparent embryos. As EDCs are accumulated in the liver, the zebrafish liver would be an ideal organ to develop into an *in vitro* platform. Zebrafish sensitivity to toxins in the water is evaluated by examining damage in the DNA or chromosomes, P450 detoxification activity, and endocrine activity at the RNA level [5]. Endocrine disruption is not species-specific; therefore, EDC effects are widespread and often irreversible [6,7]. Many studies report the zebrafish liver would make a useful model for accurate prediction of both endocrine effects and reproductive toxicity [5,8,9].

With the movement away from animal models due to ethical reasons and tight regulations on their captivity, an alternative way to test the potential toxicity of current and newly developed EDCs without using the "live" zebrafish is necessary [14], especially for the cosmetic industry due to the complete ban of animal testing in the European Union since 2013 [15]. Consequently, efforts have been increasingly made to engineer an *in vitro* 3D hepatic platform that recapitulates anatomical and physiological function of liver to test the potential impacts of chemical compounds on liver function. In particular, spheroids formed from primary trout hepatocytes were found to present canalicular structures and have similar gene expression profiles as *in vivo* trout livers, as long as the spheroids matured for 25 days [16]. Additionally, there have been efforts to create *in vitro* liver models that closely predict human metabolism and match *in vivo* clearance rates when exposed to common pharmaceuticals like propranolol [17]. Despite challenges such as extended culture periods, these results show promising advances in replacing fish models *in vitro*.

Many approaches of 2D cell culture were focused on primary liver cells or cell lines into clusters using an ultra-low-adhesion dish or the hanging drop method. Other methods culture the cells on a flat surface like tissue culture plastic or glass coated with extracellular matrix proteins. However, cells isolated from tissues lose their phenotypes quickly through uncontrolled de-differentiation [10]. It is suggested that liver cells would exhibit a reasonable reorganizational period by placing cells into a physiologically similar microenvironment. Ultimately, cells would form a more cohesive structure and well-defined functional units during the first couple of days. These insights have not been widely tested for assembling zebrafish liver hepatoids used for EDC toxicology studies. However, studies made with hydrogel coupled with cell-adherent proteins have shown positive effects of substrate softness on cell viability and metabolic secretions in primary cells as compared to the unmodified gel [11-13]. In particular, rat primary hepatocytes cultured on heparin-PEG hydrogels with an elastic modulus of 2.3 kPa showed higher cell viability, albumin secretion, and urea secretion than cells cultured on stiffer heparin-PEG hydrogels [11]. In addition, mouse primary hepatocytes on collagen-polyacrylamide hydrogels with an elastic modulus of 140 Pa showed significantly higher albumin production and HNF4α expression, a transcriptional regulatory factor that is critical in normal liver development and maintaining normal liver functions, than those cultured on a stiffer hydrogel [13]. These studies state that the elastic modulus of the substrate to which hepatocytes are cultured is an extracellular factor of modulating hepatocyte function and structure in an *in vitro* culture.

In this study, we hypothesized that the softness of a matrix modulates whether zebrafish hepatocytes can regulate their intercellular organization. In turn, the response of the resulting "hepatoid-like cluster" (hepatoid) to EDC through modulation of cell-matrix interaction. The matrix softness would mitigate the effects of EDCs on cellular detoxification activity through the urea cycle. We examined this hypothesis using

E2 as a model EDC [18,19], and studied the morphology and metabolic activity of zebrafish hepatocytes cultured on collagen-based gels with two different elastic moduli of 14 and 256 Pa. We assessed cellular oxidative stress from E2 by monitoring the reactive oxidative species activity in real-time using a fluorescent probe. The extent that E2 affects the detoxification activity of cells is monitored by the urea cycle activity of liver cells exposed to different concentrations of E2. Overall, this study aims to develop an advanced *in vitro* zebrafish liver and use it to understand the impact of EDCs on the physiological activities of urea and vitellogenin synthesis.

5.3 Materials and Methods

5.3.1 ATCC Zebrafish cell culture

Zebrafish hepatocytes (ZFL; ATCC CRL-2643) were cultured in 50% Leibovitz's L-15, 35% Dulbecco's Modified Eagle Medium high glucose, and 15% Ham's F12, all without sodium bicarbonate and supplemented with 0.15 g/L sodium bicarbonate, 15 mM 4-(2-hydroxyethyl)-1-piperazineethanesulfonic acid (HEPES), 0.01 mg/mL bovine insulin, 5% heat-inactivated fetal bovine serum, and 0.5% trout serum (Caisson Laboratory). Cells were expanded in T-75 flasks and incubated at 28°C and atmospheric carbon dioxide in a tabletop, low temperature incubator (Fisherbrand™). We used cells with a passage number of 3 to 5 for hepatoid formation on gels with controlled elastic moduli. Media was formulated in the University of Illinois Cell Media Facility, except for the trout serum, which was added separately, and the completed medium was not sterile filtered. Cells were cultured in T-75 flasks until about 80% confluent and cryopreserved using the culture medium supplemented with 10% heat-inactivated fetal bovine serum and 5% DMSO. Cells were cryopreserved in vapor phase liquid nitrogen.

5.3.2 Collagen-polyethylene glycol (PEG) hydrogel formation

Collagen-polyethylene glycol (collagen-PEG) hydrogels were prepared in 96-well plates via *in situ* cross-linking between collagen molecules by mixing PEG (Sigma, MW 7500) at mass ratios of 0 (pure collagen) and 10 to bovine Type I collagen (Advanced Biomatrix) in an equal volume of the zebrafish medium. Reconstitution solution containing 0.26 M sodium hydrogen carbonate, 0.2 M HEPES, and 0.04 M sodium hydroxide (Sigma) was added to modulate the pH of the gel to initiate gel formation. Hydrogels were then incubated at 37°C and 5% CO_2 for 30 minutes. Cells were plated directly onto hydrogels at a cell density of 1.0×10^6 cells/mL and cultured for 14 days at 28°C and atmospheric carbon dioxide. The media was replaced every two to three days.

5.3.3 Mechanical analysis

The elastic modulus of the hydrogels was measured using a rheometer (DHR-3, TA Instruments). Collagen and collagen-PEG gels were prepared as previously described and loaded onto the parallel plate (diameter = 22 mm). Gap between two plates was kept constant at 200 μm. The hydrogel was left for 20 minutes at 37°C to gel. Then, the hydrogel was oscillated at 0.1% strain while varying frequency from 0.1 to 10 Hz. The resulting stress was measured to calculate elastic and loss moduli at individual frequency. The test was conducted in triplicate.

5.3.4 Scanning electron Microscopy (SEM)

Collagen and collagen-PEG hydrogels were formed in a 96-well plate as previously described. Then, they were removed with a spatula and slowly dehydrated in 30%, 50%, and 70% w/w ethanol-water solution for at least an hour each and 100% ethanol overnight. The dehydrated gels were dried using the critical point dryer (Tousimis 931). SEM (Hitachi S4700) imaging was performed directly after drying the samples. First, the samples were mounted using copper tape and coated with a 6-8 nm layer of gold (EMITECH 575). Images were taken with an accelerating voltage of 2 kV, a working distance of 8-9 mm, and the emission current was adjusted to reduce sample damage. The pore area and fiber diameter were measured using ImageJ software. For the pore area, an automatic threshold was applied to remove the background and the particle analyzer tool was using to measure pores that were higher than 1 um^2. The average pore area was calculated by dividing the total pore area by the area of collagen. Fiber diameter was directly measured and at least 20 measurements were taken from each image. The statistical significance was calculated using the ANOVA test.

5.3.5 Immunofluorescence imaging

Cells were cultured for two weeks on collagen or collagen-PEG hydrogels installed on glass bottom dishes (Cellvis). Then they were fixed with 1:1 v/v methanol and acetone at -20°C for 20 minutes. Then, the samples were washed twice with room temperature phosphate buffered saline (PBS, Corning) for five minutes each. Cells were blocked with 2% bovine serum albumin for 1 hour. Cells fixation using this method is not needed an extra permeabilization step as they are permeabilized by acetone and methanol. The cells were stained with phalloidin-Alexa 488 (Invitrogen) overnight at 4°C (1:250) for the imaging of actin filaments and washed twice with PBS for five minutes each. 4´,6-diamidino-2-phenylindole (DAPI) was incubated at room temperature for one minute (1:500) and washed twice for one minute each immediately before imaging. For β1-integrin staining, the primary antibody P5D2 (Abcam) was incubated overnight at 4°C. The sample was then washed twice with PBS for five minutes each. Then, the secondary antibody anti-mouse conjugated AF555 (Cell Signaling Technology, 4409S) was incubated for four hours at room temperature. Then, the samples were washed with PBS twice for five minutes each. Finally, nuclei of the cells were imaged with DAPI immediately before imaging. Although the P5D2 antibody is noted as only reactive with human cells, according to the National Center for Biotechnology Information, zebrafish and humans are orthologs for β1 integrin which would suggest that the antibody will have cross-species reactivity [20].

The images were taken using a four laser, point scanning confocal microscope (Zeiss LSM 175 700), the 10x/0.3 or the 20x/0.8 air objectives were used. Images of the cells were obtained using the tile scan feature. The pinhole for all channels was set to the size of one Airy unit for the DAPI channel. The line averaging was set to 8 times and the pixel dwell time was set to 1.58 µs. Image acquisition and review were done through the Zeiss Zen (Black and Blue, respectively) programs.

5.3.6 Bicinchoninic acid (BCA) protein assay

The Pierce™ BCA Protein Assay Kit (Thermo Fisher Scientific 23225) was used to determine the total protein concentration of the zebrafish hepatoid samples. The microplate protocol was followed using the instructions provided with the assay kit. Samples were tested in triplicate. Samples were collected from the culture on days 1, 7, and 14. First, diluted albumin standards were made so that there was a range of standard from 0 to 2,000 µg/ mL of BSA concentration. Then, the working reagent was prepared by mixing 50:1 BCA reagent A to B. The solution was mixed to reduce turbidity and yielding the clear, green color as described. The working reagent was prepared fresh, immediately before starting the assay. Following the microplate procedure, 25 µL of each standard and unknown were pipetted into a 96-well plate. Then, 200 µL of the working reagent was pipetted into each well and mixed thoroughly by pipette. The plate was covered, protected from light, and placed into an incubator at 37°C for 30 minutes. Finally, the plate was cooled to room temperature and read at 562 nm wavelength on a plate reader (BioTek).

5.3.7 17β-estradiol and bisphenol A treatment

Zebrafish hepatocytes were plated at a density of 1.0×10^6 cells/mL and cultured in the conditions as described above for 14 days. A stock solution of E2 or BPA was prepared with a DMSO solution, 0.1 wt% in water. Then, for 24 hours, the cells were exposed to 0, 1, or 10 nM of E2 or BPA in cell culture media. The cells were analyzed after the 24-hour exposure period.

5.3.8 Urea colorimetric assay

Cell culture media was collected from each condition and stored at -20°C for short-term storage until testing. The low concentration urea assay kit (BioVision K375) was used to determine the urea cycle activity. The media samples and kit components were first warmed to room temperature. Then in a 96 well plate, the standard curve and samples were prepared according to the manufacturer's instructions. Each condition was tested in triplicate. The colorimetric output was read at 570 nm using a plate reader (BioTek). Then the data was analyzed using and ANOVA test to determine significance. The media was collected from each condition and stored at -5°C until use for experiments. Urea synthesis was assayed in cell culture medium using the urea assay kit (MAK006, Sigma Aldrich, Steinheim, Germany). A standard curve was created to generate 0,

1, 2, 3, 4, and 5 nmol urea/well. Then, each 50 uL of the media was applied to the 96 well for urea quantification according to the manufacturer's instruction. The colorimetric product was measured at wavelengths of 570 nm using a microplate reader (TECAN, Männedorf, Switzerland). Each condition was tested in triplicate and statistical significance was measured using and ANOVA test.

5.3.9 Vitellogenin (Vtg) measurements and immunofluorescent staining

Vtg was measured in cell pellets using an ELISA kit (10004995; Cayman Chemical, Ann Arbor, MI, USA). A cell concentration of 1.0×10^6 cells/mL was seeded on collagen and collagen-PEG coated well plates and cultured for 14 days. Then, the cells were exposed to 1 nM of E2 (Sigma Aldrich) and 10 μM of BPA (Sigma Aldrich) for 48 hours, respectively. The cell pellets were collected in 1.5 mL tubes and centrifuged for 5 minutes at 125 × *g*, and the supernatants were discarded and washed with cold PBS. The pellets were lysed with passive lysis buffer (Promega, Mannheim, Germany) after re-centrifugation. The supernatants were used for the vitellogenin quantification according to the manufacturer's instructions (Cayman Chemical). Each sample was normalized by total protein content, which was calculated using the BCA protein assay. And the ANOVA test was run to determine significance of the results for the hepatoids cultured on the collagen-PEG hydrogel. For vitellogenin staining, the primary antibody vitellogenin (LifeSpan, LS-C76845-100) was incubated overnight at 4°C. The sample was then washed twice with PBS for five minutes each. Subsequently, the secondary antibody anti-mouse conjugated FITC (Thermo Fisher Scientific, 31232) was incubated for two hours at room temperature. Then, the samples were washed with PBS three times every five minutes. Finally, nuclei of the cells were stained with DAPI immediately before imaging.

5.3.10 Live cell imaging with E2

Glass bottom dishes with dimensions of 29 mm diameter, 14 mm diameter well, #0 glass, and glass top (D29-14-0-TOP, Cellvis) were first coated with poly-D-lysine (Sigma) for 20 minutes and then washed 2x with culture media to remove the excess chemical. Zebrafish hepatocytes (ATCC CRL-2643) were seeded at 5,000 cells per dish and allowed to adhere for 10 minutes before being coated by collagen or collagen-PEG hydrogel as described above. Cells were cultured in this manner because of the short working distance of the microscope objective. Therefore, cells needed to be cultured as close to the glass cover slip as possible. After the hydrogel formed, 3 mL of culture media was added and the cells were incubated in the conditions previously described. The cells were then cultured for 2 days prior to the live cell imaging experiment to ensure that the cells were interacting with the hydrogel and each other without forming large clustered structures. Thus, individual cell ROS levels could be analyzed. Before imaging, zebrafish culture medium with 0, 1, and 10 nM of E2 (Sigma-Aldrich) replaced the media and 6 μL/3 mL of CellROX® Green Reagent (Thermo Fisher Scientific) was added to each sample. Co-localized fluorescence and phase imaging was performed on an Axio Observer Z1 (Zeiss) with GLIM Pro add-on module (Phi Optics). Gradient light interference microscopy is an upgrade to differential interference contrast microscopy that uses phase-shift

shifting to improve image quality by separating unwanted amplitude information from high detail phase information [21]. Here we use a 10x/0.3 objective and sCMOS camera (Prime BSI, Photometrics). Imaging began 20 minutes after adding the CellRox™ dye with a total of 18 representative fields of view (1150 x 1150 μm) acquired every 30 minutes for 16 hours. The images were then analyzed with ImageJ (Fiji) to measure signal intensity from the CellROX reagent as well as overlay the GLIM and fluorescent images. To measure the intensity, images from the same sample were loaded into ImageJ as a sequence in chronological order. Then, a region of interest (ROI) was enclosed using an oval, ensuring that the entire cell cluster or single cell was within the boundaries of the ROI for the entire set of images. Using the stacks menu, the Z-axis profile was plotted, and the values were exported to Excel for further analysis. The Z-axis profile plots the mean grey signal of the ROI. At least 10 ROI were chosen per sample. In Excel, the data was averaged and normalized to the control sample of 0 nM E2 for each hydrogel modulus respectively.

5.4 Results and Discussion

Increasing the pH of the pre-gelled collagen solution and the collagen-polyethylene glycol (PEG) mixture from 2.0 to 7.4 resulted in the collagen gel and collagen-PEG gel, respectively. Both hydrogels are made with interconnected fibrous networks as confirmed with scanning electron microscope images (Figure 5.1). The PEG in the collagen-PEG gel altered the diameter and spacing of collagen fibers minimally compared with the pure collagen gel (Table 5.1). In contrast, an elastic modulus of the PEG-collagen gel was 14 Pa while that of the pure collagen gel was 274 Pa. This result confirms that PEG modulates the mechanical stiffness of the collagen gel without altering the microstructure significantly.

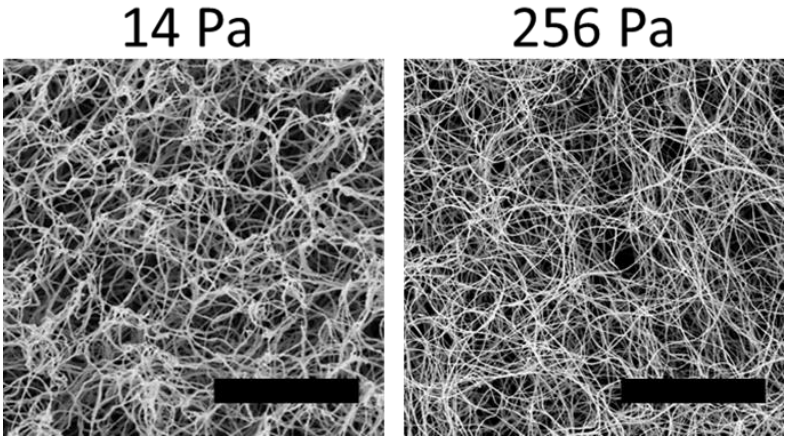

Figure 5.1. Two hydrogels were formulated; pure collagen and collagen mixed with polyethylene glycol (PEG) and imaged with scanning electron microscopy. The black scale bars represent 5 μm.

This collagen-PEG hydrogel system allows for the control of the elastic modulus without significantly altering other matrix parameters like the pore area and fiber diameter. Microscopic images of

the gel confirm that there is no significant difference in microstructure, independent of the change in softness. As analyzed previously [22], it is likely that PEG depletes the hydrogen bonds between water molecules and collagen fibers, which are major components to generate the elastic properties of the gel. As the free water molecules are depleted, the fibrillogenesis of the collagen fibers is hindered, resulting in a softer hydrogel. Such change of the intermolecular association at the molecular scale may influence the stiffness of individual collagen fibers but may not impact the pore size of the gel. This strategy to control gel softness is different from other formulations in that the PEG act as spacers between the collagen fibers instead of being used to chemically cross-link collagen molecules [23,24].

Table 5.1. The shear modulus was decreased from 256 to 14 Pa with the addition of PEG at a mass ratio of PEG to collagen being 10:1. The concentration of collagen was held constant for both hydrogel formulations at 1.5 mg/ ml. The asterisk indicates statistical significance of the difference of values between two conditions (*$P < 0.02$).

PEG: Collagen (m/ m)	Shear modulus (Pa)	Fiber diameter (μm)	Pore area (μm²)
10:1	14 ± 1 *	0.10 ± 0.02	0.53 ± 0.21
0:1	256 ± 132 *	0.09 ± 0.02	0.38 ± 0.19

The zebrafish hepatocytes were seeded onto the gels with controlled elastic moduli. Then, cell growth was monitored for two weeks by measuring total protein concentrations with a BCA protein assay kit (Figure 5.2a). The total protein concentration was increased at a comparable rate regardless of the elastic modulus of the gel. In contrast, the elastic modulus of the gel influenced cellular organization. Cells cultured on the pure collagen gel with an elastic modulus of 256 Pa proliferated independently, or in small clusters (Figure 5.2c-iv). However, cells cultured on the softer collagen-PEG gel with an elastic modulus of 14 Pa aggregated to form a large cell sheet (Figure 5.2c-i). More interestingly, the cells self-organized on the collagen-PEG gel to form a hollow lumen, or canaliculus (Figure 5.2c-ii,iii). In addition, actin molecules were localized on the cell membrane more significantly than cells cultured on the stiffer pure collagen gel. Furthermore, cells cultured on the softer collagen-PEG gel expressed more β1-integrins than those cultured on the pure collagen gel (Figure 5.2b and 5.2d). To further clarify that the zebrafish hepatoid ultrastructure was a direct result of the elastic modulus of the hydrogel, singularized hepatocytes were pre-exposed to PEG prior to plating (Supplementary Figure 5.1). After 14 days of culture, the cells were immunostained for actin filaments as well as β1-integrin expression. The cells pre-exposed to the PEG, which is the same PEG used to assemble the collagen-PEG hydrogels, did not show significant changes in actin or integrin expression from cells plated on the collagen-PEG hydrogel without pre-exposure to the soluble PEG. In addition, cells pre-exposed to PEG formed canaliculi-like structures, like cells that were not pre-exposed to the soluble PEG. Thus, it is suggested that the PEG that is present in the collagen-PEG hydrogel acts as a neutral softener with minimal interactions with the zebrafish hepatocytes during hepatoid formation.

When observing the β1-integrin expression, which indicates cellular adhesion to the matrix, the softer collagen-PEG hydrogel served to increase β1-integrin expression of cells than the stiffer, pure collagen

hydrogel. Previous studies report that cell clusters formed or placed on a bioactive 2D substrate sense and respond to biophysical properties of the matrix via integrin-ligand bonds and cell-cell junctions [25,26]. As such, we suggest that hepatocytes bound to collagen molecules of the softer gel sense the mechanical signal from the substrate, increase cellular adhesion and growth, and finally form a cell sheet in which cells are interconnected to form the canaliculi-like structure. Cells homogenously mixed into the hydrogel failed to associate with each other, thus resulting in few clusters with the physiologically relevant ultrastructure. These results indicate that the cells cultured on the 14 Pa collagen-PEG hydrogel were the most physiologically organized even though there was an independency of cell growth on the gel stiffness.

This study demonstrates that the softness of the collagen-PEG hydrogel plays a significant role in regulating the intercellular organization of engineered zebrafish hepatoids. *Ex vivo* cells frequently de-differentiate when cultured on a substrate which has a different modulus from the native tissue. By plating the hepatocytes onto a soft hydrogel with stiffness relatable to the yolk of the zebrafish egg, cells will experience a biophysical cues which will result in hepatoids with higher physiological relevance. In particular, mouse hepatocytes cultured on stiffer collagen-polyacrylamide hydrogels exhibited larger cell areas and decreased expression of HNF4α, a transcriptional regulatory factor [13]. Because this factor controls many downstream factors and functions, culturing mouse hepatocytes on stiff substrates results in reduced hepatocyte function. Specifically functional mRNA expression levels of *Baat*, *F7*, and *Gys2* are lowered in addition to HNF4α, according to the previous study made with mouse hepatocytes. Compared with this study, the cells cultured on the softer gel, with an elastic modulus of 14 Pa, formed cohesive sheet-like structures with a canaliculi-like intercellular organization as seen in the actin staining images (Figure 5.2c). Canaliculi eventually fuse to form bile ducts in the adult zebrafish [9,27]. The bile ducts and blood vessels are jointly responsible for clearing metabolic waste from the hepatocytes [8,28]. In contrast, the hepatocytes on the stiffer collagen hydrogel, with an elastic modulus of 256 Pa, formed separated, small cell clusters. By introducing the hepatocytes into a softer microenvironment, the organotypic 3D organization resembled that of a zebrafish liver.

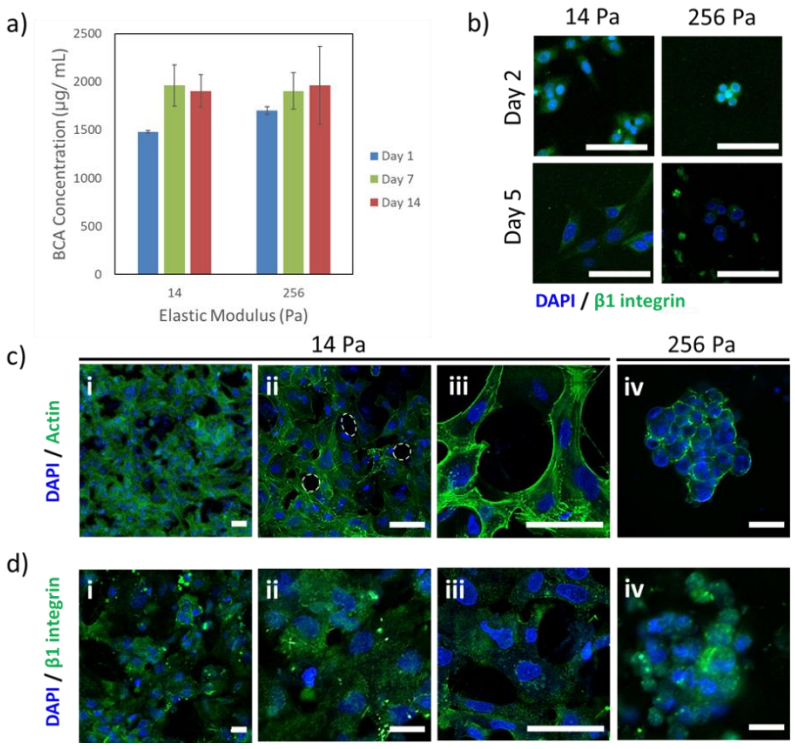

Figure 5.2. Zebrafish hepatocytes (ATCC® CRL-2643™) cultured on the collagen and collagen-PEG gels with different elastic moduli. (a) The total protein concentration assay after 1, 7, and 14 days of culture. The values and error bars represent the mean and standard deviation of three samples per condition, respectively. (b) Immunofluorescent staining of hepatocytes at days 2 and 5 for blue-colored nuclei and green-colored β1-integrin. (c–d) Immunofluorescent staining of hepatocytes after 14 days of culture on the gel. The images in (c) show blue-colored nuclei and green-colored actin filament in cells cultured on the pure collagen gel with an elastic modulus of 14 Pa (i, ii) and collagen-PEG gel with an elastic modulus of 256 Pa (iii). White dot circles mark hollow lumen formed by self-organization of hepatocytes. The images in (d) show blue-colored nuclei and green-colored β1-integrin in cells cultured on the pure collagen gel with an elastic modulus of 14 Pa (i, ii) and collagen-PEG gel with an elastic modulus of 256 Pa (iii). In each image, white scale bars represent 50 μm.

The physiological activity of hepatocytes cultured on the gels was analyzed by examining the ornithine-urea cycle, which is the primary pathway to detoxify ammonia and amino acids in the liver. Cells were analyzed at 27°C and 37°C, which represents the zebrafish and human body temperature, respectively (Figure 5.3). Cellular hepatic cycle activity increased with the cell culture period. After 2 weeks, cells cultured on the collagen-PEG gel with an elastic modulus of 14 Pa displayed higher hepatic urea activity than those on the pure collagen gel with an elastic modulus of 256 Pa (Figure 5.3a). The inverse dependency of hepatic urea activity on the elastic modulus was more significant at 37°C (Figure 5.3b).

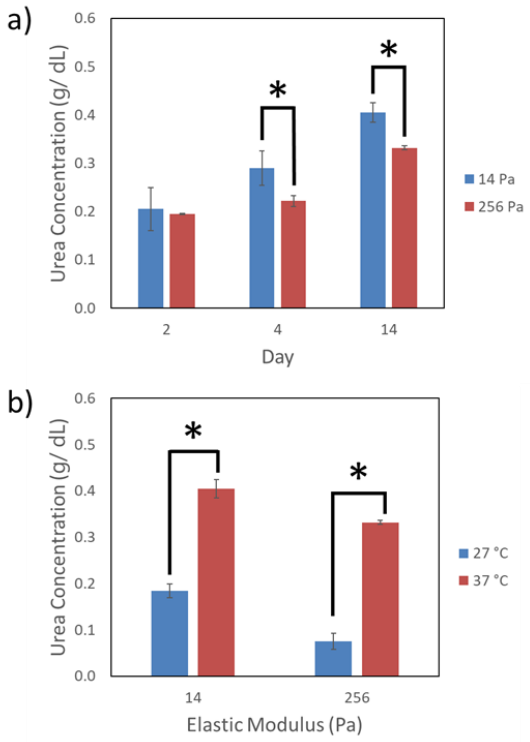

Figure 5.3. Analysis of urea cycle activity for zebrafish hepatocytes cultured on the gels with different elastic moduli. (a) The urea concentration was measured after 2, 4, and 14 days of culture. (b) Comparison of the urea cycle activity was made between 27°C and 37°C to evaluate the effects of environmental temperature. The values and error bars represent the mean and standard deviation of three samples per condition, respectively. The asterisk indicates statistical significance of the values between conditions (*$P < 0.05$).

We further assessed the extent to which the elastic modulus of the gel modulates hepatic urea cycle activities at varied concentrations of E2. E2 binds with estrogen receptors to produce Vtg in the female zebrafish and its concentration is regulated in the liver through metabolic degradation [29]. E2 stimulated the hepatic urea cycle activity as displayed, with an increase of the urea concentration with increasing E2 concentration (Figure 5.4). Interestingly, the dependency of the urea cycle activity on the E2 concentration was more substantial with cells cultured on the collagen-PEG gel with an elastic modulus of 14 Pa than those cultured on the pure collagen gel with an elastic modulus of 256 Pa. Such an inverse dependency of the urea concentration on the elastic modulus of the gel is attributed to the cellular β1-integrin expression increased with the softer gel.

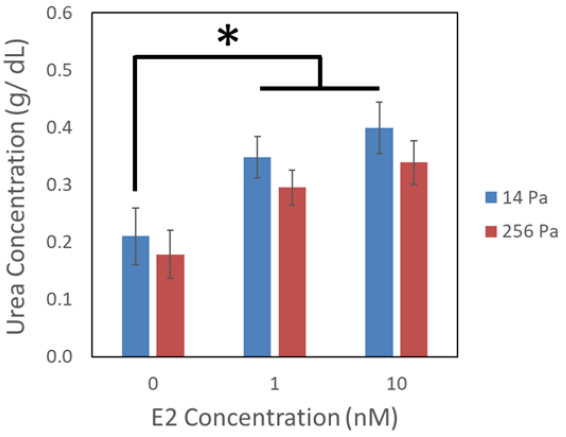

Figure 5.4. Analysis of hepatic urea cycle activity of zebrafish hepatocytes. Cells were cultured on the collagen gel with an elastic modulus of 14 Pa and the collagen-PEG hydrogel with an elastic modulus of 256 Pa for two weeks before exposure to 17β-estradiol (E2). Then, cells were exposed to 0, 1, and 10 nM of E2 for 24 hours. The values and error bars represent the mean and standard deviation of three samples per condition, respectively. The asterisk indicates statistical significance of the values between conditions (*P < 0.05).

In addition, as shown in Figure 5.5, BPA and E2 were found to have effective Vtg responses in the zebrafish hepatocyte clusters formed on collagen and collagen-PEG hydrogels. The hepatocytes cultured in a 2D monolayer on a polystyrene substrate did not markedly induce Vtg production in the presence of E2 or BPA (Figure 5.5a). In contrast, zebrafish hepatocyte clusters formed on collagen-PEG hydrogels with an elastic modulus of 14 Pa resulted in a significant increases of Vtg activity at a concentration of 10 nM of E2 or 10 μM of BPA. Hepatocyte clusters formed on the collagen gel with an elastic modulus of 256 Pa showed minimal Vtg activities after exposure to E2 or BPA, similar to cells cultured on a polystyrene substrate (Figure 5.5b). Vtg is the serum phospholipoglycoprotein precursor to egg yolk. It is potentially an ideal biomarker for environmental estrogens because estrogen receptors in the fish liver regulate vitellogenesis [30]. Vtg is typically found in the blood of female fish, whereas in male fish, the level is very low. However, Vtg synthesis can be induced in male fish if they are exposed to exogenous estrogens [31]. Therefore the presence of Vtg in a male fish can be considered a sensitive biomarker of estrogenic chemical exposure [32]. Therefore, E2 is considered as represent EDCs in environmental system and the synthesis of Vtg in aquatic organisms is very important marker for assessing endocrine disturbances by natural hormones and EDCs.

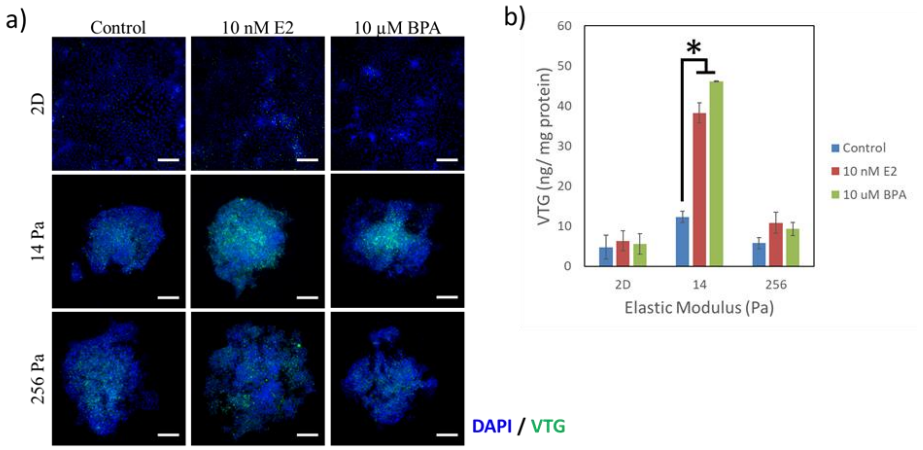

Figure 5.5. Analysis of the vitellogenin (Vtg) in zebrafish hepatocytes after 14 days of culture on a 2D polystyrene substrate, collagen-PEG (elastic modulus ~ 14 Pa), and collagen (elastic modulus ~ 256 Pa) hydrogels. (a) Immunofluorescent staining with DAPI (blue) and Vtg (green) of zebrafish hepatocytes exposed to 10 nM of E2 or 10µM of BPA for 24 hours. (b) The Vtg concentrations as measured with ELISA. The white scale bars indicate 100 µm. The asterisk indicates statistical significance of the values between conditions (*$P < 0.01$).

A previous study by the US Environmental Protection Agency (EPA) and US National Toxicology Program (NTP) set 75 µM (17.2 mg/L) as the maximum BPA concentration detected in an environmental sample [33]. In addition, François Brio et al showed that 10 µM of BPA revealed maximum estrogenic activity of the estrogen receptor and aromatase in zebrafish hepatocytes and larvae [34]. Therefore, zebrafish hepatocytes were exposed to either E2 or BPA. BPA stimulates estrogenic activity of hepatocyte clusters similar to E2. This result suggests that zebrafish hepatoids similarly metabolize both chemicals into Vtg. However, the effect is significantly different depending on the substrate on which the zebrafish hepatocytes are cultured. The hepatoids cultured on the pure collagen hydrogel with an elastic modulus of 256 Pa did not respond to the EDCs as the hepatoids on the collagen-PEG hydrogels. From the earlier result, hepatoids on the stiffer hydrogel had disorganized tissue structure as compared to the hepatoids cultured on the softer hydrogels (Figure 5.2c). Therefore, the difference in Vtg synthesis levels could be because physiologically similar tissue organization promotes high levels of hepatoid functionality. Thus, the disorganized cells on the 2D plastic substrate and the disorganized hepatoid formed on the pure collagen hydrogel had low response to EDC exposure. It is likely that the rate of estrogenic activity is altered by the substrate stiffness. This possibility will be examined systematically in future studies.

The combined effects of estrogen concentration and gel softness on the cellular urea production are further related to the change in the ROS-mediated intracellular oxidative stress level. As the liver induces Vtg synthesis using the excess E2, cells produce ROS which impacts cells negatively. In particular, we evaluated the general oxidative stress of the cells by monitoring the intracellular ROS level through the oxidation of the CellROX probe via live cell imaging for 16 hours. This study discloses that hepatoid-like clusters formed on the softer collagen-PEG hydrogels are able to return the ROS level to a baseline at the elevated E2 concentration. In contrast, cell clusters formed on the stiffer collagen hydrogel exhibited a higher ROS level for both elevated E2 conditions. In addition, cell clusters showed a drop of ROS level below baseline when

exposed to 10 nM E2, indicating that some of the cells likely lost viability and metabolic activities after exposure to excessive E2.

Because E2 is localized in the liver for biotransformation into Vtg, excessive accumulation from naturally produced and ingested E2 will increase the generation of reactive oxygen species (ROS) through mitochondrial and genomic pathways. Live cell imaging was taken to visualize the ROS response of the zebrafish hepatocytes to E2 using the positive signal from the CellROX reagent (Figure 5.6). The fluorescent intensity from the CellROX increases with increasing internal reactive oxygen species. The hepatocytes cultured on the gel with an elastic modulus of 14 Pa displayed consistent clustered cell morphology during the 16 hours (Figure 5.6a). The fluorescent signal from the control conditions demonstrates the homeostatic level of ROS as a byproduct of metabolism and as a signaling molecule. As seen in all three concentrations of E2, the hepatocytes maintained their original morphology. The ROS signal marked by oxidation of the fluorescent probe of the CellROX® reagent was also consistent from 0 to 16 hours. However, the morphology of the hepatocytes cultured on the stiffer gel with an elastic modulus of 256 Pa was changed rapidly during the 16 hours after exposure to E2 (Figure 5.6b). In particular, the change in morphology from spread to spheroidal was visible after 12 hours of exposure to 1 nM E2 (Figure 5.6b-v) and 6 hours of exposure to 10 nM E2 (Figure 5.6b-vi). Also, the hepatocytes exposed to 10 nM of E2 lost most of the ROS intensity at 16 hours.

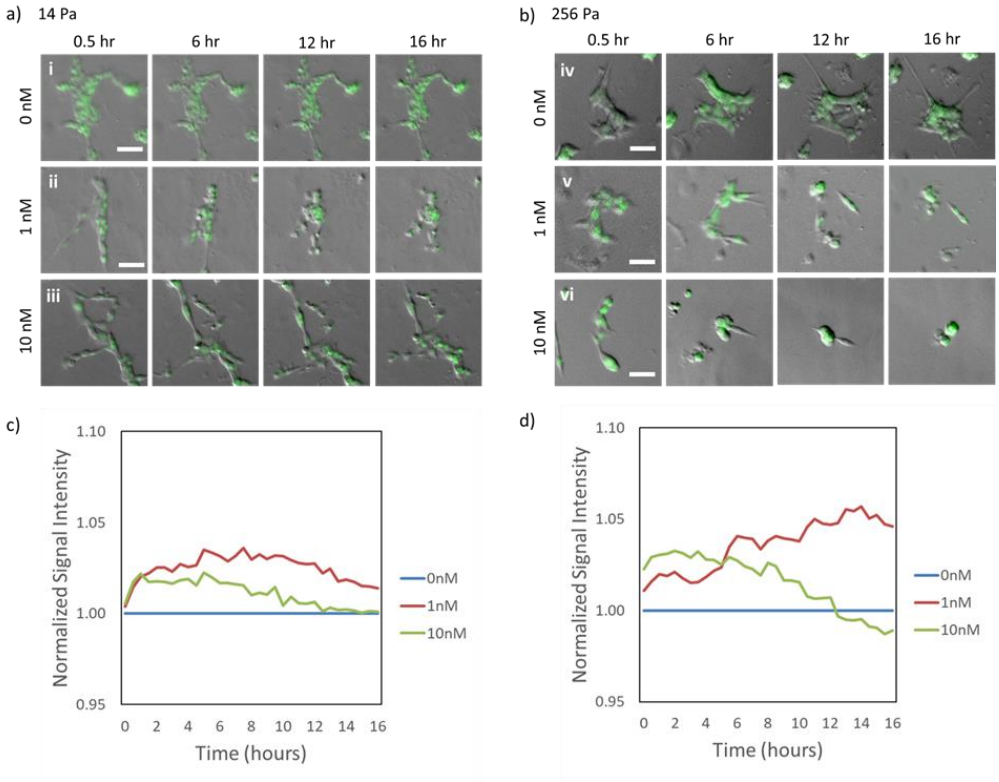

Figure 5.6. Live cell imaging of reactive oxygen species generation and morphology of zebrafish hepatocyte when exposed to 0 (i, iv), 1 (ii, v), and 10 (iii, vi) nM of 17β-estradiol (E2). Images were taken every 30 minutes over 24 hours after the addition of E2 and CellROX® reagent (green). The grey scale images are Gradient Light Interference Microscopy (GLIM) images showing the cellular morphology. (a) Zebrafish hepatocytes cultured on the collagen-PEG hydrogel with an elastic modulus of 14 Pa. (b) Zebrafish

hepatocytes cultured in a pure collagen hydrogel with an elastic modulus of 256 Pa. The white scalebars indicate 40 μm. (c–d) The normalized signal intensity of CellROX® for each hydrogel stiffness, 14 and 256 Pa, comparing their reactive oxygen species generation for increasing concentrations of E2. (c) The reactive oxygen species generation is increased for both 1 and 10 nM concentrations of E2 in the 14 Pa hydrogel and the baseline ROS concentration is recovered after 5 hours for the 1nM concentration. (d) For the 256 Pa hydrogel, the ROS levels are increased in both concentrations of E2, but the ROS level drops below the control group after 12 hours for the 10 nM concentration.

The live images of ROS signal from the cells were then analyzed with the fluorescence signal intensity (Figure 5.6c-d). According to the quantitative analysis, even with 0 nM concentration of E2, the zebrafish hepatocytes cultured on the hydrogel with an elastic modulus of 14 kPa exhibited lower ROS production than the cells cultured in the 256 Pa hydrogel (Figure 5.6c-d). When the concentration of E2 was increased to 1 nM, the hepatocytes on the gel with an elastic modulus of 14Pa showed an increase of the ROS signal up to 4 to 6 hrs, followed by the decrease of the intensity. In contrast, cells on the gel with an elastic modulus of 256 Pa displayed a steeper and continuous increase of the ROS signal up to 16 hrs.

Further increase of the E2 concentration to 10 nM resulted in transient increases of ROS signal up to 2 hrs regardless of an elastic modulus of the gel. However, the hepatocytes cultured on the gel with an elastic modulus of 14 Pa showed a relatively slower increase in the ROS level than those on the gel with an elastic modulus of 256 Pa. In the stiffer hydrogel, ROS generation was decreased after 12 hrs, indicating that the cells were no longer functioning in metabolic degradation. Taken together, the cells cultured in the collagen-PEG hydrogel with a 14 Pa modulus were better able to metabolize the increased levels of E2 without a significant impact on their morphology. In contrast, the hepatocytes cultured on the 256 Pa hydrogel demonstrated an early loss of functionality from elevated E2 concentrations. These experiments demonstrate an *in vitro* platform for the physiological impacts of endocrine-disrupting factors on zebrafish hepatoids that exhibited similar morphology and functionality as the live zebrafish. These hepatic tissues were engineered by culturing cells on the collagen-PEG gel with controlled stiffness while maintaining the pore area and fiber diameter of the hydrogels. The hepatocytes cultured on the collagen-PEG hydrogel with an elastic modulus of 14 Pa formed large sheets with intercellular canaliculi. In contrast, hepatocytes cultured on the pure collagen hydrogel with an elastic modulus of 256 Pa grew slowly without the formation of a cell sheet. Also, the hepatocytes cultured on the softer collagen-PEG hydrogel displayed elevated urea cycle activity and higher sensitivity to external E2 than those cultured on the stiffer pure collagen gel. Overall, the cellular response to the gel is attributed to the difference of the gel softness.

5.5 Summary and Conclusion

Taken together, the results of this study report that softness of cell culture substrate plays a significant role in the assembly and physiological function of zebrafish hepatoids. The hepatoids engineered to present a canaliculi-like structure was active to restore intracellular ROS level to normal by up-regulating detoxification activities upon exposure to E2. Since the zebrafish shares similar embryotic characteristics and

homology to humans, the continued study of the zebrafish hepatoid would be beneficial to understanding human liver response to endocrine-disrupting chemicals such as E2. In addition, the results of this study will significantly impact current studies that are often plagued by the loss of morphology and functionality of live embryo or primary adult liver cells *in vitro*. Therefore, this study would be broadly useful to developing an *in vitro* cell or organoid culture platform used for rapid and precise screening of potentially toxic chemicals.

5.6 Acknowledgments

This work was supported by a National Research Council of Science & Technology (NST) grant by the Korean Government (CAP-17-01-KIST Europe), partly by the National Science Foundation Research Training Grant (1735252), National Science of Foundation (STC-EBICS Grant CBET-0939511), R01CA238191, and R43GM133280-01. K. Sullivan and M. Kandel are supported by the National Science Foundation Research Training Grant (1735252) Understanding the Brain: Training the Next Generation of Researchers in Engineering and Deciphering of Miniature Brain Machinery. Chang Gyun Park was supported by the KIST Europe signature project (12001).

5.7 Bibliography

1. Thorpe, K. L.; Cummings, R. I.; Hutchinson, T. H.; Scholze, M.; Brighty, G.; Sumpter, J. P.; Tyler, C. R. Relative Potencies and Combination Effects of Steroidal Estrogens in Fish. *Environ. Sci. Technol.* **2003**, *37* (6), 1142–1149. https://doi.org/10.1021/es0201348.
2. Pang, Q.; Li, Y.; Meng, L.; Li, G.; Luo, Z.; Fan, R. Neurotoxicity of BPA, BPS, and BPB for the Hippocampal Cell Line (HT-22): An Implication for the Replacement of BPA in Plastics. *Chemosphere* **2019**, *226*, 545–552. https://doi.org/10.1016/j.chemosphere.2019.03.177.
3. Nagorka, R.; Koschorreck, J. Trends for Plasticizers in German Freshwater Environments – Evidence for the Substitution of DEHP with Emerging Phthalate and Non-Phthalate Alternatives. *Environ. Pollut.* **2020**, *262*, 114237. https://doi.org/10.1016/j.envpol.2020.114237.
4. Tian, H.; Gao, Z.; Wang, G.; Li, H.; Zheng, J. Estrogen Potentiates Reactive Oxygen Species (ROS) Tolerance to Initiate Carcinogenesis and Promote Cancer Malignant Transformation. *Tumor Biol.* **2016**, *37* (1), 141–150. https://doi.org/10.1007/s13277-015-4370-6.
5. Shao, Y.; Xiao, H.; Di Paolo, C.; Deutschmann, B.; Brack, W.; Hollert, H.; Seiler, T. B. Integrated Zebrafish-Based Tests as an Investigation Strategy for Water Quality Assessment. *Water Res.* **2019**, *150*, 252–260. https://doi.org/10.1016/j.watres.2018.11.039.
6. Bergman, Å.; Heindel, J.; Jobling, S.; Kidd, K.; Zoeller, R. T. State-of-the-Science of Endocrine Disrupting Chemicals, **2012,** Vol. 211. https://doi.org/10.1016/j.toxlet.2012.03.020.
7. Neale, P. A.; Ait-Aissa, S.; Brack, W.; Creusot, N.; Denison, M. S.; Deutschmann, B.; Hilscherová, K.; Hollert, H.; Krauss, M.; Novák, J.; Schulze, T.; Seiler, T.-B.; Serra, H.; Shao, Y.; Escher, B. I. Linking in Vitro Effects and Detected Organic Micropollutants in Surface Water Using Mixture-Toxicity Modeling. *Environ. Sci. Technol.* **2015**, *49* (24), 14614–14624. https://doi.org/10.1021/acs.est.5b04083.
8. Wilkins, B. J.; Pack, M. Zebrafish Models of Human Liver Development and Disease. *Compr. Physiol.* **2013**, *3* (3), 1213–1230. https://doi.org/10.1002/cphy.c120021.
9. Menke, A. L.; Spitsbergen, J. M.; Wolterbeek, A. P. M.; Woutersen, R. A. Normal Anatomy and Histology of the Adult Zebrafish. *Toxicol. Pathol.* **2011**, *39* (5), 759–775. https://doi.org/10.1177/0192623311409597.
10. Kiamehr, M.; Heiskanen, L.; Laufer, T.; Düsterloh, A.; Kahraman, M.; Käkelä, R.; Laaksonen, R.; Aalto-Setälä, K. Dedifferentiation of Primary Hepatocytes Is Accompanied with Reorganization of Lipid Metabolism Indicated by Altered Molecular Lipid and MiRNA Profiles. *Int. J. Mol. Sci.* **2019**,

20 (12). https://doi.org/10.3390/ijms20122910.

11. Kim, M.; Lee, J. Y.; Jones, C. N.; Revzin, A.; Tae, G. Heparin-Based Hydrogel as a Matrix for Encapsulation and Cultivation of Primary Hepatocytes. *Biomaterials* **2010**, *31* (13), 3596–3603. https://doi.org/10.1016/j.biomaterials.2010.01.068.
12. You, J.; Park, S.-A.; Shin, D.-S.; Patel, D.; Raghunathan, V. K.; Kim, M.; Murphy, C. J.; Tae, G.; Revzin, A. Characterizing the Effects of Heparin Gel Stiffness on Function of Primary Hepatocytes. *Tissue Eng. - Part A* **2013**, *19* (23–24), 2655–2663. https://doi.org/10.1089/ten.tea.2012.0681.
13. Desai, S. S.; Tung, J. C.; Zhou, V. X.; Grenert, J. P.; Malato, Y.; Rezvani, M.; Español-Suñer, R.; Willenbring, H.; Weaver, V. M.; Chang, T. T. Physiological Ranges of Matrix Rigidity Modulate Primary Mouse Hepatocyte Function in Part through Hepatocyte Nuclear Factor 4 Alpha. *Hepatology* **2016**, *64* (1), 261–275. https://doi.org/10.1002/hep.28450.
14. Simonetti, R. B.; Santos Marques, L.; Streit Jr, D. P.; Oberst3, R. Zebrafish (Danio Rerio): Ethics in Animal Experimentation. *IOSR J. Agric. Vet. Sci. Ver. I* **2016**, *9* (7), 2319–2372. https://doi.org/10.9790/2380-090701106110.
15. Couteau, C.; Coiffard, L. Regulation No 1223/2009 on Cosmetic Products. Nouv. Dermatologiques **2010**, 29 (5 PART 1).
16. Uchea, C.; Owen, S. F.; Chipman, J. K. Functional Xenobiotic Metabolism and Efflux Transporters in Trout Hepatocyte Spheroid Cultures. *Toxicol. Res.* **2015**, *4* (2), 494–507. https://doi.org/10.1039/c4tx00160e.
17. Baron, M.; Mintram, K.; Owen, S.; Hetheridge, M.; Moody, A.; Purcell, W.; Jackson, S.; Jha, A. Pharmaceutical Metabolism in Fish: Using a 3- D Hepatic In Vitro Model to Assess Clearance. *PLoS ONE* **2017**, *12*, e0168837. https://doi.org/10.1371/journal.pone.0168837.
18. vom Saal, F. S.; Nagel, S. C.; Coe, B. L.; Angle, B. M.; Taylor, J. A. The Estrogenic Endocrine Disrupting Chemical Bisphenol A (BPA) and Obesity. Mol. Cell. *Endocrinol.* **2012**, *354* (1–2), 74–84. https://doi.org/10.1016/j.mce.2012.01.001.
19. Nagel, S. C.; Bromfield, J. J. Bisphenol a: A Model Endocrine Disrupting Chemical with a New Potential Mechanism of Action. *Endocrinology* **2013**, *154* (6), 1962–1964. https://doi.org/10.1210/en.2013-1370.
20. NCBI, N. C. for B. I. itgb1bp1 integrin beta 1 binding protein 1 [Danio rerio (zebrafish)] https://www.ncbi.nlm.nih.gov/gene/641420.
21. Kandel, M. E.; Hu, C.; Naseri Kouzehgarani, G.; Min, E.; Sullivan, K. M.; Kong, H.; Li, J. M.; Robson, D. N.; Gillette, M. U.; Best-Popescu, C.; Popescu, G. Epi-Illumination Gradient Light Interference Microscopy for Imaging Opaque Structures. *Nat. Commun.* **2019**, *10* (1), 1–9. https://doi.org/10.1038/s41467-019-12634-3.
22. Clay, N. E.; Shin, K.; Ozcelikkale, A.; Lee, M. K.; Rich, M. H.; Kim, D. H.; Han, B.; Kong, H. Modulation of Matrix Softness and Interstitial Flow for 3D Cell Culture Using a Cell-Microenvironment-on-a-Chip System. *ACS Biomater. Sci. Eng.* **2016**, *2* (11), 1968–1975. https://doi.org/10.1021/acsbiomaterials.6b00379.
23. Liang, Y.; Jeong, J.; DeVolder, R. J.; Cha, C.; Wang, F.; Tong, Y. W.; Kong, H. A Cell-Instructive Hydrogel to Regulate Malignancy of 3D Tumor Spheroids with Matrix Rigidity. *Biomaterials* **2011**, *32* (35), 9308–9315. https://doi.org/10.1016/j.biomaterials.2011.08.045.
24. Cha, C.; Kim, S. Y.; Cao, L.; Kong, H. Decoupled Control of Stiffness and Permeability with a Cell-Encapsulating Poly(Ethylene Glycol) Dimethacrylate Hydrogel. *Biomaterials* **2010**, *31* (18), 4864–4871. https://doi.org/10.1016/j.biomaterials.2010.02.059.
25. Yano, H.; Mazaki, Y.; Kurokawa, K.; Hanks, S. K.; Matsuda, M.; Sabe, H. Roles Played by a Subset of Integrin Signaling Molecules in Cadherin-Based Cell-Cell Adhesion. *J. Cell Biol.* **2004**, *166* (2), 283–295. https://doi.org/10.1083/jcb.200312013.
26. Shkumatov, A.; Baek, K.; Kong, H. Matrix Rigidity-Modulated Cardiovascular Organoid Formation from Embryoid Bodies. *PLoS ONE* **2014**, *9* (4), 1–10. https://doi.org/10.1371/journal.pone.0094764.
27. Yao, Y.; Lin, J.; Yang, P.; Chen, Q.; Chu, X.; Gao, C.; Hu, J. Fine Structure, Enzyme Histochemistry, and Immunohistochemistry of Liver in Zebrafish. *Anat. Rec.* **2012**, *295* (4), 567–576. https://doi.org/10.1002/ar.22416.
28. Ip, Y. K.; Chew, S. F. Ammonia Production, Excretion, Toxicity, and Defense in Fish: A Review. *Front. Physiol.* **2010**, *1*, 1–20. https://doi.org/10.3389/fphys.2010.00134.
29. Van Der Ven, L. T. M.; Holbech, H.; Fenske, M.; Van Den Brandhof, E. J.; Gielis-Proper, F. K.; Wester, P. W. Vitellogenin Expression in Zebrafish Danio Rerio: Evaluation by Histochemistry, Immunohistochemistry, and in Situ MRNA Hybridisation. *Aquat. Toxicol.* **2003**, *65* (1), 1–11. https://doi.org/10.1016/S0166-445X(03)00103-6.
30. Cosnefroy, A.; Brion, F.; Maillot-Maréchal, E.; Porcher, J.-M.; Pakdel, F.; Balaguer, P.; Aït-Aïssa,

S. Selective Activation of Zebrafish Estrogen Receptor Subtypes by Chemicals by Using Stable Reporter Gene Assay Developed in a Zebrafish Liver Cell Line. *Toxicol. Sci.* **2011**, *125* (2), 439–449. https://doi.org/10.1093/toxsci/kfr297.

31. Mommsen, T. P.; Walsh, P. J. 5 Vitellogenesis and Oocyte Assembly. In The Physiology of Developing Fish; Hoar, W. S., Randall, D. J. B. T.-F. P., Eds.; Academic Press, **1988**; Vol. 11, pp 347–406. https://doi.org/https://doi.org/10.1016/S1546-5098(08)60202-2.
32. Sumpter, J. P.; Jobling, S. Vitellogenesis as a Biomarker for Estrogenic Contamination of the Aquatic Environment. Environ. *Health Perspect.* **1995**, *103*, 173–178. https://doi.org/10.1289/ehp.95103s7173.
33. Crain, D. A.; Eriksen, M.; Iguchi, T.; Jobling, S.; Laufer, H.; LeBlanc, G. A.; Guillette, L. J. An Ecological Assessment of Bisphenol-A: Evidence from Comparative Biology. *Reprod. Toxicol.* **2007**, *24* (2), 225–239. https://doi.org/https://doi.org/10.1016/j.reprotox.2007.05.008.
34. Le Fol, V.; Aït-Aïssa, S.; Sonavane, M.; Porcher, J.-M.; Balaguer, P.; Cravedi, J.-P.; Zalko, D.; Brion, F. In Vitro and in Vivo Estrogenic Activity of BPA, BPF and BPS in Zebrafish-Specific Assays. *Ecotoxicol. Environ. Saf.* **2017**, *142*, 150–156. https://doi.org/https://doi.org/10.1016/j.ecoenv.2017.04.009.

5.8 Supporting Information

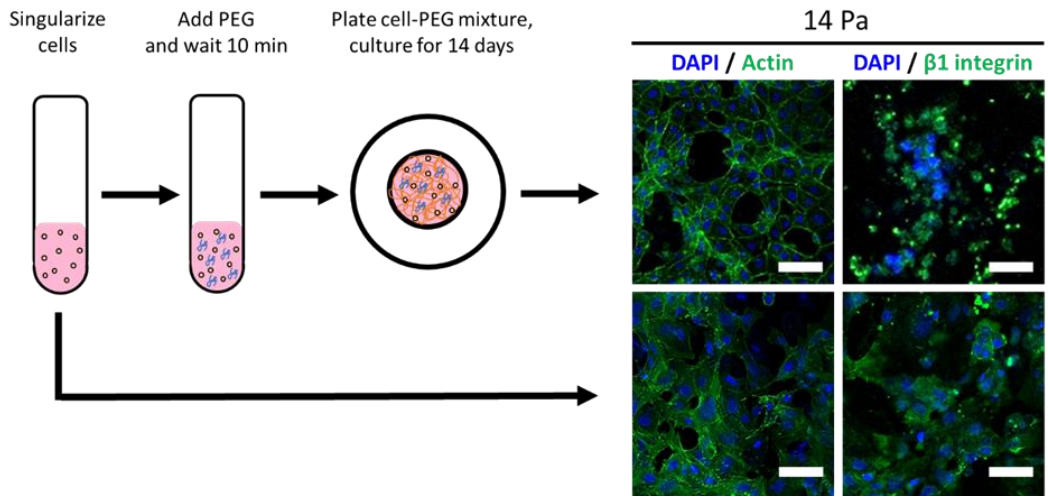

Supplementary Figure 5.1. Scheme of pre-coating zebrafish hepatocytes (ZF-L) with PEG and immunofluorescence imaging of hepatoids cultured on collagen-PEG hydrogels after 14 days. Zebrafish hepatocytes interacted with PEG monomers for 10 minutes prior to plating on collagen-PEG hydrogels with an elastic modulus of 14 Pa. The hepatoids had similar structure as those that were not mixed with PEG prior to plating when visualizing the nucleus (DAPI, blue) and actin filaments (green). Cell-matrix adhesions as visualized by β1 integrin (green) showed that the cells were adhering to the collagen fibers similarly.

Materials and Methods

Pre-treatment of zebrafish hepatocytes with polyethylene glycol (PEG)

Zebrafish hepatocytes were singularized in culture medium and mixed with 1:1 ratio of PEG (Sigma, MW 7500) for 10 minutes. After pre-treating the cells with PEG, the suspension was plated at a cell density of 1.0×10^6 cells/ mL onto pre-formed collagen-PEG hydrogels in glass bottom dishes (Cellvis). Then, they were cultured for 14 days at 28 °C and atmospheric carbon dioxide. The hepatoids were then stained using the immunofluorescence imaging method for the nucleus, actin filaments (phalloidin-Alexa 555, Invitrogen), and β1-integrin. Images were taken using a scanning confocal microscope (Zeiss LSM 710) using the 20x/0.8 air objective. Image acquisition and review were performed through the Zeiss Zen (Black and Blue, respectively) programs.

Chapter 6. Hybrid-spheroid culture with nanofibers

Contributions

As published in: **Chang Gyun Park**, Indong Jun, Sangmin Lee, Chang Seon Ryu, Sang-Ah Lee, Jaeho Park, Hyung-Seop Han, Honghyun Park, Andreas Manz, Heungsoo Shin, and Young Jun Kim, "Integration of bioinspired fibrous strands with 3D spheroids for environmental hazard monitoring" *Small* **2022**, *18*(22), e2200757. https://doi.org/10.1002/smll.202200757

Authorship contributions

Chang Gyun Park: writing - original draft, data curation, formal analysis, writing - review & editing.
Indong Jun: writing - writing - original draft, conceptualization, data curation, formal analysis, writing - review & editing.
Sangmin Lee: formal analysis, methodology, writing - review & editing.
Chang Seon Ryu: conceptualization, writing - review & editing.
Sang-Ah Lee: formal analysis, writing - review & editing.
Jaeho Park: formal analysis, methodology, writing - review & editing.
Hyung-Seop Han: conceptualization, data curation, formal analysis, writing - review & editing.
Honghyun Park: investigation, methodology, resources, writing - review & editing.
Andreas Manz: investigation, methodology, resources, writing - review & editing.
Heungsoo Shin: conceptualization, investigation, methodology, writing - review & editing.
Young Jun Kim: writing - original draft, conceptualization, funding acquisition, investigation, methodology, writing - review & editing.

Relation to the thesis

This study describes the attempt to produce a unique 3D culture platform that features bioinspired strands of electrospun nanofibers (BSeNs) and aquatic cell lines to compensate for shortcomings in the current cell spheroid generation techniques. The integrating 3D spheroids with BSeNs mitigated against the problems associated with hypoxia, and that the produced system is suitable for the testing of endocrine disrupting chemicals without the need for vertebrate platforms. I believe that this study makes a significant contribution to the literature because the use of animals for environmental testing is increasingly subjected to control, meaning that new means of testing the toxicity of environmental chemicals is required. 3D spheroids generally have issues involving hypoxia, and 2D platforms cannot provide results of sufficient accuracy. The results indicate that the novel BSeN-treated spheroid can provide answers to such problems. Furthermore, bioinspired materials that closely mimic ECM environments can yield efficient zebrafish cells with intrinsic functions and xenobiotic metabolism similar to those of zebrafish embryos. These findings have profound implications for designing *in vitro* cell culture-based monitoring platforms for alternative testing.

6.1 Abstract

Numerous methods have been introduced to produce three-dimensional (3D) cell cultures that can reduce the need for animal experimentation. This study presents a unique 3D culture platform that features bioinspired strands of electrospun nanofibers (BSeNs) and aquatic cell lines to compensate for shortcomings in the current cell spheroid generation techniques. The use of BSeNs in 3D zebrafish liver cell cultures is found to improve liver and reproductive functions through spheroid-based *in vitro* assays such as whole transcriptome sequencing and reproductive toxicity testing, with optimized properties exhibiting results similar to those obtained for fish embryo acute toxicity (FET, OECD TG 236) following exposure to environmental endocrine-disrupting chemicals (17β-Estradiol (E2), 4-hydroxytamoxifen (4-HT), and bisphenol compounds (bisphenol A (BPA) and 9,9-Bis(4-hydroxyphenyl)fluorene (BPFL)). These findings have beneficial effects of bioinspired materials that closely mimic ECM environments can yield efficient zebrafish cells with intrinsic functions and xenobiotic metabolism similar to those of zebrafish embryos. As a closer analog for the *in vivo* conditions that are associated with exposure to potentially hazardous chemicals, the straightforward culture model introduced in this study shows promise as an alternative tool that can be used to further eco-environmental assessment.

Keywords: biomimetics; fibrous strands; spheroids; environmental hazard assessment

6.2 Introduction

The misuse of chemicals can partially explain the increasing incidences of environmental and human health problems [1–3]. The multidisciplinary field termed ecotoxicology investigates how environmental pollutants affect the aquatic and terrestrial environment [4], and is aimed primarily at understanding undesirable events in the natural environment by performing ecotoxicological testing and risk evaluations of new chemicals that are used, discarded, or reach the environment. Ecotoxicologists also conduct detailed monitoring studies elucidating the physiological and biochemical responses of organisms following pollutant exposure, which often reflect toxic effects [5]. Over the past few decades, government agencies have mandated testing toxicity on live animals to determine the environmental risk of new chemicals or products on the market [6]. However, the use of animals in scientific and medical tests is generally subject to animal welfare protection [7], and the European Commission (EC) has produced a directive to ban animal testing for cosmetics or household products [8]. The need for alternative approaches to the use of vertebrate animals for hazard assessments of chemicals and pollutants has thus become increasingly important [9], with the use of vertebrates for environmental risk assessment banned for several regulatory purposes. Therefore, the first consideration when starting a vertebrate ecotoxicity test is to minimize the unnecessary use of vertebrate organisms as far as possible.

Fish are ideal sentinels for evaluating aquatic toxicity in vertebrates and have become a popular alternative model system in aquatic ecotoxicology [10,11]. The zebrafish is a particularly convenient model

because of its easy maintenance and high numbers of offspring. In particular, fish embryo toxicity (FET) tests using zebrafish have attracted attention as an alternative method for animal experiments [12,13]. Many studies have indicated that fish embryos provide excellent versatility for environmental and biological assessment applications, ranging from acute system toxicity, sub-chronic toxicity, and teratogenicity to endocrine disruption [13–16]. Lee et al. comprehensively analyzed acute toxic and thyroid hormone disturbances effect of endocrine-disrupting chemicals (EDCs) in zebrafish embryos [17]. In particular, zebrafish embryos are considered to suffer from no sentinel, minor pain, or discomfort when exposed to chemicals prior to 120 h post-fertilization (hpf) [18]. According to EU Directive 2010/63/E.U. on the protection of animals used for scientific purposes, animals in the early life stages are not defined objects for protection [19]. Therefore, zebrafish embryos do not fall within the regulatory framework for animal experiments when still within 120 hpf.

An excellent alternative *in vitro* ecotoxicity monitoring platform using cells can evaluate acute and subchronic toxicity or mechanistic pathways without any restrictions [20]. Cellular studies are essential in ecotoxicity studies because the primary interaction between hazardous chemicals and environmental species begins at the cellular level [21]. Cytotoxicology, for instance, provides an essential concept for understanding ecotoxicological processes because it plays a crucial role in explaining the mode by which toxins act. Therefore, the relationship between the cytotoxic response and toxicity can be a valuable starting point for ecotoxicological studies. Furthermore, cell culture systems can provide valuable information that can be used better to control cellular functions and processes for *in vivo* experiments. Even today, most studies are based on experiments using 2D cell cultures as *in vitro* tests. However, several heterogeneous disparities are associated with 2D cultures in the *in vivo* environment, such as perturbations in the interaction between cells and the extracellular environment and changes in the cell morphology, polarity, and methods of division [22]. These shortcomings have instigated high demand for new approach methodologies (NAMs) that can more closely mimic *in vivo* conditions [23]. Thus, over the past few decades, 3D cell cultures have gained increased recognition as a highlighted evaluation tool in biological research. Spheroids are the simplest 3D culture models that are used in studies in which the physiological representation of underlying tissue is compared with other commonly used models such as cells grown in monolayers (2D) [24]. Numerous studies have demonstrated the suitability of the 3D spheroid culture system as an *in vitro* alternative to evaluate chemical toxicity and environmental samples in biological and ecotoxicity studies. Several studies have shown that 3D spheroid models exhibit several *in vivo* environmental features, such as cell–cell interactions, drug penetration, and resistance [25,26]. For example, Mandon et al. reported that 3D hepaRG spheroids are possible models for genotoxicity assessment to detect carcinogens *in vitro* [27]. Sirenko et al. reported that human 3D culture models derived from iPSC-differentiated cells could provide valuable systems for analyzing drug-induced toxicity [33]. However, spheroids that are produced by the universal method are subjected to challenges associated with viability, hypoxia, and long-term culture because of the strong cell-to-cell interactions within the spheroids [28]. One significant disadvantage in using conventional spheroid cultures is that nutrients and oxygen are not supplied at sufficient abundance to the core of the spheroids because the diffusion gradient increases alongside the size of a spheroid [29]. In addition, 3D spheroid platforms have been established for *in vitro* mammalian toxicity studies but have not been actively considered for investigating model aquatic species in environmental applications. Therefore, the overall interspecies response difference between highly

simplified 3D rotating ellipsoids and potentially dangerous chemicals in fish models is one of the challenges that researchers must overcome.

Previous studies have revealed that bioinspired materials overcome the limitations posed by the conventional spheroid system and offer advantages such as improved viability, proliferation, and oxygen transport. For example, we previously reported on the use of bioinspired strands of electrospun nanofibers (BSeNs) that were assembled using human cell lines such as fibroblasts, chondrocytes, HUVECs, and stem cells [30–34]. BSeNs are fibrous strands of several micrometers in length with nanoscale diameters that are obtained by electrospinning and mimic the structures of collagen fibrils [33]. BSeN-incorporated spheroids have demonstrated improved viability and reduced hypoxia and apoptosis [30]. Here, we further hypothesized that BSeN would improve the toxicity evaluation of potentially hazardous chemicals and could serve as an *in vitro* platform for environmental hazard assessment. The objectives of this study were: 1) investigate the effect of using BSeN in 3D spheroids composed of zebrafish liver cells, 2) examine the effect of BSeN in regulating the viability, hypoxia, and functioning of cells in spheroids through spheroid-based *in vitro* assays, and 3) verify the similarity in using BSeN-incorporated 3D spheroids and fish embryo acute toxicity tests to investigate the correlation between potentially hazardous chemicals and reproductive toxicity (FET, OECD TG 236). We suggest that combining bioinspired materials with cell lines in the aquatic environment may serve as a starting point for an *in vitro* test method that can be used as a monitoring platform for environmental risk assessment.

6.3 Materials and Methods

6.3.1 Materials

Poly(l-lactic acid) (PLLA) was obtained from Samyang (Seoul, Korea), and isopropyl alcohol, Tris-HCl, dopamine, dimethyl sulfoxide (DMSO), 17β-estradiol (E2), 4- Hydroxytamoxifen (4-HT), Bisphenol A (BPA), and 9,9-Bis(4-hydroxyphenyl)fluorene (BPFL) were purchased with high purity from Sigma–Aldrich (Steinheim, Germany). For ZFL cell culture, Leibowitz-15 medium and 0.25% trypsin–EDTA were obtained from ATCC® (Wesel, Germany). Ham's F12 and Dulbecco's modified Eagle's mediums (DMEM), mouse epidermal growth factor, fetal bovine serum (FBS), and phosphate-buffered saline (PBS; pH 7.4) were purchased from Thermo Scientific (Karlsruhe, Germany). Other supplements, including HEPES, sodium bicarbonate, penicillin-streptomycin, and bovine insulin, were purchased from Sigma–Aldrich. Trout serum was obtained from Caisson Laboratories (Smithfield, UT, USA).

6.3.2 Fabrication and preparation of BSeN

PLLA electrospun nanofiber sheets were fabricated and prepared as previously described. Briefly, a 4% PLLA solution was prepared in a DCM and trifluoroethanol (TFE) mixture (8:2, v/v), and 10 mL of the solution was ejected by a syringe pump at a rate of 5 mL/h (KDS200; K.D. Scientific, New Hope, PA, USA) through a 23-gauge needle under 12.8 kV. The solution was then deposited on a rotating mandrel collector

(SPG, Incheon, Korea) and the electrospun collected sheet was dried overnight. To fabricate BSeN, PLLA electrospun nanofiber sheets were immersed in 10% (v/v) ethylenediamine solution in isopropyl alcohol (IPA) and incubated for 30 min at 37°C under vigorous shaking at 200 rpm. The BSeNs were then collected by centrifugation at 4000 rpm for 5 min and washed with IPA (3 times), 70% EtOH (once), and distilled water (DW, 3 times) before they were lyophilized for 24 h. For the polydopamine coating, 50 mg of BSeN was suspended in 70% EtOH and washed with DW. Subsequently, the BSeN was dispersed in dopamine hydrochloride solution dissolved in 10 mM Tris-HCl buffer (2 mg/mL, pH 8.5) and stirred at 100 rpm for 10 min. Thereafter, the resulting polydopamine-coated BSeN (PD-BSeN) was washed twice with DW and lyophilized overnight.

6.3.3 Characterization of strand electrospun fibers

The surface morphology of strand electrospun fibers was observed using scanning electron microscopy (SEM; Quanta 250 FEG, FEI Company, Eindhoven, Netherlands) at a low vacuum mode (200 Pa) with a LFD sensor. The accelerating voltages were 5.0 and 7.0 kV, respectively. The samples were prepared on a silica wafer, and air-dried at room temperature. The diameter of BSeNs was analyzed by ImageJ software. A total of 50 single fibers captured from SEM images were analyzed for the diameter measurement (n = 50). Surface roughness was observed by atomic force microscopy (AFM; XE-100, Park system, Suwon, Korea). Samples were scanned at the repetition rate of 0.4 Hz in the non-contact mode on a 5 x 5 μm^2 surface area. The bundle form samples were dispersed in ethanol and dried on the stub for the detailed analysis of single form fiber. The roughness of the surface before and after polydopamine coating was evaluated on a 1μm x 1μm magnified surface. The images were then processed via a software package (XEI, Park system, Korea). The surface chemical composition of the fibers was also analyzed by highresolution X-ray photoelectron spectra (XPS) (Theta Probe Base System, Thermo Scientific).

6.3.4 Cell Culture and incorporation of ZFL spheroids with BSeN and PD-BSeN

The zebrafish liver (ZFL) cell line was obtained from ATCC (CRL2643) and cultured in a complete growth medium in T-75 flasks at 28°C in a cell incubator (Thermo Scientific). The complete growth medium was composed of 50% Leibowitz-15, 35% DMEM, and 15% Ham's F12 supplemented with 15 mM HEPES, 0.15 g/L sodium bicarbonate, 1% penicillin-streptomycin, 0.01 mg/mL of bovine insulin, 50 ng/mL mouse epidermal growth factor, 5% heat-inactivated FBS, and 0.5% trout serum. For comparative experiments, cells from the same batch were used, and the density was fixed at 50,000 cells per well. ZFL cells in T-75 flasks were washed with PBS and treated with 0.25% trypsin–EDTA. The cells were then suspended in a complete growth medium and centrifuged at 125 × g for 5 min. The pelleted cells were resuspended in the medium and counted using a cell counter (TC20 automated cell counter (Bio-Rad Laboratories, Feldkirchen, Germany). After counting, the cells were seeded in a six-well flat-bottom plate (Thermo Scientific) to produce the monolayer culture. The cells were seeded in BIOFLOAT 96-well U-bottom plates (faCellitate, Mannheim,

Germany) and centrifuged at 125 × *g* for 5 min for the spheroid culture. To fabricate hybrid spheroids, BSeN and PD-BSeN were sterilized using 70% ethanol under UV exposure for 30 min and then washed twice with distilled water. Then, ≈ 50,000 cells were combined with 1 μg of BSeN or PD-BSeN and seeded into each well of BIOFLOATTM 96-well U-bottom plates. The mixture was centrifuged at 125 × *g* for 5 min and cultured in an incubator at 28 °C. The complete growth medium was replaced at a half-ratio every 2–3 days.

6.3.5 Zebrafish and fish embryo acute toxicity (FET)

Adult wild-type zebrafish were obtained from the European Zebrafish Resource Center (EZRC; Karlsruhe, Germany). Fish maintenance, breeding conditions, and egg production were performed under internationally accepted standards (temperature 26.0 ± 1.0°C and 10/14 h dark/light cycle). The zebrafish were fed twice daily with freshly hatched brine shrimp. The embryo acute toxicity test was conducted according to OECD TG 236 with slight modifications. Briefly, freshly laid eggs were transferred to sterilized dishes filled with clean fish water (E3 medium). After controlling fertilization, eleuthero embryos were transferred to multiple wells (6 well, Corning) at 72 hpf with 6 mL of test solution added per well. The exposure concentrations of E2, 4-HT, BPA, and BPFL used in the toxicity assessment were selected through a preliminary range-finding test (Supplementary Figure 6.11). For the FET, stock solutions of E2, 4-HT, BPA, and BPFL were prepared by dissolving each chemical in dimethyl sulfoxide (DMSO). Diluted solutions were prepared by diluting these stocks at least 100-fold using culture media. The chemicals were exposed to eleutheroembryos for 48 h, and the embryos were employed for Vtg measurement.

6.3.6 Construction of transfected cell line and luciferase reporter assay

The human embryonic kidney 293 cell line (HEK293, CRL-1573; ATCC, Wesel, Germany) was used as a transfection host for the zebrafish estrogen receptor alpha (zESR1) construct. The HEK293 cells were cultured in DMEM with 10% fetal bovine serum and 1% penicillin-streptomycin (Thermo Scientific), at 37°C and 5% CO2. The HEK293 cells were transduced using the pGreenFire Lenti-reporter plasmid (pGF2-ERE-rFLuc-T2A-GFP-mPGK-Puro, TR455VA-P; System Biosciences, Palo Alto, USA) that encodes GFP reporter and red-shifted luciferase, under the control of ERE response elements with the puromycin resistance, according to a previously described methodology [51]. The transduced cells were selected with the addition of puromycin (10 μg/mL) in the culture medium. Then, the cells (HEK293-ERE) were transfected with the piggyBac transposon gene expression system. The zESRα expression vector was custom-cloned by vectorbuilder (pPB-Neo-CAG>zESRα, VB210426-1022cns; Vectorbuilder Inc. Chicago, USA) and the pRP-mCherry-CAG>hyPBase plasmid (VB160216-10057; Vectorbuilder Inc) encodes the hyperactive version of piggyBac transposase. After transfection, the transfected cells (HEK293-ERE-zESRα) were selected with the culture medium containing puromycin (10 μg/mL) and neomycin (2 μg/mL). The constructed cells were utilized to evaluate (anti)estrogenic activities. E2 and 4-HT were used as reference chemicals for estrogenic and antiestrogenic activities, respectively. The test chemicals were purchased with high purity (≥ 98%) from Sigma–Aldrich and were dissolved in dimethyl sulfoxide (DMSO). Cells were exposed to half-logarithmic

(3.16-fold) dilutions of test chemicals and the concentrations of which did not exceed 0.5% (v/v). The transfected cells were seeded at a rate of 2.0×10^4 cells per well on a 96-well plate. After overnight, the chemical solutions were treated with a ratio of 1:1 in each well containing the medium, and cultured for 24 h. The cells were lysed with passive lysis buffer (Promega, Mannheim, Germany), and the lysates were applied to evaluate luciferase activity using the Luciferase Reporter Assay (Promega). Luminescence was measured as relative luminescence units. The luminescence units for each condition were replicated for eight wells, and a mean value was calculated. The experiment was repeated three times from independent cultures ($n = 3$).

6.3.7 ATP (cell viability) measurement

To measure the cell viability of 3D, Hybrid-1, and Hybrid-2 groups, each condition was prepared in the same manner as described in the method section and was evaluated at 1, 28, and 56 days, respectively. The complete medium with a spheroid (100 μL) was transferred from the ultra-low attachment plates to 96-well white opaque culture plates (Thermo Scientific). Then, each well of the different cell concentrations was treated with 100 μL of CellTiter-Glo® 3D reagent (Promega, Mannheim, Germany), and the luminescent signal was recorded after 30 min using a microplate reader (Tecan, Männedorf, Switzerland). Each group was replicated to eight spheroids and calculated as the mean value. The experiment was repeated three times from independent cultures ($n = 3$).

6.3.8 DNA measurement

For the measurement of DNA content, a Quant-iT PicoGreen dsDNA Assay Kit was purchased from Invitrogen (Carlsbad, CA, USA). The assay was conducted for the spheroid and spheroids with nanofibers cultured for 1, 28, and 56 days, respectively. First, each spheroid was pooled in a tube and washed with PBS. Next, the pooled spheroids were lysed in 100 μL of RIPA lysis buffer and centrifuged at 10,000 × *g* for 10 min after vortexing for 2 min. Then, each supernatant was transferred into a new tube and used for the DNA assay. Each supernatant (10 μL) was reacted with working reagents provided from the Quant-iT Picogreen dsDNA assay kit. The fluorescent intensity was measured using a fluorescent microplate reader (Tecan, Männedorf, Switzerland) with excitation and emission wavelengths of 480 and 520 nm, respectively. In the experiment of polydopamine coating condition, each fiber group was replicated to four spheroids and calculated as the mean value. The experiment was repeated eight times from independent cultures ($n = 8$). In the experiment of spheroid long-term culture, each group was replicated to eight spheroids and calculated as a mean value. The experiment was repeated three times from independent cultures ($n = 3$).

6.3.9 Fluorescence observation

Cell cytoskeleton (F-actin), nuclei, hypoxia factor, viability, and Vtg were observed by using fluorescence microscopies. The cytoskeleton of cells was analyzed at 1 and 3 days using Alexa Fluor 568-Phalloidin (Cat. #A12380; Thermo Scientific). Each sample of different cultures was washed with PBS and fixed in 3.7% paraformaldehyde at room temperature (RT) for 15 min. Thereafter, the samples were permeabilized with 0.1% Triton X-100 at RT for 5 min. After permeabilization, the samples were washed three times with PBS and blocked with 3% bovine serum albumin (BSA; Sigma–Aldrich) at RT for 30 min. Next, samples were incubated with the phalloidin staining solution for 2 h at RT After washing three times with 1% of BSA, and the samples were stained with 4′,6- diamidino-2-phenylindole (DAPI; Vector Laboratories, Burlingame, CA, USA). For the observation of FITC-coated BSeN, the lyophilized BSeN was dispersed in 1 mL of PBS. FITC was dissolved in DMSO at a concentration of 30 mM, and 10 μL of the FITC solution was added to the suspension. The reaction was proceeded in the dark at RT under constant stirring for 4 h. The coated BSeNs were collected by centrifugation at 4,000 rpm for 10 min after washing with PBS (3 times). Then, 50,000 cells were combined with 1 μg of the FITC-coated BSeN and seeded in each well of BIOFLOATTM 96-well U-bottom plates. The spheroids with FITC-coated BSeN were cultured for 3 days. Then, the samples were prepared in the same manner with the cytoskeleton staining. The hypoxia of cells was stained at 7 and 14 days by BioTracker 520 green hypoxia dye (Cat. #SCT033; EMD Millipore, CA, USA). The culture medium of cells was removed and rinsed twice with PBS. The staining solution that was composed of the hypoxia dye and the culture medium was treated for 24 hours. After incubation, each sample was prepared in the same manner with the cytoskeleton staining. The cell viability was measured by live and dead staining. Samples were cultivated for 14 days, and then the culture medium was removed. Fluorescein diacetate (FDA; Sigma–Aldrich) and propidium iodide (PI; Sigma–Aldrich) were dissolved in a culture medium without FBS and trout serum. Next, the staining solution was added to each well. After incubation in the dark for 20 min, the staining solution was removed, and the samples were washed with PBS. The Vtg was detected on day 14 culture using an immunofluorescence assay. Samples were prepared with fixation, permeabilization, and blocking processes. Then, each sample was incubated with the primary antibody (Cat. #LS-C76845; LSBio, WA, USA) overnight at 4°C, and then washed three times with 1% of BSA. Each sample was incubated with the secondary antibody (Cat. #31232; Thermo Scientific) for 2 hours and rewashed three times with 1% of BSA. The samples were embedded in a mounting medium containing DAPI.

The monolayer cells were imaged under an inverted fluorescence optical microscope (DMi8, Leica-Microsystems, Wetzlar, Germany) equipped with a digital camera (DCF295, Leica-Microsystems), a fluorescence excitation light source CoolLED pE300-lite (CoolLED Ltd. Andover, U.K.), and a software (LAS AF version 3.1.0, Leica-Microsystems, Mannheim, Germany). The spheroid cultures were imaged using a Lightsheet Z.1 microscope (Carl Zeiss Microscopy GmbH, Jena, Germany) with two-sided 10×/0.2 illumination optics and a 20×/1.0 detection optic equipped with a pco.edge 4.2 camera (PCO AG, Kelheim, Germany). The captured images were analyzed using ZEN imaging software (Carl Zeiss, Jena, Germany).

6.3.10 Observation of spheroid-incorporating BSeNs by SEM

The spheroid were cultured for 3 days to investigate the distribution of BSeN in the spheroids. Then, the spheroids were fixed in 3.7% paraformaldehyde, then attached to carbon conductive adhesive tape, and

lyophilized overnight. The samples were observed using SEM (Quanta 250 FEG) at a low vacuum mode (200 Pa) with an LFD sensor. The accelerating voltage was 5.0.

6.3.11 Fluorescence-activated single-cell sorting (FACS)

Cell viability, hypoxia, and proliferation analyses were performed using flow cytometry. The cell viability was analyzed at day 3 culture using Live/dead fixable staining kits (Cat. #PK-CA707-32006; PromoCell, Heidelberg, Germany). Hypoxia and proliferation were analyzed at day 7 culture using BioTracker 520 green hypoxia dye (Cat. #SCT033; Sigma–Aldrich) and Click-iT EdU flow cytometry assay kits (Cat. #C10418; Invitrogen, Carlsbad, CA, USA), respectively. All experiments were conducted according to the manufacturer's instructions. For the analysis of the 2D group, 50,000 cells were seeded into each well of a 6-well flat-bottom plate. The cells from the three wells were detached as single cells by trypsinization and pooled in a tube. In spheroid groups, eight spheroids were collected into a tube and separated as single cells by trypsinization. Each tube of pooled 2D, 3D, Hybrid-1, and Hybrid-2 groups was considered a sample. Five replicate samples of each group were prepared from independent culture ($n = 5$). Then, each sample was fixed 3.7% paraformaldehyde at RT for 15 min. Thereafter, the fixed cells were permeabilized with 0.1% Triton X-100 at RT for 5 min. Next, the cells were rinsed twice with PBS containing 1% BSA, and the cells were immediately analyzed by ZE5 Cell Analyzer (Bio-Rad Laboratories, Munchen, Germany). Qualitative and quantitative analysis was performed using FCS Express software (De NovoTM software, Glendale, CA, USA).

6.3.12 Whole transcriptome sequencing (RNA-Seq) analysis

Total RNA samples of 2D, 3D, and Hybrid-2 groups were extracted for RNA-Seq analysis. To extract the total RNA sample from monolayer cell culture, 1 mL of ZFL cells (50,000 cells/mL) were seeded in each well of a 6-well flat-bottom plate and cultured for 7 days. The cells of three wells were collected in a tube and lysed with RLT buffer (Qiagen, Hilden, Germany) after washing with cold PBS. For the total RNA samples from the spheroid and with nanofibers cultures, 100 µL of 50,000 cells were seeded in each well of BIOFLOAT^{TM} 96-well U-bottom plates and cultured for 7 days, respectively. We collected 48 spheroids in a tube and centrifuged them at 125 × g for 5 min. After washing with cold PBS and centrifugation again, the samples were lysed in the same manner as monolayer cells. Each tube of pooled conditions was considered a sample, and twelve total RNA samples (each condition in quadruplicates; $n = 4$) were sent to a Novogene for RNA-Seq (Novogene, Cambridge, UK). Total RNA samples were purified using poly-T oligo-attached magnetic beads after quality control checks. Paired-end sequencing (150 bp) was conducted using an Illumina NovaSeq 6000 system. Samples were sequenced at a sequencing depth of at least 48 million clean reads, and 15 G raw bases were generated per sample. Raw sequences were filtered for contaminant adapter sequences and reads with > 10% uncertain nucleotides or > 50% low-quality nucleotides (Qphred ≤ 5). Filtered reads were considered clean reads, and the reads of each sample were used for data analysis. Data analysis was

conducted by Novogene. Paired-end clean reads were aligned to the reference genome (genome assembly: GRCz11_gca_000002035_4, Taxon ID: 7955) using HISAT2 to count the read numbers mapped to each gene. The FPKMs in each sample was determined based on the gene length and read count mapped to the gene. Differential expression analyses of two conditions/groups (in quadruplicates for each condition) were conducted using the *DESeq2* R package, which identifies differential expression among genes using a model based on the negative binomial distribution. *P* values were adjusted (P_{adj}) using the Benjamini and Hochberg method to control the false discovery rate. Differentially expressed genes (DEGs) were evaluated at a level of $P_{adj} < 0.05$.

6.3.13 qRT-PCR analysis

Total RNA samples of 2D, 3D, Hybrid-1, and Hybrid-2 groups were extracted in the same manner as RNA-Seq analysis except for the culture time (14 days). Each tube of pooled conditions was considered a sample, and eight replicate samples were prepared for each condition ($n = 8$). Total RNA of each sample was extracted using an RNeasy Plus Mini kit (Cat. #74136; Qiagen, Hilden, Germany). The concentration and purity of samples were determined spectrophotometrically using a NanoDrop™ 2000 spectrophotometer (Thermo Scientific). The reverse transcription was performed when the purity of samples was higher than 2.0 (OD260/280 and OD260/230). According to the manufacturer's instructions, the reverse transcription was conducted using a High-Capacity RNA-to-cDNATM kit (Applied Biosystems, Waltham, MA, USA). The total RNA (1 μg) was used for the reverse transcription. Reverse transcription was performed for samples with purity > 2.0 (OD260/OD280 and OD260/OD230). Thereafter, real-time PCR (7500 FAST Real-Time PCR System, Applied Biosystems) was conducted using the TaqMan Gene Expression Master Mix (Thermo Scientific) and PowerUp™ SYBR™ Green Master Mix (Applied Biosystems). The probe assay identifications and reaction cycles are described in Supplementary Table 6.1 and Supplementary Table 6.2. The relative mRNA expressions were determined using the $2^{-\Delta\Delta CT}$ method [52].

6.3.14 Enzyme-linked immunosorbent assay (ELISA)

In the monolayer culture, 1 mL of 50,000 cells were seeded in each well of a 6-well flat-bottom plate and cultured for 5 and 14 days, respectively. The 1.0×10^6 cells were collected from three wells into a tube by centrifugation at 125 × *g* for 5 min after trypsinization and cell counting. Then, the cells were washed with PBS and centrifuged again. The pooled cells were homogenized with cold RIPA buffer (Thermo Scientific) by vortex for 2 min. For spheroids and with nanofibers cultures, 100 μL of 50,000 cells were seeded in each well of BIOFLOAT™ 96-well U-bottom plates and cultured for 5 and 14 days, respectively. About 48 spheroids of the 96-well plate were collected into a tube and centrifuged at 125 × *g* for 5 min. After washing with PBS and centrifugation again, cold RIPA buffer was added to a tube and homogenized by vortex for 2 min. The homogenates in each tube were centrifuged at 14,000 × *g*, 4°C for 10 min. The supernatants were transferred to new tubes and were stored at −80°C until the Vtg quantification. Each tube of pooled cells or

spheroids was considered as a sample, and five replicate samples of each condition were prepared (n = 5).

In the experiment of Vtg levels upon EDCs exposure, 30 embryos of each group were pooled into a tube. Then, the tubes were centrifuged at 125 × g and 4°C for 5 min. The centrifuged embryos were washed with deionized water and centrifuged again. Next, 500 μL of cold RIPA buffer was added to each pooled tube and homogenized with beads using a homogenizer for 2 min. After centrifugation at 14,000 × g and 4°C for 10 min, the supernatants were transferred to new tubes. The tubes were stored at −80°C until being used for the quantification. Each pooled tube was considered as a sample, and six replicate samples of each condition were prepared for the quantification (n = 6). According to the manufacturer's instructions, the quantification was measured using an ELISA kit (Cat. #10004995; Cayman Chemical, MI, USA).

6.3.15 Analysis of correlation coefficient

Before calculating each correlation coefficient, the data set conducted the Shapiro-Wilk test using the basic function in R-open source software. All of the test groups followed the Gaussian distribution (P-values > 0.05). The Pearson's correlation coefficients were calculated/visualized using the "psych" package in R to investigate the relationship among the test groups (https://cran.rproject.org/web/packages/psych/psych.pdf).

6.3.16 Statistical analysis

All the graphs, calculations, and statistical analyses were performed using GraphPad Prism software version 8.0 (GraphPad Software, San Diego, CA, USA). All data are expressed as means ± standard deviation (SD). Data were tested for normality and homogeneity of variance to determine whether to perform parametric or non-parametric statistical tests. Statistical differences among test groups were determined using one-way analysis of variance (ANOVA) followed by post hoc Dunnett's T3 test (non-homogeneous variance) or Scheffe's test (homogeneous variances). All statistical analyses for RNA-Seq were performed using the *DESeq2* R package; heatmaps were generated based on FPKM cluster analysis according to the log2(FPKM+1) value, and a volcano plot was created from DEG gene expression levels according to $-\log10(P_{adj})$.

6.4 Results and Discussion

Over the past few decades, the most common method of evaluating the toxicity of a chemical mixture has been through animal testing. However, the use of animals for toxicity testing can raise concerns about animal ethics, and the need for alternative animal testing methods is growing worldwide. In addition, there is growing confidence in the substitution of animal testing as many studies have already demonstrated that the results of alternative animal testing are reproducible and predictable. In this context, different approaches to cell-based

platforms should be studied to investigate the effectiveness of alternative tests, even in environmental toxicity assessment. This study uses a combination of aquatic cell lines and bioinspired materials to present high potential as a screening platform for *in vitro* environmental hazard assessment. A 3D spheroid-based evaluation platform using bioinspired materials can provide results similar to *in vivo* experiments and has the advantages of microarrays such as high throughput and simplicity.

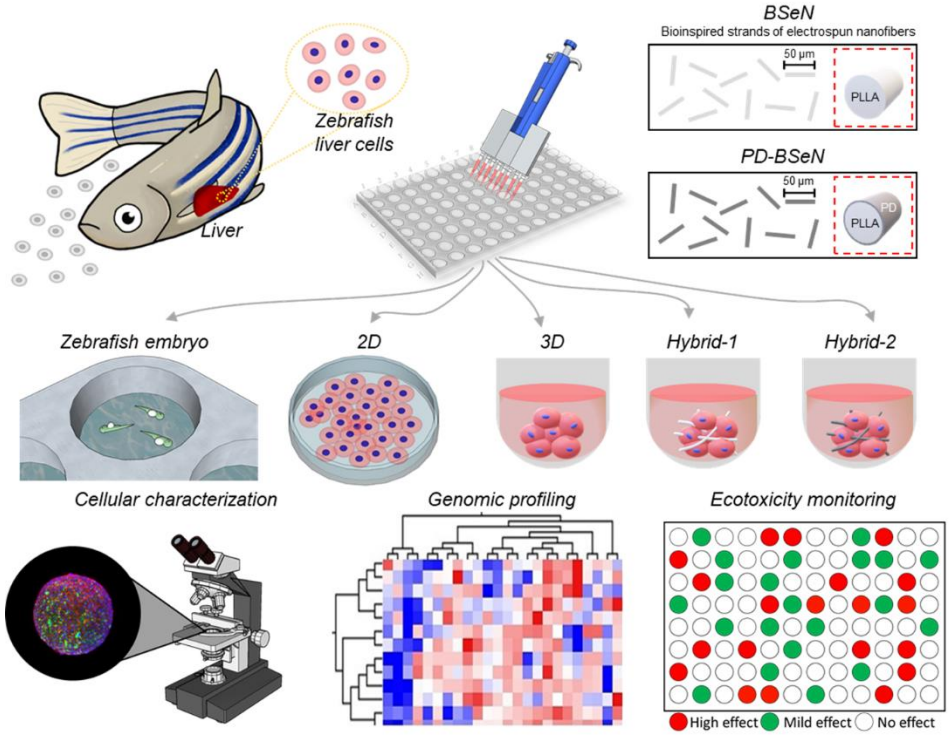

Figure 6.1. Schematic illustration of this study. Zebrafish liver (ZFL) cells were cultured as monolayers, spheroids, and hybrid-spheroids. BSeN and PD-BSeN were fabricated for use in the hybrid-spheroid cultures. Comparative analyses of the generated groups were conducted using cellular characterization, genomic profiling, and ecotoxicity monitoring techniques depending on culture time.

6.4.1 Characterization of BSeNs

Several methods have been used to generate 3D spheroid cultures and extensive reviews of these efforts have been produced elsewhere. One of the most critical issues associated with the most commonly used spheroid cultures is problems with the distribution of oxygen. Increasing the size of a spheroid can lead to oxygen depletion (hypoxia) and causes cell necrosis in the core, and the presence of necrotic cells within a spheroid may render it useless for toxicity screening. Zebrafish liver cells are known to be useful in forming spheroids on non-adhesive plates; however, we previously demonstrated the problem of hypoxia and the changes in the inner structure of the spheroid upon increasing the cell number or prolonging the culture period [35]. Therefore, a multidisciplinary approach is required to overcome the limitations in the existing methods that are used for spheroid generation. Moreover, it is a priority to develop an innovative toxicity assessment platform that can improve the function of a cell while improving the viability of cells inside the spheroid, as

this is the main reason for generating spheroids for environmental toxicity assessment using bioinspired materials. In this study, we present a multidisciplinary approach for the production of in vitro toxicological screening platforms using a combination of aquatic cell lines (zebrafish liver cells) and bioinspired materials (Figure 6.1). Our core technique involves the assembly of 3D spheroid cultures of zebrafish cells using BSeNs. We hypothesize that this form of BSeN serves as a physical bridge for the transportation of oxygen and nutrients into the core of spheroids, thereby overcoming the limitations posed by conventional spheroids and providing advantages such as improving viability and increasing proliferation, and supporting the transport of oxygen.

The extracellular matrix (ECM) is a non-cellular 3D macromolecular fibrillar network that can provide a physical platform for cells and stimulate interactive biochemical and biomechanical signals [36]. We previously reported the preparation of ECM-mimicking fibrous strands through the aminolysis-based partial degradation of electrospun nanofibers to produce individual short fibers by cleaving the ester linkage of poly L-lactic acid (PLLA) with ethylenediamine and generating an amide bond with amine functionality (Figure 6.2a and Supplementary Figure 6.1) [30,32]. However, substrates that are prepared using PLLA, a synthetic biodegradable material, may not have cell-interactive properties, leading to poor cell interaction. Therefore, we used a mussel-inspired coating method to increase the cell affinity of the BSeN surface. The SEM images showed changes in form from a mesh of aligned nanofibers to well-distributed relatively minor individual short fibers following the fragmentation process (Figure 6.2b). It was confirmed that aminolysis of partially degraded electrospun nanofibers resulted in the production of individualized fibers with lengths of 50–80 μm, regardless of the presence or absence of polydopamine coating on the BSeN. Since BSeN described above has similar dimensions to fibrillar proteins, the major fibrous proteins of the ECM, it will mimic the nanoscale structural aspects of ECM and positively affect the activity of cell–ECM interactions [37,38]. Figure 6.2c depicts BSeN group surfaces that have been subjected to polydopamine coating, as confirmed by AFM (atomic force microscopy). The AFM images revealed that PD-BSeN increased the roughness. For example, the roughness value (Ra) of the original BSeN surface was 5.35 ± 2.29 nm, while the roughness of the surface of PD-BSeN increased to 79.42 ± 12.44 nm (Figure 6.2e). The chemical composition of BSeN was evaluated using XPS, and clear nitrogen peaks (N1s) were observed (Figure 6.2f and Supplementary Figure 6.2). In addition, we provided clear evidence for the presence of catecholamines in the PD-BSeN group using micro-BCA analysis (Figure 6.2g). Dopamine is considered a small-molecule mimetic of Mytilus edulis foot protein-5 (Mefp-5) in that it contains both catechol and the primary amine functional groups that are present in the side chains of 3,4-dihydroxyphenylalanine (DOPA) and Lys residues [39,40]. Incubation of the target substances in an alkaline dopamine solution (pH 8.0–8.5) leads to the oxidative polymerization of dopamine and the formation of a polymeric coating [41]. It has been proven that various functional coatings can be created on biomaterials via various immobilization reactions using polydopamine coating as a base. Several studies have reported that polydopamine (PD)-coated surfaces become negatively charged because of the deprotonation of one catechol (OH) group, resulting in improved hydrophilicity and biological performance (i.e., cell attachment and proliferation) [42,43].

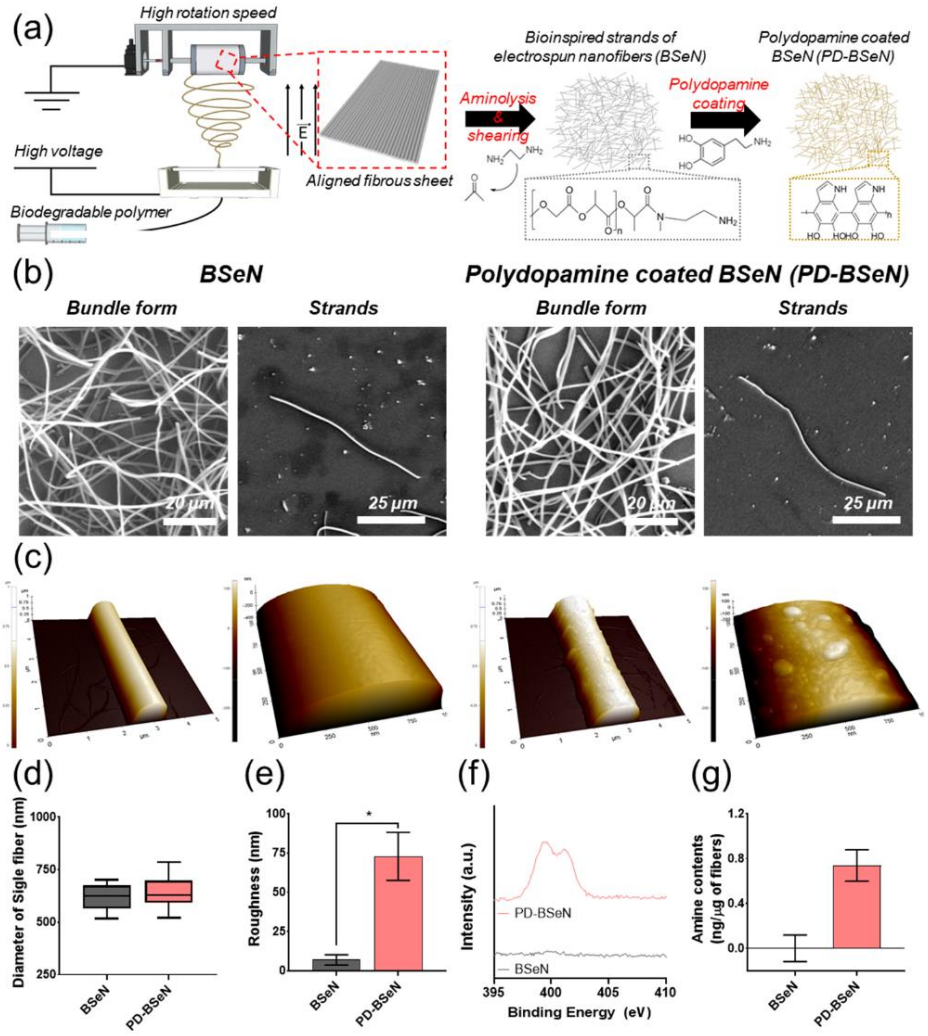

Figure 6.2. Fabrication and characterizations of nanofibers. (a) Schematic representation of BSeN and PD-BSeN generation. (b) SEM micrography images and (c) 3D AFM images of BSeN and PD-BSeN. (d) Diameter of single BSeN and PD-BSeN fibers. The diameter was analyzed by ImageJ software. A total of 50 single fibers were analyzed from SEM images obtained using FEI Quanta 250 FEG Scanning Electron Microscope. Data are expressed as mean ± SD (n = 50). (e) Surface roughness measurement of BSeN and PD-BSeN. A total of ten single fibers from AFM images were analyzed by ImageJ software. Comparison of the means between two groups was performed using one-way analysis of variance (ANOVA; $*P < 0.05$, n = 10). (f) XPS spectrum of nanofibers with and without polydopamine coating. (g) Quantification of catecholamine in nanofibers. The quantification was analyzed using Micro-BCA assay (n = 6).

6.4.2 Effect of BSeN on 3D spheroid formation

We previously investigated and determined the optimal conditions for spheroid formation based on screening under various BSeN conditions (Supplementary Figure 6.3a). As a result, the DNA content did not affect the spheroids regardless of the amount of BSeN present. In contrast, the DNA content was significantly reduced in BSeN that was coated with PD for >20 min and showed limitation in spheroid formation (Supplementary Figure 6.3b–d and Supplementary Figure 6.4). These trends are contrary to the previous results obtained from incorporating BSeN into human cell-based spheroids [30–32]. Human cell lines and fish cell lines were significantly different in size, which is presumed to be one of the reasons why different results can be obtained

under the same conditions. Our results suggest that relatively small fish cells are more sensitive to external environmental factors than human cell lines. We plan to focus on studying the fate regulation of fish cells according to the physical parameters of the ECM environment in the future (i.e., topography, stiffness, and roughness). As illustrated in Figure 6.3a, spheroids comprising cells that incorporated BSeN or PD-BSeN were designated Hybrid-1 and Hybrid-2, respectively. 2D and 3D refer to monolayer cells and spheroids, respectively, which were cultured using the generic methods (as a control group).

Figure 6.3b shows the morphology of the zebrafish liver cell spheroids after incubation for 24 h. The superposed fluorescence images of the actin filament and FITC-coated BSeN showed that the fibrous strands were well distributed throughout the spheroid (Supplementary Figure 6.5). SEM images confirmed the distribution of homogenous cells and fibrous strands within the spheroids. High-magnification SEM analysis showed that the cells were firmly attached to the surface of the fibrous strands, resulting in the formation of stable spheroids (Figure 6.3b; Supplementary Figure 6.6).

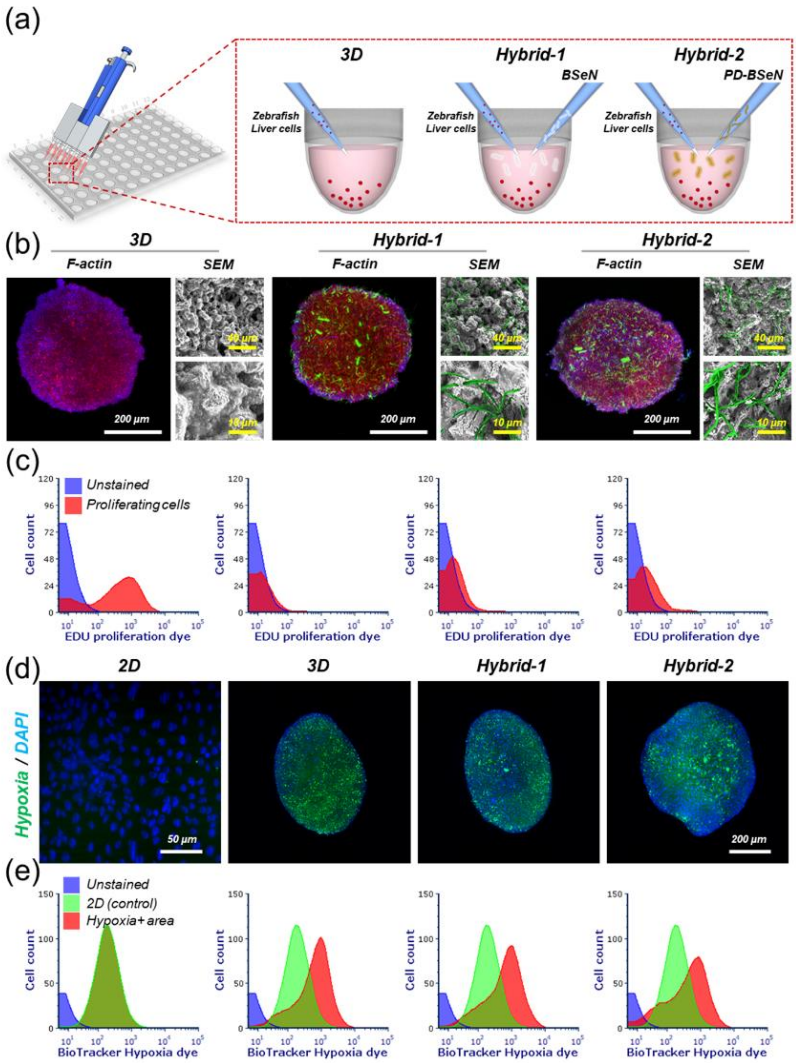

Figure 6.3. Formation of hybrid-spheroids with BSeN and PD-BSeN and their effects on cell proliferation and hypoxia. (a) Schematic illumination of method used to fabricate spheroids (3D), spheroids with BSeN (Hybrid-1), and spheroids with PD-BSeN (Hybrid-2). (b) Representative cytoskeletal structure and SEM micrography images of spheroids at day 3. The cytoskeletal structure images were acquired by fluorescence staining for DAPI (nuclei; blue) and F-actin (red), and BSeN and PD-BSeN were also stained by FITC

labeling (green). (c) FACS results of cell proliferation after 7 days of culture in 2D, 3D, Hybrid-1, and Hybrid-2 groups (2D from left, Hybrid-2 to the right). (d) Representative hypoxia images at day 7. Images were acquired by fluorescence staining for DAPI (nuclei; blue) and hypoxia (green). (e) FACS results of hypoxia after culturing for 7 days in 2D, 3D, Hybrid-1, and Hybrid-2 groups (2D from left, Hybrid-2 to the right).

BSeN was found to improve the proliferation of zebrafish liver cells, which can be attributed to the facilitation of mass transport resulting from the formation of spheroids with a loosely arranged structure (Figure 6.3c–e, Supplementary Figure 6.7, and Supplementary Figure 6.8). This speculation was partially demonstrated by hypoxic staining. As shown in Figure 6.3d,e, Hybrid-2 showed reduced hypoxia, while strong hypoxic signals were distributed throughout the spheroids in the 3D group. Although intense cell–cell and cell–material contact within spheroids may be analogous to the physiological environment of natural tissue, the drawbacks of coexisting with materials with low cell affinity limit the proliferation of normal cells in spheroids during long-term culture with a lack of nutrient supply. This phenomenon was clearly observed in Hybrid-1. After culturing for seven days, Hybrid-1 showed a significantly higher proliferation rate than the 3D group (Supplementary Figure 6.7). However, under long-term culture conditions, the proliferation capacity of Hybrid-1 was not different from that of the 3D group. (Supplementary Figure 6.8). In contrast, the cells in the Hybrid-2 group continued to metabolize, even when cultured for 8 weeks. The antioxidant role of polydopamine [44] may partly explain the differences observed in the Hybrid-1 and Hybrid-2 groups; allowing the cells to improve the cell–material interactions is likely to have improved the problems of apoptosis and necrosis by preventing oxidative stress.

Although spheroids have been widely studied as *in vitro* analytical assessment tools, concerns about the long-term viability of cells within spheroids have constrained studies evaluating the health effects of long-term exposure to low-level chemicals in the field of environmental toxicity. Nevertheless, the results suggest that applying BSeN to aquatic cells can enable meaningful discovery and provide significant advances in the development of engineering platforms for toxicity assessment and monitoring in ecotoxicology.

6.4.3 Evaluation of functions using spheroid-based *in vitro* assays

The differential gene expression in spheroids that were cultured for 7 days was also analyzed using whole-transcriptome sequencing analysis (Figure 6.4). A hierarchical clustering heatmap revealed distinct expression profiles between the 2D and 3D spheroids. The 3D spheroids exhibited significant upregulation of 2,507 genes and downregulation of 2,969 genes compared to the 2D group. This result is consistent with the findings of previous studies, and the trend was consistently observed in the relationship between the 2D and the Hybrid-2 groups. Contrary to our expectations, no distinct differences were observed in the Hybrid-2 group as compared to the 3D group. Both the 3D and Hybrid-2 groups had higher abundances of genes that are related to metabolic pathways than the 2D groups, as shown in Figure 6.4c. Depending on the cell type and microenvironment, various metabolic adaptations are associated with cell proliferation [45]. It is known that mitochondria produce most of the cellular adenosine triphosphate (ATP) via substrate-level-phosphorylation, primarily through the oxidative phosphorylation system [46]. Studies have suggested that oxidative phosphorylation provides the majority of ATP during cell proliferation. As shown in Figure 6.4c,

the oxidative phosphorylation in the Hybrid-2 group differed significantly from that of the 2D group. Although a clear explanation for our results may not be within the scope of this study, we speculate that this is part of an adaptation strategy to hypoxic environments. In other words, these results suggest that cells coexisting with PD-BSeN can maintain their proliferative capacity through oxidative phosphorylation, even under inadequate oxygen levels.

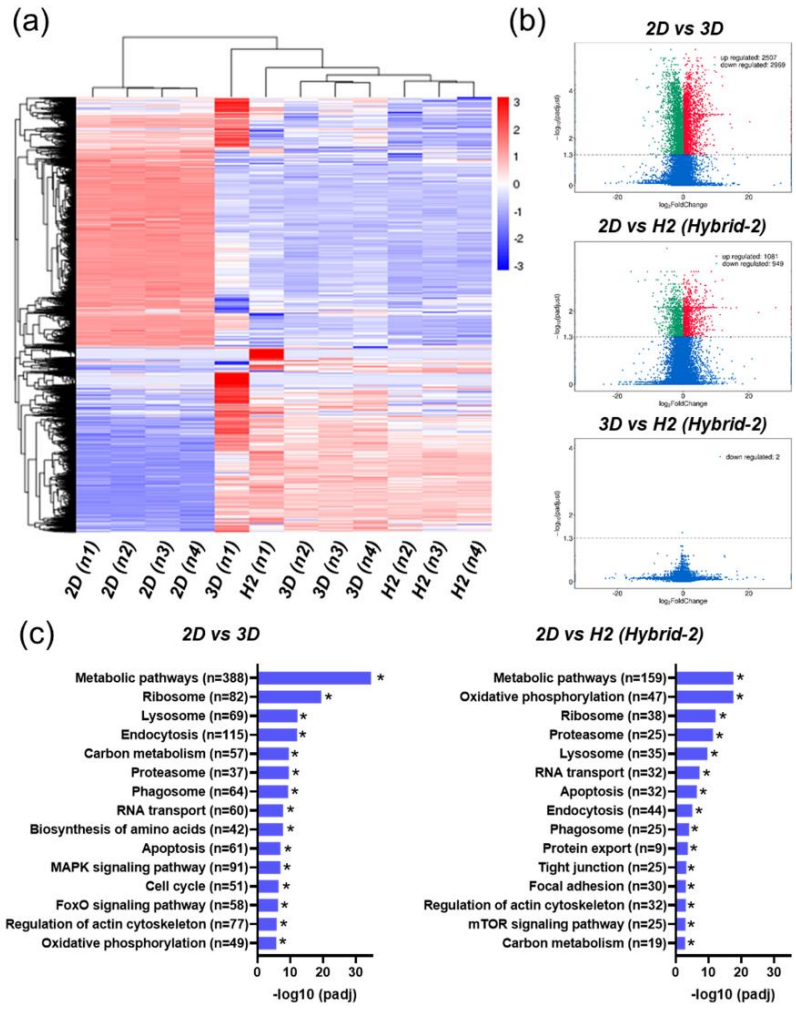

Figure 6.4. RNA sequencing (RNA-Seq) analysis of 2D, 3D, and Hybrid-2 groups cultured for 7 days (n = 4). (a) Heatmap hierarchical clustering according to log2(FPKM+1) indicates differentially expressed genes (DEGs) in the groups. Red and blue indicate genes with high and low expression levels, respectively. (b) Volcano plot analysis results. Plots indicate overall DEG distribution. (c) KEGG enrichment histogram of transcripts (*$P_{adj} < 0.05$).

To complement the whole-transcriptome sequencing analysis, we investigated the effect of BSeN on the gene expression levels of spheroids that were cultured for 14 days (Figure 6.5a–d). Zebrafish cell lines that are established from the livers of zebrafish show promise for fundamental studies into estrogen, liver, and reproductive functions. We found that improved estrogen receptors were achieved in all spheroid groups (3D, Hybrid-1, and Hybrid-2) as compared to the 2D group. For example, the relative gene expression of

ESR-1 was 1.27 ± 0.11, 1.15 ± 0.50, and 1.77 ± 0.60 times higher in the 3D, Hybrid-1, and Hybrid-2 groups, respectively, compared with the control (2D). In addition, analysis of the liver-related gene expression showed interesting results. HNFs are a group of transcription factor families whose expression is enriched in the liver compared to other organs [47]. Cells in the 2D group showed similar HNF4A gene expression to the 3D group. However, both Hybrid groups showed more pronounced HNF4A gene expression than the 2D group. Since zebrafish liver cells can perform metabolic functions associated with the liver, they are an excellent cellular tool with which it is possible to determine the effect of exogenous metabolites [35]. We demonstrated that Hybrid-2 incorporated with PD-BSeN had similar or higher expression of drug-metabolizing genes (GSTA1, PXR, and CYP3C1) than the other three groups (1.88 ± 0.16 fold for PXR, 4.02 ± 0.42 fold for GSTA1, and 1.36 ± 0.13 fold CYP3C1) as compared to 2D.

Vtg is generally produced in the liver of female vertebrate ovaries in response to circulating endogenous estrogen [48,49] and is a precursor to the turbulence protein. Once produced in the liver, it follows the blood flow to the ovary, where it is absorbed. Many studies have reported that Vtg induction can be measured both *in vivo* and *in vitro* in fish liver cells (hepatocytes) [35,49]. In addition, *in vitro* Vtg assays that use cells have been widely recognized as advantageous for detecting the effects of estrogen metabolites because hepatocytes maintain their metabolic state and can detect both estrogenic and anti-estrogenic effects. As shown in Figure 6.5d, the relative gene expression of Vtg was higher in the Hybrid-2 group than in the 2D, 3D, and Hybrid-1 groups. Consistent with the trend observed in the gene expression results, the protein detection of Vtg in cells cultured for 5 d indicated its overexpression in the spheroid-based groups (3D, Hybrid-1, and Hybrid-2) compared to the 2D groups (Figure 6.5e and Supplementary Figure 6.8). For example, the Vtg expression (ng mg-1 of proteins) detected after 5 days had dramatically increased from 7.92 ± 0.61 in the 2D group to 19.91 ± 0.09, 16.80 ± 2.77, and 19.63 ± 2.07 in the 3D, Hybrid-1, and Hybrid-2 groups, respectively. We also hypothesized that if the spheroids contain too few cells, the benefit of the enhanced 3D cell-cell adhesion was reduced compared to the 2D culture. In a previous study, we demonstrated that almost negligible levels of Vtg were detected in a 2D group with 5,000 cells [35]. However, low levels of Vtg were also detected in the 2D group with 50,000 cells. We also measured the amount of Vtg on day 5 in spheroids with low cell numbers under the same conditions (Supplementary Figure 6.10). An average Vtg level of 5.69 ± 0.42 ng/mg of proteins was detected in the spheroid-based groups with or without BSeN. These results indicate that the advantages gained for 3D spheroids containing too few cells may be comparable or even inferior to those using monolayer culture conditions (2D group).

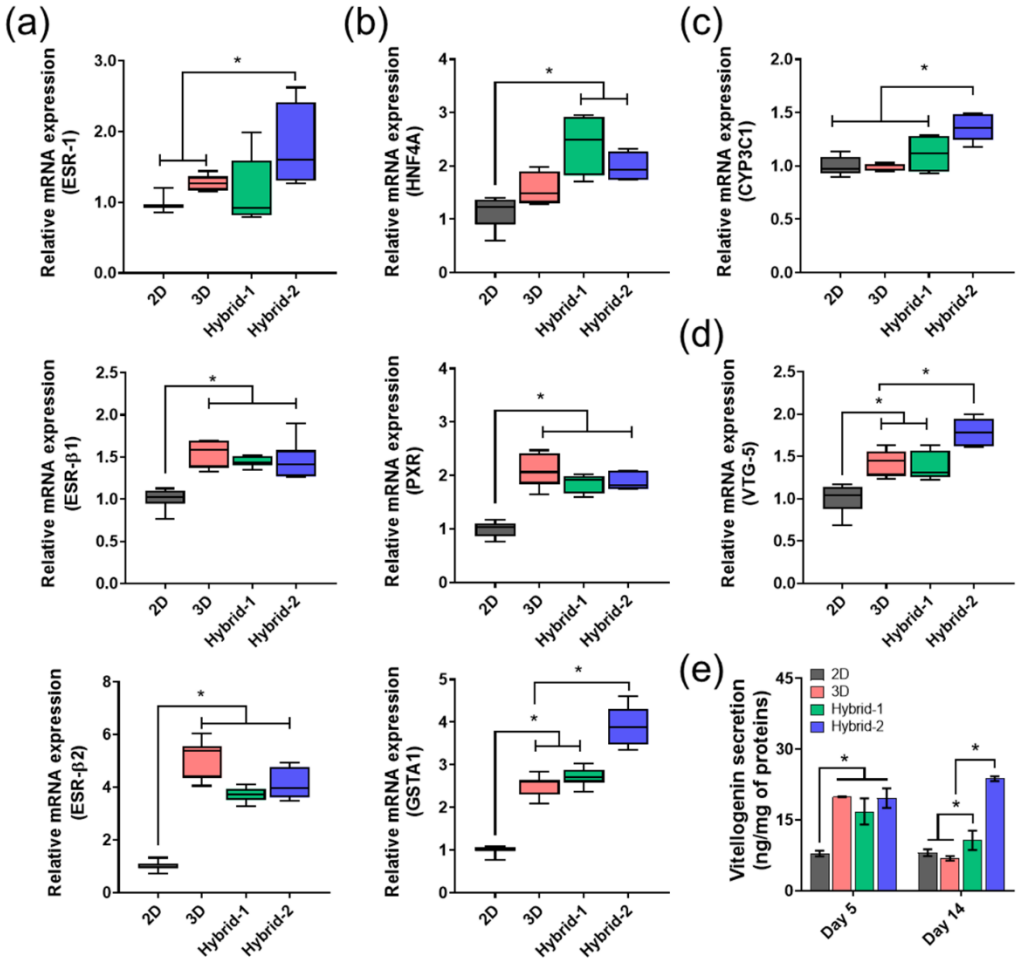

Figure 5. Fold-change in mRNA expression of (a) estrogen receptor genes, (b) liver-relative genes, (c) CYP3C1 gene, (d) VTG-5 gene. Each group was cultured for 14 days. Samples were prepared in the same manner as the RNA sequencing analysis. Data are presented as mean ± SD (n = 8). (e) ELISA quantification of vitellogenin (Vtg). The Vtg was normalized to total protein concentration, and data are presented as mean ± SD (n = 5). (a–e) Comparisons of the means between each group were performed using one-way analysis of variance (ANOVA; *$p < 0.05$), followed by Dunnett's T3 test (non-homogeneous variance) or Scheffe's test (homogeneous variance).

Interestingly, different Vtg expression levels were observed after the cells were cultured for 14 days. The results confirmed that the Vtg expression was significantly reduced in groups 3D and Hybrid-1 on day 14 as compared to day 5. In contrast, the Hybrid-2 group showed Vtg protein expression stability, even when cultured for 14 days. We speculate that these findings may be due to the long-term central hypoxia and necrotic hypoxia in spheroids that occurs under long-term culture. We, therefore, examined the viability of and hypoxia in spheroids at 14 days (Supplementary Figure 6.9). The live and dead staining images revealed that the cells in the 3D group were densely distributed throughout the spheroid, and a large number of dead cells were detected on day 14. The overall trend of dead cells was similar to that observed with hypoxia staining. Although some dead cells were observed, the cells observed in the 2D, Hybrid-1, and Hybrid-2 groups were generally living. In addition, hypoxic staining revealed that the hybrid group with incorporated BSeN showed low fluorescence intensity. These results suggest that the 3D culture method can improve cell

functioning but is not valuable as a long-term *in vitro* evaluation model unless it provides an environment where the cells can live for a long time. The 3D spherical culture methods were found to improve the liver function of the cells, suggesting that the use of BSeN with cell-friendly chemical/structural characteristics positively regulates cell-to-cell interactions with excellent efficacy.

6.4.4 Comparison of reproductive toxicity in *in vitro* cell-based platforms and zebrafish embryos as a result of EDC exposure

Zebrafish embryos have been successfully used for highthroughput toxicity screening [9]. Eleutheroembryos (of <120 hpf) are preferred *in vitro* testing models because it is thought that embryos in the earliest stages feel less pain than adult fish [13]. Therefore, the eleuthero embryo (developmental stage of 96–120 hpf) has been proposed as a promising toxicity monitoring tool, and international standardized test guidelines have been developed and validated for embryos at his stage (i.e., fish embryo acute toxicity (FET, OECD TG 236) [12,13]. Vtg assessments are considered one of the primary reproductive indicators for EDCs. This study aimed to compare the acute short-term reproductive toxicity observed in zebrafish embryos with that obtained via cell-based assessment platforms. First, representative EDCs (E2, 4HT, BPA, and BPFL) were selected (Supplementary Figure 6.11). The expression of Vtg showed little change in the zebrafish embryo with low-dose E2 treatment, but this increased markedly under high-dose E2 concentrations, reaching 1.35 ± 0.10 times the control level. In contrast, exposing zebrafish embryos to 4HT led to a significant reduction of 0.50 ± 0.03 and 0.42 ± 0.05 times that observed in the control at 10×10^{-9} and 1×10^{-6} M, respectively. Compared with the control group, the Vtg level increased by 1.36 ± 0.04 times when exposed to BPA and decreased by 0.61 ± 0.02 times when exposed to BPFL.

There is an ongoing debate concerning the extent to which *in vitro* cell systems are viable for toxicity testing and risk assessment. In general, cell-based assays exhibit lower sensitivity than *in vivo* experiments when comparing toxic effects. Prior attempts to compare the toxic efficacy of aquatic cell lines with whole fish test systems showed weak correlations [50]. Similarly, we confirmed no difference in the Vtg expression as the result of exposure to any substance in the 2D group using zebrafish liver cell lines. In contrast, in the 3D group, high-dose E2 and BPFL produced a similar tendency to that observed using zebrafish embryos, with very low sensitivity to 4HT and BPA substances. These results indicate that the monolayer cell culture platform (2D) exhibits negligible xenobiotic metabolism capacity and that the cell-only 3D culture platform has lower sensitivity to exogenous substances than zebrafish embryos. However, remarkable results were obtained in the Hybrid-2 group. As shown in Figure 6.6, the Vtg levels in cells exposed to E2 and BPA increased, while those in cells exposed to 4HT and BPFL decreased compared to the control group. To verify the reliability of the reproductive toxicity data describing the cell-based culture platforms (2D, 3D, Hybrid-1, and Hybrid-2) and the zebrafish embryos, we analyzed the correlation between the expression levels of the groups in a given set of Vtg libraries (Figure 6.6b–e). Consistent with previous results, negligible correlations were obtained between reproductive toxicity and EDC substances in 2D cultured monolayered fish cells and embryos. In the 3D group, although reproductive toxicity endpoints showed a potential correlation with zebrafish embryos, the two groups differed in sensitivity and

predictability, with Pearson correlation coefficients of 0.54 and 0.65 as a result of E2 and 4-HT exposure, respectively. Based on the group correlation, it was found that the Hybrid-2 group had a similar response to E2 as the zebrafish embryo (Pearson correlation coefficient of 0.83 (Figure 6.6b,c). These results indicate that the toxicity data obtained with the 3D spheroid platform with integrated biomimetic material adequately correlated with the FET results. Therefore, we can conclude that the incorporation of biomimetic materials into 3D spheroid platforms produces an appropriate and preferable *in vitro* assessment tool for alternative testing. An ideal *in vitro* toxicological assessment platform should be a 3D co-culture model composed of one or more fish cell lines and should have a system similar to the physiological and morphological properties of the fish model. This study (proof-of-concept stage) proposes that bioinspired materials with aquatic cell lines can be the starting point for *in vitro* test platforms that can be used as alternative testing. We suggest that a culture platform using bioinspired materials will become more useful *in vitro* evaluation system, and therefore conducted a follow-up study to investigate the toxic reactivity *in vivo* fish at the cellular level by studying the fate regulation of fish cells according to parameters (physical/chemical) that can further imitate the cell-matrix environment.

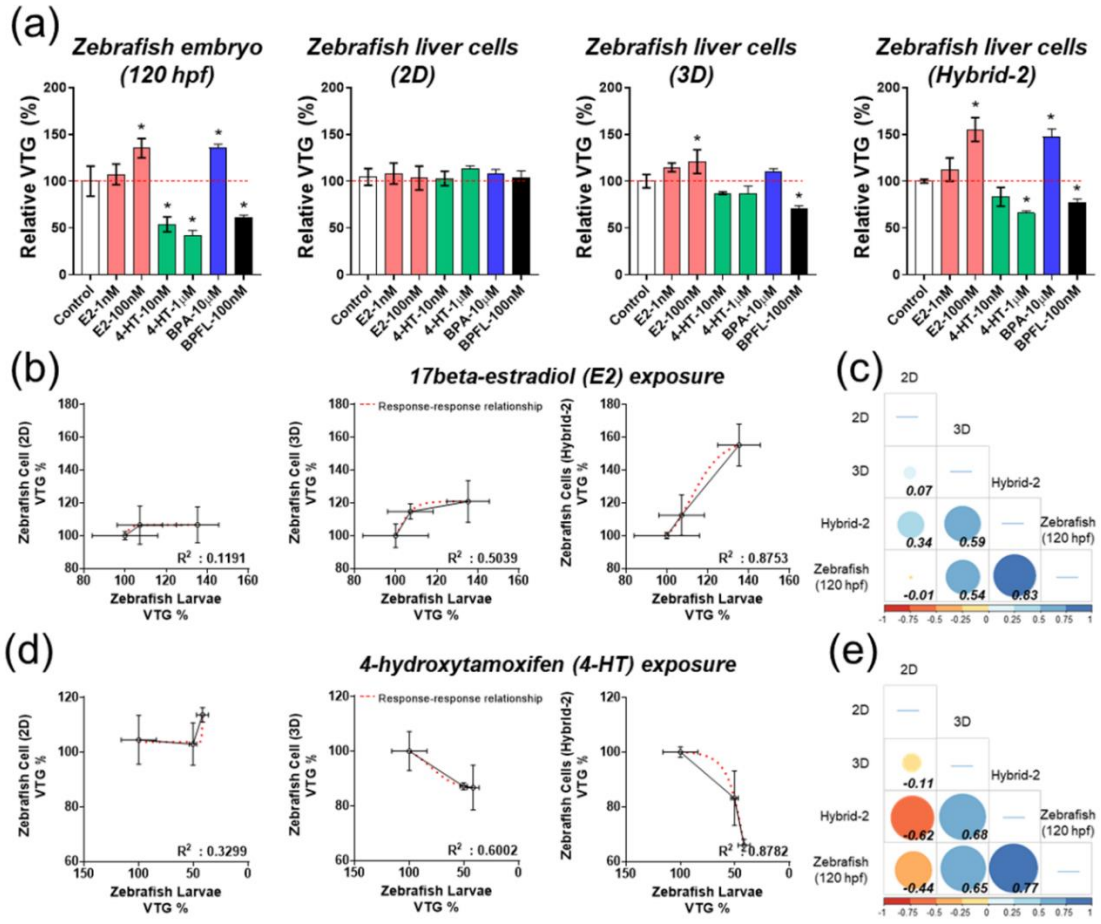

Figure 6.6. Comparison of vitellogenin (Vtg) levels upon endocrine-disrupting chemicals (EDCs) exposure. (a) Relative Vtg levels in zebrafish larvae, 2D, 3D, and Hybrid-2 groups. All groups were cultured for 3 days and exposed to each chemical for 48 h. Six replicate samples of each condition were prepared for comparison. Data are presented as mean ± SD (n = 6). Comparisons of the means between each group were performed using one-way analysis of variance (ANOVA), followed by Scheffe's test (homogeneous variance). Asterisk means a significant difference compared to the control condition ($p < 0.05$). (b–e) Correlation analysis of Vtg

levels in groups. (b-c) Correlation matrix plot for 17β-estradiol (E2) exposure. Pearson correlation coefficient (*r*) was calculated between groups. (d-e) Correlation matrix plot for 4-hydroxytamoxifen (HT) exposure. Pearson correlation coefficient (*r*) was calculated between groups.

6.5 Summary and Conclusion

Because environmental pollutants adversely affect various molecular mechanisms, cellular models for monitoring and functional studies are needed as an alternative to in vivo exposure studies in ecotoxicology. The present study introduces 3D culture screening platforms that feature BSeNs and aquatic cell lines and investigated the possibility of an alternative animal test method in environmental toxicity evaluation. Our results suggest that the use of BSeN overcomes the limitations posed by conventional spheroid systems and offers advantages such as improved viability, proliferation, and oxygen transport. Furthermore, analysis of the spheroid-based in vitro assays demonstrated that combining BSeN with 3D zebrafish liver cell cultures improved the liver and reproductive functions. Results from the Hybrid-2 group indicated substantial effects on the expression of reproductive proteins such as Vtg and showed a high correlation with the reproductive toxicity data of zebrafish embryos that are exposed to EDCs. Our results indicate that the beneficial effects of biomaterials that closely mimic ECM environments can yield efficient zebrafish cells with intrinsic functions and xenobiotic metabolism similar to those of zebrafish embryos. These findings have profound implications for designing in vitro cell culture-based monitoring platforms for alternative testing.

6.6 Acknowledgments

I.J. and C.G.P. contributed equally to this work. This research was supported by a National Research Council of Science & Technology (NST) grant by the Korean Government (MSIP, No. CAP-17-01-KIST Europe) and the Korea Institute of Science and Technology Europe Basic Research Program (12201). This research was supported by a National Research Foundation of Korea (NRF) grant funded by the Korean government (MEST) (Grant No. NRF-2020R1A4A3078645 and NRF-2019R1A2C2084965).

6.7 Bibliography

1. Adeola, F. O. Global Impact of Chemicals and Toxic Substances on Human Health and the Environment, in *Handbook of Global Health* (Eds: I. Kickbusch, D. Ganten, M. Moeti), Springer International Publishing, Cham **2021**, p. 2227.
2. Birnbaum, L. S. The effect of environmental chemicals on human health. *Fertil. Steril.* **2008**, *89*, e31.
3. Tweedale, A. C. The inadequacies of pre-market chemical risk assessment's toxicity studies-the implications. *J. Appl. Toxicol.* **2017**, *37*, 92.
4. Ford, A.T.; Agerstrand, M.; Brooks, B.W.; Allen, J.; Bertram, M.G.; Brodin, T.; Dang, Z.; Duquesne, S.; Sahm, R.; Hoffmann, F.; Hollert, H.; Jacob, S.; Kluver, N.; Lazorchak, J.M.; Ledesma, M.; Melvin, S.D.; Mohr, S.; Padilla, S.; Pyle, G.G.; Scholz, S.; Saaristo, M.; Smit, E.; Steevens, J.A.; van den Berg, S.; Kloas, W.; Wong, B.B.M.; Ziegler, M.; Maack, G. The Role of Behavioral

Ecotoxicology in Environmental Protection. *Environ. Sci. Technol.* **2021**, *55*, 5620.
5. Schuijt, L.M.; Peng, F.J.; van den Berg, S.J.P.; Dingemans, M.M.L.; Van den Brink, P.J. (Eco)toxicological tests for assessing impacts of chemical stress to aquatic ecosystems: Facts, challenges, and future. *Sci. Total Environ.* **2021**, *795*, 148776.
6. Krewski, D.; Acosta, D. Jr.; Andersen, M.; Anderson, H.; Bailar, J.C.; Boekelheide, K.; Brent, R.; Charnley, G.; Cheung, V.G.; Green, S.Jr.; Kelsey, K.T.; Kerkvliet, N.I.; Li, A.A.; McCray, L.; Meyer, O.; Patterson, R.D.; Pennie, W.; Scala, R.A.; Solomon, G.M.; Stephens, M.; Yager, J.; Zeise, L. Toxicity testing in the 21st century: a vision and a strategy. *J. Toxicol. Environ. Health, Part B* **2010**, *13*, 51.
7. Grune, B.; Hensel, A.; Schönfelder, G. Animal welfare: Rules for assessing pain in lab animals. *Nature* **2014**, *512*, 28.
8. Knight, J.; Rovida, C.; Kreiling, R.; Zhu, C.; Knudsen, M.; Hartung, T. Continuing animal tests on cosmetic ingredients for REACH in the EU. *ALTEX* **2021**, *38*, 653.
9. Lillicrap, A.; Belanger, S.; Burden, N.; Pasquier, D.D.; Embry, M.R.; Halder, M.; Lampi, M.A.; Lee, L.; Norberg-King, T.; Rattner, B.A.; Schirmer, K.; Thomas, P. Alternative approaches to vertebrate ecotoxicity tests in the 21st century: A review of developments over the last 2 decades and current status. *Environ. Toxicol. Chem.* **2016**, *35*, 2637.
10. OECD, Test No. 203: Fish, Acute Toxicity Test. **2019**.
11. Bambino, K.; Chu, J. Zebrafish in Toxicology and Environmental Health. *Curr. Top. Dev. Biol.* **2017**, *124*, 331.
12. OECD, Test No. 236: Fish Embryo Acute Toxicity (FET) Test. **2013**.
13. Sobanska, M.; Scholz, S.; Nyman, A.M.; Cesnaitis, R.; Gutierrez Alonso, S.; Klüver, N.; Kühne, R.; Tyle, H.; de Knecht, J.; Dang, Z.; Lundbergh, I.; Carlon, C.; De Coen, W. Applicability of the fish embryo acute toxicity (FET) test (OECD 236) in the regulatory context of Registration, Evaluation, Authorisation, and Restriction of Chemicals (REACH). *Environ. Toxicol. Chem.* **2018**, *37*, 657.
14. Ortiz-Villanueva, E.; Jaumot, J.; Martínez, R.; Navarro-Martín, L.; Piña, B.; Tauler, R. Assessment of endocrine disruptors effects on zebrafish (Danio rerio) embryos by untargeted LC-HRMS metabolomic analysis. *Sci. Total Environ.* **2018**, *635*, 156.
15. Ibrahim, M.A.; Zulkifli, S.Z.; Azmai, M.N.A.; Mohamat-Yusuff, F.; Ismail, A. Embryonic toxicity of 3,4-dichloroaniline (3,4-DCA) on Javanese medaka (Oryzias javanicus Bleeker, 1854). *Toxicol. Rep.* **2020**, *7*, 1039.
16. Jarque, S.; Rubio-Brotons, M.; Ibarra, J.; Ordoñez, V.; Dyballa, S.; Miñana, R.; Terriente, J. Morphometric analysis of developing zebrafish embryos allows predicting teratogenicity modes of action in higher vertebrates. *Reprod. Toxicol.* **2020**, *96*, 337.
17. Lee, J.; Kim, S.; Park, Y.J.; Moon, H.B.; Choi, K. Thyroid Hormone-Disrupting Potentials of Major Benzophenones in Two Cell Lines (GH3 and FRTL-5) and Embryo-Larval Zebrafish. *Environ. Sci. Technol.* **2018**, *52*, 8858.
18. Scholz S. Zebrafish embryos as an alternative model for screening of drug-induced organ toxicity. *Arch. Toxicol.* **2013**, *87*, 767.
19. Busquet, F.; Kleensang, A.; Rovida, C.; Herrmann, K.; Leist, M.; Hartung, T. New European Union statistics on laboratory animal use - what really counts!. *ALTEX* **2020**, *37*, 167.
20. Macko, P.; Palosaari, T.; Whelan, M. Extrapolating from acute to chronic toxicity in vitro. *Toxicol. In Vitro* **2021**, *76*, 105206.
21. Prinz, N.; Korez, Š.; Understanding How Microplastics Affect Marine Biota on the Cellular Level Is Important for Assessing Ecosystem Function: A Review, in *YOUMARES 9 - The Oceans: Our Research, Our Future: Proceedings of the 2018 conference for YOUng MArine RESearcher in Oldenburg, Germany* (Eds: S. Jungblut, V. Liebich, M. Bode-Dalby), Springer International Publishing, Cham **2020**, p. 101.
22. Edmondson, R.; Broglie, J.J.; Adcock, A.F.; Yang, L. Three-dimensional cell culture systems and their applications in drug discovery and cell-based biosensors. *Assay Drug Dev. Technol.* **2014**, *12*, 207.
23. Punt, A.; Bouwmeester, H.; Blaauboer, B.J.; Coecke, S.; Hakkert, B.; Hendriks, D.; Jennings, P.; Kramer, N.I.; Neuhoff, S.; Masereeuw, R.; Paini, A.; Peijnenburg, A.; Rooseboom, M.; Shuler, M.L.; Sorrell, I.; Spee, B.; Strikwold, M.; Van der Meer, A.D.; Van der Zande, M.; Vinken, M.; Yang, H.; Bos P.M.J; Heringa, M. B. (2020). New approach methodologies (NAMs) for human-relevant biokinetics predictions. Meeting the paradigm shift in toxicology towards an animal-free chemical risk assessment. *ALTEX* **2020**, *37*, 607.
24. Laschke, M.W.; Menger, M.D. Life is 3D: Boosting Spheroid Function for Tissue Engineering. *Trends Biotechnol.* **2017**, *35*, 133.

25. Fong, E.L.; Lamhamedi-Cherradi, S.E.; Burdett, E.; Ramamoorthy, V.; Lazar, A.J.; Kasper, F.K.; Farach-Carson, M.C.; Vishwamitra, D.; Demicco, E.G.; Menegaz, B.A.; Amin, H.M.; Mikos, A.G.; Ludwig, J.A. Modeling Ewing sarcoma tumors in vitro with 3D scaffolds. *Proc. Natl. Acad. Sci. U. S. A.* **2013**, *110*, 6500.
26. Langhans, S.A. Three-Dimensional in Vitro Cell Culture Models in Drug Discovery and Drug Repositioning. *Front. Pharmacol.* **2018**, *9*, 6.
27. Mandon, M.; Huet, S.; Dubreil, E.; Fessard, V.; Le Hégarat, L. Three-dimensional HepaRG spheroids as a liver model to study human genotoxicity in vitro with the single cell gel electrophoresis assay. *Sci. Rep.* **2019**, *9*, 10548.
28. Sirenko, O.; Hancock, M.K.; Hesley, J.; Hong, D.; Cohen, A.; Gentry, J.; Carlson, C. B.; Mann, D.A. Phenotypic Characterization of Toxic Compound Effects on Liver Spheroids Derived from iPSC Using Confocal Imaging and Three-Dimensional Image Analysis. *Assay Drug Dev. Technol.* **2016**, *14*, 381.
29. Tse, H.M.; Gardner, G.; Dominguez-Bendala, J.; Fraker, C.A. The Importance of Proper Oxygenation in 3D Culture. *Front. Bioeng. Biotechnol.* **2021**, *9*, 634403.
30. Ahmad, T.; Lee, J.; Shin, Y.M.; Shin, H.J.; Madhurakat Perikamana, S.K.; Park, S.H.; Kim, S.W.; Shin, H. Hybrid-spheroids incorporating ECM like engineered fragmented fibers potentiate stem cell function by improved cell/cell and cell/ECM interactions. *Acta Biomater.* **2017**, *64*, 161.
31. Ahmad, T.; Shin, H.J.; Lee, J.; Shin, Y.M.; Perikamana, S.; Park, S.Y.; Jung, H.S.; Shin, H. Fabrication of in vitro 3D mineralized tissue by fusion of composite spheroids incorporating biomineral-coated nanofibers and human adipose-derived stem cells. *Acta Biomater.* **2018**, *74*, 464.
32. Lee, J.; Lee, S.; Ahmad, T.; Madhurakkat Perikamana, S.K.; Lee, J.; Kim, E.M.; Shin, H. Human adipose-derived stem cell spheroids incorporating platelet-derived growth factor (PDGF) and bio-minerals for vascularized bone tissue engineering. *Biomaterials* **2020**, *255*, 120192.
33. Lee, J.; Lee, S.; Huh, S.J.; Kang, B.J.; Shin, H. Directed Regeneration of Osteochondral Tissue by Hierarchical Assembly of Spatially Organized Composite Spheroids. *Adv. Sci.* **2022**, *9*, 2103525.
34. Lee, J.; Lee, S.; Kim, S.M.; Shin, H. Size-controlled human adipose-derived stem cell spheroids hybridized with single-segmented nanofibers and their effect on viability and stem cell differentiation. *Biomater. Res.* **2021**, *25*, 14.
35. Park, C.G.; Ryu, C.S.; Sung, B.; Manz, A.; Kong, H.; Kim, Y.J. Transcriptomic and physiological analysis of endocrine disrupting chemicals Impacts on 3D Zebrafish liver cell culture system. *Aquat. Toxicol.* **2022**, *245*, 106105.
36. Gattazzo, F.; Urciuolo, A.; Bonaldo, P. Extracellular matrix: a dynamic microenvironment for stem cell niche. *Biochim. Biophys. Acta* **2014**, *1840*, 2506.
37. Nicolas, J.; Magli, S.; Rabbachin, L.; Sampaolesi, S.; Nicotra, F.; Russo, L. 3D Extracellular Matrix Mimics: Fundamental Concepts and Role of Materials Chemistry to Influence Stem Cell Fate. *Biomacromolecules* **2020**, *21*, 1968.
38. Sun, B. The mechanics of fibrillar collagen extracellular matrix. *Cell Rep. Phys. Sci.* **2021**, *2*, 100515
39. Li, Y.; Cheng, J.; Delparastan, P.; Wang, H.; Sigg, S.J.; DeFrates, K.G.; Cao, Y.; Messersmith, P.B. Molecular design principles of Lysine-DOPA wet adhesion. *Nat. Commun.* **2020**, *11*, 3895.
40. Lee, H.; Dellatore, S.M.; Miller, W.M.; Messersmith, P.B. Mussel-inspired surface chemistry for multifunctional coatings. *Science* **2007**, *318*, 426.
41. Park, J.; Brust, T.F.; Lee, H.J.; Lee, S.C.; Watts, V.J.; Yeo, Y. Polydopamine-based simple and versatile surface modification of polymeric nano drug carriers. *ACS Nano* **2014**, *8*, 3347.
42. Barclay, T.G.; Hegab, H.M.; Clarke, S.R.; Ginic-Markovic, M. Versatile Surface Modification Using Polydopamine and Related Polycatecholamines: Chemistry, Structure, and Applications. *Adv. Mater. Interfaces* **2017**, *4*, 1601192.
43. Xue, M.; Zhou, D.; Ji, Y.; Xie, Y.; Li, C.; Zhao, J. The polydopamine-enhanced superadhesion and fracture strength of honeycomb polyurethane porous membranes. *RSC Adv.* **2020**, *10*, 1639.
44. Mollica, F.; Lucernati, R.; Amorati, R. Expanding the spectrum of polydopamine antioxidant activity by nitroxide conjugation. *J. Mater. Chem. B* **2021**, *9*, 9980.
45. Giralt, A.; Fajas, L. Editorial: Metabolic Adaptation to Cell Growth and Proliferation in Normal and Pathological Conditions. *Front. Endocrinol.* **2017**, *8*, 362.
46. Wilson, D.F. Oxidative phosphorylation: regulation and role in cellular and tissue metabolism. *J. Physiol.* **2017**, *595*, 7023.
47. Zhou, Z.; Xu, M.J.; Gao, B. Hepatocytes: a key cell type for innate immunity. *Cell Mol. Immunol.* **2016**, *13*, 301.
48. Robitaille, J.; Denslow, N.D.; Escher, B.I.; Kurita-Oyamada, H.G.; Marlatt, V.; Martyniuk, C.J.; Navarro-Martín, L.; Prosser, R.; Sanderson, T.; Yargeau, V.; Langlois, V.S. Towards regulation of

Endocrine Disrupting chemicals (EDCs) in water resources using bioassays - A guide to developing a testing strategy. *Environ. Res.* **2022**, *205*, 112483.

49. Dang, Z. Interpretation of fish biomarker data for identification, classification, risk assessment and testing of endocrine disrupting chemicals. *Environ. Int.* **2016**, *92-93*, 422.
50. Rodrigues, E.T.; Varela, A.T.; Pardal, M.A.; Oliveira, P.J. Cell-based assays seem not to accurately predict fish short-term toxicity of pesticides. *Environ. Pollut.* **2019**, *252*, 476.
51. Elegheert, J.; Behiels, E.; Bishop, B.; Scott, S.; Woolley, R.E.; Griffiths, S.C.; Byrne, E.; Chang, V.T.; Stuart, D.I.; Jones, E.Y.; Siebold, C.; Aricescu, A.R. Lentiviral transduction of mammalian cells for fast, scalable and high-level production of soluble and membrane proteins. *Nat Protoc*, **2018**, *13*, 2991.
52. Schmittgen, T.D.; Livak, K.J. Analyzing real-time PCR data by the comparative C(T) method. *Nat Protoc*, **2008**, *3*, 1101.

6.8 Supporting Information

Supplementary Table 6.1. The information of assay identification and probes

Gene Name	Gene symbol	Ref Seq Identification	Assay Identification	Source
Estrogen receptor 1	ESR-1	NM_152959.1	Dr03093579	Thermo
Estrogen receptor 2a	ESR-β2	NM_180966.2	Dr03074408	Thermo
Estrogen receptor 2b	ESR-β1	NM_174862.3	Dr03150586	Thermo
Hepatocyte nuclear factor 4 alpha	HNF4A	NM_194368.1	Dr03433679	Thermo
Pregnane X receptor	PXR	NM_001098617.2	Dr03105193	Thermo
Glutathione S-transferase alpha 1	GSTA1	NM_213394	PPZ05128A	Qiagen
Cytochrome P450, family 3, subfamily c, polypeptide 1	CYP3C1	NM_212673	PPZ01717A	Qiagen
Vitellogenin 5	VTG-5	NM_001025189.2	PPZ00676A	Qiagen
Glucose-6-phosphate dehydrogenase	g6pd	XM_694076	PPZ12949A	Qiagen
Eukaryotic translation elongation factor 1 alpha 1, like 1	eef1a1l1	NM_131263.1	Dr03432748	Thermo

Supplementary Table 6.2. Condition of reaction cycles

Mode	Cycles	Temperature (°C)	Duration (sec)	Step
SYBR green assay	Hold	95	20	AmpliTaq Fast DNA polymerase and Up activation
	40	95	3	Denature
		60	30	Anneal/Extend
TaqMan assay	Hold	50	120	UNG incubation
		95	120	Polymerase activation
	40	95	3	Denature
		60	30	Anneal/Extend

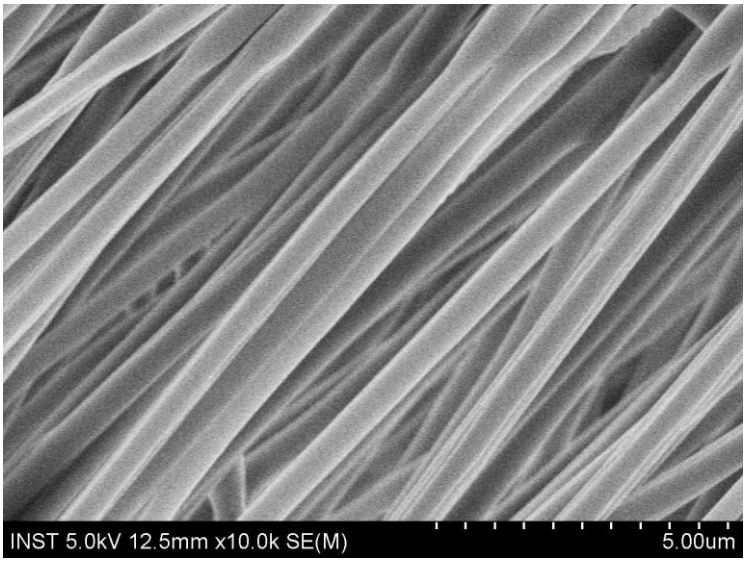

Supplementary Figure 6.1. SEM images of the morphology of fibrous sheet by electrospinning.

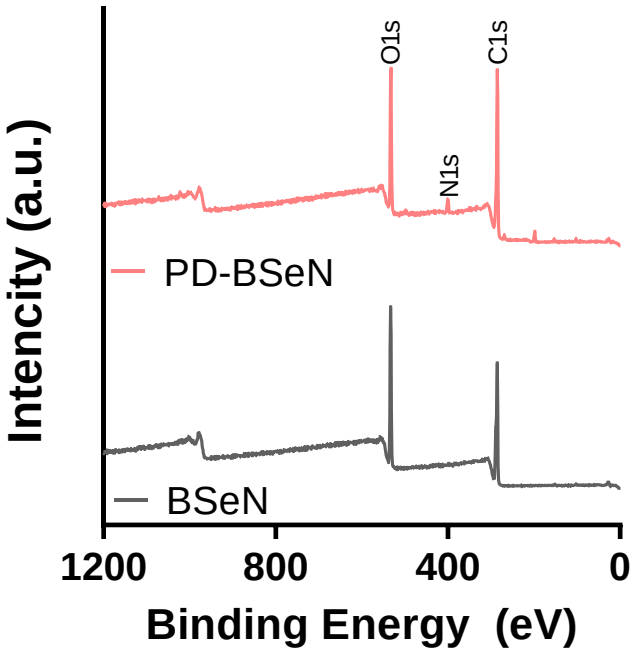

Supplementary Figure 6.2. XPS surface chemical composition of BSeN and PD-BSeN.

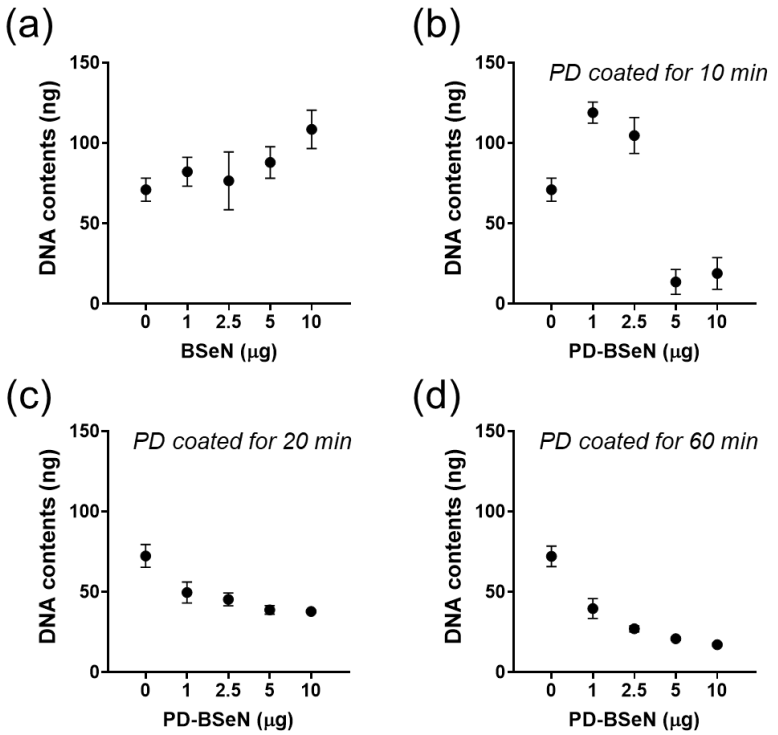

Supplementary Figure 6.3. Optimization of polydopamine coating condition. DNA contents in hybrid-spheroid with PD-BSeN (day 1) were measured depending on different coating times and amounts of PD-BSeN. Spheroids with (a) BSeN, (b) BSeN coated with PD for 10 min, (c) BSeN coated with PD for 20 min, and (d) BSeN coated with PD for 60 min. Each fiber group was replicated to four spheroids and calculated as the mean value. The experiment was repeated eight times from independent cultures. All data are expressed as mean ± SD (n = 8).

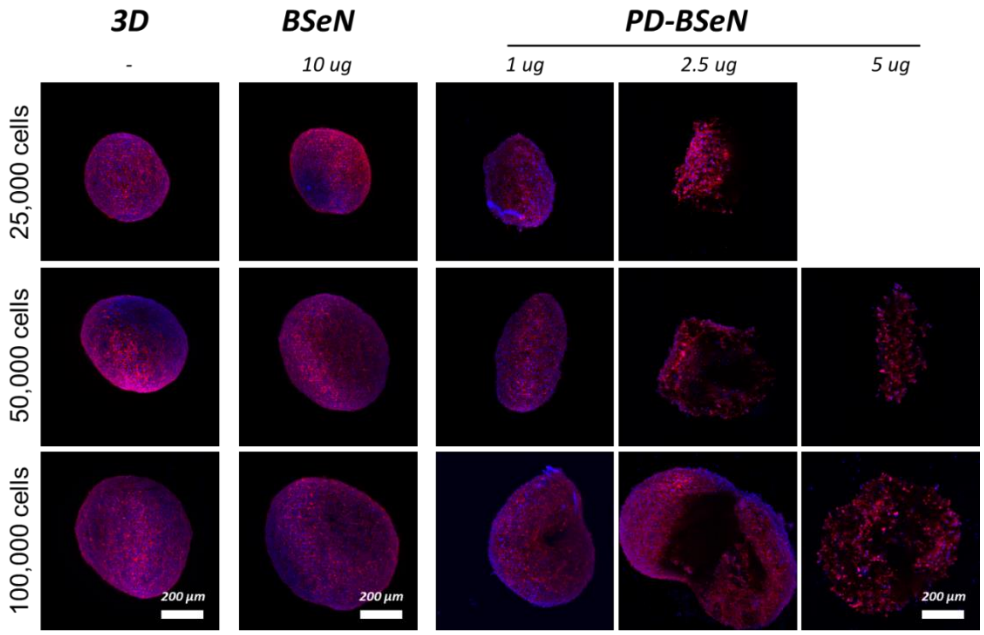

Supplementary Figure 6.4. Fabrication of hybrid-spheroids depending on cell density and PD-BSeN amount. Spheroids and hybrid-spheroids were cultured for 3 days, and their cytoskeletal structure images were obtained by fluorescence staining for DAPI (nuclei; blue) and F-actin (red). In hybrid-spheroids with BSeN,

different cell densities were incorporated with 10 μg of BSeN. In hybrid-spheroids with PD-BSeN, different cell densities were incorporated with 1, 2.5, and 5 μg of PD-BSeN, respectively. PD-BSeN was prepared in a condition of BSeN coated with PD for 60 min.

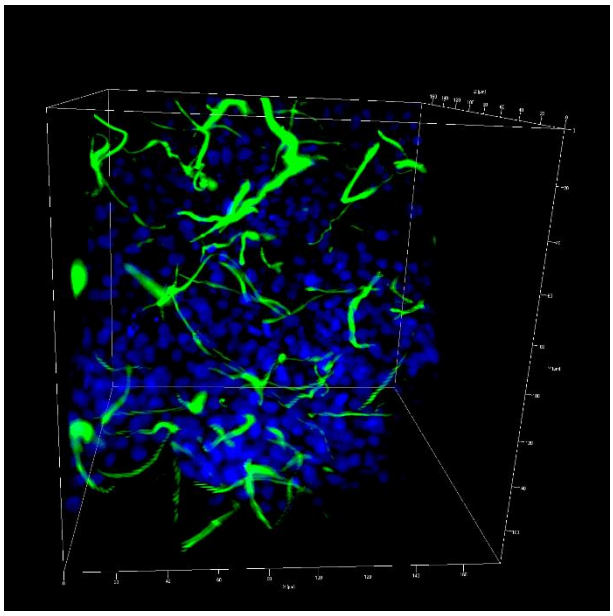

Supplementary Figure 6.5. Representative 3D rendering images of FITC-coated BSeN distributed inside a spheroid. FITC-coated BSeN (green) and DAPI (blue) fluorescence in a spheroid were observed using light-sheet microscopy. The ZFL cells (50,000 cells) were combined with 1 μg of the FITC-coated BSeN and seeded into each well of the BIOFLOATTM 96-well U-bottom plate. The spheroid was cultured for 3 days.

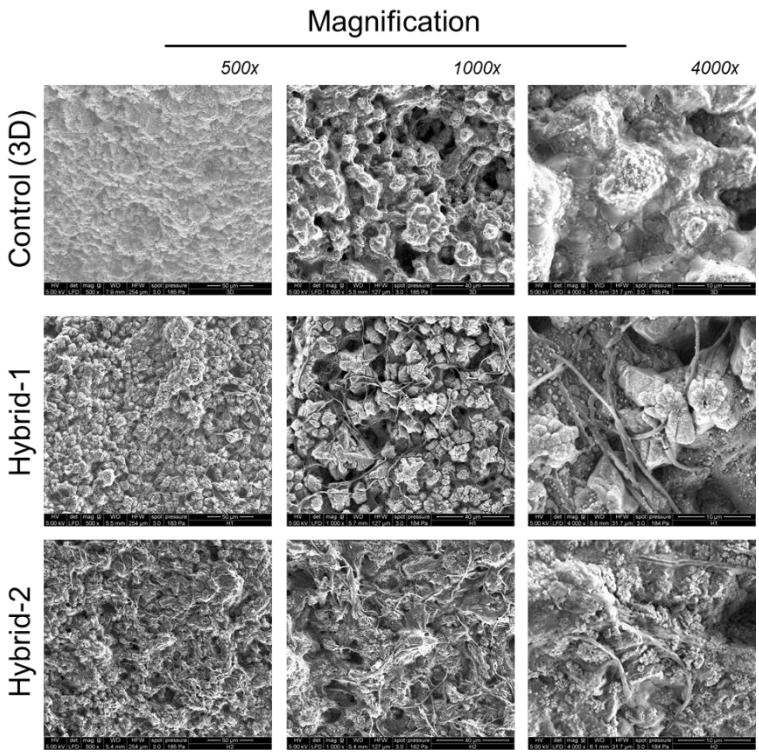

Supplementary Figure 6.6. Representative SEM images of BSeN distributed inside a spheroid. The ZFL cells (50,000 cells) were combined with 1 μg of the BSeN or PD-BSeN were seeded into each well of BIOFLOATTM 96-well U-bottom plates. SEM images were taken at day 3 with Quanta 250 FEG scanning electron microscope. Scale bars are shown on all images. Images of each group were obtained at 500X, 1000X, and 4000X magnifications, respectively.

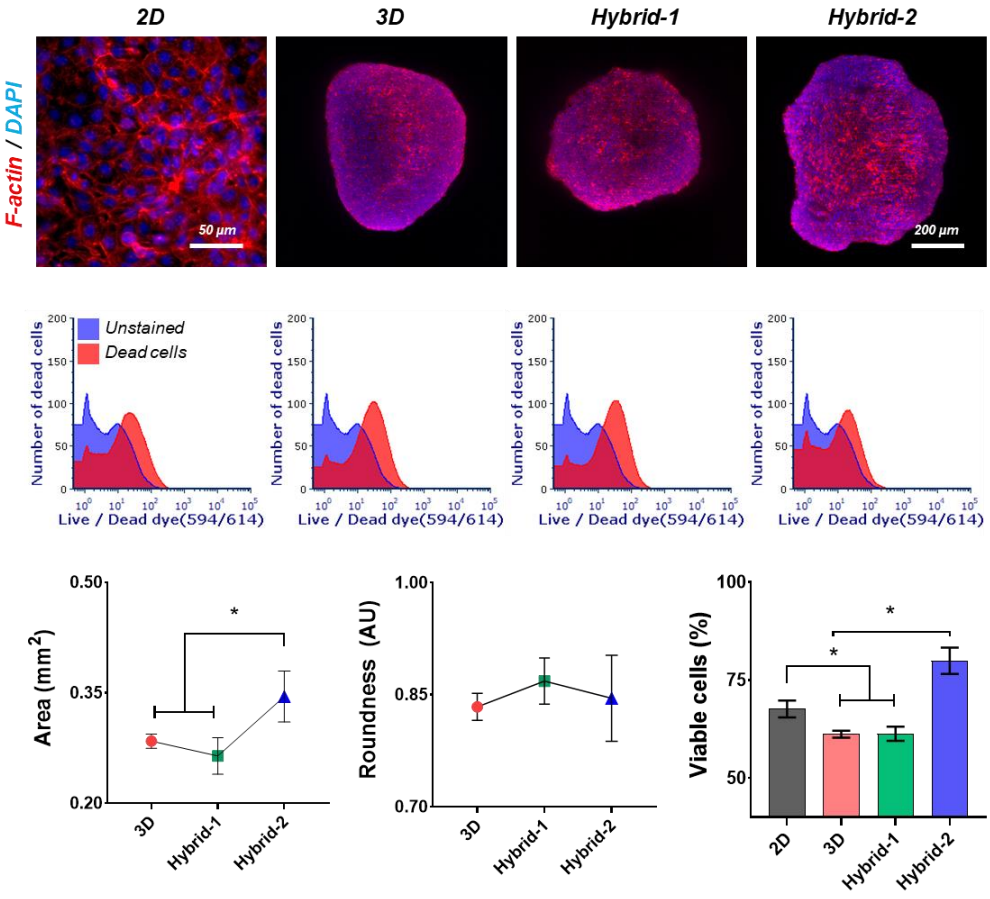

Supplementary Figure 6.7. Morphological observation and viability of monolayer cells and spheroids cultured for 3 days. The cytoskeletal structure images were acquired by fluorescence staining for DAPI (nuclei; blue) and F-actin (red). Area and roundness of spheroids were analyzed by ImageJ software. Data are expressed as mean ± SD (n = 10). FACS results of cell viability after 3 days of culture in 2D, 3D, Hybrid-1, and Hybrid-2 groups (2D from left, Hybrid-2 to the right). The detail of sample preparations is described in the experimental section of Supporting Information. Five replicate samples were prepared for each condition from independent culture, and data are expressed as mean ± SD (n = 5). In the graphs, comparisons of the means between each group were performed using one-way analysis of variance (ANOVA), followed by Scheffe's test (*, $P < 0.05$).

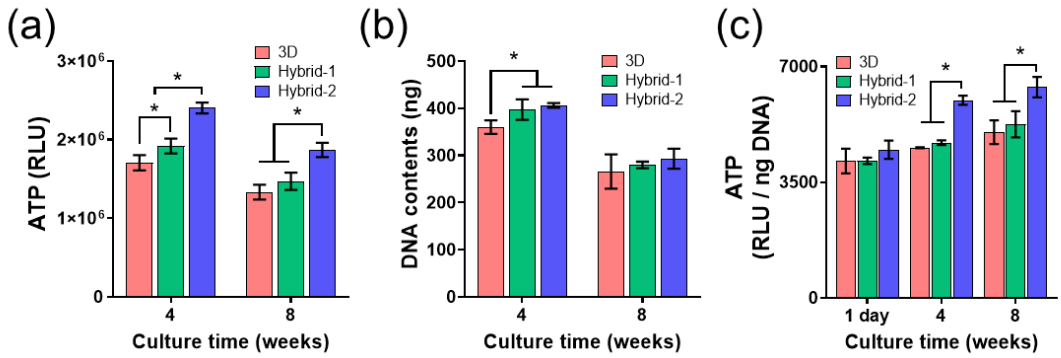

Supplementary Figure 6.8. Measurements of ATP and DNA contents in spheroids cultured for long terms. Each group was replicated to eight spheroids and calculated as a mean value. The experiment was repeated three times, and data are expressed as mean ± SD (n = 3). Comparisons of the means between each group were performed using one-way analysis of variance (ANOVA), followed by Scheffe's test (*, $P < 0.05$).

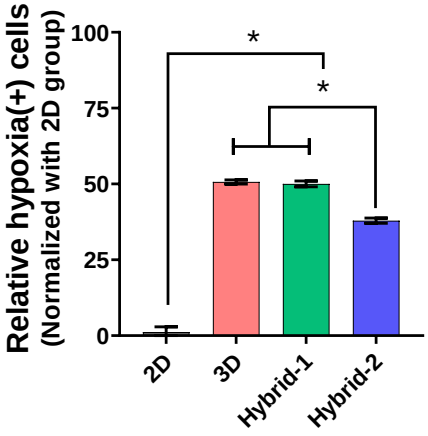

Supplementary Figure 6.9. Relative quantification of hypoxia from the FACS results in Figure 3e. Five replicate samples were prepared for each condition from independent culture, and all groups were normalized with the 2D group, and data are expressed as mean ± SD (n = 5). Comparison of the means between each group was performed using one-way analysis of variance (ANOVA), followed by Scheffe's test (*, $P < 0.05$).

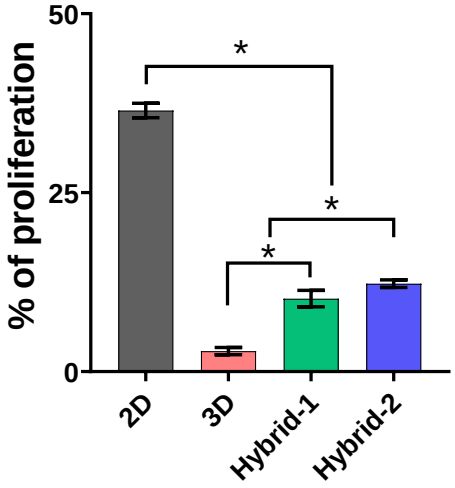

Supplementary Figure 6.10. Relative quantification of cell proliferation from the FACS results in Figure 3c. Five replicate samples were prepared for each condition from independent culture, and data are expressed as mean ± SD (n = 5). Comparison of the means between each group was performed using one-way analysis of variance (ANOVA), followed by Scheffe's test (*, $P < 0.05$).

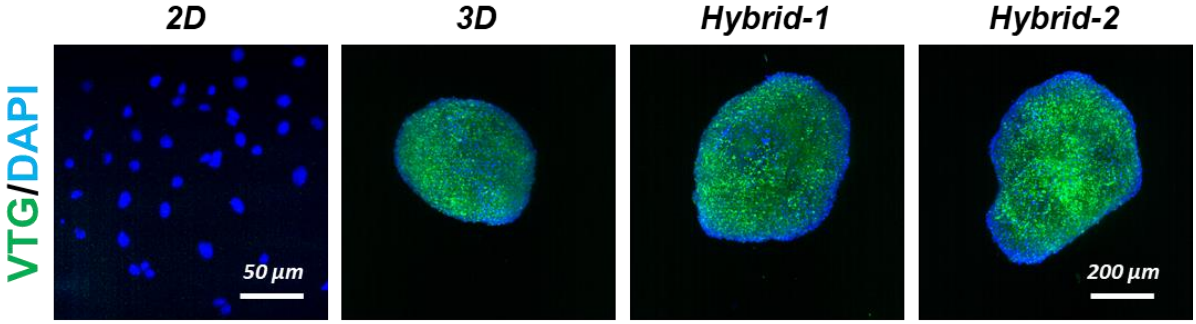

Supplementary Figure 6.11. Immunofluorescence staining for vitellogenin expression of each group at day 5. Each group was stained with DAPI (blue) and Vtg (green).

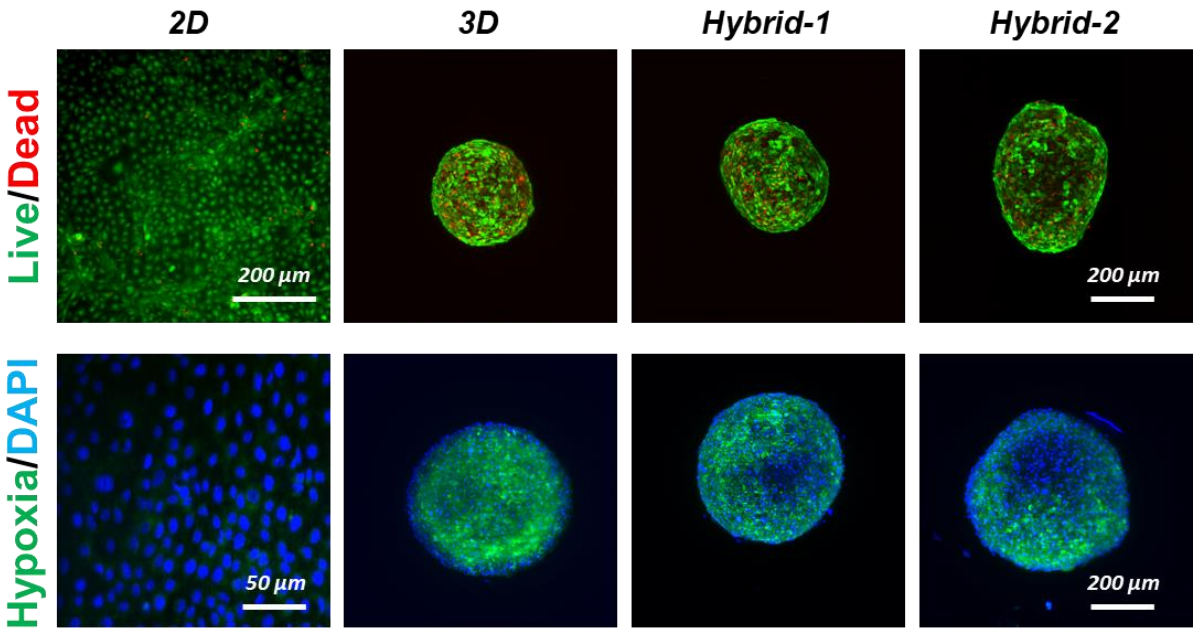

Supplementary Figure 6.12. Viability and hypoxia images of each group at day 14. The viability images were measured by live and dead staining. The hypoxia images were acquired by fluorescence staining for DAPI (nuclei; blue) and hypoxia (green).

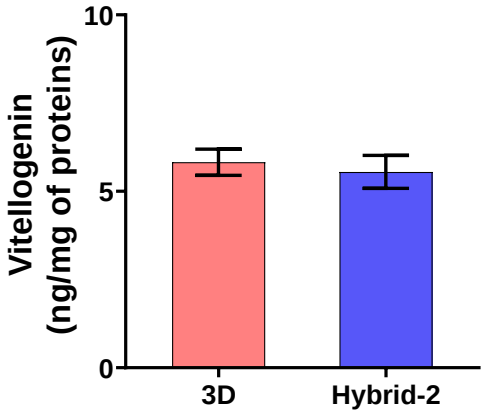

Supplementary Figure 6.13. ELISA quantification of vitellogenin. The 3D and Hybrid-2 groups (5,000 cells/well) were cultured for 5 days. Vitellogenin was normalized to total protein concentration. One hundred spheroids (5,000 cells/well) for each condition were collected into a tube. Each tube was considered a sample, and six replicate samples were prepared for the quantification. Data are presented as mean ± SD (n = 6).

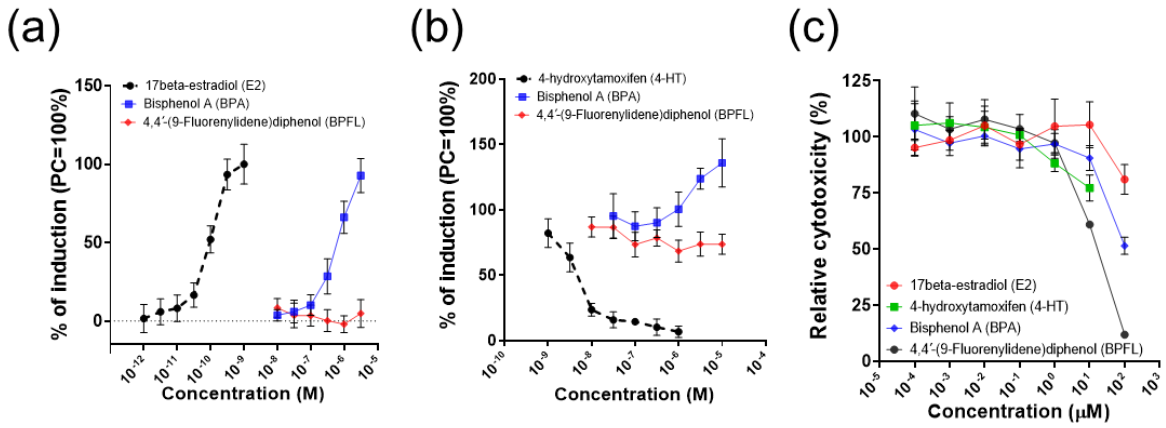

Supplementary Figure 6.14. (a) Estrogenic and (b) anti-estrogenic activities in zebrafish estrogen receptor alpha. The induction value at the maximum concentration of 17β-estradiol (E2; 1 nM for estrogenic assay and 0.32 nM for anti-estrogenic assay) was set to 100%. In anti-estrogenic activity, 0.32 nM E2 was co-treated with EDCs chemicals. The graphs present the means of three replicates of eight wells for each condition. Data are expressed as mean ± SD (n = 3). (c) Cytotoxicity of zebrafish liver cells upon chemical exposure. The graph presents the means of three replicates of five wells. Data are expressed as mean ± SD (n = 3).

Chapter 7. Conclusion

This thesis aims to 3D *in vitro*-based alternative approaches to ecotoxicity assessment. Precise and reliable alternative tests to animal testing are necessary as increasing the presence of EDCs in the ecosystem. Thereby, various *in silico* and *in vitro* approaches have been introduced and tested as alternatives to animal testing.

In the first chapter, the 3D structure of zEsr1-LBD was generated using homology modeling, and the model was docked and simulated with EDCs. The results showed moderate or high correlations with the results of *in vitro* reporter gene assays. The model can be useful for predicting and evaluating the estrogenic activities of EDCs. The combined approaches are useful to evaluate modes of action as a molecular initiating event upon estrogenic chemical exposure. Following the chapter, the ZFL cell line was applied to various three-dimensional (3D) cell culture techniques to develop novel *in vitro* platforms. The 3D spheroid culture of ZFL cells showed higher transcriptional regulation of genes related to reproductive toxicological response and liver functions compared to monolayer cells. Significantly, 3D ZFL spheroids treated with estrogenic chemicals were activated to synthesize a higher level of Vtg than monolayer cells. These findings indicate that 3D cell culture is crucial to ZFL cell sensitization and activation for transcription, and ultimately to physiological function. The results suggest that the engineering of novel 3D *in vitro* platforms for screening harmful chemicals and improving understanding of the underlying liver toxicity mechanisms at the molecular and cellular levels.

However, the 3D spheroid culture revealed limitations such as simplified architecture, agglomeration, and limited diffusion. Thus, hydrogels and nanofibers that could mimic ECM environments were applied to the ZFL cell culture to implement those limitations. In the ZFL cluster culture on hydrogels, the softer gel drove cells to form a cell sheet with a canaliculi-like structure compared to its stiffer gel counterpart. The hepatoids cultured on the softer gel exhibited the more active urea production and Vtg levels upon exposure to estrogenic compounds. In addition, the use of nanofibers in 3D ZFL cell cultures is found to improve liver and reproductive functions through assays such as whole transcriptome sequencing and reproductive toxicity testing, with optimized properties exhibiting results similar to those obtained for fish embryo acute toxicity (FET, OECD TG 236) following exposure to environmental EDCs. These findings have beneficial effects of bioinspired materials that closely mimic ECM environments can yield efficient ZFL with intrinsic functions and xenobiotic metabolism similar to those of zebrafish embryos.

Collectively, the 3D *in vitro* systems show improved cell functionality and physiology by forming tissue-like environments. Besides, the systems show promise as tools that are useful for further eco-environmental assessment and can narrow the gap between *in vitro* and *in vivo* systems. I believe that the integrated approaches can be applied to evaluate potential EDCs with screening from a mode of action as a MIE to AOs induced by KEs and can construct methods that cover relevant mechanisms as alternative platforms to animal and primary cells. Therefore, this thesis can contribute to reducing the animal testing under the 3Rs principles.

Chapter 8. Appendix

8.1 Original Paper - Combined *in silico* and *in vitro* approaches for identifying EDCs

Environmental Toxicology and Chemistry—Volume 00, Number 00—pp. 1–13, 2022
Received: 31 March 2022 | Revised: 12 May 2022 | Accepted: 12 July 2022

Environmental Toxicology

Species Differences in Response to Binding Interactions of Bisphenol A and its Analogs with the Modeled Estrogen Receptor 1 and In Vitro Reporter Gene Assay in Human and Zebrafish

Chang Gyun Park,[a,b] Nancy Singh,[a,b] Chang Seon Ryu,[a] Ju Yong Yoon,[a] Maranda Esterhuizen,[c,d] and Young Jun Kim[a,*]

[a]Environmental Safety Group, Korea Institute of Science and Technology Europe, Saarbrucken, Germany
[b]Universität des Saarlandes, Saarbrücken, Germany
[c]Ecosystems and Environment Research Programme, Faculty of Biological and Environmental Sciences, University of Helsinki, Lahti, Finland
[d]Helsinki Institute of Sustainability Science, Fabianinkatu, Helsinki, Finland

Abstract: Adverse impacts associated with the interactions of numerous endocrine-disruptor chemicals (EDCs) with estrogen receptor 1 play a pivotal role in reproductive dysfunction. The predictive studies on these interactions thus are crucial in the risk assessment of EDCs but rely heavily on the accuracy of specific protein structure in three dimensions. As the three-dimensional (3D) structure of zebrafish estrogen receptor 1 (zEsr1) is not available, the 3D structure of zEsr1 ligand-binding domain (zEsr1-LBD) was generated using MODELLER and its quality was assessed by the PROCHECK, ERRAT, ProSA, and Verify-3D tools. After the generated model was verified as reliable, bisphenol A and its analogs were docked on the zEsr1-LBD and human estrogen receptor 1 ligand-binding domain (hESR1-LBD) using the Discovery Studio and Autodock Vina programs. The molecular dynamics followed by molecular docking were simulated using the Nanoscale Molecular Dynamics program and compared to those of the in vitro reporter gene assays. Some chemicals were bound with an orientation similar to that of 17β-estradiol in both models and in silico binding energies showed moderate or high correlations with in vitro results ($0.33 \leq r^2 \leq 0.71$). Notably, hydrogen bond occupancy during molecular dynamics simulations exhibited a high correlation with in vitro results ($r^2 \geq 0.81$) in both complexes. These results show that the combined in silico and in vitro approaches is a valuable tool for identifying EDCs in different species, facilitating the assessment of EDC-induced reproductive toxicity. *Environ Toxicol Chem* 2022;00:1–13. © 2022 SETAC

Keywords: In silico methods; Homology modeling; Estrogen receptor 1; Zebrafish; Bisphenol A and its analogs; In vitro assay

INTRODUCTION

Estrogen-induced actions promote various physiological processes, such as growth, homeostasis, and reproduction (Barkhem et al., 2004; Hewitt et al., 2016; Khalid & Krum, 2016; Kovats, 2015; Shen & Shi, 2015). In addition, estrogens regulate the pubertal development and function of the female reproductive system (Hewitt et al., 2016), bone density (Khalid & Krum, 2016), immune system (Kovats, 2015), and lipid and glucose metabolism (Shen & Shi, 2015). Most of these processes are mediated by estrogen receptors (ESRs), which can be divided into two subtypes: estrogen receptor 1 (ESR1) and estrogen receptor 2 (ESR2). Both receptors have been observed in nonmammalian vertebrates and mammals (Hawkins et al., 2000). Estrogen receptor 1 is predominantly expressed in various tissues and organs, such as the liver, bones, glands, uterus, ovaries, testes, and prostate (Dahlman-Wright et al., 2006; Heldring et al., 2007), and plays more important roles than ESR2 in the mammary glands and uterus, maintenance of skeletal homeostasis, and regulation of lipid and glucose metabolism (Barros & Gustafsson, 2011; Paterni et al., 2014). Estrogen receptors are structurally composed of N-terminal, DNA-binding, and ligand-binding domains (LBDs; Kumar et al., 2011). Ligand-binding domains include the ligand-binding pocket, which can activate ESRs by interacting with ligands, such as 17β-estradiol (E2). Owing to this interaction, many exogenous chemicals, which mimic estrogens,

This article includes online-only Supporting Information.
* Address correspondence to youngjunkim@kist-europe.de
Published online 25 July 2022 in Wiley Online Library (wileyonlinelibrary.com).
DOI: 10.1002/etc.5433

can alter the functions of the endocrine system and cause various adverse effects (Bardet et al., 2002). Therefore, concern regarding the possible threats posed by endocrine-disrupting chemicals (EDCs) in wildlife and humans is increasing (Mills & Chichester, 2005; Zhang & Zhou, 2005).

Bisphenol A (BPA) has been reported to adversely affect the reproductive and developmental systems of humans, fish, and amphibians (Kang et al., 2007; Mathieu-Denoncourt et al., 2015; Rochester, 2013), and is a precursor to plastics, epoxy resins, and thermal paper (Geens et al., 2012). Although substitutes have recently been manufactured to replace BPA, some exert endocrine effects similar to those of BPA (Chen et al., 2016; Keminer et al., 2020; Rosenmai et al., 2014; Usman & Ahmad, 2016). As a large number of comprehensive studies are required to evaluate potential endocrine disruption caused by BPA substitutes, molecular docking is a promising tool for predicting and screening potential EDCs, and has been conducted to predict the types of interactions, binding affinity, and orientations of the docked ligands at the binding site of the target receptor (Babu et al., 2012; Cavaliere et al., 2020; Montes-Grajales & Olivero-Verbel, 2013; Sliwoski et al., 2013). However, because most static docking protocols lack receptor flexibility, the reliability of the complexes might be uncertain (Kalé et al., 1999). Hence, molecular dynamic simulation has been applied to understand the dynamic behavior of complexation and to complement the limitations of molecular docking. Molecular dynamic simulation can offer fundamental molecular mechanisms and conformational changes (Kalé et al., 1999; Phillips et al., 2005). Although most docking studies have been conducted on BPA and its analogs for human ESRs, docking and molecular dynamic simulations for aquatic organisms remain limited because there are currently no available crystal structures (Babu et al., 2012; Zhang et al., 2018).

The present study aimed to generate the structure of an zEsr1 ligand-binding domain (zEsr1-LBD) using homology modeling. Zebrafish (*Danio rerio*) have been utilized as a model organism for toxicity testing by the Organization for Economic Co-operation and Development (OECD) guidelines. Furthermore, zebrafish exhibit rapid development and growth, and signaling pathways highly similar to those in humans (Kari et al., 2007; MacRae & Peterson, 2015). The zEsr1-LBD was generated using the MODELLER program and the structural quality was then verified using PROCHECK, ERRAT, ProSA, and Verify-3D tools. Consequently, the generated zEsr1-LBD model was used to investigate its interactions with E2, BPA, 4,4′-(9-fluorenyliden)-diphenol (BPFL), tetramethyl bisphenol A (TMBPA), and 4-phenylphenol. Tetramethyl bisphenol A, BPFL, and 4-phenylphenol are classified as alternative substances of BPA, and these analogs are introduced mainly for usage in thermal paper, polymers, polycarbonates, and fire retardants (Keminer et al., 2020). Because these applications cause exposure of chemicals in the environment, the analogs have been detected in water and sediment samples from lakes or rivers (Banaderakhshan et al., 2022; Chafi et al., 2022; Jin & Zhu, 2016). These chemicals have been reported to have endocrine disruptor potential by exhibiting anti- or estrogenic activities in humans (Keminer et al., 2020). In addition, BPFL showed an antiestrogenic effect in mice and zebrafish, and hormetic effects on regulating the hypothalamic–pituitary–thyroid axis in zebrafish (Jin et al., 2021; Mi et al., 2019; Zhang et al., 2017). However, there is still a lack of studies on their estrogenic disruptive activities and their modes of action in aquatic species. Thus, the complex geometry and putative chemical-receptor binding energies of BPA and its analogs were calculated and validated by conducting in vitro assays. The correlations between the in silico and in vitro analyses confirmed that the newly generated zEsr1-LBD is useful for predicting and evaluating the estrogenic activities of EDCs.

MATERIALS AND METHODS

Sequence alignment, template selection, and homology modeling

Sequence alignment was conducted to observe sequence identity between human ESRs (hESRs) and zebrafish Esrs (zEsrs). Multiple sequence alignment and principal components analysis (PCA) were conducted, and a phylogenetic tree was generated using JalView (Procter et al., 2021). The PCA and phylogenetic tree were constructed using amino acid sequences of ESRs available from Uniprot. The sequence sources and UniProt IDs were as follows: human ESR1 (hESR1, P03372), zebrafish estrogen receptor 1 (zEsr1, P57717), human ESR 2 (hESR2, Q92731), zebrafish ESR2a (zEsr2a, Q7ZU32), and zebrafish ESR2b (zEsr2b, Q90WS9).

The crystal structure of hESR1 (protein data bank [PDB] ID: 2YJA) was selected as hESR1-LBD, which is bound to stapled peptides and E2 (Phillips et al., 2011). The LBD structure of zEsr1 was created using homology modeling. First, the LBD sequence of zEsr1 (P57717) was retrieved from the UniProt database to build the model. The query sequence was then used to search for an optimal template with the protein-basic local alignment search tool (BLASTp; Altschul et al., 1990). The hESR1-LBD (2YJA) was selected as the optimal template after utilizing BLASTp. The software MODELLER 9.25 was used to create the homology model for zEsr1-LBD. The program is a homology or comparative modeling tool that conducts comparative protein structure modeling based on satisfaction of spatial restraints. Comparative modeling predicts the three-dimensional (3D) structure of a given protein target sequence based primarily on its alignment with one or more proteins with known template structures to generate a zebrafish Esr1 model (Webb & Sali, 2016). The LBD sequence of zEsr1 and template structure (2YJA) were used as the inputs in MODELLER v9.25 (https://salilab.org/modeller/9.25/release.html). When target-template alignment is conducted, the program automatically calculates a 3D model of the target using its automodel class (Webb & Sali, 2016). Finally, MODELLER generates a 3D model containing all the main chain and sidechain nonhydrogen atoms as the output of the given target sequence. Ten models were generated, and one structure with the lowest discrete optimized protein energy (DOPE) score was selected as the zEsr1-LBD model for molecular docking (Shen & Sali, 2006).

Homology model validation

The structural qualities of zEsr1-LBD and hESR1-LBD were validated using the ERRAT program (Colovos & Yeates, 1993), PROCHECK (Morris et al., 1992), ProSA (Wiederstein & Sippl, 2007), and Verify 3D tools (Lüthy et al., 1992). The ERRAT program analyzes the relative frequencies of noncovalent interactions between various types of atoms (Colovos & Yeates, 1993), whereas PROCHECK uses the Ramachandran plot for structural verification, which assesses the quality and accuracy of the stereochemical properties of a model (Morris et al., 1992). The Protein Structure Analysis (ProSA) program is an established tool with a large user base that is frequently used to refine and validate experimental protein structures and for structural prediction and modeling (Wiederstein & Sippl, 2007). The program Verify 3D measures the compatibility of a protein model with its own amino acid sequence (Lüthy et al., 1992).

Molecular docking

The hESR1-LBD and generated zEsr1-LBD structures were used for molecular docking with BPA analogues including E2, BPA, BPFL, TMBPA, and 4-phenylphenol as the test ligands from the PubChem database (E2: 5757, BPA: 6623, BPFL: 76716, TMBPA: 79717, and 4-phenylphenol: 7103). All the chemicals were saved as a structure data file format, and their geometries were optimized following the MM2 energy minimization method. The files were converted into protein data bank format using Discovery Studio Visualizer 2016 (Accelrys Software).

Molecular docking simulations were conducted using the CDOCKER module of Discovery Studio (Wu et al., 2003) and AutoDock Vina (Trott & Olson, 2010), which uses the CHARMM-based molecular dynamics method. The CDOCKER module generates the conformation using high-temperature molecular dynamics and then forwards the conformations to the binding site for binding pose analysis. The CDOCKER interaction energy is taken as an estimate of the molecular binding affinity, with lower values suggesting more favorable binding between the protein and ligand (Wu et al., 2003). Autodock Vina utilizes protein and ligand information, along with the grid box properties, in the docking configuration file and assumes that the receptor is rigid and ligands are flexible during docking (Trott & Olson, 2010). Root mean squared deviation (RMSD) values below 1.0 Å were clustered and the results with the most favorable binding free energy were considered. The grid size was set to 40 points each in the *x*, *y*, and *z* directions, with a grid spacing of 1.0 Å. The energetic map was determined using the distance-dependent function of the dielectric constant, and the default settings were applied to all the other parameters. All docked poses were determined using rankings based on binding energies. The pose with the lowest binding energy was extracted and aligned with the receptor structure for further analysis.

Molecular dynamics simulations

All simulations were performed using nanoscale molecular dynamics (NAMD) 2.14 software with a CHARMM27 force field (Phillips et al., 2005). System preparations for molecular dynamic simulations and analysis of the computed trajectories were performed using visual dynamics studio (VMD) Ver 1.9 (Humphrey et al., 1996). The CHARMM GUI web server was utilized to prepare the system for the molecular dynamic simulations, including ligand parameter files. Coordinates for the missing hydrogen atoms and amino acid side chains were added with AutoPSF plugin from VMD and based on the CHARMM27 force field (Kalé et al., 1999). The system was solvated with TIP3P water using the solvate plugin from VMD with a spacing of 10Å in all directions (Jorgensen et al., 1983). Charges of the system were neutralized by Na^+ and Cl^- ions using the autoionize plugin from VMD. After the minimization of the solvated system, the system was equilibrated at a temperature of 310 K. The simulations were conducted in an isothermal-isobaric ensemble with periodic boundary conditions. Electrostatic interactions were computed using the particle mesh Ewald method (Cheatham et al., 1995). The van der Waals interactions were calculated at cutoff and switching distances of 12 and 10 Å, respectively. The temperature and pressure were maintained constant using a Langevin thermostat and a Langevin barostat, respectively. All simulations were conducted for at least 20 ns using 2 fs time steps (Feller et al., 1995).

The RMSD of protein Cα atoms was calculated in each simulation. Moreover, the hydrogen bonding (H-bonding) occupancy was analyzed using the H-bond plugin. The cutoff distance and angle of occupancy were set to 3.5 Å and 120°, respectively. The simulation of binding free energy (ΔG_{bind}) was calculated by molecular mechanics/Poisson–Boltzmann surface area (MM/PBSA) in the CaFE plugin. Each simulation extracted at least 5000 snapshots from the last 5 ns of the trajectories. The calculation of MM/PBSA was performed according to a methodology described previously (Hou et al., 2011).

Recombinant yeast assay

All the chemicals were purchased from Sigma-Aldrich and dissolved in dimethyl sulfoxide (DMSO), the concentration of which did not exceed 1% (v/v) of the test chemicals. *Saccharomyces cerevisiae* recombinant yeast was purchased from Xenometrix AG (XenoScreen YES) and was genetically integrated to express hESR1 (YES). The expression plasmid of the reporter gene *lac*-Z was also inserted into the yeast, which induces the β-galactosidase enzyme. Therefore, when an agonist bound to the hESR1 in the yeast, yeast was activated and expressed β-galactosidase, which converts chlorophenol red-β-D-galactopyranoside (CPRG) into chlorophenol red (Xenometrix, 2018). Based on this principle, the yeast could be used to evaluate the estrogenic activity of chemicals; for this, we used E2 as a reference chemical. The test yeast was exposed to half-logarithmic (3.16-fold) dilutions of E2 and other chemicals. The exposure ranges were 10^{-11}–10^{-8} M for E2, 10^{-7}–10^{-4} M for BPA and TMBPA, and 10^{-8}–10^{-5} M for BPFL and 4-phenylphenol. The medium containing yeast and CPRG (200 µl) was exposed to the test chemicals (2 µl) in 96-well

plates and incubated at 31 °C with shaking (100 rpm) for 48 h. 17β-Estradiol treatment resulted in the cleavage of CPRG into chlorophenol red by the induction of β-galactosidase. We analyzed optical density at 690 nm (OD_{690}) and 570 nm (OD_{570}) using a spectrophotometer (Tecan). Data analysis was conducted according to the yeast assay manufacturer's protocol (Xenometrix, 2018).

Cell culture, transfection, and luciferase reporter assay

The human embryonic kidney 293 cell line (HEK293, CRL-1573; ATCC) was utilized as a transfection host for the zEsr1 construct. The HEK293 cells were cultured in Dulbecco's modified Eagle's medium without phenol red (Thermo Scientific), with 10% fetal bovine serum (Thermo Scientific) and 1% penicillin–streptomycin (Thermo Scientific) at 37 °C and 5% CO_2.

The HEK293 cells were transduced with the pGreenFire Lenti-reporter plasmid (pGF2-ERE-rFLuc-T2A-GFP-mPGK-Puro, TR455VA-P; System Biosciences) that encodes green fluorescent protein (GFP) reporter and red-shifted luciferase, under the control of estrogen response element (ERE) with the puromycin resistance, according to a previously described methodology (Elegheert et al., 2018). Briefly, the cells were plated with 3×10^5 cells per well in a six-well plate (Thermo Scientific) before transduction. After overnight culture, the old medium was aspirated and the virus-containing medium was treated with 5 μg/ml of polybrene for 8 h. Subsequently, the virus-containing medium was removed and the transduced cells were allowed to recover overnight before the addition of puromycin (10 μg/ml) for selection in the medium. In the second step, the transduced cells (HEK293-ERE) were transfected with the piggyBac transposon gene expression system. The zEsr1 expression vector was custom-cloned by vectorbuilder (pPB-Neo-CAG > zEsr1, VB210426-1022cns; Vectorbuilder) and the pRP-mCherry-CAG > hyPBase plasmid (VB160216-10057; Vectorbuilder) encodes the hyperactive version of piggyBac transposase. The cells were plated with 1×10^5 cells per well in a six-well plate. After overnight culture, 1 μg of the vector and 0.75 μl of the lipofectamine 3000 reagent were mixed in 250 μl of Opti-MEM medium and incubated for 15 min for DNA–lipid complex formation. The mixture of the DNA-lipid complex formation was treated to each well and incubated for 6 h. Afterwards, the medium was removed, and the cells were allowed to recover overnight before the addition of puromycin and neomycin (10 and 2 μg/ml, respectively). Finally, the transfected cells (HEK293-ERE-zEsr1) were collected.

The HEK293-ERE-zEsr1 cells were used to assess the estrogenic activity of chemicals. 17β-Estradiol was used as a reference chemical and the cells were exposed to half-logarithmic (3.16-fold) dilutions of E2 and other chemicals. The exposure ranges were 10^{-12}–10^{-9} M for E2 and 10^{-10}–10^{-5} M for other chemicals. The test chemicals were obtained with high purity (≥98%) from Sigma-Aldrich and were dissolved in DMSO, with a concentration not exceeding 0.5% (v/v). The cells were seeded at a rate of 1.0×10^4 cells per well on a 96-well plate. After overnight culture, the chemical solutions were treated with a ratio of 1:1 in each well containing the medium and cultured for 24 h. The cells were lysed with passive lysis buffer (Promega), and the lysates were applied to evaluate Firefly luciferase activity using the Luciferase Reporter Assay System (Promega). Luminescence was measured as relative luminescence units with an integration time of 10 s and a settling time of 1 s using a microplate reader.

Statistical analysis

All data of the in vitro studies are presented as the mean of triplicate per concentration and are presented as the mean ± standard deviation. Graphs are prepared using SigmaPlot (Ver 12.0; Systat Software). The correlation analysis was performed using Pearson correlation test in R Ver 3.5.1 through RStudio Ver 1.2.5042.

RESULTS AND DISCUSSION

Sequence alignment, template selection, and homology modeling

Sequence alignments of hESRs and zEsrs were obtained and are compared in Figure 1. The sequence identity between hESR1 and zEsr1 is 47% (Figure 1A). Notably, the sequence identity of LBD between hESR1 and zEsr1 increased to 62%, which indicates better conservation compared to other domains. The sequence similarity of the LBD regions between both sequences is 78%. The PCA results indicated clear separations between ESR1 and ESR2, regardless of the species (Figure 1B). The hESR1 and zEsr1 isoforms are closer to each other than the hESR2 and zEsr2 isoforms. The phylogenetic tree reveals the close inter-relationship of 1 and 2 isoforms of hESR and zEsr in terms of evolutionary distance metric (Figure 1C).

Sequence alignment is a pivotal step in generating a homology model, because sequence misalignment can result in homology model errors and the generation of different models (Chang & Swaan, 2006; Venclovas, 2003). Phylogenetic analysis confirmed that zEsr1 is derived from the ESR1 ancestral subtype and that zEsr2 isoforms belong to the ESTR2 subgroup. Moreover, the LBD is highly conserved following the DNA binding domain (Menuet et al., 2002). Consequently, the LBD sequences of hESR1 and zEsr1 were considered well conserved within the same subtype.

A homology model of zEsr1-LBD was generated using MODELLER based on sequence alignment (Figure 2). Human ESR1-LBD (PDB ID: 2YJA; Figure 2A) was selected as a template, with query coverage, sequence identity, *e*-value, and bit score of 44%, 62.1%, 6e−109, and 327, respectively. Ten homology models were generated, and the optimal zEsr1-LBD model was selected according to the lowest discrete optimized protein energy (DOPE score −32,888; Figure 2B). The X-ray crystal structure of hESR1-LBD and the homology model of zEsr1-LBD are superimposed in Figure 2C. The backbone positional RMSD between the two structures was 0.162 Å, indicating that the zEsr1-LBD model has high similarity and

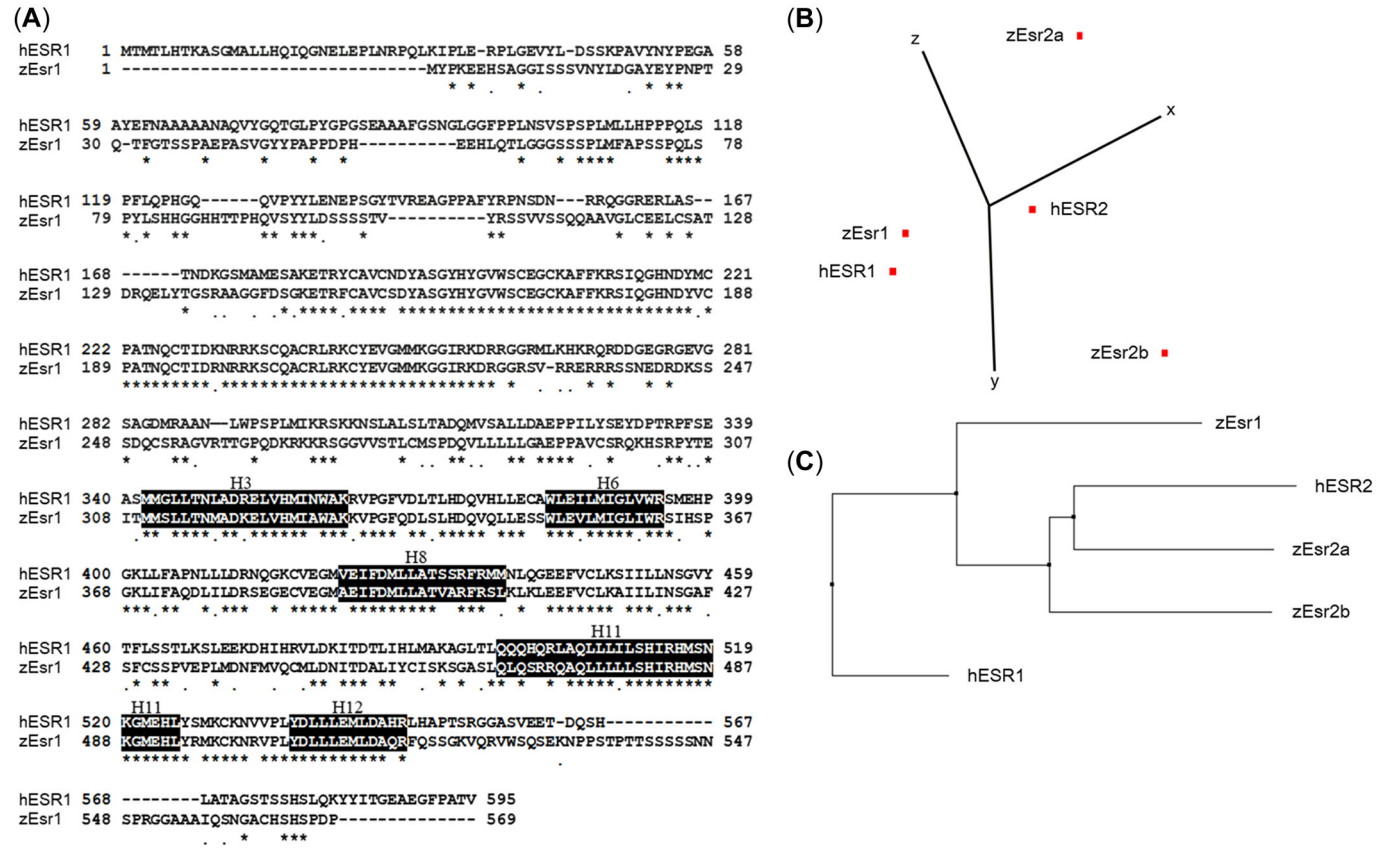

FIGURE 1: Sequence alignment comparison. (**A**) Sequence alignment between human estrogen receptor 1 (hESR1) and zebrafish estrogen receptor 1 (zEsr1). The conserved amino acids are marked with asterisks and similar properties between different amino acids are marked as dots. The helices surrounding the ligand-binding cavity are colored black in the E/F domain. Gaps are denoted with a hyphen. (**B**) Principal component analysis of human and zebrafish estrogen receptors. (**C**) Phylogenetic analysis showing the relationships between human and zebrafish estrogen receptors.

structural comparability with the hESR1-LBD structure (Martí-Renom et al., 2000; Shehadi et al., 2020). The ligand-binding cavities when both receptors were bound to E2 are superimposed in Figure 2D. Three residues at corresponding positions of the ligand-binding cavities of hESR1 and zEsr1 were involved in hydrogen bonding and each residue of the two receptors formed hydrogen bonding interactions with the identical atoms of E2. Moreover, the distances of each corresponding hydrogen bond are comparable between the two species. Taken together, these results confirmed the reliability of the generated zEsr1-LBD and binding similarity between the hESR1- and zEsr1-LBDs.

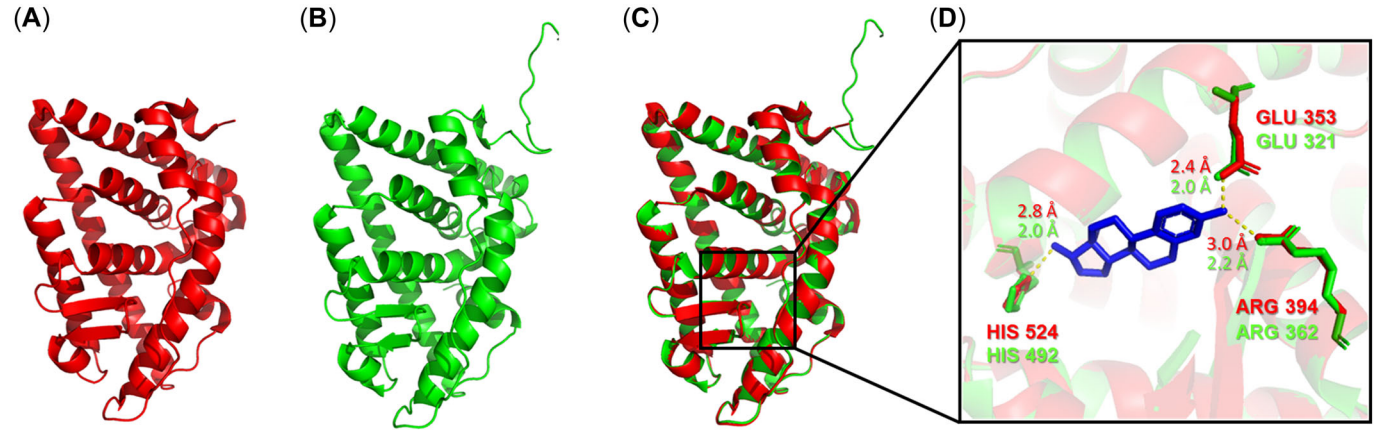

FIGURE 2: Three-dimensional ligand-binding domain structures of the human estrogen receptor 1 (hESR1) and modeled zebrafish estrogen receptor 1 (zEsr1). (**A**) Ligand-binding domain of hESR1 (hESR1-LBD; PDB:2YJA). (**B**) Ligand-binding domain of zEsr1 (zEsr1-LBD) generated by homology modeling using MODELLER. (**C**) Superimposed images of hESR1-LBD (red) and zEsr1-LBD (green). (**D**) Hydrogen bond interactions of 17β-estradiol with both structures. Red and green residues indicate hESR1-LBD and zEsr1-LBD, respectively. GLU = glutamic acid; HIS = histidine; ARG = arginine.

Model validation

The generated model, including the conformation-dependent backbone geometry, was validated using PROCHECK, ERRAT, ProSA, and Verify-3D (Supporting Information, Table S1 and Figure S1). The PROCHECK software was used to obtain a Ramachandran plot (Morris et al., 1992) for evaluating the stereochemical properties of hESR1-LBD and zEsr1-LBD, which presents the phi (φ) and psi (ψ) distributions of backbone conformation angles for each residue in a protein structure consistent with a right-handed α-helix (Supporting Information, Figure S1A). A good-quality model is expected to occupy greater than 90% of the most favorable region in the Ramachandran plot (Morris et al., 1992; Otero et al., 2010). For the plots of hESR1-LBD and zEsr1-LBD, amino acids occupied 96.6% and 97.5% of the most favorable region, respectively. None of the residues were present in the disallowed region in the plot generated for zEsr1-LBD, while 0.4% of the residues were present in the disallowed region of the plot for hESR1-LBD, indicating that both structures were good stereochemical models. To assess the relative distributions of different atom types in the test structure and determine the overall quality factor for noncovalent bonded atomic interactions, ERRAT was used; with scoring exceeding 90% which resulted in 97.0% and 90.8% for hESR1-LBD and zEsr1-LBD, respectively, indicating that the backbone conformation and noncovalent bonding interactions of hESR1-LBD and zEsr1-LBD were acceptable for high-quality structure models (Supporting Information, Figure S1B; Colovos & Yeates, 1993; Shamsara, 2019).

The structures were also cross-validated using ProSA-web (*z*-score), which resulted in −6.80 and −6.76 for hESR1-LBD and zEsr1-LBD, respectively, and plotted within the range for entire proteins determined by the nuclear magnetic resonance and X-ray-derived structures (Supporting Information, Figure S1C). The results suggest that the prediction accuracy of the 3D protein structure models is acceptable when compared to previous studies (Otero et al., 2010; Shehadi et al., 2020; Wiederstein & Sippl, 2007). Finally, the Verify-3D server was used to predict the hESR1-LBD and zEsr1-LBD structures as profile-3D scores, which are presented as a table computed from the atomic coordinates of the structure (Supporting Information, Figure S1D). A 3D-1D score exceeding 0.2 for greater than 65% of a structure indicates high quality in a general manner, according to previous studies (Lüthy et al., 1992; Shamsara, 2019). The verify-3D server predicted that 79.2% of the residues in hESR1-LBD had an average 3D-1D score of >0.2, while 78.0% of the residues in zEsr1-LBD had an average 3D-1D score of >0.2. Both structures effectively met the criteria with high scores. Overall, the modeled zEsr1-LBD was comparatively robust and could be applied to the subsequent evaluation of binding activities.

Molecular docking and molecular dynamic simulations

The docking of chemicals on hESR1-LBD and zEsr1-LBD was successfully simulated and revealed multiple docking poses for each ligand binding site. The binding poses of the docked complexes are illustrated in Figure 3. In particular, the docked complexes of E2/hESR1-LBD and E2/zEsr1-LBD exhibited an identical pattern of interactions between ligand and receptor, consisting of three hydrogen bonds and nine hydrophobic interactions. The hydrogen bonds were glutamic acid (Glu) 353, arginine (Arg) 394, and histidine (His) 524 for hESR1-LBD, and Glu321, Arg362, and His492 for zEsr1-LBD. However, the interactions with BPA differed between hESR1-LBD and zEsr1-LBD. The interactions of BPA with hESR1-LBD consisted of two hydrogen bonds and nine hydrophobic interactions, while three hydrogen bonds and 10 hydrophobic interactions were observed in the BPA/zEsr1-LBD complex. Notably, two hydrogen bonds (Glu353 and His524 for hESR1-LBD, and Glu321 and His492 for zEsr1-LBD) were shared between both structures. The docked complex between BPFL and hESR1-LBD consisted of one hydrogen bond and five hydrophobic interactions. The hydrogen bond was observed in serine (Ser) 512 residue. The docked complex with BPFL/zEsr1-LBD exhibited one hydrogen bond, two electrostatic interactions, and five hydrophobic interactions. Tetramethyl BPA exhibited the same hydrogen bonds as BPA in hESR1-LBD. Two phenolic hydroxyl groups formed hydrogen bonds with polar residues of Glu353 and His524, respectively. Tetramethyl BPA formed an electrostatic interaction with the methionine (Met) 343 residue. Only one hydrogen bond (His492) was observed in the TMBPA/zEsr1-LBD complex. In addition, 4-phenylphenol formed the same hydrogen bonds and hydrophobic interactions in both receptors. The van der Waals interactions of only three residues differed, and the hydrogen bonds were Glu353 and Arg394 for hESR1-LBD, and Glu321 and Arg362 for zEsr1-LBD.

Before analyzing the molecular dynamic simulation results, each ligand–receptor complex was evaluated for dynamic stability based on the RMSD values of all atoms (Supporting Information, Figures S2 and S3). The RMSD values were between 0.8 and 2.2 Å in ligand/hESR1-LBD complexes, and between 1.6 and 4.5 Å in ligand/zEsr1-LBD complexes. All complexes reached a stable equilibrated state after 10 ns of simulation. The H-bonding occupancies between 10 and 15 ns in the molecular dynamic trajectory analysis were analyzed with Glu353, Arg394, and His524 for hESR1-LBD and Glu321, Arg362, and His492 for zEsr1-LBD (Figure 4). These residues interact with E2 as major hydrogen bonds, as previously described (Asnake et al., 2019; Kalaiarasi et al., 2019). In contrast, TMBPA, E2, BPA, BPFL, and 4-phenylphenol exhibited similar patterns in the docked complexes with hESR1-LBD and zEsr1-LBD. Considering the sum of three H-bonding occupancies, E2/hESR1- and E2/zEsr1-LBD ratios exhibited superiority when compared with those of other chemicals, in the order of E2 > BPA > 4-phenylphenol > TMBPA > BPFL. Similar to E2, BPA formed mainly hydrogen bonds with Glu353 and His524 in hESR1-LBD, and with Glu321 and His492 in zEsr1-LBD. None of the H-bonding occupancies with the residues was observed for BPFL. High occupancy with Glu353 was observed in the TMBPA/hESR1-LBD complex, whereas high occupancy with His492 was observed in the TMBPA/zEsr1-LBD complex. Lastly, 4-phenylphenol exhibited similar H-bonding occupancy trends

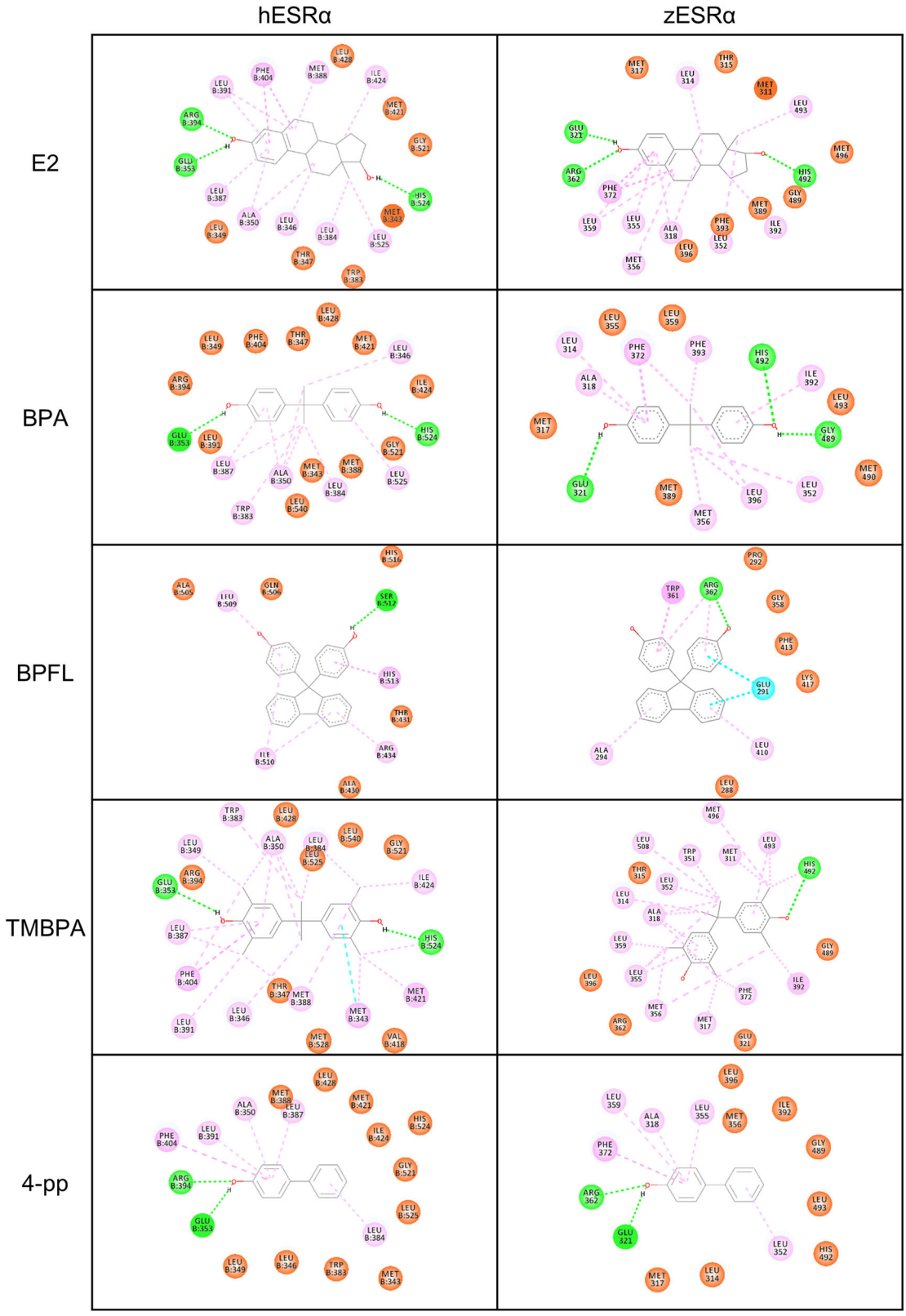

FIGURE 3: Interactions of the ligand–receptor complexes. Two-dimensional docking results for receptor–ligand complex indicating hydrogen bonding (green), hydrophobic interactions (pink), van der Waals interactions (orange), and electrostatic interactions (cyan). hESRα = human estrogen receptor 1; zESRα = zebrafish estrogen receptor 1; E2 = 17β-estradiol; BPA = bisphenol A; BPFL = 4,4′-(9-fluorenyliden)-diphenol; TMBPA = tetramethyl bisphenol A; 4-pp = 4-phenylphenol; PHE = phenylalanine; MET = methionine; LEU = leucine; ILE = isoleucine; GLY = glycine; HIS = histidine; TRP = tryptophan; THR = threonine; ALA = alanine; GLU = glutamic acid; ARG = arginine; GLN = glutamine; SER = serine; PRO = proline; LYS = lysine; VAL = valine.

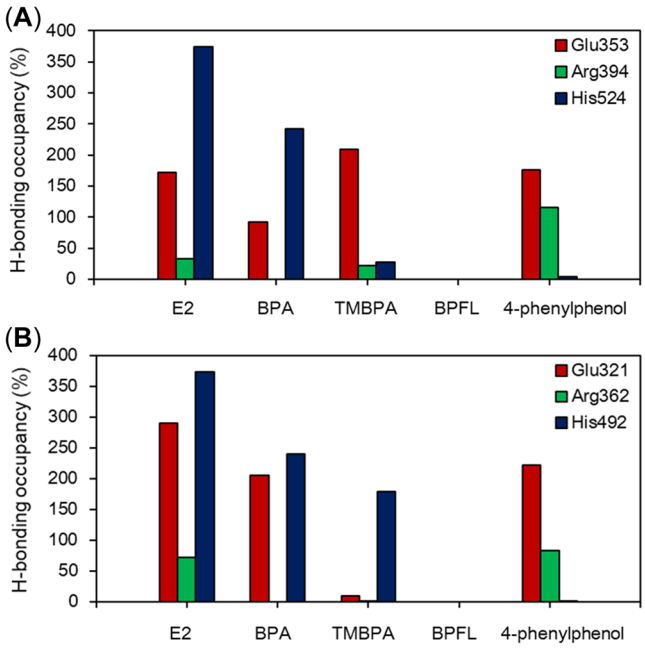

FIGURE 4: Occupancies of hydrogen bonds between ligands and Glu353, Arg394, and His524 residues for ligand-binding domain of human estrogen receptor 1 (hESR1-LBD) (**A**), and between ligands and Glu321, Arg362, and His492 residues for ligand-binding domain of zebrafish estrogen receptor 1 (zEsr1-LBD) (**B**) during molecular dynamic simulations (10–15 ns). E2 = 17β-estradiol; BPA = bisphenol A; BPFL = 4,4′-(9-fluorenyliden)-diphenol; TMBPA = tetramethyl bisphenol A; H = hydrogen; Glu = glutamic acid; Arg = arginine; His = histidine.

in both structures. Glu353 and Arg394 were observed in the hESR1-LBD complex, and Glu321 and Arg362 were observed in the zEsr1-LBD complex.

Previous studies have attempted to determine the major amino acid residues involved in ligand recognition by hESR (Danielian et al., 1993; Ekena et al., 1996; Pakdel & Katzenellenbogen, 1992). The 515–535 residue region has been identified as being responsible for ligand recognition through an alanine-scanning mutagenesis assay (Pakdel & Katzenellenbogen, 1992). Consequently, glycine (Gly) 521, His524, leucine (Leu) 525, and Met528 in helix 11 were identified as the key residues for ligand recognition (Ekena et al., 1996). The His524 residue has recently been recognized as a key player with a critical role in maintaining agonist conformation in hESR1-LBD (Cao et al., 2017; Zhang et al., 2018). Furthermore, the hydrogen bonds with Glu353 and Arg394 residues also have been reported to stabilize ligands embedded in the hESR1 cavity, thereby providing a stable recognition site (Lee & Barron, 2017; Miller, 2015; Mu et al., 2011). In the present study, hydrogen bonds with the Glu353, Arg394, and His524 residues were observed in the E2/hESR1-LBD complex, and the interactions corresponded with previously reported docking results (Cao et al., 2017; Kalaiarasi et al., 2019; Park et al., 2021; Wang et al., 2020). Collectively, the docking results of the present study indicated that BPA and its analogs were located in hESR1-LBD, forming diverse interactions. Bisphenol A, TMBPA, and 4-phenylphenol shared some similarity to E2 in hydrogen-bonding interactions. Bisphenol A and TMBPA formed hydrogen bonds with Glu353 and His524, which were associated with the ligand recognition site. Although 4-polyphenol interacted with two other hydrogen bonds, Gly521, His524, Leu525, and Met528 in H11 formed van der Waals interactions. Two to four hydrogen bonds were observed in the BPA/hESR1-LBD complex: Glu353, Arg394, Gly521, and His524. Glu353 and His524 interactions have been commonly observed in previous studies (Cao et al., 2017; Cavaliere et al., 2020; Delfosse et al., 2012; Jeong et al., 2019; Li et al., 2015). Such differences regarding hydrogen bonds appear to be due to the different calculations and simulation methods used in different docking programs. Cao et al. (2017) docked TMBPA on hESR1-LBD and reported that TMBPA interacted as hydrogen bonds with Glu353 and His524 during molecular dynamic simulations, which is consistent with our results. Several docking simulations have been conducted using zEsr1-LBD and have shown that E2 forms three hydrogen bonds corresponding to those (Glu321, Arg362, and His492) observed in the present study (Asnake et al., 2019; Costache et al., 2005). Mu et al. (2018) reported that BPA forms the same hydrogen bonds as E2, which are similar to those (Glu321 and His492) observed in our results. When considering the key residues for ligand recognition in hESR1-LBD, BPA, TMBPA, and 4-phenylphenol were fitted to zEsr1-LBD and interacted with the residues for ligand recognition. Considering the similarity of their ligand recognition patterns to E2, these interactions were assumed to contribute to agonism. Like hESR1-LBD, the interactions of TMBPA and 4-phenylphenol with zEsr1-LBD indicated that BPA and its analogs exhibited similar binding modes, which may explain how they mimic endogenous hormones that disrupt the zebrafish endocrine system.

Binding energy analysis

To assess the binding affinity of ligand–receptor complexes, binding energies were calculated with molecular docking and molecular dynamic simulations. The binding energies of each chemical are listed in Table 1 and Supporting Information, Table S2. Docking simulations were conducted using CHARMm-based (CDOCKER) and AutoDock Vina, and all chemicals were docked in hESR1-LBD and zEsr1-LBD. In the hESR1-LBD simulations, the E2/hESR1-LBD complex exhibited the lowest binding energy among the test chemicals in both docking programs, whereas the BPFL/hESR1-LBD complex exhibited the highest energy. The binding energies in hESR1-LBD were ranked as follows: E2 > TMBPA ≥ BPA > 4-phenylphenol > BPFL. In the zEsr1-LBD simulations, a similar pattern to hESR1-LBD was observed, with the lowest binding energy occurring for the E2/zEsr1-LBD complex, and the highest occurring for the BPFL/hESR1-LBD complex among the test chemicals. The binding energies were ranked as follows: E2 > BPA ≒ TMBPA > 4-phenylphenol > BPFL. The steady state of 10 and 15 ns molecular dynamic simulations revealed the order TMBPA > E2 > BPA > 4-phenylphenol > BPFL, in which TMBPA revealed a lower binding free energy than E2 in the hESR1. For the zEsr1 complexes, the binding free energies were ranked as follows: E2 > BPA > TMBPA > 4-phenylphenol > BPFL. The binding energies differed

TABLE 1: Binding energies of molecular docking and molecular dynamic (MD) simulations

	Molecular docking				MD simulation (10–15 ns)	
	Discovery studio		AutoDock Vina		MMPBSA	
Docking program	Cdocker interaction energy (kcal/mol)		Binding free energy (kcal/mol)		Binding free energy, ΔG_{bind} (kcal/mol)	
Ligands/receptors	hESR1-LBD	zEsr1-LBD	hESR1-LBD	zEsr1-LBD	hESR1-LBD	zEsr1-LBD
Estradiol	−53.2 ± 0.00	−49.8 ± 0.00	−11.1 ± 0.00	−10.7 ± 0.00	−18.8 ± 2.76	−18.6 ± 2.55
Bisphenol A	−38.2 ± 0.00	−38.0 ± 0.00	−8.13 ± 0.10	−8.36 ± 0.04	−17.8 ± 3.09	−17.3 ± 3.17
Bisphenol FL	−14.5 ± 0.00	−12.3 ± 0.00	−7.26 ± 0.05	−7.02 ± 0.12	−7.23 ± 2.61	−3.48 ± 4.67
Tetramethyl bisphenol A	−41.8 ± 0.00	−42.3 ± 0.00	−8.10 ± 0.08	−8.13 ± 0.12	−22.9 ± 3.46	−16.8 ± 3.79
4-Phenylphenol	−30.4 ± 0.00	−29.7 ± 0.00	−7.80 ± 0.00	−7.60 ± 0.00	−13.1 ± 2.64	−12.3 ± 3.53

MMPBSA = molecular mechanics Poisson-Boltzmann surface area; hESR1 = human estrogen receptor; zEsr1 = zebrafish estrogen receptor; LBD = ligand-binding domain.

according to the chemicals used. The docking programs exhibited similar binding energy patterns and corresponded with the results of previous studies (Cavaliere et al., 2020; Jeong et al., 2019; Makarova et al., 2016). Bisphenol A and its analogs were docked, and their binding energies with hESR1-LBD were compared. Bisphenol A and its substitutes exhibited higher binding energy than E2/hESR1-LBD. Cavaliere et al. (2020) reported the same binding energy pattern for hESR1-LBD (E2 > TMBPA > BPA). Makarova et al. (2016) simulated E2 and BPA docking on simulated hESR1-LBD and zEsr1-LBD using AutoDock, and E2 exhibited lower binding energy than BPA. The binding energies were −11.5 and −7.73 kcal/mol for hESR1-LBD and −11.0 and −7.56 kcal/mol for zEsr1-LBD, respectively. The E2/hESR1-LBD manifested lower binding free energy than BPA/hESR1-LBD using MM/PBSA and molecular mechanics generalized Born surface area (MMGBSA) methods (Li et al., 2015, 2018). Notably, the TMBPA/hESR1-LBD displayed a lower binding free energy than the E2 complex during molecular dynamic simulation, which is not consistent with docking calculation. This can be explained by van der Waals and hydrophobic interactions (Supporting Information, Table S2). The calculated van der Waals (ΔG_{vdw}) and nonpolar solvation (ΔG_{SA}) of TMBPA interactions revealed the lowest energies among the complexes. Previous reports have shown that the energies of the apolar ($\Delta G_{vdw} + \Delta G_{SA}$) and electrostatic ($\Delta G_{elec}$) components significantly contribute to the estimate of binding free energy in MM/PBSA (Tan et al., 2006; Verma et al., 2016). Therefore, TMBPA resulted in a lower binding free energy than E2 in hESR1-LBD, whereas, the TMBPA/zEsr1-LBD complex exhibited a higher binding free energy than E2 due to the electrostatic interactions. The electrostatic energy was markedly lower in the zEsr1-LBD than in the hESR1-LBD complex. Collectively, each complex showed different binding energies and the patterns were confirmed by docking programs and molecular dynamic simulation.

Comparison of in silico and in vitro experiments

The in silico and in vitro results were compared to evaluate their correlation, as shown in Figure 5. The human estrogenic activities of BPA and its analogs were evaluated by conducting an in vitro reporter gene assay (Figure 5A). The maximum concentration of each chemical with a nontoxic effect on the yeast strain was selected based on the results of the cytotoxicity test. 17β-Estradiol was used as the reference chemical and exhibited a dose–response depending on the concentration. Bisphenol A and its analogs also exhibited dose–response curves, excluding BPFL. The median effect concentration (EC50) values for E2, BPA, TMBPA, and 4-phenylphenol were 1.25, 14,657, 10,216, and 4,594 nM, respectively. The maximal induction rates of BPA and its analogs were ranked in the following order: BPA > TMBPA > 4-phenylphenol > BPFL. Even though the EC50 value of BPA was higher than those of TMBPA and 4-phenylphenol, BPA exhibited the highest induction rate (90.7%) at the maximum concentration except E2. Similar results have been reported in other reporter gene studies (Bergmann et al., 2020; Cao et al., 2017; Pelch et al., 2019; Sun et al., 2008). Tetramethyl bisphenol A exhibited lower EC20 and EC50 values than BPA; however, the estrogenic activity at the maximum concentration of BPA was higher than that of TMBPA (Cao et al., 2017; Pelch et al., 2019). Two studies reported that the EC50 value of 4-phenylphenol is lower than that of BPA (Bergmann et al., 2020; Sun et al., 2008). Conversely, Li et al. (2010) reported a higher EC50 value for 4-phenylphenol than for BPA. Such differences can be attributed to the different reporter systems, and the different host cells and their cytotoxicity and ligand-binding affinity. Our in vitro assay showed that BPFL and 4-phenylphenol appeared to be more cytotoxic (>10 μM) than BPA and TMBPA (>100 μM). Keminer et al. (2020) recently conducted a ligand-binding assay using a commercially available fluorescence polarization-based technique. Bisphenol A inhibited the fluorescent ligand by 61.2%, followed by 4-phenylphenol (53.1%), TMBPA (24.2%), and BPFL (−2.06%). Therefore, it seems that BPA exhibited the highest estrogenic activity compared to BPA analogs, despite the lower EC50 values of TMBPA and 4-phenylphenol.

In the present study, zebrafish estrogenic activities of BPA and its analogs were evaluated using an in vitro reporter gene assay (Figure 5B). The maximum concentrations of compounds with a nontoxic effect on the cells were selected based on the results of the cytotoxicity test. Bisphenol A, E2, and 4-phenylphenol exhibited dose–response curves. The EC50 values for E2, BPA, and 4-phenylphenol were 0.09, 583, and 9,787 nM, respectively. Tetramethyl bisphenol A induced weak estrogenic activity (16.6% as the maximal induction), which was different from the estrogenic activity in the human in vitro assay.

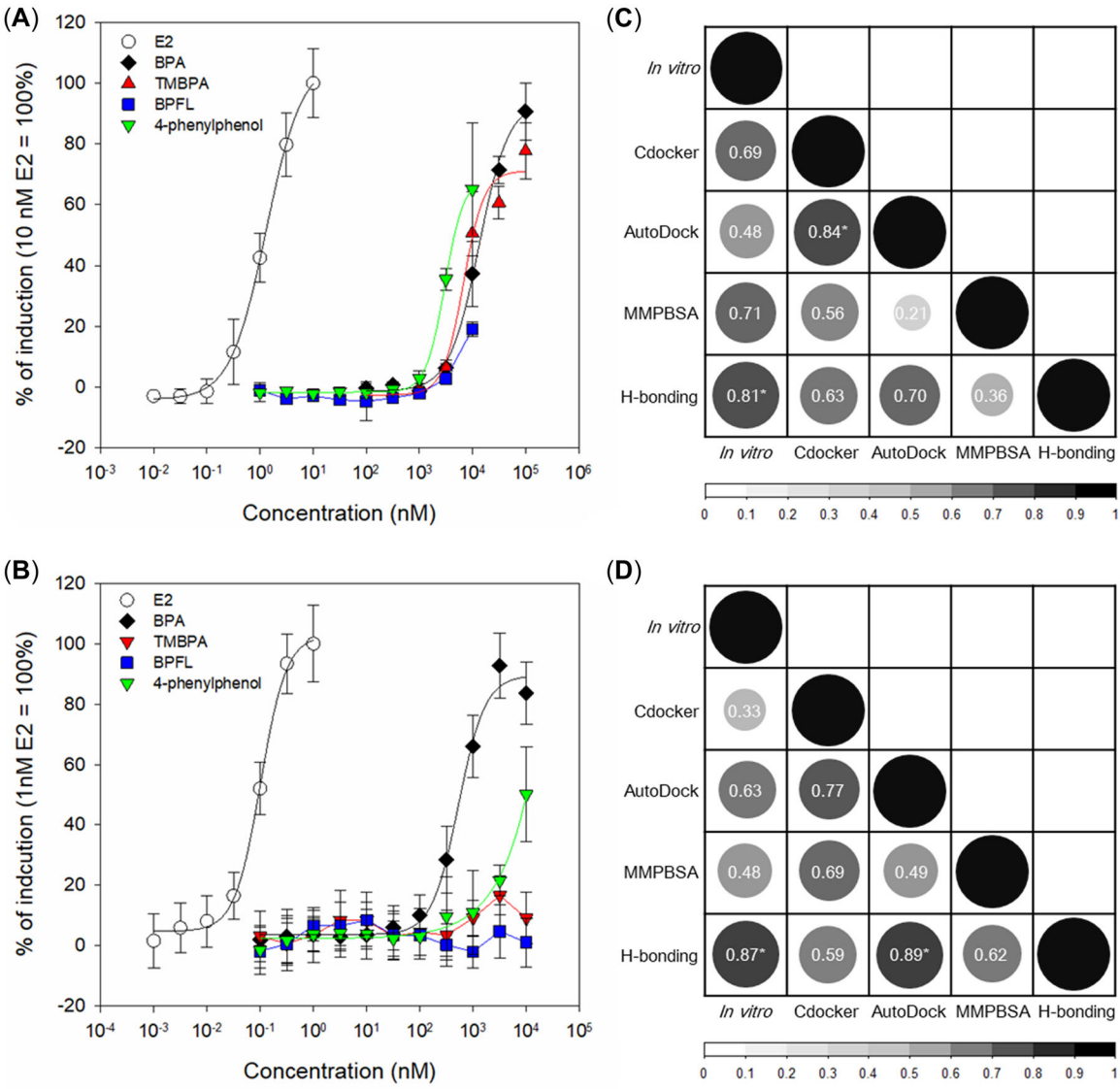

FIGURE 5: Comparisons of in silico and in vitro assays. (**A**, **B**) In vitro assays for estrogenic activity in human estrogen receptor 1 (hESR1), (**A**) and zebrafish estrogen receptor 1 (zEsr1) (**B**), respectively. The induction value at the maximum concentration of 17β-estradiol (E2; 10 nM for hESR1 and 1 nM for zEsr1) was set to 100%. (**C**, **D**) Correlation matrix plot. Pearson correlation coefficient (r) between in silico and in vitro results in hESR1 (**C**) and zEsr1 (**D**). Values are indicated as r^2. The color intensity and the size of rounds are proportional to r^2. Asterisks indicate significant correlation ($p < 0.05$). The applied in vitro data are the maximal induction ratios of each chemical. The binding energies computed by Discovery studio, Autodock Vina, and MMBPSA, were applied in the analysis. The hydrogen bonding (H-bonding) data are the sum of H-bonding occupancies of each complex during molecular dynamics simulations. E2 = 17β-estradiol; BPA = bisphenol A; BPFL = 4,4′-(9-fluorenyliden)-diphenol; TMBPA = tetramethyl bisphenol A; MMPBSA = molecular mechanics Poisson-Boltzmann surface area.

The maximal induction rates of BPA and its analogs were ranked in the following order: BPA > 4-phenylphenol > TMBPA > BPFL. Each chemical exhibited different estrogenic activities in this reporter assay. None of the previous studies showed estrogenic activity with BPFL, TMBPA, and 4-phenylphenol in zEsr1, while estrogenic activity has been observed with BPA (Cosnefroy et al., 2012; Le Fol et al., 2017; Pinto et al., 2019).

Lastly, the in silico and in vitro results were compared to evaluate their correlation. All the factors computed by in silico experiments revealed moderate or high correlations with in vitro results (Figure 5C,D). High correlation was observed between Cdocker and AutoDock Vina ($r^2 = 0.84$ for hESR1 and $r^2 = 0.77$ for zEsr1). Notably, the hydrogen-bonding occupancy exhibited high correlations with in vitro results ($r^2 = 0.81$ for hESR1 and $r^2 = 0.87$ for zEsr1). The results indicate that hydrogen bond interactions with certain residues have pivotal roles for ligand recognition and its activation. The interaction of modelled zEsr1 with TMBPA resulted in relatively poor correlations, especially compared to the correlations of hESR1, although the TMBPA complex in both receptors revealed comparable binding free energies compared with BPA and 4-phenylphenol interactions. The in vitro results of weak estrogenic activity of TMBPA can be explained by the MM/PBSA calculated lowest energies in van der Waals and nonpolar solvation among the complexes. In addition, TMBPA formed a hydrogen bond with the His492 residue in the docking programs and the molecular dynamic simulation. The

residue is considered to be critical in ligand recognition and maintenance of the agonist conformation (Babu et al., 2012; Shehadi et al., 2020). The results are inconsistent with previous reports and the present in vitro result. However, the inconsistency can be elucidated with other residues such as Glu353 and Arg394 in hESR1-LBD. Considering the reported functions of Glu353 and Arg394 residues, and the results in H-bonding occupancy, we speculate that even though the His492 residue plays critical roles, other residues such as Glu321 and Arg362 are necessary as well for the complex stabilization and its activation. For these reasons, it seems TMBPA induced different estrogenic activities on human ESRα and zebrafish ESRα. Overall, the present study found good agreement between the results from in silico and in vitro approaches using the hESR1-LBD and zEsr1-LBD structures. The structures can be useful for screening EDCs that have potential estrogenic disruptive activities. However, the current approach also reveals some limitations that must be considered for better prediction. A relatively smaller scale of the test and limited sampling conditions in pose prediction and approximated scoring might cause poor correlation of results with experimental in vitro data. Moreover, this structure only predicts estrogenic activity between the LBD and a ligand, therefore it is impossible to predict estrogenic activities related to other mechanisms or domains. In light of these limitations, more studies with diverse ligands are necessary to draw a solid conclusion, and detailed analyses of binding energy and interaction modes are required to predict estrogenic activity. Our future study will be the assessment of other EDCs and investigations to reveal other mechanisms inducing (anti)estrogenic activities.

CONCLUSION

Because the 3D structure of zebrafish ESRα is not available, a homology-based 3D model of zEsr1-LBD was constructed and validated using PROCHECK, ERRAT, ProSA, and Verify-3D tools, which have suitable models to represent the 3D structure. After validation, BPA and its analogs were docked on zEsr1- and hESR1-LBDs. Molecular dynamic simulation was conducted to understand the dynamic behavior of each complex and to complement the limitations of molecular docking. Bisphenol A and some of its analogs were bound with an orientation similar to that of E2 in both models. In addition, the in vitro results demonstrated that the in silico and in vitro results were in good agreement with moderate to high correlations. Therefore, the combined in silico and in vitro approaches provide useful prediction models for identifying EDCs by taking into account the difference between the two species.

Supporting Information—The Supporting information is available on the Wiley Online Library at https://doi.org/10.1002/etc.5433.

Acknowledgments—The present study was supported by the National Research Council of Science & Technology grant by the Korea Government (No. CAP-17-01-KIST Europe) and the Korea Institute of Science and Technology Europe Basic Research Program (Project No. 12201).

Disclaimer—The authors declare that they have no known competing financial interests or personal relationships that could have appeared to influence the work reported in the present study.

Author Contributions Statement—**Chang Gyun Park**: Writing—original draft; Data curation; Formal analysis; Writing—review and editing. **Nancy Singh**: Data curation; Formal analysis; Resources; Methodology; Writing—review and editing. **Chang Seon Ryu**: Writing—original draft; Data curation; Formal analysis; Writing—review and editing. **Ju Yong Yoon**: Formal analysis; Methodology; Writing—review and editing. **Maranda Esterhuizen**: Conceptualization; Investigation; Methodology; Writing—review and editing. **Young Jun Kim**: Writing—original draft; Conceptualization; Funding acquisition; Investigation; Methodology; Writing—review and editing. All persons who meet authorship criteria are listed as authors, and all authors certify that they have participated sufficiently in the present study to take public responsibility for the content, including participation in the concept, design, analysis, writing, or revision of the manuscript. Furthermore, each author certifies that this material or similar material has not been and will not be submitted to or published in any other publication before its appearance in *Environmental Toxicology and Chemistry*. All authors contributed equally to this study. The final version of the manuscript has been approved by all authors.

Data Availability Statement—The authors confirm that the data supporting the findings of the present study are available within the article and its Supporting Information. All data of this study are available from https://drive.google.com/drive/folders/1B3LnXhZQDRkgXs6YykEcduuO0j9IMWQw?usp=sharing.

REFERENCES

Altschul, S. F., Gish, W., Miller, W., Myers, E. W., & Lipman, D. J. (1990). Basic local alignment search tool. *Journal of Molecular Biology*, *215*(3), 403–410.

Asnake, S., Modig, C., & Olsson, P.-E. (2019). Species differences in ligand interaction and activation of estrogen receptors in fish and human. *The Journal of Steroid Biochemistry and Molecular Biology*, *195*, 105450.

Babu, S., Vellore, N. A., Kasibotla, A. V., Dwayne, H. J., Stubblefield, M. A., & Uppu, R. M. (2012). Molecular docking of bisphenol A and its nitrated and chlorinated metabolites onto human estrogen-related receptor-gamma. *Biochemical and Biophysical Research Communications*, *426*(2), 215–220.

Banaderakhshan, R., Kemp, P., Breul, L., Steinbichl, P., Hartmann, C., & Fürhacker, M. (2022). Bisphenol A and its alternatives in Austrian thermal paper receipts, and the migration from reusable plastic drinking bottles into water and artificial saliva using UHPLC-MS/MS. *Chemosphere*, *286*, 131842.

Bardet, P. L., Horard, B., Robinson-Rechavi, M., Laudet, V., & Vanacker, J. M. (2002). Characterization of oestrogen receptors in zebrafish (*Danio rerio*). *Journal of Molecular Endocrinology*, *28*(3), 153–163.

Barkhem, T., Nilsson, S., & Gustafsson, J. A. (2004). Molecular mechanisms, physiological consequences and pharmacological implications of estrogen receptor action. *American Journal of PharmacoGenomics*, *4*(1), 19–28.

Barros, R. P., & Gustafsson, J. (2011). Estrogen receptors and the metabolic network. *Cell Metabolism*, *14*(3), 289–299.

Bergmann, A. J., Simon, E., Schifferli, A., Schönborn, A., & Vermeirssen, E. L. M. (2020). Estrogenic activity of food contact materials—Evaluation of 20 chemicals using a yeast estrogen screen on HPTLC or 96-well plates. *Analytical and Bioanalytical Chemistry*, *412*(19), 4527–4536.

Cao, H., Wang, F., Liang, Y., Wang, H., Zhang, A., & Song, M. (2017). Experimental and computational insights on the recognition mechanism between the estrogen receptor α with bisphenol compounds. *Archives of Toxicology*, *91*(12), 3897–3912.

Cavaliere, F., Lorenzetti, S., & Cozzini, P. (2020). Molecular modelling methods in food safety: Bisphenols as case study. *Food and Chemical Toxicology*, *137*, 111116.

Chafi, S., Azzouz, A., & Ballesteros, E. (2022). Occurrence and distribution of endocrine disrupting chemicals and pharmaceuticals in the river Bouregreg (Rabat, Morocco). *Chemosphere*, *287*, 132202.

Chang, C., & Swaan, P. W. (2006). Computational approaches to modeling drug transporters. *European Journal of Pharmaceutical Sciences*, *27*(5), 411–424.

Cheatham, T. E., III, Miller, J. L., Fox, T., Darden, T. A., & Kollman, P. A. (1995). Molecular dynamics simulations on solvated biomolecular systems: The particle mesh Ewald method leads to stable trajectories of DNA, RNA, and Proteins. *Journal of the American Chemical Society*, *117*(14), 4193–4194.

Chen, D., Kannan, K., Tan, H., Zheng, Z., Feng, Y.-L., Wu, Y., & Widelka, M. (2016). Bisphenol analogues other than BPA: Environmental occurrence, human exposure, and toxicity—A review. *Environmental Science & Technology*, *50*(11), 5438–5453.

Colovos, C., & Yeates, T. O. (1993). Verification of protein structures: Patterns of nonbonded atomic interactions. *Protein Science*, *2*(9), 1511–1519.

Cosnefroy, A., Brion, F., Maillot-Maréchal, E., Porcher, J. M., Pakdel, F., Balaguer, P., & Aït-Aïssa, S. (2012). Selective activation of zebrafish estrogen receptor subtypes by chemicals by using stable reporter gene assay developed in a zebrafish liver cell line. *Toxicological Sciences*, *125*(2), 439–449.

Costache, A. D., Pullela, P. K., Kasha, P., Tomasiewicz, H., & Sem, D. S. (2005). Homology-modeled ligand-binding domains of zebrafish estrogen receptors alpha, beta1, and beta2: From in silico to in vivo studies of estrogen interactions in *Danio rerio* as a model system. *Molecular Endocrinology*, *19*(12), 2979–2990.

Dahlman-Wright, K., Cavailles, V., Fuqua, S. A., Jordan, V. C., Katzenellenbogen, J. A., Korach, K. S., Maggi, A., Muramatsu, M., Parker, M. G., & Gustafsson, J. A. (2006). International union of pharmacology. LXIV. Estrogen receptors. *Pharmacological Reviews*, *58*(4), 773–781.

Danielian, P. S., White, R., Hoare, S. A., Fawell, S. E., & Parker, M. G. (1993). Identification of residues in the estrogen receptor that confer differential sensitivity to estrogen and hydroxytamoxifen. *Molecular Endocrinology*, *7*(2), 232–240.

Delfosse, V., Grimaldi, M., Pons, J. L., Boulahtouf, A., le Maire, A., Cavailles, V., Labesse, G., Bourguet, W., & Balaguer, P. (2012). Structural and mechanistic insights into bisphenols action provide guidelines for risk assessment and discovery of bisphenol A substitutes. *Proceedings of the National Academy of Sciences of the United States of America*, *109*(37), 14930–14935.

Ekena, K., Weis, K. E., Katzenellenbogen, J. A., & Katzenellenbogen, B. S. (1996). Identification of amino acids in the hormone binding domain of the human estrogen receptor important in estrogen binding. *Journal of Biological Chemistry*, *271*(33), 20053–20059.

Elegheert, J., Behiels, E., Bishop, B., Scott, S., Woolley, R. E., Griffiths, S. C., Byrne, E. F. X., Chang, V. T., Stuart, D. I., Jones, E. Y., Siebold, C., & Aricescu, A. R. (2018). Lentiviral transduction of mammalian cells for fast, scalable and high-level production of soluble and membrane proteins. *Nature Protocols*, *13*(12), 2991–3017.

Feller, S. E., Zhang, Y., Pastor, R. W., & Brooks, B. R. (1995). Constant pressure molecular dynamics simulation: The Langevin piston method. *The Journal of Chemical Physics*, *103*(11), 4613–4621.

Geens, T., Aerts, D., Berthot, C., Bourguignon, J. P., Goeyens, L., Lecomte, P., Maghuin-Rogister, G., Pironnet, A. M., Pussemier, L., Scippo, M. L., Van Loco, J., & Covaci, A. (2012). A review of dietary and non-dietary exposure to bisphenol-A. *Food and Chemical Toxicology*, *50*(10), 3725–3740.

Hawkins, M. B., Thornton, J. W., Crews, D., Skipper, J. K., Dotte, A., & Thomas, P. (2000). Identification of a third distinct estrogen receptor and reclassification of estrogen receptors in teleosts. *Proceedings of the National Academy of Sciences of the United States of America*, *97*(20), 10751.

Heldring, N., Pike, A., Andersson, S., Matthews, J., Cheng, G., Hartman, J., Tujague, M., Ström, A., Treuter, E., Warner, M., & Gustafsson, J. A. (2007). Estrogen receptors: How do they signal and what are their targets. *Physiological Reviews*, *87*(3), 905–931.

Hewitt, S. C., Winuthayanon, W., & Korach, K. S. (2016). What's new in estrogen receptor action in the female reproductive tract. *Journal of Molecular Endocrinology*, *56*(2), R55–71.

Hou, T., Wang, J., Li, Y., & Wang, W. (2011). Assessing the performance of the MM/PBSA and MM/GBSA methods. 1. The accuracy of binding free energy calculations based on molecular dynamics simulations. *Journal of Chemical Information and Modeling*, *51*(1), 69–82.

Humphrey, W., Dalke, A., & Schulten, K. (1996). VMD: Visual molecular dynamics. *Journal of Molecular Graphics*, *14*(1), 33–38.

Jeong, J., Kim, H., & Choi, J. (2019). In silico molecular docking and In vivo validation with *Caenorhabditis elegans* to discover molecular initiating events in adverse outcome pathway framework: Case study on endocrine-disrupting chemicals with estrogen and androgen receptors. *International Journal of Molecular Sciences*, *20*(5), 1209.

Jin, H., & Zhu, L. (2016). Occurrence and partitioning of bisphenol analogues in water and sediment from Liaohe River Basin and Taihu Lake, China. *Water Research*, *103*, 343–351.

Jin, M., Dang, J., Paudel, Y. N., Wang, X., Wang, B., Wang, L., Li, P., Sun, C., & Liu, K. (2021). The possible hormetic effects of fluorene-9-bisphenol on regulating hypothalamic-pituitary-thyroid axis in zebrafish. *Science of the Total Environment*, *776*, 145963.

Jorgensen, W. L., Chandrasekhar, J., Madura, J. D., Impey, R. W., & Klein, M. L. (1983). Comparison of simple potential functions for simulating liquid water. *The Journal of Chemical Physics*, *79*(2), 926–935.

Kalé, L., Skeel, R., Bhandarkar, M., Brunner, R., Gursoy, A., Krawetz, N., Phillips, J., Shinozaki, A., Varadarajan, K., & Schulten, K. (1999). NAMD2: Greater scalability for parallel molecular dynamics. *Journal of Computational Physics*, *151*(1), 283–312.

Kalaiarasi, C., Manjula, S., & Kumaradhas, P. (2019). Combined quantum mechanics/molecular mechanics (QM/MM) methods to understand the charge density distribution of estrogens in the active site of estrogen receptors. *RSC Advances*, *9*(69), 40758–40771.

Kang, J. H., Asai, D., & Katayama, Y. (2007). Bisphenol A in the aquatic environment and its endocrine-disruptive effects on aquatic organisms. *Critical Reviews in Toxicology*, *37*(7), 607–625.

Kari, G., Rodeck, U., & Dicker, A. P. (2007). Zebrafish: An emerging model system for human disease and drug discovery. *Clinical Pharmacology & Therapeutics*, *82*(1), 70–80.

Keminer, O., Teigeler, M., Kohler, M., Wenzel, A., Arning, J., Kaßner, F., Windshügel, B., & Eilebrecht, E. (2020). A tiered high-throughput screening approach for evaluation of estrogen and androgen receptor modulation by environmentally relevant bisphenol A substitutes. *Science of the Total Environment*, *717*, 134743.

Khalid, A. B., & Krum, S. A. (2016). Estrogen receptors alpha and beta in bone. *Bone*, *87*, 130–135.

Kovats, S. (2015). Estrogen receptors regulate innate immune cells and signaling pathways. *Cellular Immunology*, *294*(2), 63–69.

Kumar, R., Zakharov, M. N., Khan, S. H., Miki, R., Jang, H., Toraldo, G., Singh, R., Bhasin, S., & Jasuja, R. (2011). The dynamic structure of the estrogen receptor. *Journal of Amino Acids*, *2011*, 812540.

Lüthy, R., Bowie, J. U., & Eisenberg, D. (1992). Assessment of protein models with three-dimensional profiles. *Nature*, *356*(6364), 83–85.

Le Fol, V., Ait-Aissa, S., Sonavane, M., Porcher, J.-M., Balaguer, P., Cravedi, J.-P., Zalko, D., & Brion, F. (2017). In vitro and in vivo estrogenic activity of BPA, BPF and BPS in zebrafish-specific assays. *Ecotoxicology and Environmental Safety*, *142*, 150–156.

Lee, S., & Barron, M. G. (2017). Structure-based understanding of binding affinity and mode of estrogen receptor α agonists and antagonists. *PLoS One*, *12*(1), e0169607.

Li, L., Wang, Q., Zhang, Y., Niu, Y., Yao, X., & Liu, H. (2015). The molecular mechanism of bisphenol A (BPA) as an endocrine disruptor by interacting with nuclear receptors: Insights from molecular dynamics (MD) simulations. *PLoS One*, *10*(3), e0120330.

Li, J., Ma, M., & Wang, Z. (2010). In vitro profiling of endocrine disrupting effects of phenols. *Toxicology In Vitro*, *24*(1), 201–207.

Li, Y., Perera, L., Coons, L. A., Burns, K. A., Tyler Ramsey, J., Pelch, K. E., Houtman, R., van Beuningen, R., Teng, C. T., & Korach, K. S. (2018). Differential in vitro biological action, coregulator interactions, and

molecular dynamic analysis of bisphenol A (BPA), BPAF, and BPS ligand-ERα complexes. *Environmental Health Perspectives*, *126*(1), 017012.

MacRae, C. A., & Peterson, R. T. (2015). Zebrafish as tools for drug discovery. *Nature Reviews Drug Discovery*, *14*(10), 721–731.

Makarova, K., Siudem, P., Zawada, K., & Kurkowiak, J. (2016). Screening of toxic effects of bisphenol A and products of its degradation: Zebrafish (*Danio rerio*) embryo test and molecular docking. *Zebrafish*, *13*(5), 466–474.

Martí-Renom, M. A., Stuart, A. C., Fiser, A., Sánchez, R., Melo, F., & Sali, A. (2000). Comparative protein structure modeling of genes and genomes. *Annual Review of Biophysics and Biomolecular Structure*, *29*, 291–325.

Mathieu-Denoncourt, J., Wallace, S. J., de Solla, S. R., & Langlois, V. S. (2015). Plasticizer endocrine disruption: Highlighting developmental and reproductive effects in mammals and non-mammalian aquatic species. *General and Comparative Endocrinology*, *219*, 74–88.

Menuet, A., Pellegrini, E., Anglade, I., Blaise, O., Laudet, V., Kah, O., & Pakdel, F. (2002). Molecular characterization of three estrogen receptor forms in zebrafish: Binding characteristics, transactivation properties, and tissue distributions. *Biology of Reproduction*, *66*(6), 1881–1892.

Mi, P., Zhang, Q.-P., Zhang, S.-H., Wang, C., Zhang, S.-Z., Fang, Y.-C., Gao, J.-Z., Feng, D.-F., Chen, D.-Y., & Feng, X.-Z. (2019). The effects of fluorene-9-bisphenol on female zebrafish (*Danio rerio*) reproductive and exploratory behaviors. *Chemosphere*, *228*, 398–411.

Miller, C. (2015). *A brief on the structure and function of estrogen receptor alpha (BCMB8010 Enzyme Project)*. https://doi.org/10.13140/RG.2.1.4082.5044

Mills, L. J., & Chichester, C. (2005). Review of evidence: Are endocrine-disrupting chemicals in the aquatic environment impacting fish populations? *Science of the Total Environment*, *343*(1–3), 1–34.

Montes-Grajales, D., & Olivero-Verbel, J. (2013). Computer-aided identification of novel protein targets of bisphenol A. *Toxicology Letters*, *222*(3), 312–320.

Morris, A. L., MacArthur, M. W., Hutchinson, E. G., & Thornton, J. M. (1992). Stereochemical quality of protein structure coordinates. *Proteins*, *12*(4), 345–364.

Mu, X., Huang, Y., Li, X., Lei, Y., Teng, M., Li, X., Wang, C., & Li, Y. (2018). Developmental effects and estrogenicity of bisphenol A alternatives in a zebrafish embryo model. *Environmental Science & Technology*, *52*(5), 3222–3231.

Mu, Y., Peng, S., Zhang, A., & Wang, L. (2011). Role of pocket flexibility in the modulation of estrogen receptor alpha by key residue arginine 394. *Environmental Toxicology and Chemistry*, *30*(2), 330–336.

Otero, J. M., Papadakis, M. A., Udatha, D. B., Nielsen, J., & Panagiotou, G. (2010). Yeast biological networks unfold the interplay of antioxidants, genome and phenotype, and reveal a novel regulator of the oxidative stress response. *PLoS One*, *5*(10), e13606.

Pakdel, F., & Katzenellenbogen, B. S. (1992). Human estrogen receptor mutants with altered estrogen and antiestrogen ligand discrimination. *Journal of Biological Chemistry*, *267*(5), 3429–3437.

Park, C. G., Jung, K. C., Kim, D.-H., & Kim, Y. J. (2021). Monohaloacetonitriles induce cytotoxicity and exhibit different mode of action in endocrine disruption. *Science of the Total Environment*, *761*, 143316.

Paterni, I., Granchi, C., Katzenellenbogen, J. A., & Minutolo, F. (2014). Estrogen receptors alpha (ERα) and beta (ERβ): Subtype-selective ligands and clinical potential. *Steroids*, *90*, 13–29.

Pelch, K. E., Li, Y., Perera, L., Thayer, K. A., & Korach, K. S. (2019). Characterization of estrogenic and androgenic activities for bisphenol A-like chemicals (BPs): In vitro estrogen and androgen receptors transcriptional activation, gene regulation, and binding profiles. *Toxicological Sciences*, *172*(1), 23–37.

Phillips, C., Roberts, L. R., Schade, M., Bazin, R., Bent, A., Davies, N. L., Moore, R., Pannifer, A. D., Pickford, A. R., Prior, S. H., Read, C. M., Scott, A., Brown, D. G., Xu, B., & Irving, S. L. (2011). Design and structure of stapled peptides binding to estrogen receptors. *Journal of the American Chemical Society*, *133*(25), 9696–9699.

Phillips, J. C., Braun, R., Wang, W., Gumbart, J., Tajkhorshid, E., Villa, E., Chipot, C., Skeel, R. D., Kalé, L., & Schulten, K. (2005). Scalable molecular dynamics with NAMD. *Journal of Computational Chemistry*, *26*(16), 1781–1802.

Pinto, C., Hao, R., Grimaldi, M., Thrikawala, S., Boulahtouf, A., Aït-Aïssa, S., Brion, F., Gustafsson, J., Balaguer, P., & Bondesson, M. (2019). Differential activity of BPA, BPAF and BPC on zebrafish estrogen receptors in vitro and in vivo. *Toxicology and Applied Pharmacology*, *380*, 114709.

Procter, J. B., Carstairs, G. M., Soares, B., Mourão, K., Ofoegbu, T. C., Barton, D., Lui, L., Menard, A., Sherstnev, N., Roldan-Martinez, D., Duce, S., Martin, D. M. A., & Barton, G. J. (2021). Alignment of biological sequences with Jalview. *Methods in Molecular Biology*, *2231*, 203–224.

Rochester, J. R. (2013). Bisphenol A and human health: A review of the literature. *Reproductive Toxicology*, *42*, 132–155.

Rosenmai, A. K., Dybdahl, M., Pedersen, M., Alice van Vugt-Lussenburg, B. M., Wedebye, E. B., Taxvig, C., & Vinggaard, A. M. (2014). Are structural analogues to bisphenol A safe alternatives? *Toxicological Sciences*, *139*(1), 35–47.

Shamsara, J. (2019). Homology modeling of 5-alpha-reductase 2 using available experimental data. *Interdisciplinary Sciences, Computational Life Sciences*, *11*(3), 475–484.

Shehadi, I. A., Rashdan, H. R. M., & Abdelmonsef, A. H. (2020). Homology modeling and virtual screening studies of antigen MLAA-42 protein: Identification of novel drug candidates against leukemia—An in silico approach. *Computational and Mathematical Methods in Medicine*, *2020*, 8196147.

Shen, M., & Shi, H. (2015). Sex hormones and their receptors regulate liver energy homeostasis. *International Journal of Endocrinology*, *2015*, 294278.

Shen, M. Y., & Sali, A. (2006). Statistical potential for assessment and prediction of protein structures. *Protein Science*, *15*(11), 2507–2524.

Sliwoski, G., Kothiwale, S., Meiler, J., & Lowe, E. W., Jr. (2013). Computational methods in drug discovery. *Pharmacological Reviews*, *66*(1), 334–395.

Sun, H., Xu, X.-L., Qu, J.-H., Hong, X., Wang, Y.-B., Xu, L.-C., & Wang, X.-R. (2008). 4-Alkylphenols and related chemicals show similar effect on the function of human and rat estrogen receptor α in reporter gene assay. *Chemosphere*, *71*(3), 582–588.

Tan, J. J., Chen, W. Z., & Wang, C. X. (2006). Investigating interactions between HIV-1 gp41 and inhibitors by molecular dynamics simulation and MM–PBSA/GBSA calculations. *Journal of Molecular Structure*, *766*(2), 77–82.

Trott, O., & Olson, A. J. (2010). AutoDock Vina: Improving the speed and accuracy of docking with a new scoring function, efficient optimization, and multithreading. *Journal of Computational Chemistry*, *31*(2), 455–461.

Usman, A., & Ahmad, M. (2016). From BPA to its analogues: Is it a safe journey? *Chemosphere*, *158*, 131–142.

Venclovas, C. (2003). Comparative modeling in CASP5: Progress is evident, but alignment errors remain a significant hindrance. *Proteins*, *53*, 380–388.

Verma, S., Grover, S., Tyagi, C., Goyal, S., Jamal, S., Singh, A., & Grover, A. (2016). Hydrophobic interactions are a key to MDM2 inhibition by polyphenols as revealed by molecular dynamics simulations and MM/PBSA free energy calculations. *PLoS One*, *11*(2), e0149014.

Wang, T., Wang, Y., Zhuang, X., Luan, F., Zhao, C., & Cordeiro, M. N. D. S. (2020). Interaction of coumarin phytoestrogens with ERα and ERβ: A molecular dynamics simulation study. *Molecules*, *25*(5), 1165.

Webb, B., & Sali, A. (2016). Comparative protein structure modeling using MODELLER. *Current Protocols in Bioinformatics*, *54*(7), 5.6.1–5.6.3.

Wiederstein, M., & Sippl, M. J. (2007). ProSA-web: Interactive web service for the recognition of errors in three-dimensional structures of proteins. *Nucleic Acids Research*, *35*, W407–W410.

Wu, G., Robertson, D. H., Brooks Iii, C. L., & Vieth, M. (2003). Detailed analysis of grid-based molecular docking: A case study of CDOCKER—A CHARMm-based MD docking algorithm. *Journal of Computational Chemistry*, *24*(13), 1549–1562.

Xenometrix. (2018). *XenoScreen YES/YAS instructions for use*. Retrieved 2022 January 10, from: https://www.aniara.com/mm5/PDFs/IFU/IFU_AN05-233-Y.pdf

Zhang, J., Li, T., Wang, T., Yuan, C., Zhong, S., Guan, T., Li, Z., Wang, Y., Yu, H., Luo, Q., Wang, Y., & Zhang, T. (2018). Estrogenicity of halogenated bisphenol A: In vitro and in silico investigations. *Archives of Toxicology*, *92*(3), 1215–1223.

Zhang, Y., & Zhou, J. L. (2005). Removal of estrone and 17β-estradiol from water by adsorption. *Water Research*, *39*(16), 3991–4003.

Zhang, Z., Hu, Y., Guo, J., Yu, T., Sun, L., Xiao, X., Zhu, D., Nakanishi, T., Hiromori, Y., Li, J., Fan, X., Wan, Y., Cheng, S., Li, J., Guo, X., & Hu, J. (2017). Fluorene-9-bisphenol is anti-oestrogenic and may cause adverse pregnancy outcomes in mice. *Nature Communications*, *8*(1), 14585.

8.2 Original Paper - 3D spheroid culture of zebrafish liver cell

Aquatic Toxicology 245 (2022) 106105

Contents lists available at ScienceDirect

Aquatic Toxicology

journal homepage: www.elsevier.com/locate/aqtox

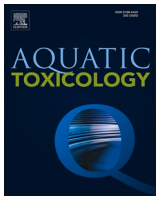

Transcriptomic and physiological analysis of endocrine disrupting chemicals Impacts on 3D Zebrafish liver cell culture system

Chang Gyun Park [a,c,1], Chang Seon Ryu [a,1], Baeckkyoung Sung [a,b], Andreas Manz [a,c], Hyunjoon Kong [d,*], Young Jun Kim [a,b,*]

[a] Environmental Safety Group, KIST Europe Forschungsgesellschaft mbH, 66123 Saarbrücken, Germany
[b] Division of Energy & Environment Technology, University of Science & Technology, 34113 Daejeon, Republic of Korea
[c] Department of Systems Engineering, Universität des Saarlandes, 66123 Saarbrücken, Germany
[d] Department of Chemical and Biomolecular Engineering, University of Illinois at Urbana-Champaign, Urbana, IL 61801, USA

ARTICLE INFO

Keywords:
3D spheroid culture
17β-estradiol
In vitro platforms
Vitellogenin
Zebrafish liver cell

ABSTRACT

In recent decades, extensive efforts have focused on developing in vitro platforms mimicking fish livers to better understand the acute or chronic effects of toxicants on lower aquatic vertebrates. Fish liver cell lines have emerged as a promising culture system for these in vitro platforms because they complement the currently limited in vitro tools that mostly consist of mammalian cell lines and adhere to the 3Rs: replacement, reduction, and refinement of living animal tests. However, monolayer cell lines have lower transcriptional and physiological responses upon exposure to toxic chemicals than freshly isolated primary cells. To overcome this challenge, we utilized a three-dimensional (3D) spheroid-based in vitro platform, in which hepatocyte cells had self-organized into spheroid forms via E-cadherin bonds. This platform exhibited augmented transcriptomic and phenotypic regulation of liver cells in comparison to monolayer cells. We examined the organoid platform using the zebrafish liver (ZFL) cell line as a model system. ZFL cells spontaneously clustered into 3D spheroids with long-term viability by optimizing cell seeding density on a non-adherent substrate. Interestingly, 3D ZFL spheroids treated with estrogenic chemicals were activated to synthesize a higher level of vitellogenin (Vtg) than monolayer cells. Whole-transcriptome sequencing analysis confirmed that 3D ZFL spheroids had greater transcriptional regulation of genes related to reproductive toxicological response and liver functions, such as the urea cycle, estrogen receptors, and vitellogenin, compared to monolayer cells. These results may contribute to the engineering of novel 3D in vitro platforms for screening harmful chemicals and improving understanding of the underlying liver toxicity mechanisms at the molecular and cellular levels.

1. Introduction

Hepatic and reproductive toxicity in fish has been extensively evaluated within the adverse outcome pathway framework during assessments of environmental disturbances caused by various contaminants (Garcia-Reyero and Murphy, 2018). Many of these contaminants are endocrine-disrupting chemicals (EDCs), which can mimic the modes-of-action of sex hormones (Mills and Chichester, 2005). These EDCs have adverse effects on wildlife population dynamics (Mills and Chichester, 2005). For example, EDCs inhibit the biosynthesis of enzymes including steroidogenic cytochrome p450, steroid hydroxylase, and hydroxysteroid dehydrogenases. Some EDCs can also interact with nuclear receptors such as estrogen receptors (ERs), androgen receptors, peroxisome proliferator-activated receptors, and other physiologically critical nuclear receptors, including retinoid X receptors (Sanderson, 2006; Grimaldi et al., 2015). In particular, the binding of estrogenic EDCs to ERs triggers the transcription of vitellogenin (Vtg), a precursor of the egg yolk proteins (Cosnefroy et al., 2012). Vtg is present not only in females but also in males that express Vtg in response to exposure with xenoestrogens (Hara et al., 2016). Therefore, Vtg is a critical biomarker of endocrine disturbances in aquatic organisms (Hara et al., 2016).

Zebrafish (*Danio rerio*) have been used as a model vertebrate organism globally and are part of several Organization for Economic Co-

* Corresponding authors.
E-mail addresses: hjkong06@illinois.edu (H. Kong), youngjunkim@kist-europe.de (Y.J. Kim).
[1] These authors contributed equally to this work.

https://doi.org/10.1016/j.aquatox.2022.106105
Received 21 May 2021; Received in revised form 23 January 2022; Accepted 27 January 2022
Available online 29 January 2022

operation and Development (OECD) test guidelines because of their rapid growth, development, and high conservation of signaling pathways compared to those of humans (MacRae and Peterson, 2015; Kari et al., 2007). Zebrafish are increasingly used in single-chemical toxicity testing (OECD, 1992, 1998, 2000). High numbers of zebrafish are also required for long-term studies on toxin bioaccumulation and reproduction. Due to growing concerns about the welfare of laboratory animals in toxicity testing, the reduction, refinement, and replacement principles (3Rs) have been actively attempted in vertebrate animal studies, including those using fish. Among alternative approaches, in vitro cell-based systems represent a promising technology for the predictive assessment of in vivo toxicity, allowing for more controlled manipulation of cellular functions and biological processes. Both freshly isolated primary hepatocytes and the zebrafish liver (ZFL) cell line are commonly cultured on two-dimensional (2D) substrates to study liver response dynamics to EDCs at the molecular and cellular level (Ghosh et al., 1994; Chen and Chan, 2011; Park et al., 2020). In particular, the ZFL cell line offers continued cell proliferation and adheres to the 3Rs (EU, 2010). However, monolayer-cultured cells exhibit decreased hepatic polarity and detoxification processes than 3D cell cultures (Godoy et al., 2013). It is difficult to conduct long-term chronic toxicity assessments using monolayer-cultured cells due to cellular detachment (Braunbeck and Segner, 2000). Furthermore, ZFL cells have a limited capacity for synthesizing Vtg upon exposure to estrogen hormones under monolayer culture conditions (Wallace and Selman, 1985; Eide et al., 2014). Therefore, there is an urgent need to develop a novel in vitro system to enhance the physiological activity of ZFL cells for robust reproductive toxicity assessment. *In vivo*-like cell aggregates such as a three-dimensional (3D) cell cultures represent a promising approach to address this need because they show higher cell-to-cell interactions, metabolic activity, and the tissue-like environment than monolayer cell cultures. Therefore, 3D cell culture is increasingly being employed in various fields including toxicology, pharmacology, and biomedical applications (Bell et al., 2016; dit Faute et al., 2002; Hirschhaeuser et al., 2010; Ramaiahgari et al., 2014; Tung et al., 2011).

In this study, we hypothesized that ZFL cells cultured in 3D spheroids would present genetic profiles and physiological functionality more similar to liver tissue due to enhanced E-cadherin-mediated intercellular adhesion. E-cadherin plays pivotal roles in the formation of hepatocyte spheroids, the maintenance of epithelial cell behavior, and the prevention of cell death (van Roy and Berx, 2008; Capra and Eskelinen, 2017; Luebke-Wheeler et al., 2009). The resulting ZFL spheroids are expected to exhibit enhanced liver-specific functions and tissue-like environments compared with monolayer cell cultures. To achieve this objective, we optimized the cell-seeding conditions under which ZFL spheroids remain viable and metabolically active over 28 days, and prepared a monolayer ZFL cell culture as the control. We conducted comparative analyses of Vtg synthesis, detoxification, and transcriptional regulation using these two systems based on immunofluorescence, enzyme-linked immunosorbent assay (ELISA), quantitative reverse-transcription polymerase chain reaction (RT-qPCR), and whole-transcriptome RNA sequencing (RNA-Seq) techniques. We anticipate that the results of this study will contribute to improving understanding of EDC-induced endocrine disorders and the ability to design toxicity tests that empower fit-for-purpose chemical regulation.

2. Materials and methods

2.1. Formation of 3D ZFL spheroids

The zebrafish liver (ZFL) cell line was purchased from ATCC (CRL2643, Wesel, Germany) and then cultured and maintained in complete growth medium within T-75 flasks at 28 °C in a cell incubator (Thermo Scientific, Karlsruhe, Germany). The complete growth medium consisted of 50% Leibowitz-15 (ATCC), 35% Dulbecco's modified Eagle's medium (DMEM; Thermo Scientific), and 15% Ham's F12 (Thermo Scientific), supplemented with 15 mM of HEPES (Sigma-Aldrich, Steinheim, Germany), 0.15 g/L sodium bicarbonate (Sigma-Aldrich), 1% penicillin–streptomycin (Sigma–Aldrich), 0.01 mg/mL bovine insulin (Sigma-Aldrich), 50 ng/mL mouse epidermal growth factor (Thermo Scientific), 5% heat-inactivated fetal bovine serum (FBS), and 0.5% trout serum (Caisson Laboratories, Smithfield, UT, USA). For the generation of 3D spheroids, cells in the T-75 flask were washed with phosphate buffered saline (PBS; pH 7.4, Thermo Scientific). Next, the cells were treated with 0.25% trypsin–EDTA (ATCC), suspended in complete growth medium, and spun at 125 × *g* for 5 min. The pelleted cells were re-suspended in the medium and counted using a hemocytometer after staining with 0.4% trypan blue (Sigma-Aldrich). Cells from the same batch were seeded into a 96-well flat-bottomed plate (Thermo Scientific) for monolayer cell culture, and ultra-low-attachment 96-well round-bottomed plates (Corning B.V. Life Sciences, Amsterdam, Netherlands) for 3D spheroid culture, respectively. The initial spheroid cell densities were 5000, 10,000, 25,000, 50,000, and 100,000 cells/well. The 3D ZFL spheroids formed in ultra-low-attachment 96-well round-bottomed plates (Fig. 1A). Seeded cells were cultured in an incubator at 28 °C, and 50% of the complete growth medium was replaced every 2–3 days in both monolayer cells and 3D spheroid cultures. To analyze changes in size and shape, bright-field images of the 3D ZFL spheroids were obtained at 1, 3, 7, 14, 21, and 28 days of culture using an inverted light microscope (Olympus CKX41, Olympus, Tokyo, Japan) equipped with a digital camera (C5060-ADUS, Olympus, Tokyo, Japan).

2.2. ZFL cell viability measurement

To measure cell viability in 3D ZFL spheroids, the cells were seeded at different densities in ultra-low-attachment 96-well round-bottomed plates and measured at 1 and 28 days. Complete medium containing a 3D spheroid (100 μL) was transferred from the ultra-low-attachment plates to 96-well white opaque culture plates (Thermo Scientific). Next, each well was treated with 100 μL CellTiter-Glo 3D reagent (Promega, Mannheim, Germany), and luminescent signals were recorded after 30 min using a microplate reader (Tecan, Männedorf, Switzerland). Bioluminescence from viable cells among the spheroids on day 1 was correlated to the cell seeding density (Fig. 2A). Each cell density group was replicated for eight spheroids and a mean value was calculated. The experiment was repeated three times from independent cultures (n= 3). Measured response values revealed a non-linear trend at higher cell seeding densities (≥ 25,000 cells/well) and fit a polynomial regression equation. The expected linear fit was calculated for accurate cell viability measurement (Zanoni et al., 2016). Based on the linear fit equation, the fractions of viable cells were measured on days 1 and 28. Each cell density group was replicated for five spheroids and a mean value was calculated. The experiment was repeated three times from independent cultures (n= 3). For live and dead staining, each cell concentration was cultivated for 28 days, and then the medium was removed. Fluorescein diacetate (FDA; Sigma-Aldrich) and propidium iodide (PI; Sigma-Aldrich) were dissolved in culture medium without FBS and trout serum, and the solution was added to each well. After incubation in the dark for 10 min, the staining solution was removed, and the cells were washed with PBS. The stained cells were observed under an inverted fluorescence optical microscope (DMi8, Leica Microsystems, Wetzlar, Germany) equipped with a digital camera (DCF295, Leica Microsystems), N PLAN 40 × /0.55 CORR objective lens (11,506,297, Leica Microsystems), a fluorescence excitation light source CoolLED pE300-lite (CoolLED Ltd. Andover, UK), fluorescence filters [350/50 4′,6-diamidino-2-phenylindole (DAPI) excitation filter and 460/40 emission, 480/40 excitation fluorescein isothiocyanate (FITC) filter and 527/30 emission, and 546/10 RHOD excitation filter and emission 585/40], and fluorescence overlay software (LAS AF v3.1.0, Leica Microsystems).

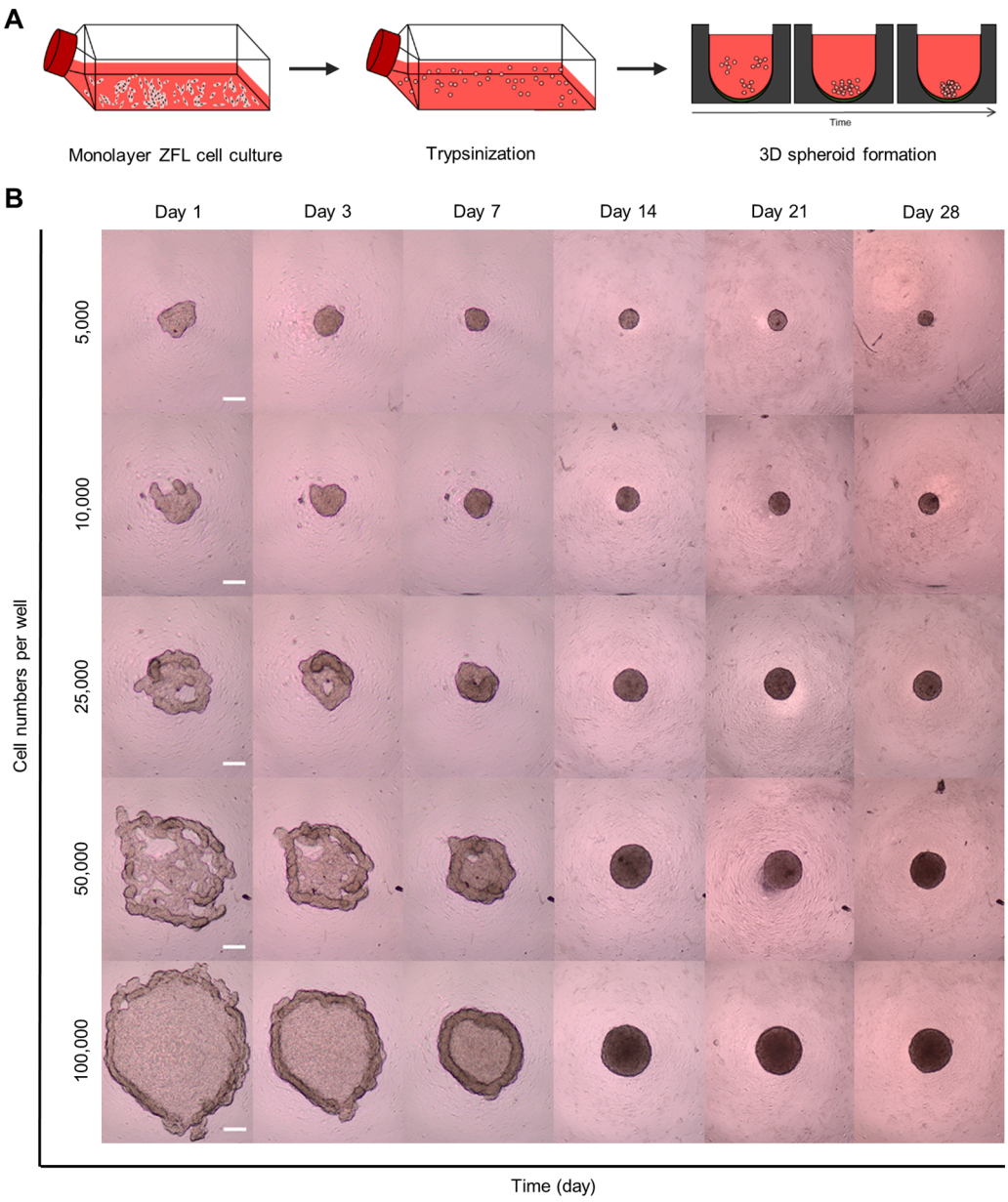

Fig. 1. Process of three-dimensional (3D) spheroid formation and morphological changes. (**A**) Schematic of 3D spheroid formation. A monolayer culture of zebrafish liver (ZFL) cells was trypsinized for cell dissociation and collected by centrifugation at 125 × *g*. The collected cells were transferred to an ultra-low-attachment plate and cultured. (**B**) Representative bright-field images of 3D spheroids seeded at different cell densities over 28 days of culture. Cells were seeded into an ultra-low attachment plate, and bright-field images were captured at 1, 3, 7, 14, 21, and 28 days. White scale bar: 200 μm.

2.3. Chemical exposure

The test chemicals were dissolved in dimethyl sulfoxide (DMSO) and the concentration of which did not exceed 0.5% (v/v). We obtained high-purity (≥ 98%) 17β-estradiol (E2), 17α-ethynylestradiol (EE2), bisphenol A (BPA), and bisphenol S (BPS) from Sigma-Aldrich. The concentrations of the E2, EE2, BPA, and BPS working stocks were 0.0002, 0.002, 2, and 2 mM, respectively. From these stocks, diluted solutions were prepared through 100 × dilution with complete medium. Each diluted solution was treated to wells containing spheroid or monolayer cells and complete medium at a 1:1 ratio. After exposure for 24 or 48 h, the spheroid and monolayer cells were used for assays.

2.4. Immunofluorescence assay

Cells with nuclear non-histone, cytoskeleton, and nuclei were stained with Ki67, F-actin, and DAPI, respectively. To obtain fluorescence images, monolayer cells and 3D spheroids were fixed in 3.7% paraformaldehyde at room temperature (RT) for 15 min, washed with PBS, and permeabilized in PBS supplemented with 0.1% Triton X-100 at RT for 5 min. After permeabilization, the samples were washed three times with PBS and blocked with 3% bovine serum albumin (BSA; Sigma–Aldrich) at RT for 30 min. Next, the samples were incubated with primary antibodies at 4 °C overnight. After being washed three times with 1% BSA, the samples were incubated with secondary antibodies for 2 h and rewashed three times with 1% BSA. Finally, the samples were embedded in mounting medium containing DAPI (Vector Laboratories, Burlingame, CA, USA). Table 1 lists the primary and secondary antibodies used in this experiment. F-actin staining was performed using phalloidin-iFluor (ab176753, Abcam). Images of the monolayer cells were obtained by using a fluorescence microscope (DMi8, Leica) and analyzed using the ImageJ software (NIH and LOCI). The 3D spheroids were imaged using a Lightsheet Z.1 microscope (Carl Zeiss Microscopy GmbH, Jena, Germany) with two-sided 10 × /0.2 illumination optics and a 20 × /1.0 detection optic equipped with a pco.edge 4.2 camera (PCO AG, Kelheim, Germany). The captured images were analyzed using the ZEN imaging software (Carl Zeiss). The relative intensity of Vtg was calculated using the ImageJ software. Fluorescence microscope images of the samples were measured at the same exposure time and laser power, and the corrected total cell fluorescence (CTCF) were calculated

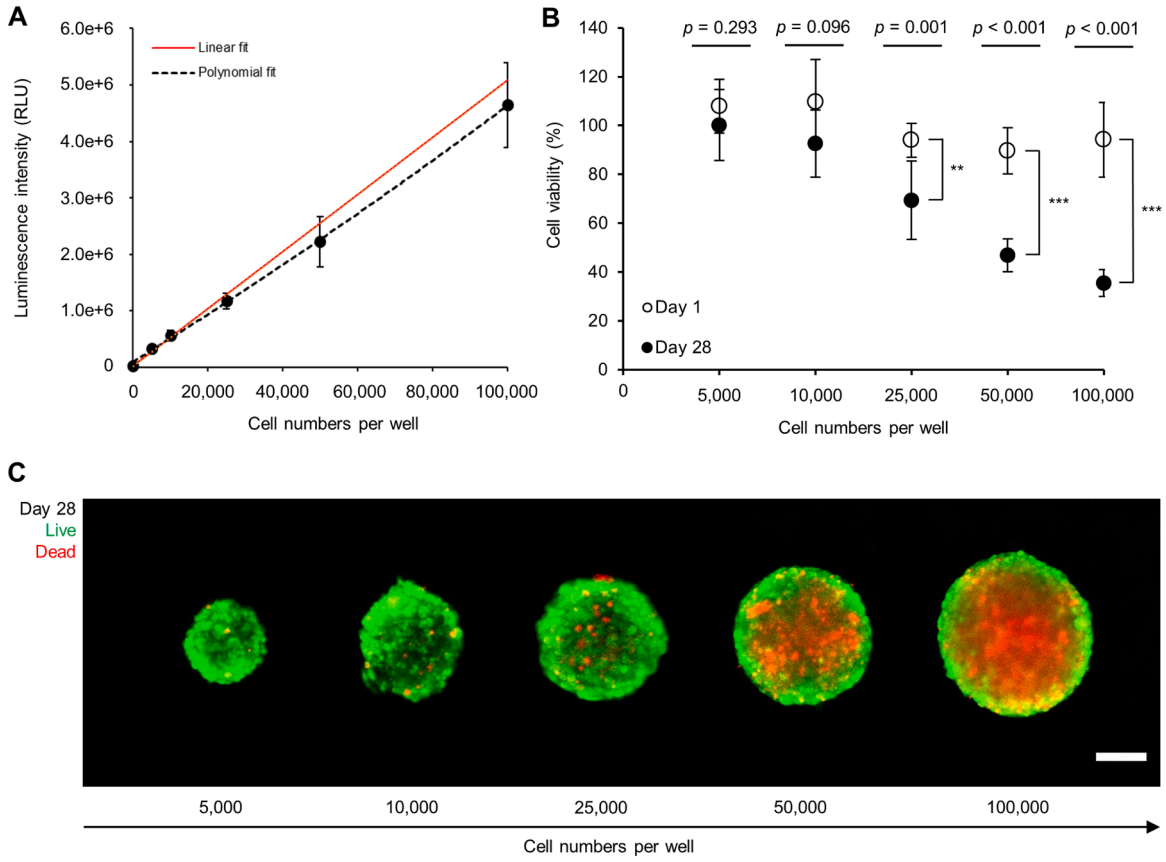

Fig. 2. Cell viability in 3D spheroid cultures over 28 days of culture. (**A**) Cell viability of 3D spheroids cultured in an ultra-low-attachment plate. Different cell densities (5000–100,000 cells/well) were seeded into an ultra-low-attachment plate and cultured for 24 h. The CellTiter-Glo 3D cell viability assay was used to measure luminescence intensity according to cell numbers. The polynomial fit indicates the measured relationship between luminescence and cell number, and the linear fit (red line) is the expected relationship. The graph presents means of three replicates of eight spheroids for each cell number condition. Data are means ± standard deviation (SD; n= 3). (**B**) Comparison of cell viability between days 1 and 28. Cell viability rates (%) were calculated based on the linear fit in (**A**). The graph presents means of three replicates of five spheroids for each cell number condition. Data are means ± SD (n= 3). Student's t-test was performed to compare means between days 1 and 28 of cell number groups (*$P < 0.05$; **$P < 0.01$; ***$P < 0.001$). (**C**) Images of live and dead 3D spheroids cultured for 28 days as a function of increasing cell number (5000 cells from left, 100,000 cells to the right). White scale bar: 100 μm. Green and red fluorescence indicates live and dead cells, respectively.

Table 1
Antibody information.

Antibodies	Source	Catalog	RRID
Anti-E-cadherin	Thermo	PA5–19,479	AB_10,988,711
Anti-Ki67	GeneTex	GTX16667	AB_422,351
Anti-Total ERK	Cell signaling	4696	AB_390,780
Anti-Vitiellogenin	LifeSpan	LS-C76845–100	AB_1,602,614
Anti-Rabbit IgG Alexa Fluor 546	Thermo	A-11,010	AB_2,534,077
Anti-Mouse IgG1 FITC	Thermo	31,232	AB_429,670
Goat Anti-Mouse IgG H&L (HRP)	Abcam	Ab6789	AB_955,439
Goat Anti-Rabbit IgG H&L (HRP)	Abcam	Ab6721	AB_955,447

as follows (Banerjee et al., 2013):

$$\text{Whole} - \text{cellsignal} = \text{Sumofpixelintensityvaluesforonecell} \quad (1)$$

$$\text{Backgroundsignal} = \text{Averageintensityperpixelforaselectedregionadjacent tothecell} \quad (2)$$

$$\text{CTCF} = \text{Whole} - \text{cellsignal}(\text{Numberofpixelsinthecell} = \text{Areaoftheselectedsurface} \times \text{Backgroundsignal}) \quad (3)$$

Images obtained from eight replicates of each condition were analyzed as mean relative intensity values. The experiment was repeated three times with independent cultures (n= 3).

2.5. Urea assay

Cellular synthesis of urea was measured to evaluate hepatic functionality. The urea cycle converts toxic ammonia to urea in the liver for excretion, thereby acting as a detoxification mechanism (Atkinson, 1992). The urea content of cell pellets was analyzed using a urea assay kit (MAK006, Sigma-Aldrich). In the monolayer culture, 1 mL of ZFL cells (50,000 cells/mL) was seeded into each well of a 6-well flat-bottomed plate and cultured for 7 and 28 days. After trypsinization and cell counting, 1.0×10^6 cells were collected from three wells into a tube by centrifugation at 125 × g for 5 min. For the 3D spheroids, 100 μL (i.e., 5000 cells at a density of 50,000 cell/mL) were seeded into each well of an ultra-low-attachment 96-well round-bottomed plate and cultured for 7 and 28 days. About 200 spheroids were collected into a tube and centrifuged at 125 × g for 5 min. Each tube of pooled monolayer cells and spheroids was considered a sample, and six replicate samples of each condition were prepared from independent cultures

(n= 6). After washing with PBS and another centrifugation at 125 × g for 5 min, 100 μL of cold urea assay buffer was added to a tube and homogenized by vortexing for 2 min. The homogenates were centrifuged at 14,000 × g and 4 °C for 10 min. The supernatants were used for urea quantification according to the manufacturer's instructions. This assay determined the urea concentration: a coupled enzyme reaction resulted in a colored product that was measured by reading the absorbance at 570 nm on a microplate reader (Tecan). The supernatants of each sample were normalized to total protein content, quantified using a bicinchoninic acid (BCA) protein assay.

2.6. ELISA

Vtg synthesis was measured using an ELISA kit (10,004,995, Cayman Chemical, Ann Arbor, MI, USA). Monolayer cells and 3D spheroids were cultivated for 7, 14, and 28 days, and collected in the same manner as for the urea assay. Each tube of pooled monolayer cells and spheroids was considered a sample, and three replicate samples of each condition were prepared from independent cultures (n= 3). After washing with PBS and another centrifugation at 125 × g for 5 min, 100 μL of passive lysis buffer (Promega) was added to a tube and homogenized by vortexing for 2 min. The homogenates were centrifuged at 14,000 × g and 4 °C for 10 min. The supernatants were used for Vtg quantification according to the manufacturer's instructions (Cayman Chemical). The supernatants of each sample were normalized to total protein content and quantified using a BCA protein assay.

2.7. mRNA expression analysis

To extract total RNA samples from monolayer cell cultures, 1 mL of ZFL cells (50,000 cells/mL) were seeded into each well of a 6-well flat-bottom plate and cultured for 7 days. The cells of three wells were collected in a tube and lysed with RLT buffer (Qiagen, Hilden, Germany) after washing with cold PBS. For 3D spheroids, 100 μL of cells (i.e., 5000 cells at a density of 50,000 cell/mL) were seeded into each well of an ultra-low-attachment 96-well round-bottomed plate and cultured for 7 days. We collected 100 spheroids in a tube and centrifuged them at 125 × g for 5 min. After washing with cold PBS and another centrifugation at 125 × g for 5 min, 3D spheroids were lysed in the same manner as monolayer cells. Each tube of pooled monolayer cells and spheroids was considered a sample, and three replicate samples were prepared from independent cultures for each condition (n= 3). Total RNA of each sample was extracted using an RNeasy Plus mini kit (74,136, Qiagen). Sample concentration and purity were determined spectrophotometrically using a NanoDrop 2000 spectrophotometer (Thermo Scientific). Reverse transcription was performed for samples with purity > 2.0 (OD_{260}/OD_{280} and OD_{260}/OD_{230}) using the High-Capacity RNA-to-cDNA kit (Applied Biosystems, Waltham, MA, USA) according to the manufacturer's instructions. Total RNA (1 μg) was used for reverse transcription. Next, qRT-PCR (7500 FAST Real-Time PCR System, Applied Biosystems) was conducted using the TaqMan Gene Expression Master Mix (Thermo Scientific) and PowerUp SYBR Green Master Mix (Applied Biosystems). Tables 2 and 3 describe the probe assay identifications and reaction cycles. Relative mRNA expression was determined using the $2^{-\Delta\Delta CT}$ method (Schmittgen and Livak, 2008).

2.8. RNA-Seq analysis

Total RNA samples of monolayer cells and 3D spheroids were extracted in the same manner as those subjected to mRNA expression analysis. Six total RNA samples (monolayer cells and 3D spheroids in triplicate) were sent to a Novogene for RNA-Seq (Novogene, Cambridge, UK). Total RNA samples were purified using poly-T oligo-attached magnetic beads after quality control checks. Paired-end sequencing (150 bp) was conducted using an Illumina NovaSeq 6000 system. Samples were sequenced at a sequencing depth of at least 48 million clean reads, and 15 G raw bases were generated per sample. Raw sequences were filtered for contaminant adapter sequences and reads with > 10% uncertain nucleotides or > 50% low-quality nucleotides (Qphred ≤ 5). Filtered reads were considered clean, and the reads of each sample were used for data analysis. Data analysis was conducted by Novogene. Paired-end clean reads were aligned to the reference genome (genome assembly: GRCz11_gca_000002035_4, Taxon ID: 7955) using HISAT2 to count the read numbers mapped to each gene, and the expected FPKM number was determined for each gene based on the gene length and read count mapped to the gene. Differential expression analyses of two conditions/groups (in triplicate for each condition) were conducted using the *DESeq2* R package, which identifies differential expression among genes using a model based on the negative binomial distribution. To control the false discovery rate, P values were adjusted (P_{adj}) using the Benjamini and Hochberg method. Differentially expressed genes (DEGs) were evaluated at a level of $P_{adj} < 0.05$.

Table 2
The information of assay identification and probes.

Gene Name	Gene symbol	RefSeq Identification	Assay Identification	Source
Estrogen receptor 1	*esr1*	NM_152,959.1	Dr03093579	Thermo
Estrogen receptor 2a	*esr2a*	NM_180,966.2	Dr03074408	Thermo
Estrogen receptor 2b	*esr2b*	NM_174,862.3	Dr03150586	Thermo
Vitellogenin 1	*vtg1*	NM_001044897.3	PPZ09938A	Qiagen
Vitellogenin 2	*vtg2*	NM_001044913.1	PPZ10052A	Qiagen
Vitellogenin 3	*vtg3*	NM_131,265.1	PPZ00317A	Qiagen
Vitellogenin 4	*vtg4*	NM_001045294.2	Dr03191564	Thermo
Vitellogenin 5	*vtg5*	NM_001025189.2	PPZ00676A	Qiagen
Glucose-6-phosphate dehydrogenase	*g6pd*	XM_694,076	PPZ12949A	Qiagen
Eukaryotic translation elongation factor 1 alpha 1, like 1	*eef1a1l1*	NM_131,263.1	Dr03432748	Thermo

Table 3
Condition of reaction cycles.

Mode	Cycles	Temperature (°C)	Duration (sec)	Step
SYBR green assay	Hold	95	20	AmpliTaq Fast DNA polymerase and Up activation
	40	95	3	Denature
		60	30	Anneal/Extend
TaqMan assay	Hold	50	120	UNG incubation
		95	120	Polymerase activation
	40	95	3	Denature
		60	30	Anneal/Extend

2.9. Statistical analyses

Statistical analyses were performed using the SPSS Statistics v21 software (SPSS, Inc, IBM, Chicago, IL, USA). All data are expressed as means ± standard deviation (SD). Data were tested for normality using the Shapiro–Wilk test and for homogeneity of variance using Levene's test to determine whether to perform parametric or non-parametric statistical tests. Statistical differences among test groups were determined using Student's t-test or one-way analysis of variance (ANOVA) followed by post hoc Dunnett's T3 test (non-homogeneous variance) or Scheffe's test (homogeneous variances). Data for cell viability, urea synthesis, and Vtg intensity analyses were evaluated using Student's t-test. Data for Vtg synthesis and gene transcript abundance analyses were evaluated using one-way ANOVA. All statistical analyses for RNA-Seq

were performed using the *DESeq2* R package; heatmaps were generated based on FPKM cluster analysis according to the log2(FPKM+1) value, and a volcano plot was created from DEG gene expression levels according to $-\log10(P_{adj})$. For principal component analysis (PCA), six samples from two groups were scaled to unit variance and calculated as PC1 (85.5%) and PC2 (6.05%).

3. Results

3.1. Formation of 3D ZFL spheroids

The ultra-low-attachment plate inhibited cellular attachment, and cells gradually aggregated to form spheroids during cultivation (Fig. 1B). Bright-field microscopy images revealed that the initial cell seeding densities influenced spheroid morphology. Morphological changes were evaluated by measuring the 2D surface area, diameter, solidity, and roundness of the spheroids over a period of 28 days (Supplementary Fig. 1 and Supplementary Table 1). The surface area and diameter of spheroids decreased over time, whereas their roundness and solidity increased continuously over 28 days of cell culture (Supplementary Table 1). Initial cell densities > 25,000 cells/well resulted in more significant changes in spheroidal area and diameter. Notably, initial seeding densities of 5000 and 10,000 cells/well resulted in high solidity values (> 0.9) on day 3. In monolayer cell culture, cells had a typical epithelial appearance (Supplementary Fig. 2A). After cells were plated at a density of 5000 cells/well, cell numbers increased over time, finally reaching confluency on day 7 (Supplementary Fig. 2A). Cells continued to grow, but a delay in cell doubling time coincided with overconfluency at day 14 (Supplementary Fig. 2B).

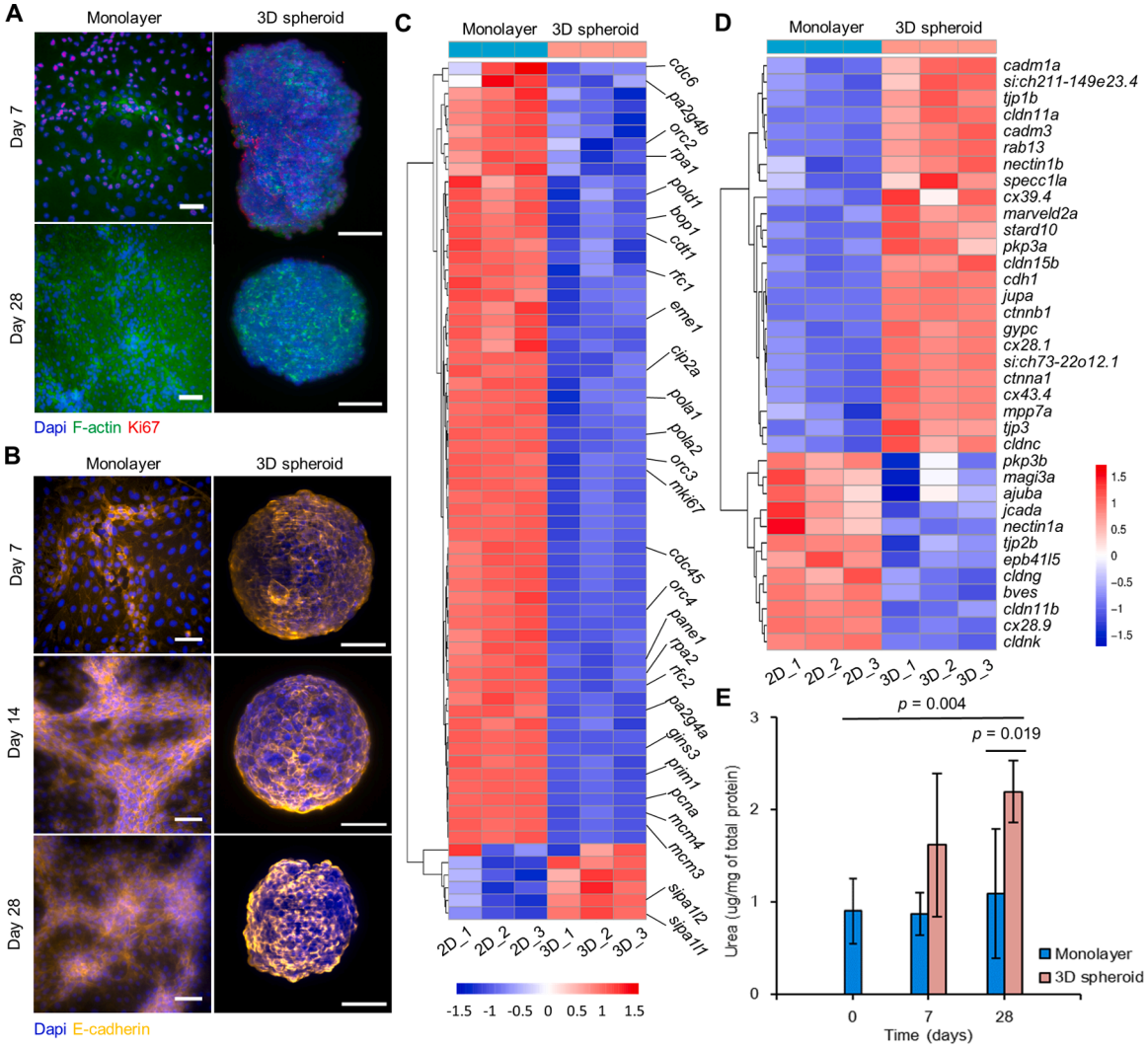

Fig. 3. Evaluation of 3D spheroid properties and urea synthesis. (**A, B**) Immunofluorescence observations of monolayer cells and 3D spheroids using fluorescence optical and lightsheet microscopies. Cells seeded at a density of 5000 cells/well were cultured for 7, 14, and 28 days. Scale bars: 50 μm. (**A**) Representative images of Ki67 (red), F-actin (green), and 4′,6-diamidino-2-phenylindole (DAPI; blue) staining to investigate cell proliferation and cell structure. (**B**) Representative images of E-cadherin (orange) and DAPI (blue) staining to investigate cell–cell interaction. (**C, D**) RNA-seq analysis. Heatmaps of gene expression differences between monolayer and 3D spheroid cells at day 7. For monolayer cells, 50,000 cells/mL were seeded into each well of a 6-well flat-bottom plate; cells were collected from three wells into a tube. For 3D spheroids, 100 spheroids (5000 cells/well) were collected into a tube. Each tube of pooled monolayer cells or spheroids was considered a sample, and three replicate samples were prepared for each condition from independent cultures (n= 3). (**C**) Heatmap of expression differences in genes related to cell proliferation and replication, (**D**) Heatmap of expression differences in genes related to cell–cell junctions. (**E**) Urea synthesis analysis. We collected 1.0×10^6 monolayer cells or 200 spheroids (5000 cells/well) into a tube. Each tube was considered a sample, and six replicate samples were prepared for each condition from independent cultures (n= 6). Urea concentrations were normalized to total protein concentration. Error bars indicate means ± SD. Student's t-test was performed to compare means between groups. Significant differences were observed between monolayer cells (day 0) and 3D spheroids cultured for 28 days (P= 0.004) and between monolayer cells and 3D spheroids cultured for 28 days (P= 0.019).

3.2. Long-term viability of 3D ZFL spheroids

Cell viability measurements using bioluminescence differed significantly between days 1 and 28 for cell seeding densities > 25,000 cells/well, indicating cell death during culture (Fig. 2B). In contrast, no significant difference was observed in the fraction of viable cells for cell seeding densities of 5000 and 10,000 cells/well between days 1 and 28. Cell viability was further assessed using a live/dead cell staining method (Fig. 2C). Cell seeding densities of ≥ 50,000 cells/well showed red fluorescence in the spheroid cores, indicating cell death. In contrast, spheroids formed from cell seeding densities of 5000 and 10,000 cells/well remained viable for 28 days. Therefore, we selected a seeding density of 5000 cells/well as the optimal condition for subsequent experiments.

3.3. Comparative studies of growth, cell–cell adhesion, and hepatic functionality

Phenotypic properties and physiological functions of 3D ZFL spheroids prepared at a seeding density of 5000 cells/well were assessed by monitoring cell proliferation, cell-to-cell interaction, and urea synthesis (Fig. 3). Ki-67 is expressed only during active cell cycle phases with its effects on cell proliferation. Positive Ki67 expression was observed at the periphery of 3D spheroids on day 7, but became minimal by day 28. Monolayer cells also had decreased Ki67 expression throughout the 28-day culture period (Fig. 3A). A separate analysis of cellular adhesion to neighboring cells revealed that cells in the 3D ZFL spheroids had more active cell-to-cell interactions induced by E-cadherin bonds responsible for hepatic junction formation in the liver. Immunofluorescence images revealed that E-cadherin expression increased over time in 3D spheroids compared to cell monolayers (Fig. 3B). Western blot analysis of E-cadherin expression confirmed higher expression by cells constituting 3D spheroids than monolayer cells (Supplementary Fig. 3A). However, according to our RNA-Seq results, 3D spheroids cultured for 7 days had significantly lower expression of genes related to cell proliferation and replication (e.g., *mki67* and *pcna*) than monolayer cells (Fig. 3C). Genes related to cell-to-cell junctions such as *cdh1, cadm, cldn*, and *tjp* had enhanced expression within 3D spheroids (Fig. 3D). Section 3.5 provides more detailed hepatic functional gene expression analysis results.

The hepatic functionality of cells was evaluated by quantifying the cellular synthesis of urea (Fig. 3E). Interestingly, 3D spheroids had significantly more urea synthesis activity than monolayer cells over 28 days. Additionally, 3D spheroids displayed a 2-fold increase in urea synthesis activity over time, whereas monolayer cells exhibited constant urea synthesis activity. Overall, the difference in the urea synthesis activity between 3D spheroids and monolayer cells became more prominent over the cell culture period.

3.4. Comparative analysis of Vtg synthesis

Immunostaining revealed that monolayer cells produced a limited amount of Vtg even after stimulation with exogenous E2 (Fig. 4A). In contrast, 3D ZFL spheroids actively synthesized Vtg even without the addition of exogenous E2 (Fig. 4B). Cellular Vtg synthesis levels continued to increase over 28 days in both the presence and absence of exogenous E2 (Fig. 4C). The relative intensity of Vtg demonstrated that BPA and BPS, both of which are agonists to ERs, resulted in a significant increase in Vtg synthesis by 3D spheroids (1.6-fold with 10 μM BPA; 3.2-fold with 10 μM BPS; Fig. 4D and Supplementary Fig. 3C). The 3D spheroids also exhibited increased Vtg synthesis in response to 17α-ethynylestradiol (EE2), which is a synthetic hormone for ER activation (Supplementary Fig. 3C). The transcript abundance of genes involved in Vtg synthesis was also compared between monolayer cells and 3D spheroids after 7 days of culture (Fig. 4E). Each condition was treated with 1 nM E2 for 24 h to activate Vtg transcript abundance. E2 decreased e*sr2b* expression levels in 3D spheroids and increased e*sr2a* expression more significantly than monolayer cells (2.1- and 1.8-fold in the absence and presence of exogenous E2, respectively). We further examined the effects of E2 on transcript abundance among Vtg sub-family genes. *Vtg1* and *vtg5* are major precursors for ovulation and egg maturation. The abundance of *vtg1* transcripts was 2.9-fold higher in 3D spheroids than in monolayer cells following E2 exposure. Similarly, 3D spheroids had 5.3-fold higher *vtg5* transcript abundance than monolayer cells.

3.5. Analysis of whole transcriptome sequence (RNA-Seq) related to hepatic function

We further analyzed differential gene expression in 3D spheroids using whole-transcriptome sequencing analysis (Fig. 5). A heatmap of hierarchical clustering revealed distinct expression profiles between monolayer cells and 3D spheroids (Fig. 5A). Principal component analysis (PCA) also revealed clear separation between monolayer cells and 3D spheroids sets (Fig. 5B). The 3D spheroids exhibited significant upregulation of 4324 genes and downregulation of 4363 genes compared to monolayer cells (Fig. 5C). Interestingly, 3D spheroids expressed greater transcript abundance of genes related to hepatic functions than monolayer cells (Fig. 5D–H). Supplementary Tables 2–6 present detailed gene functions associated with the heatmap data. The 3D spheroids had more transcript abundance of genes related to the urea cycle, such as *acy1* (a marker of aminoacylase) and *oat* (a marker of ornithine aminotransferase), than monolayer cells. However, they expressed lower levels of some markers such as *ass1* (a marker of argininosuccinate synthase), *cad* (a pyrimidine biosynthesis marker), and *otc* (a marker of ornithine carbamoyltransferase) (Fig. 5D). This trend is consistent with our urea synthesis results (Fig. 3E). We observed significantly more *vtg3* and *vtg5* gene transcript abundance in spheroids compared to monolayer cells (Fig. 5E). The 3D spheroids had greater expression of *cyp2* family genes such as *cyp2aa*s and *cyp2k*s (markers of endogenous and xenobiotics compound metabolism) than monolayer cells (Fig. 5F). Moreover, the expression of other *cyp* genes increased, including *cyp1d1* (a marker of testosterone 6-beta-hydroxylase function), *cyp7a1* (a marker of a rate-limiting factor for synthesizing bile acids), and *cyp39a1* (a bile acid synthesis marker). In contrast, monolayer cells expressed more *cyp17a1* and *cyp2ad*s genes, which encode proteins involved with hydroxylase activity and metabolic functions, respectively, than 3D spheroids. The 3D ZFL spheroids had more transcript abundance of genes related to glucose and glycogen synthesis and metabolism activity than monolayer cells, as shown by higher levels of *pdk*s (a glucose homeostasis marker), *irs1* (an insulin receptor binding activity marker), and *gcgra* (a glucose metabolism marker) (Fig. 5G).

Nuclear receptor genes *esr2a* and *esr2b* (estrogen receptor activity markers) were increased in 3D spheroids (Fig. 5H). The 3D spheroids also had more transcript abundance of *ppar* genes than monolayer cells. These genes regulate energy homeostasis and metabolic function; *ppardb* regulates cholesterol storage, and *pparaa* regulates fatty acid metabolism. Other markers such as *arntl1b* (a photoperiodism regulation marker), *thrb* (thyroid hormone-mediated signaling pathway), *pgr* (steroid binding and steroid hormone receptor activity), and *nr1i2* (*pxr*, responses to diverse xenobiotic and endogenous chemicals) were also enhanced in 3D spheroids. These markers play critical roles in regulating numerous biological processes such as cell proliferation, development, metabolism, and reproduction (Sever and Glass, 2013).

4. Discussion

In this study, we systematically examined the extent to which 3D culture of the ZFL cell line provides improved and more realistic assessments of cell viability, detoxification activity, and sensitivity to reproductive toxicants. We successfully assembled 3D ZFL spheroids that remained viable and metabolically active for 28 days in vitro by tuning the initial cell seeding density to 5000 cells/non-adherent wells. At optimized cell densities (5000 cells and 10,000 cells/well), uniform

spheroidal shapes were achieved during cultivation, without necrotic cores. The consistent maintenance of 3D spheroid morphology is a key factor in their viability, functionality, and application (Zanoni et al., 2016; Hirschhaeuser et al., 2010). In contrast, at cell seeding densities ≥ 25,000 cells/well, excess cells aggregated within the limited space of the concave well and rolled up the boundary of the cell layer, causing irregular cell aggregates > 500 μm in size. The resulting spheroids had an internal quiescent zone and necrotic core, probably due to limited diffusion of nutrients and oxygen (Zanoni et al., 2016; Hirschhaeuser et al., 2010). These findings suggest that the optimized cell densities have reproducible and consistent viability and function. In contrast, monolayer cells reached 100% confluency after 7 days of culture,

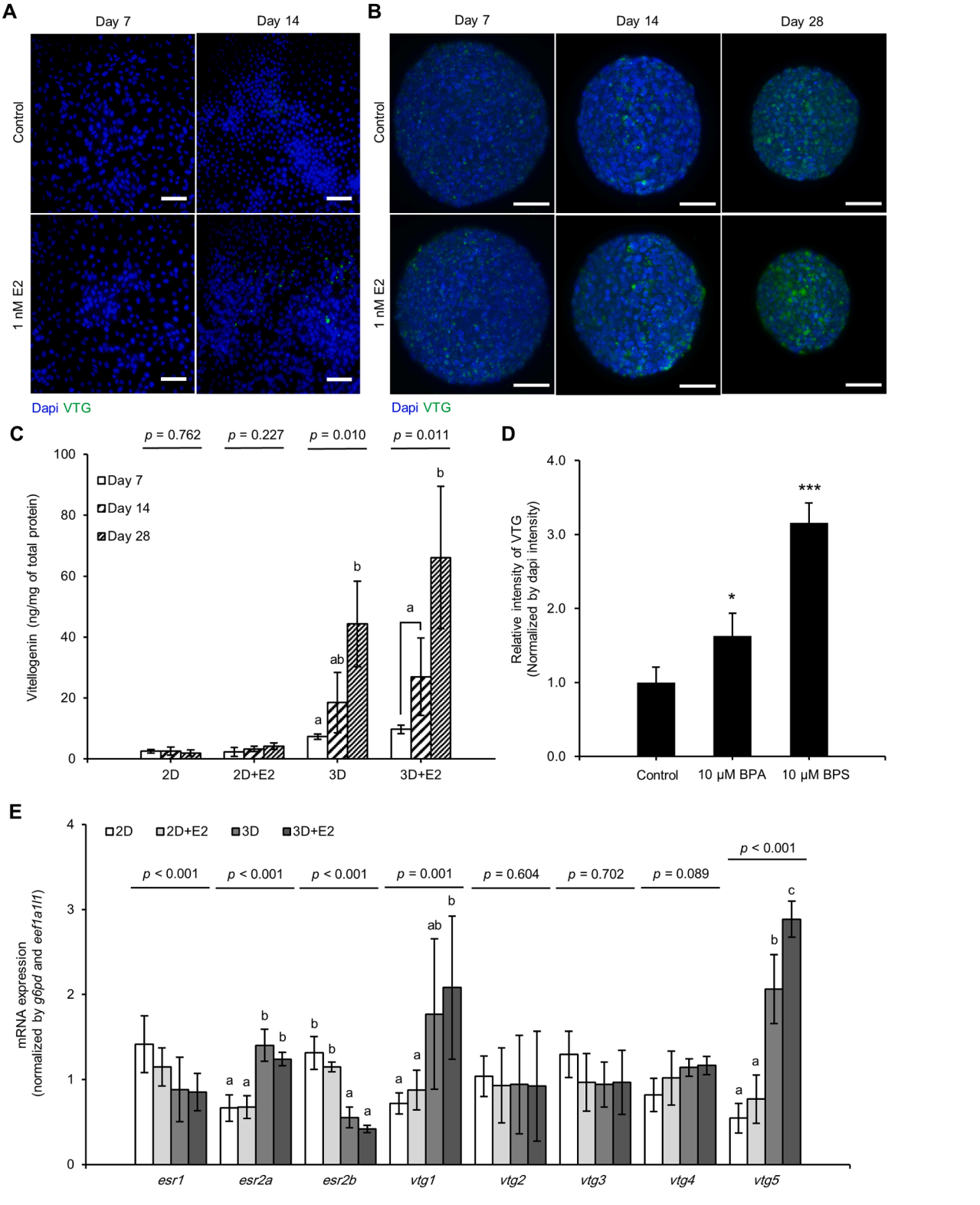

(caption on next page)

Fig. 4. Analysis of Vtg synthesis in 3D spheroids. (**A, B**) Fluorescence images of monolayer cells and 3D spheroids stained with DAPI (blue) and Vtg (green). Cells seeded at a density of 5000 cells/well were cultured for 7, 14, and 28 days. On days 7 and 28, cell cultures were treated with 1 nM 17β-estradiol (E2) for 24 h. Scale bar: 50 μm. (**C**) Quantification of Vtg synthesis in two-dimensional (2D) monolayer cells and 3D spheroids. Cells were treated with 1 nM E2 for 24 h. We collected 1.0 × 10^6 cells or 200 spheroids (5000 cells/well) into a tube. Each tube was considered a sample, and three replicate samples were prepared for each condition from independent cultures (n= 3). Vtg was normalized to total protein concentration. Error bars indicate means ± SD. Comparisons of means between culture days in each group were performed using one-way analysis of variance (ANOVA; $P < 0.05$), followed by Dunnett's T3 test (non-homogeneous variance) or Scheffe's test (homogeneous variance). Different letters indicate significant differences. (**D**) Relative intensity of Vtg, normalized by DAPI intensity. The 3D spheroids (5000 cells/well) were cultured for 7 days with charcoal stripped fetal bovine serum (FBS); subsequently, 10 μM of bisphenol A (BPA), and bisphenol S (BPS) were treated for 48 h. Eight replicate spheroids of each group were measured and the mean relative intensity was calculated. Measurements were repeated three times from independent cultures. Error bars indicate means ± SD (n= 3). Student's t-test was performed to compare means between the control and chemical treatment groups (99.9% confidence interval; $^*P < 0.05$; $^{**}P < 0.01$; $^{***}P < 0.001$). (**E**) mRNA expression related to vitellogenesis in 2D and 3D measured by a TaqMan gene expression assay and SYBR Green gene expression assay, as described in the Methods section. For monolayer cells, 50,000 cells/mL were seeded into each well of a 6-well flat-bottomed plate, and cells were collected from three wells into a tube. For 3D spheroids, 100 spheroids (5000 cells/well) were collected into a tube. Each tube was considered a sample, and three replicate samples were prepared for each condition from independent cultures (n= 3). Data were normalized to the transcript abundance of *eef1a1l1* (TaqMan assay) or *g6pd* (SYBR Green assay). After 7 days of culture, both groups were treated with 1 nM E2 for 24 h. Error bars indicate means ± SD. Comparisons of means between sample groups for each gene were performed using one-way ANOVA ($P < 0.05$), followed by Dunnett's T3 test for non-homogeneous variance or Scheffe's test for homogeneous variance.

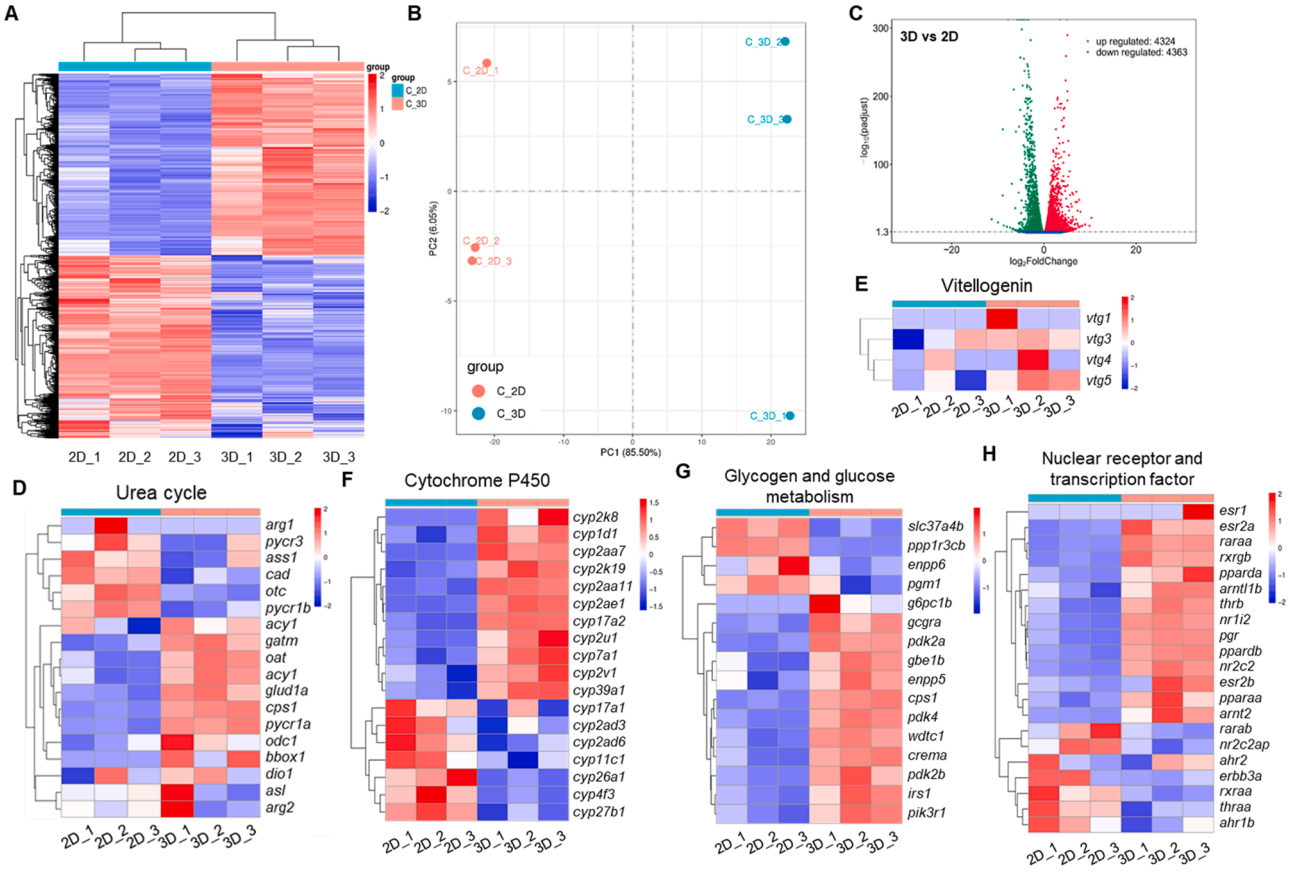

Fig. 5. RNA sequencing (RNA-Seq) analysis of monolayer cells and 3D spheroids. (A–H) RNA-Seq analysis. Heatmaps of differences in expression between monolayer and 3D spheroid cells at day 7 (n= 3). Samples were prepared as described for mRNA expression. (**A**) Heatmap hierarchical clustering according to log2 (FPKM+1) indicates differentially expressed genes (DEGs) between groups. Red and blue indicate genes with high and low expression levels, respectively. (**B**) The 2D principal component analysis (PCA) results for both groups. (**C**) Volcano plot analysis results. Plots indicate overall DEG distribution. (**D–H**) Heatmaps of differential expression between groups. (**D**) Urea cycle; (**E**) vitellogenin; (**F**) cytochrome P450 activity; (**G**) glycogen and glucose metabolism; (**H**) nuclear receptor and transcription factor.

followed by over-confluency. A previous study reported that an over-confluent environment altered signaling and led to irreproducible behavior (Han et al., 2006). Therefore, monolayer cell culture and 3D ZFL spheroids at high cell density (≥ 25,000 cells/well) are inappropriate for long-term culture experiments.

Compared to monolayer cells, 3D ZFL spheroids had increased cell–cell interaction driven by E-cadherin and urea synthesis, and decreased cell proliferation and replication. These results are consistent with previous studies reporting that 3D spheroids display more realistic hepatic functions and properties (Ramaiahgari et al., 2014; Jung et al., 2017). In human cell lines, E-cadherin inhibition in primary hepatocytes prevented cell–cell attachment and spheroid formation, subsequently leading to cell death through a caspase-independent mechanism (Luebke-Wheeler et al., 2009). E-cadherin also plays a crucial role in cell–cell interactions related to contact formation and junction remodeling (Kim et al., 2011). Several studies have reported that 3D spheroids exhibit enhanced cell–cell interactions and hepatic functions, such as albumin secretion and urea synthesis, compared to monolayer culture

(Chua et al., 2019; Ramaiahgari et al., 2014; Jung et al., 2017). The results of whole-transcriptome sequencing analysis revealed distinct differences in cell–cell interaction and cell proliferation and replication between monolayer cells and 3D spheroids. One representative finding is the upregulation of *ctnnb* in 3D spheroids. The *ctnnb1* gene encodes β-catenin; this is a major participant in the Wnt signaling pathway, which is important in liver metabolism and the development and maintenance of liver functions (Behari, 2010). However, the roles of other genes within the same category according to the heatmap have not yet been fully evaluated. *Cldn* genes encode claudin, a family of proteins important in tight junction formation and function. The functions of claudin proteins remain poorly understood, except for claudin-1 (Roehlen et al., 2020). Additionally, 3D spheroids had increased the expression of genes relevant to primary hepatic functions including the urea cycle, hepatic cytochrome P450, glycogen and glucose metabolism, nuclear receptors, and transcriptional factors compared to 2D cultures. These expression patterns were previously reported in other 3D human hepatocyte spheroids (Bell et al., 2016), where they were found to be similar to those of in vivo liver samples through whole-proteome analysis. The 3D spheroid model of hepaRG cells was more similar to liver tissue-specific gene expression profiles than monolayer cell culture (Kim et al., 2017). The *cyp2* family (e.g., *cyp2aas* and *cyp2ks*) can be markers of endogenous and xenobiotics compounds. In addition, *cyp7a1 and cyp39a1* are used as bile acid synthesis markers. Nuclear receptors such as *pxr* and *ppar*, which have important regulatory functions in the liver, were also more abundant in 3D spheroids compared to monolayer cells, which may indicate enhanced hepatic functionality; however, the regulation of enzymatic activity and metabolites via these receptors should be confirmed in further studies, as well as differences in the responses of related pathways. Future studies should focus on the effects of receptor ligand upregulation on xenobiotic and lipid metabolism.

The 3D spheroid culture increased vitellogenesis over time, suggesting that the spheroid model can be further developed as a suitable model system for screening reproductive toxicity. According to OECD Test Guidelines 229, 230 and 240 for in vivo reproductive screening assays, Vtg levels are measured as an endpoint to predict the potential reproductive effects of chemicals on fish (OECD, 2012, 2009, 2015). Compared to the test guidelines, our model is able to measure Vtg levels in chemical exposure up to 28 days without the need for live animal testing. Another important finding is that 3D ZFL spheroids synthesize Vtg in response to ER signaling, as shown by antibody fluorescence staining and ELISA. The transcript abundance of *vtg5* gene in the 3D spheroids was further increased through exposure to exogenous E2, whereas monolayer cells did not respond to this stimulus. Interestingly, we found a correlation between the improved Vtg synthesis by 3D ZFL spheroids and ER gene transcriptional activity. Exogenous E2 induces *esr1* and *esr2a* expression, but downregulates *esr2b* expression, in the liver (Chandrasekar et al., 2010). Esr2a and esr2b are essential for female zebrafish reproduction: esr2a plays a vital role in follicle cell proliferation and trans-differentiation, follicle growth, and chorion formation (Lu et al., 2017) and esr2a-knockout female medaka fish (*Oryzias latipes*) are completely infertile (Kayo et al., 2019). Our 3D ZFL spheroids had increased *esr2a* expression compared with monolayer cells, consistent with responses observed in vivo during increased vitellogenesis (Tingaud-Sequeira et al., 2012). The increased Vtg expression was also correlated with the elevation of *esr1* expression by E2 induction (Menuet et al., 2004). A previous zebrafish embryo study reported that exogenous E2 also induced *vtg1, 3*, and *5* (Hao et al., 2013). Similarly, 3D ZFL spheroids expressed *vtg1* and *vtg5* more actively than monolayer cells. Therefore, we propose that 3D ZFL spheroids are more receptive than monolayer cells to ER signaling and vitellogenesis activation. The results of this study also indicate that 3D ZFL spheroids are sensitive to BPA and BPS, as demonstrated by the increased Vtg intensity during exposure. BPA and BPS have been shown to bind with ERs and stimulate Vtg synthesis (Cosnefroy et al., 2012; Le Fol et al., 2017; Pinto et al., 2019). Interestingly, BPS had greater Vtg intensity than BPA in the present study. This tendency can be interpreted according to relative estrogenic potency (REP). Previous studies have found that BPA has higher REP in esr1 than esr2s (Cosnefroy et al., 2012; Pinto et al., 2019), whereas BPS has the highest REP in esr2a among ERs (Le Fol et al., 2017). These findings confirm that the 3D ZFL spheroid model responds with Vtg synthesis upon exposure to EDCs with estrogenic potency.

In summary, the results of this study demonstrate that 3D ZFL spheroids are advantageous to retaining hepatic functions and vitellogenesis via phenotypic and whole-RNA-Seq analysis. Compared with monolayer cells, 3D spheroids exhibited increased intercellular interactions marked by E-cadherin, as well as increased urea and Vtg synthesis activity. Interestingly, these increases in phenotypic activity were correlated with increased expression of genetic markers of hepatic functions and Vtg. Together, these findings indicate that 3D cell culture is crucial to ZFL cell sensitization and activation for transcription, and ultimately to physiological function. Therefore, this study has yielded a robust alternative in vitro platform to animal and primary cells for accurate and rapid in vitro screening of estrogenic or anti-estrogenic substances.

Authorship contributions

Conceptualisation: YJK, HK; Data curation: CGP, CSR and BS; Formal data analysis: CGP, CSR and BS; Funding acquisition: YJK; Investigation: HJK, YJK and AM; Methodology; HJK, YJK, AM; Resources, AM; Writing - original draft: CGP, CSR, YJK; Writing - review & editing: CGP, CSR, YJK, BS, HJK and AM.

Declaration of Competing Interest

The authors declare that they have no known competing financial interests or personal relationships that could have appeared to influence the work reported in this paper.

Acknowledgments

This research was supported by a National Research Council of Science & Technology (NST) grant by the Korean Government (MSIP, No. CAP-17–01-KIST Europe) and the Korea Institute of Science and Technology Europe Basic Research Program (Project no. 12001).

Supplementary materials

Supplementary material associated with this article can be found, in the online version, at doi:10.1016/j.aquatox.2022.106105.

References

Atkinson, D.E., 1992. Functional roles of urea synthesis in vertebrates. Physiol. Zool. 65, 243–267. https://doi.org/10.1086/physzool.65.2.30158252 https://doi.org/.

Banerjee, A., Sahana, A., Lohar, S., Hauli, I., Mukhopadhyay, S.K., Safin, D.A., Babashkina, M.G., Bolte, M., Garcia, Y., Das, D, 2013. A rhodamine derivative as a "lock" and scn- as a "key": visible light excitable scn- sensing in living cells. Chem. Commun. (Camb.) 49, 2527–2529. https://doi.org/10.1039/c3cc40582f https://doi.org/.

Behari, J., 2010. The wnt/β-catenin signaling pathway in liver biology and disease. Expert Rev. Gastroenterol. Hepatol. 4, 745–756. https://doi.org/10.1586/egh.10.74 https://doi.org/.

Bell, C.C., Hendriks, D.F., Moro, S.M., Ellis, E., Walsh, J., Renblom, A., Fredriksson Puigvert, L., Dankers, A.C., Jacobs, F., Snoeys, J., et al., 2016. Characterization of primary human hepatocyte spheroids as a model system for drug-induced liver injury, liver function and disease. Sci Rep 6, 25187. https://doi.org/10.1038/srep25187 https://doi.org/.

Braunbeck, T. and Segner, H. (2000). Isolation and cultivation of teleost hepatocytes. In M. N. Berry and A. M. Edwards (eds.), The Hepatocyte Review. Dordrecht: Springer Netherlands. doi:https://10.1007/978-94-017-3345-8_6.

Capra, J., Eskelinen, S., 2017. Correlation between e-cadherin interactions, survivin expression, and apoptosis in mdck and ts-src mdck cell culture models. Lab. Invest. 97, 1453–1470. https://doi.org/10.1038/labinvest.2017.89 https://doi.org/.

Chandrasekar, G., Archer, A., Gustafsson, J.-.Å., Andersson Lendahl, M., 2010. Levels of 17β-estradiol receptors expressed in embryonic and adult zebrafish following in vivo treatment of natural or synthetic ligands. PLoS One 5, e9678. https://doi.org/10.1371/journal.pone.0009678 https://doi.org/.

Chen, D.S., Chan, K.M., 2011. Differentially expressed proteins in zebrafish liver cells exposed to copper. Aquat. Toxicol. 104, 270–277. https://doi.org/10.1016/j.aquatox.2011.05.004 https://doi.org/.

Chua, A.C.Y., Ananthanarayanan, A., Ong, J.J.Y., Wong, J.Y., Yip, A., Singh, N.H., Qu, Y., Dembele, L., McMillian, M., Ubalee, R., et al., 2019. Hepatic spheroids used as an in vitro model to study malaria relapse. Biomaterials 216, 119221. https://doi.org/10.1016/j.biomaterials.2019.05.032 https://doi.org/.

Cosnefroy, A., Brion, F., Maillot-Maréchal, E., Porcher, J.M., Pakdel, F., Balaguer, P., Aït-Aïssa, S., 2012. Selective activation of zebrafish estrogen receptor subtypes by chemicals by using stable reporter gene assay developed in a zebrafish liver cell line. Toxicol. Sci. 125, 439–449. https://doi.org/10.1093/toxsci/kfr297 https://doi.org/.

dit Faute, M.A., Laurent, L., Ploton, D., Poupon, M.F., Jardillier, J.C., Bobichon, H., 2002. Distinctive alterations of invasiveness, drug resistance and cell-cell organization in 3d-cultures of mcf-7, a human breast cancer cell line, and its multidrug resistant variant. Clin. Exp. Metastasis 19, 161–168. https://doi.org/10.1023/a:1014594825502 https://doi.org/.

Eide, M., Rusten, M., Male, R., Jensen, K.H., Goksoyr, A., 2014. A characterization of the zfl cell line and primary hepatocytes as in vitro liver cell models for the zebrafish (danio rerio). Aquat. Toxicol. 147, 7–17. https://doi.org/10.1016/j.aquatox.2013.11.023 https://doi.org/.

EU, 2010. Directive 2010/63/eu of the european parliament and of the council of 22 september 2010 on the protection of animals used for scientific purposes. Off J EU 276, 33–79.

Garcia-Reyero, N., Murphy, C.A., 2018. A Systems Biology Approach to Advancing Adverse Outcome Pathways for Risk Assessment, 1. Springer, Cham. https://doi.org/10.1007/978-3-319-66084-4.

Ghosh, C., Zhou, Y.L., Collodi, P., 1994. Derivation and characterization of a zebrafish liver cell line. Cell Biol. Toxicol. 10, 167–176. https://doi.org/10.1007/bf00757560 https://doi.org/.

Godoy, P., Hewitt, N.J., Albrecht, U., Andersen, M.E., Ansari, N., Bhattacharya, S., Bode, J.G., Bolleyn, J., Borner, C., Bottger, J., et al., 2013. Recent advances in 2d and 3d in vitro systems using primary hepatocytes, alternative hepatocyte sources and non-parenchymal liver cells and their use in investigating mechanisms of hepatotoxicity, cell signaling and adme. Arch. Toxicol. 87, 1315–1530. https://doi.org/10.1007/s00204-013-1078-5 https://doi.org/.

Grimaldi, M., Boulahtouf, A., Delfosse, V., Thouennon, E., Bourguet, W., Balaguer, P., 2015. Reporter cell lines for the characterization of the interactions between human nuclear receptors and endocrine disruptors. Front. Endocrinol (Lausanne) 6, 62. https://doi.org/10.3389/fendo.2015.00062 https://doi.org/.

Han, J., Farnsworth, R.L., Tiwari, J.L., Tian, J., Lee, H., Ikonomi, P., Byrnes, A.P., Goodman, J.L., Puri, R.K., 2006. Quality prediction of cell substrate using gene expression profiling. Genomics 87, 552–559. https://doi.org/10.1016/j.ygeno.2005.11.017 https://doi.org/.

Hao, R., Bondesson, M., Singh, A.V., Riu, A., McCollum, C.W., Knudsen, T.B., Gorelick, D. A., Gustafsson, J.A., 2013. Identification of estrogen target genes during zebrafish embryonic development through transcriptomic analysis. PLoS One 8, e79020. https://doi.org/10.1371/journal.pone.0079020 https://doi.org/.

Hara, A., Hiramatsu, N., Fujita, T., 2016. Vitellogenesis and choriogenesis in fishes. Fish. Sci. 82, 187–202. https://doi.org/10.1007/s12562-015-0957-5 https://doi.org/.

Hirschhaeuser, F., Menne, H., Dittfeld, C., West, J., Mueller-Klieser, W., Kunz-Schughart, L.A., 2010. Multicellular tumor spheroids: an underestimated tool is catching up again. J. Biotechnol. 148, 3–15. https://doi.org/10.1016/j.jbiotec.2010.01.012 https://doi.org/.

Jung, H.-.R., Kang, H.M., Ryu, J.-.W., Kim, D.-.S., Noh, K.H., Kim, E.-.S., Lee, H.-.J., Chung, K.-.S., Cho, H.-.S., Kim, N.-.S., et al., 2017. Cell spheroids with enhanced aggressiveness to mimic human liver cancer in vitro and in vivo. Sci. Rep. 7, 10499. https://doi.org/10.1038/s41598-017-10828-7 https://doi.org/.

Kari, G., Rodeck, U., Dicker, A.P., 2007. Zebrafish: an emerging model system for human disease and drug discovery. Clin. Pharmacol. Ther. 82, 70–80. https://doi.org/10.1038/sj.clpt.6100223 https://doi.org/.

Kayo, D., Zempo, B., Tomihara, S., Oka, Y., Kanda, S., 2019. Gene knockout analysis reveals essentiality of estrogen receptor beta1 (esr2a) for female reproduction in medaka. Sci. Rep. 9, 8868. https://doi.org/10.1038/s41598-019-45373-y https://doi.org/.

Kim, D.-.S., Ryu, J.-.W., Son, M.-.Y., Oh, J.-.H., Chung, K.-.S., Lee, S., Lee, J.-.J., Ahn, J.-.H., Min, J.-.S., Ahn, J., et al., 2017. A liver-specific gene expression panel predicts the differentiation status of in vitro hepatocyte models. Hepatology 66, 1662–1674. https://doi.org/10.1002/hep.29324 https://doi.org/.

Kim, S.A., Tai, C.-.Y., Mok, L.-.P., Mosser, E.A., Schuman, E.M., 2011. Calcium-dependent dynamics of cadherin interactions at cell–cell junctions. Proc. Natl. Acad. Sci. 108, 9857–9862. https://doi.org/10.1073/pnas.1019003108 https://doi.org/.

Le Fol, V., Aït-Aïssa, S., Sonavane, M., Porcher, J.M., Balaguer, P., Cravedi, J.P., Zalko, D., Brion, F, 2017. In vitro and in vivo estrogenic activity of bpa, bpf and bps in zebrafish-specific assays. Ecotoxicol. Environ. Saf. 142, 150–156. https://doi.org/10.1016/j.ecoenv.2017.04.009 https://doi.org/.

Lu, H., Cui, Y., Jiang, L., Ge, W., 2017. Functional analysis of nuclear estrogen receptors in zebrafish reproduction by genome editing approach. Endocrinology 158, 2292–2308. https://doi.org/10.1210/en.2017-00215 https://doi.org/.

Luebke-Wheeler, J.L., Nedredal, G., Yee, L., Amiot, B.P., Nyberg, S.L., 2009. E-cadherin protects primary hepatocyte spheroids from cell death by a caspase-independent mechanism. Cell Transplant 18, 1281–1287. https://doi.org/10.3727/096368909x474258 https://doi.org/.

MacRae, C.A., Peterson, R.T., 2015. Zebrafish as tools for drug discovery. Nat. Rev. Drug Discov. 14, 721–731. https://doi.org/10.1038/nrd4627 https://doi.org/.

Menuet, A., Le Page, Y., Torres, O., Kern, L., Kah, O., Pakdel, F., 2004. Analysis of the estrogen regulation of the zebrafish estrogen receptor (er) reveals distinct effects of eralpha, erbeta1 and erbeta2. J. Mol. Endocrinol. 32, 975–986. https://doi.org/10.1677/jme.0.0320975 https://doi.org/.

Mills, L.J., Chichester, C., 2005. Review of evidence: are endocrine-disrupting chemicals in the aquatic environment impacting fish populations? Sci. Total Environ. 343, 1–34. https://doi.org/10.1016/j.scitotenv.2004.12.070 https://doi.org/.

OECD, 1992. Test no. 210: Fish, Early-Life Stage Toxicity Test. OECD Publishing.

OECD, 1998. Test no. 212: Fish, Short-Term Toxicity Test on Embryo and Sac-Fry Stages. OECD Publishing.

OECD, 2000. Test no. 215: Fish, Juvenile Growth Test. OECD Publishing.

OECD (2009). Test no. 230: 21-day Fish assay: A Short-Term Screening for Oestrogenic and Androgenic activity, and Aromatase Inhibition.

OECD (2012). Test no. 229: Fish Short Term Reproduction Assay.

OECD (2015). Test no. 240: Medaka extended One Generation Reproduction Test (meogrt).

Park, C.G., Sung, B., Ryu, C.S., Kim, Y.J., 2020. Mono-(2-ethylhexyl) phthalate induces oxidative stress and lipid accumulation in zebrafish liver cells. Comp. Biochem. Physiol. C Toxicol. Pharmacol. 230, 108704 https://doi.org/10.1016/j.cbpc.2020.108704 https://doi.org/.

Pinto, C., Hao, R., Grimaldi, M., Thrikawala, S., Boulahtouf, A., Aït-Aïssa, S., Brion, F., Gustafsson, J., Balaguer, P., Bondesson, M., 2019. Differential activity of bpa, bpaf and bpc on zebrafish estrogen receptors in vitro and in vivo. Toxicol. Appl. Pharmacol. 380, 114709 https://doi.org/10.1016/j.taap.2019.114709 https://doi.org/.

Ramaiahgari, S.C., den Braver, M.W., Herpers, B., Terpstra, V., Commandeur, J.N., van de Water, B., Price, L.S., 2014. A 3d in vitro model of differentiated hepg2 cell spheroids with improved liver-like properties for repeated dose high-throughput toxicity studies. Arch. Toxicol. 88, 1083–1095. https://doi.org/10.1007/s00204-014-1215-9 https://doi.org/.

Roehlen, N., Roca Suarez, A.A., El Saghire, H., Saviano, A., Schuster, C., Lupberger, J., Baumert, T.F, 2020. Tight junction proteins and the biology of hepatobiliary disease. Int. J. Mol. Sci. 21 https://doi.org/10.3390/ijms21030825 https://doi.org/.

Sanderson, J.T., 2006. The steroid hormone biosynthesis pathway as a target for endocrine-disrupting chemicals. Toxicol. Sci. 94, 3–21. https://doi.org/10.1093/toxsci/kfl051 https://doi.org/.

Schmittgen, T.D., Livak, K.J., 2008. Analyzing real-time pcr data by the comparative c(t) method. Nat. Protoc. 3, 1101–1108.

Sever, R. and Glass, C.K. (2013). Signaling by nuclear receptors. Cold Spring Harbor Perspect. Biol. 5, a016709-a016709. doi:https://doi.org/ 10.1101/cshperspect.a016709.

Tingaud-Sequeira, A., Knoll-Gellida, A., Andre, M., Babin, P.J., 2012. Vitellogenin expression in white adipose tissue in female teleost fish. Biol. Reprod. 86, 38. https://doi.org/10.1095/biolreprod.111.093757 https://doi.org/.

Tung, Y.C., Hsiao, A.Y., Allen, S.G., Torisawa, Y.S., Ho, M., Takayama, S., 2011. High-throughput 3d spheroid culture and drug testing using a 384 hanging drop array. Analyst 136, 473–478. https://doi.org/10.1039/c0an00609b https://doi.org/.

van Roy, F., Berx, G., 2008. The cell-cell adhesion molecule e-cadherin. Cell. Mol. Life Sci. 65, 3756–3788. https://doi.org/10.1007/s00018-008-8281-1 https://doi.org/.

Wallace, R.A., Selman, K., 1985. Major protein changes during vitellogenesis and maturation of fundulus oocytes. Dev. Biol. 110, 492–498. https://doi.org/10.1016/0012-1606(85)90106-X https://doi.org/.

Zanoni, M., Piccinini, F., Arienti, C., Zamagni, A., Santi, S., Polico, R., Bevilacqua, A., Tesei, A., 2016. 3d tumor spheroid models for in vitro therapeutic screening: a systematic approach to enhance the biological relevance of data obtained. Sci. Rep. 6, 19103. https://doi.org/10.1038/srep19103 https://doi.org/.

8.3 Original Paper - Zebrafish liver cell cluster culture on collagen-based hydrogel

Environmental Science & Technology

pubs.acs.org/est

Article

Matrix Softness-Mediated 3D Zebrafish Hepatocyte Modulates Response to Endocrine Disrupting Chemicals

Kathryn M. Sullivan, Chang Gyun Park, John D. Ito, Mikhail Kandel, Gabriel Popescu, Young Jun Kim,* and Hyunjoon Kong*

Cite This: *Environ. Sci. Technol.* 2020, 54, 13797−13806

Read Online

ACCESS | Metrics & More | Article Recommendations | Supporting Information

ABSTRACT: Endocrine disrupting chemicals (EDC) include synthetic compounds that mimic the structure or function of natural hormones. While most studies utilize live embryos or primary cells from adult fish, these cells rapidly lose functionality when cultured on plastic or glass substrates coated with extracellular matrix proteins. This study hypothesizes that the softness of a matrix with adhered fish cells can regulate the intercellular organization and physiological function of engineered hepatoids during EDC exposure. We scrutinized this hypothesis by culturing zebrafish hepatocytes (ZF-L) on collagen-based hydrogels with controlled elastic moduli by examining morphology, urea production, and intracellular oxidative stress of hepatoids exposed to 17β-estradiol. Interestingly, the softer gel drove cells to form a cell sheet with a canaliculi-like structure compared to its stiffer gel counterpart. The hepatoids cultured on the softer gel exhibited more active urea production upon exposure to 17β-estradiol and displayed faster recovery of intracellular reactive oxygen species level confirmed by gradient light interference microscopy (GLIM), a live-cell imaging technique. These results are broadly useful to improve screening and understanding of potential EDC impacts on aquatic organisms and human health.

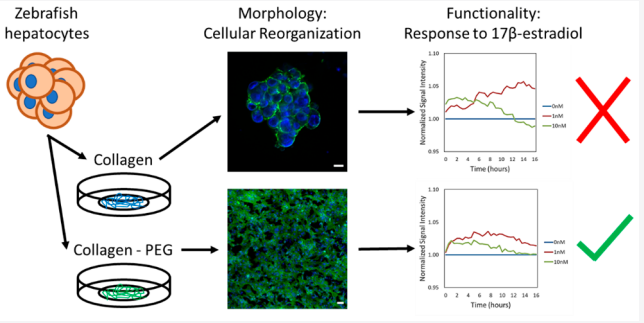

INTRODUCTION

For the last few decades, endocrine disrupting chemicals (EDCs) have been extensively used in various industrial and household products and medicine. It is well documented that the majority of endocrine disruption effects in fish field populations are due to exposure to natural and synthetic steroidal estrogens and their breakdown products such as 17β-estradiol.[1] Certain industrial chemicals also have shown an estrogenic activity. For example, bisphenol A is a precursor of polycarbonate plastics and resins.[2] Another chemical, di(2-ethylhexyl) phthalate, is used as a plasticizer of food packaging and medical devices.[3] The subsequent increase in EDC levels in the river and potential drinking water prompted efforts to understand their impacts on the human endocrine system. EDCs may disrupt endocrine pathways through mimicking naturally occurring hormones or by blocking receptors. As they are transported into the liver for metabolic degradation, chronic exposure can result in nonalcoholic fatty liver disease which severely impacts metabolism, potentially leading to cirrhosis or cancer.[4] Thus, a platform must be developed to test chemical substitutes for their potentially adverse effects on liver morphology and function.

One common way to examine the potential toxicity of EDCs is through the examination of the zebrafish (*Danio rerio*), a standard testing fish species for biomonitoring due to their small size, easy cultivation, and transparent embryos. As EDCs are accumulated in the liver, the zebrafish liver would be an ideal organ to develop into an *in vitro* platform. Zebrafish sensitivity to toxins in the water is evaluated by examining damage in the DNA or chromosomes, P450 detoxification activity, and endocrine activity at the RNA level.[5] Endocrine disruption is not species-specific; therefore, EDC effects are widespread and often irreversible.[6,7] Many studies report the zebrafish liver would make a useful model for accurate prediction of both endocrine effects and reproductive toxicity.[5,8,9]

With the movement away from animal models due to ethical reasons and tight regulations on their captivity, an alternative way to test the potential toxicity of current and newly developed EDCs without using the "live" zebrafish is necessary,[14] especially for the cosmetic industry due to the complete ban of animal testing in the European Union since 2013.[15] Consequently, efforts have been increasingly made to engineer an *in vitro* 3D hepatic platform that recapitulates anatomical and physiological

Received: March 30, 2020
Revised: August 7, 2020
Accepted: September 25, 2020
Published: September 25, 2020

https://dx.doi.org/10.1021/acs.est.0c01988
Environ. Sci. Technol. 2020, 54, 13797−13806

function of liver to test the potential impacts of chemical compounds on liver function. In particular, spheroids formed from primary trout hepatocytes were found to present canalicular structures and have similar gene expression profiles as *in vivo* trout livers, as long as the spheroids matured for 25 days.[16] Additionally, there have been efforts to create *in vitro* liver models that closely predict human metabolism and match *in vivo* clearance rates when exposed to common pharmaceuticals like propanolol.[17] Despite challenges such as extended culture periods, these results show promising advances in replacing fish models *in vitro*.

Many approaches of 2D cell culture were focused on culturing primary liver cells or cell lines into clusters using an ultra-low-adhesion dish or the hanging drop method. Other methods culture the cells on a flat surface like tissue culture plastic or glass coated with extracellular matrix proteins. However, cells isolated from tissues lose their phenotypes quickly through uncontrolled dedifferentiation.[10] It is suggested that liver cells would exhibit a reasonable reorganizational period by placing cells into a physiologically similar microenvironment. Ultimately, cells would form a more cohesive structure and well-defined functional units during the first couple of days. These insights have not been widely tested for assembling zebrafish liver hepatoids used for EDC toxicology studies.

However, studies made with hydrogel coupled with cell-adherent proteins have shown positive effects of substrate softness on cell viability and metabolic secretions in primary cells as compared to the unmodified gel.[11−13] In particular, rat primary hepatocytes cultured on heparin-PEG hydrogels with an elastic modulus of 2.3 kPa showed higher cell viability, albumin secretion, and urea secretion than cells cultured on stiffer heparin-PEG hydrogels.[11] In addition, mouse primary hepatocytes on collagen-polyacrylamide hydrogels with an elastic modulus of 140 Pa showed significantly higher albumin production and HNF4α expression, a transcriptional regulatory factor that is critical in normal liver development and maintaining normal liver functions, than those cultured on a stiffer hydrogel.[13] These studies state that the elastic modulus of the substrate on which hepatocytes are cultured is an extracellular factor of modulating hepatocyte function and structure in an *in vitro* culture.

In this study, we hypothesized that the softness of a matrix modulates whether zebrafish hepatocytes can regulate their intercellular organization. In turn, the response of the resulting "hepatoid-like cluster" (hepatoid) to EDCs can be tuned through modulation of cell-matrix interactions. The matrix softness would mitigate the effects of EDCs on cellular detoxification activity through the urea cycle. We examined this hypothesis using 17β-estradiol as a model EDC,[18,19] and studied the morphology and metabolic activity of zebrafish hepatocytes cultured on collagen-based gels with two different elastic moduli of 14 and 256 Pa. We assessed cellular oxidative stress from 17β-estradiol by monitoring the reactive oxidative species activity in real-time using a fluorescent probe. The extent to which 17β-estradiol affects the detoxification activity of cells is monitored by the urea cycle activity of liver cells exposed to different concentrations of 17β-estradiol. Overall, this study aims to develop an advanced *in vitro* zebrafish liver and use it to understand the impact of EDCs on the physiological activities of urea and vitellogenin synthesis.

MATERIALS AND METHODS

ATCC Zebrafish Cell Culture. Zebrafish hepatocytes [ZF-L] (ATCC CRL-2643) were cultured in 50% Leibovitz's L-15, 35% Dulbecco's Modified Eagle Medium high glucose, and 15% Ham's F12, all without sodium bicarbonate and supplemented with 0.15 g/L sodium bicarbonate, 15 mM 4-(2-hydroxyethyl)-1-piperazineethanesulfonic acid (HEPES), 0.01 mg/mL bovine insulin, 5% heat-inactivated fetal bovine serum, and 0.5% trout serum (Caisson Laboratory). Cells were expanded in T-75 flasks and incubated at 28 °C and atmospheric carbon dioxide in a tabletop, low temperature incubator (Fisherbrand). We used cells with a passage number of 3 to 5 for hepatoid formation on gels with controlled elastic moduli. Media was formulated in the University of Illinois Cell Media Facility, except for the trout serum which was added separately, and the completed medium was not sterile filtered. Cells were cultured in T-75 flasks until about 80% confluent and cryopreserved using the culture medium supplemented with 10% heat-inactivated fetal bovine serum and 5% DMSO. Cells were cryopreserved in vapor phase liquid nitrogen.

Collagen-Polyethylene Glycol (PEG) Hydrogel Formation. Collagen-polyethylene glycol (collagen-PEG) hydrogels were prepared in 96-well plates via *in situ* cross-linking between collagen molecules by mixing PEG (Sigma, MW 7500) at mass ratios of 0 (pure collagen) and 10 to bovine Type I collagen (Advanced Biomatrix) in an equal volume of the zebrafish medium. Reconstitution solution containing 0.26 M sodium hydrogen carbonate, 0.2 M HEPES, and 0.04 M sodium hydroxide (Sigma) was added to modulate the pH of the gel to initiate gel formation. Hydrogels were then incubated at 37 °C and 5% CO_2 for 30 min. Cells were plated directly onto hydrogels at a cell density of 1.0×10^6 cells/mL and cultured for 14 days at 28 °C and atmospheric carbon dioxide. The media was replaced every two to three days.

Mechanical Analysis. The elastic modulus of the hydrogels was measured using a rheometer (DHR-3, TA Instruments). Collagen and collagen-PEG gels were prepared as previously described and loaded onto the parallel plate (diameter = 22 mm). The gap between the two plates was kept constant at 200 μm. The hydrogel was left for 20 min at 37 °C to gel. Then, the hydrogel was oscillated at 0.1% strain while varying frequency from 0.1 to 10 Hz. The resulting stress was measured to calculate elastic and loss moduli at individual frequency. The test was conducted in triplicate.

Scanning Electron Microscopy (SEM). Collagen and collagen-PEG hydrogels were formed in a 96-well plate as previously described. Then, they were removed with a spatula and slowly dehydrated in 30%, 50%, and 70% w/w ethanol−water solution for at least 1 h each and 100% ethanol overnight. The dehydrated gels were dried using the critical point dryer (Tousimis 931). SEM (Hitachi S4700) imaging was performed directly after drying the samples. First, the samples were mounted using copper tape and coated with a 6−8 nm layer of gold (EMITECH 575). Images were taken with an accelerating voltage of 2 kV, a working distance of 8−9 mm, and the emission current was adjusted to reduce sample damage.

The pore area and fiber diameter were measured using ImageJ software. For the pore area, an automatic threshold was applied to remove the background and the particle analyzer tool was used to measure pores that were larger than 1 um^2. The average pore area was calculated by dividing the total pore area by the area of collagen. Fiber diameter was directly measured, and at

https://dx.doi.org/10.1021/acs.est.0c01988
Environ. Sci. Technol. 2020, 54, 13797−13806

least 20 measurements were taken from each image. The statistical significance was calculated using the ANOVA test.

Immunofluorescence Imaging. Cells were cultured for two weeks on collagen or collagen-PEG hydrogels installed on glass bottom dishes (Cellvis). Then they were fixed with 1:1 v/v methanol and acetone at −20 °C for 20 min. Then, the samples were washed twice with room temperature phosphate buffered saline (PBS, Corning) for 5 min each. Cells were blocked with 2% bovine serum albumin for 1 h. Cells fixation using this method does not need an extra permeabilization step as permeabilization is obtained by acetone and methanol.

The cells were stained with phalloidin-Alexa 488 (Invitrogen) overnight at 4 °C (1:250) for the imaging of actin filaments and washed twice with PBS for 5 min each. 4′,6-Diamidino-2-phenylindole (DAPI) was incubated at room temperature for 1 min (1:500) and washed twice for 1 min each immediately before imaging.

For β1-integrin staining, the primary antibody P5D2 (Abcam) was incubated overnight at 4 °C. The sample was then washed twice with PBS for 5 min each. Then, the secondary antibody antimouse conjugated AF555 (Cell Signaling Technology, 4409S) was incubated for 4 h at room temperature. Then, the samples were washed with PBS twice for 5 min each. Finally, nuclei of the cells were imaged with DAPI immediately before imaging. Although the P5D2 antibody is noted as only reactive with human cells, according to the National Center for Biotechnology Information, zebrafish and humans are orthologs for β1 integrin which would suggest that the antibody will have cross-species reactivity.[20]

The images were taken using a four laser, point scanning confocal microscope (Zeiss LSM 700). The 10x/0.3 or the 20x/0.8 air objectives were used. Images of the cells were obtained using the tile scan feature. The pinhole for all channels was set to the size of one Airy unit for the DAPI channel. The line averaging was set to 8 times, and the pixel dwell time was set to 1.58 μs. Image acquisition and review were done through the Zeiss Zen (Black and Blue, respectively) programs.

Bicinchoninic Acid (BCA) Protein Assay. The Pierce BCA Protein Assay Kit (Thermo Fisher Scientific 23225) was used to determine the total protein concentration of the zebrafish hepatoid samples. The microplate protocol was followed using the instructions provided with the assay kit. Samples were tested in triplicate. Samples were collected from the culture on days 1, 7, and 14.

First, diluted albumin standards were made so that there was a range of standard from 0 to 2000 μg/mL of BSA concentration. Then, the working reagent was prepared by mixing 50:1 BCA reagent A to B. The solution was mixed to reduce turbidity to yield the clear, green color as described. The working reagent was prepared fresh, immediately before starting the assay.

Following the microplate procedure, 25 μL each of the standard and unknown were pipetted into a 96-well plate. Then, 200 μL of the working reagent was pipetted into each well and mixed thoroughly by pipet. The plate was covered, protected from light, and placed into an incubator at 37 °C for 30 min. Finally, the plate was cooled to room temperature and read at 562 nm wavelength on a plate reader (BioTek).

17β-Estradiol and Bisphenol A Treatment. Zebrafish hepatocytes were plated at a density of 1.0×10^6 cells/mL and cultured in the conditions as described above for 14 days. A stock solution of 17β-estradiol (E2) or bisphenol A (BPA) was prepared with a DMSO solution, 0.1 wt % in water. Then, for 24 h, the cells were exposed to 0, 1, or 10 nM of 17β-estradiol (E2) or bisphenol A (BPA) in cell culture media. The cells were analyzed after the 24-h exposure period.

Urea Colorimetric Assay. Cell culture media was collected from each condition and stored at −20 °C for short-term storage until testing. The low concentration urea assay kit (BioVision K375) was used to determine the urea cycle activity. The media samples and kit components were first warmed to room temperature. Then, in a 96-well plate, the standard curve and samples were prepared according to the manufacturer's instructions. Each condition was tested in triplicate. The colorimetric output was read at 570 nm using a plate reader (BioTek). Then, the data was analyzed with an ANOVA test to determine significance.

The media was collected from each condition and stored at −5 °C until it was used for experiments. Urea synthesis was assayed in cell culture medium using the urea assay kit (MAK006, Sigma-Aldrich, Steinheim, Germany). A standard curve was created to generate 0, 1, 2, 3, 4, and 5 nmol urea/well. Then, 50 uL of the media was applied to the 96 wells for urea quantification according to the manufacturer's instruction. The colorimetric product was measured at wavelengths of 570 nm using a microplate reader (TECAN, Männedorf, Switzerland). Each condition was tested in triplicate, and statistical significance was measured using an ANOVA test.

Vitellogenin (VTG) Measurements and Immunofluorescent Staining. Vitellogenin was measured in cell pellets using an ELISA kit (10004995; Cayman Chemical, Ann Arbor, MI, USA). A cell concentration of 1.0×10^6 cells/mL was seeded on collagen and collagen-PEG coated well plates and cultured for 14 days. Then, the cells were exposed to 1 nM of 17β-estradiol (Sigma-Aldrich) and 10 μM of BPA (Sigma-Aldrich) for 48 h, respectively. The cell pellets were collected in 1.5 mL tubes and centrifuged for 5 min at 125 × g, and the supernatants were discarded and washed with cold PBS. The pellets were lysed with passive lysis buffer (Promega, Mannheim, Germany) after recentrifugation. The supernatants were used for the vitellogenin quantification according to the manufacturer's instructions (Cayman Chemical). Each sample was normalized by total protein content, which was calculated using the BCA protein assay. The ANOVA test was run to determine significance of the results for the hepatoids cultured on the collagen-PEG hydrogel.

For vitellogenin staining, the primary antibody vitellogenin (LifeSpan, LS-C76845−100) was incubated overnight at 4 °C. The sample was then washed twice with PBS for 5 min each. Subsequently, the secondary antibody antimouse conjugated FITC (Thermo, 31232) was incubated for 2 h at room temperature. Then, the samples were washed with PBS three times every 5 min. Finally, nuclei of the cells were stained with DAPI immediately before imaging.

Live Cell Imaging with 17β-Estradiol. Glass bottom dishes (29 mm diameter), the well (14 mm diameter), #0 glass, and the glass top (D29-14-0-TOP, Cellvis) were first coated with poly-D-lysine (Sigma) for 20 min and then washed twice with culture media to remove excess chemical. Zebrafish hepatocytes (ATCC CRL-2643) were seeded at 5000 cells per dish and allowed to adhere for 10 min before being coated by collagen or collagen-PEG hydrogel as described above. Cells were cultured in this manner because of the short working distance of the microscope objective. Therefore, cells needed to be cultured as close to the glass coverslip as possible. After the hydrogel was formed, 3 mL of culture media was added and the cells were incubated in the conditions previously described. The

https://dx.doi.org/10.1021/acs.est.0c01988
Environ. Sci. Technol. 2020, 54, 13797−13806

cells were then cultured for 2 days prior to the live cell imaging experiment to ensure that the cells were interacting with the hydrogel and each other without forming large clustered structures. Thus, individual cell ROS levels could be analyzed.

Before imaging, zebrafish culture medium with 0, 1, and 10 nM of 17β-estradiol (Sigma-Aldrich) replaced the media and 6 μL/3 mL of CellROX Green Reagent (Thermo Fisher Scientific) was added to each sample. Co-localized fluorescence and phase imaging was performed on an Axio Observer Z1 (Zeiss) with GLIM Pro add-on module (Phi Optics). Gradient light interference microscopy is an upgrade to differential interference contrast microscopy that uses phase-shift shifting to improve image quality by separating unwanted amplitude information from high detail phase information.[21] Here, we use a 10x/0.3 objective and sCMOS camera (Prime BSI, Photometrics). Imaging began 20 min after addition of the CellRox dye with a total of 18 representative fields of view (1150 × 1150 μm) acquired every 30 min for 16 h.

The images were then analyzed with ImageJ (Fiji) to measure signal intensity from the CellROX reagent as well as to overlay the GLIM and fluorescent images. To measure the intensity, images from the same sample were loaded into ImageJ as a sequence in chronological order. Then, a region of interest (ROI) was enclosed using an oval, ensuring that the entire cell cluster or single cell was within the boundaries of the ROI for the entire set of images. Using the stacks menu, the Z-axis profile was plotted, and the values were exported to Excel for further analysis. The Z-axis profile plots the mean gray signal of the ROI. At least 10 ROI were chosen per sample. In Excel, the data was averaged and normalized to the control sample of 0 nM 17β-estradiol for each hydrogel modulus, respectively.

RESULTS AND DISCUSSION

Increasing the pH of the pre-gelled collagen solution and the collagen-polyethylene glycol (PEG) mixture from 2.0 to 7.4 resulted in the collagen gel and collagen-PEG gel, respectively. Both hydrogels are made with interconnected fibrous networks as confirmed by scanning electron microscope images (Figure 1). The PEG in the collagen-PEG gel altered the diameter and spacing of collagen fibers minimally compared with the pure collagen gel (Table 1). In contrast, the elastic modulus of the PEG-collagen gel was 14 Pa while that of the pure collagen gel was 256 Pa. This result confirms that PEG modulates the mechanical stiffness of the collagen gel without altering the microstructure significantly.

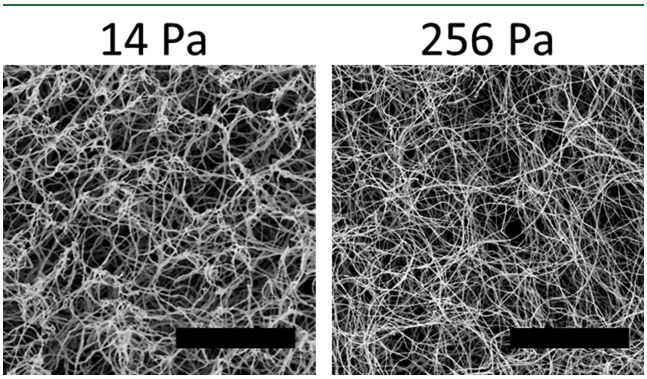

Figure 1. Two hydrogels were formulated; pure collagen and collagen mixed with polyethylene glycol (PEG) and imaged with scanning electron microscopy. The black scale bars represent 5 μm.

Table 1. Collagen Hydrogel Shear Moduli and Microstructure Properties[a]

PEG/Collagen (m/m)	Shear modulus (Pa)	Fiber diameter (μm)	Pore area (μm^2)
10:1	14 ± 1	0.10 ± 0.02	053 ± 0.21
0:1	256 ± 132	0.09 ± 0.02	0.38 ± 0.19

[a]The shear modulus was decreased from 256 to 14 Pa with the addition of PEG at a mass matio of PEG to collagen being 10:1. The concentration fo collagen was held constant for both hydrogel formulations at 1.5 ng/ mL. The asterisk indicates statistical significance of the difference of values between two conditions (*p < 0.02).

This collagen-PEG hydrogel system allows for the control of the elastic modulus without significantly altering other matrix parameters like the pore area and fiber diameter. Microscopic images of the gel confirm that there is no significant difference in microstructure, independent of the change in softness. As analyzed previously,[22] it is likely that PEG depletes the hydrogen bonds between water molecules and collagen fibers, which are major components to generate the elastic properties of the gel. As the free water molecules are depleted, the fibrillogenesis of the collagen fibers is hindered, resulting in a softer hydrogel. Such change of the intermolecular association at the molecular scale may influence the stiffness of individual collagen fibers but may not impact the pore size of the gel. This strategy to control gel softness is different from other formulations, in that the PEG act as spacers between the collagen fibers instead of being used to chemically cross-link collagen molecules.[23,24]

The zebrafish hepatocytes were seeded onto the gels with controlled elastic moduli. Then, cell growth was monitored for two weeks by measuring the total protein concentrations with a BCA protein assay kit (Figure 2a). The total protein concentration was increased at a comparable rate regardless of the elastic modulus of the gel. In contrast, the elastic modulus of the gel influenced cellular organization. Cells cultured on the pure collagen gel with an elastic modulus of 256 Pa proliferated independently or in small clusters (Figure 2c-iv). However, cells cultured on the softer collagen-PEG gel with an elastic modulus of 14 Pa aggregated to form a large cell sheet (Figure 2c-i). More interestingly, the cells self-organized on the collagen-PEG gel to form a hollow lumen, or canaliculus (Figure 2c-ii,iii). In addition, actin molecules were localized on the cell membrane more significantly than cells cultured on the stiffer pure collagen gel. Furthermore, cells cultured on the softer collagen-PEG gel expressed more β1 integrins than those cultured on the pure collagen gel (Figure 2b,d).

To further clarify that the zebrafish hepatoid ultrastructure was a direct result of the elastic modulus of the hydrogel, singularized hepatocytes were pre-exposed to PEG prior to plating (Figure S1). After 14 days of culture, the cells were immunostained for actin filaments as well as β1 integrin expression. The cells pre-exposed to the PEG, which is the same PEG used to assemble the collagen-PEG hydrogels, did not show significant changes in actin or integrin expression from cells plated on the collagen-PEG hydrogel without pre-exposure to the soluble PEG. In addition, cells pre-exposed to PEG formed canaliculi-like structures, like cells that were not pre-exposed to the soluble PEG. Thus, it is suggested that the PEG that is present in the collagen-PEG hydrogel acts as a neutral softener with minimal interactions with the zebrafish hepatocytes during hepatoid formation.

https://dx.doi.org/10.1021/acs.est.0c01988
Environ. Sci. Technol. 2020, 54, 13797−13806

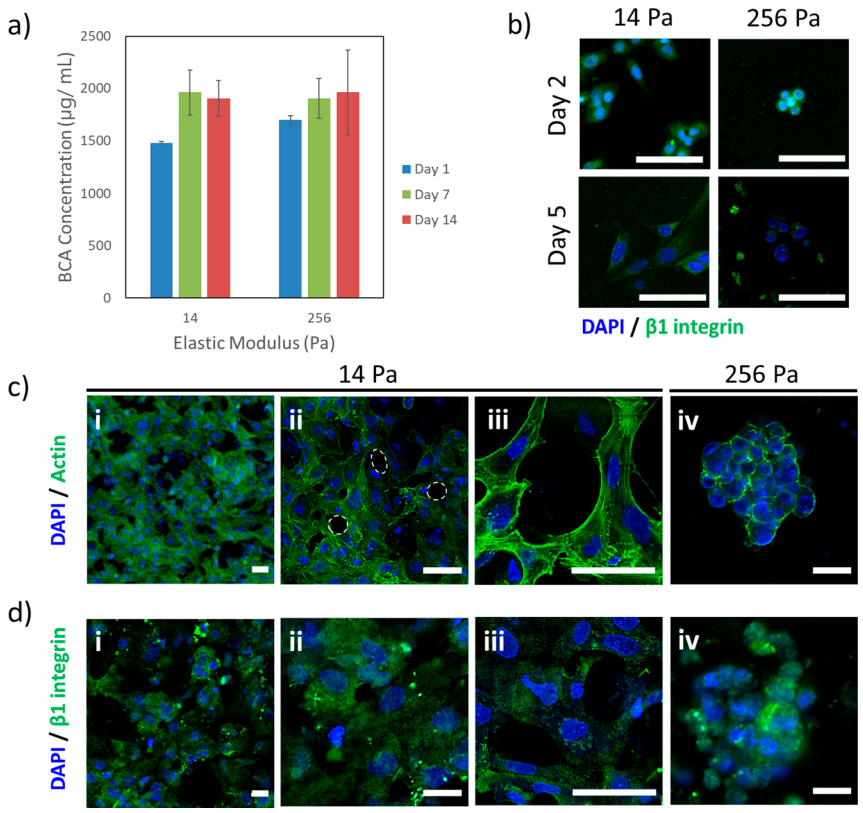

Figure 2. Zebrafish hepatocytes (ATCC CRL-2643) cultured on the collagen and collagen-PEG gels with different elastic moduli. (a) The total protein concentration assay after 1, 7, and 14 days of culture. The values and error bars represent the mean and standard deviation of three samples per condition, respectively. (b) Immunofluorescent staining of hepatocytes at days 2 and 5 for blue-colored nuclei and green-colored β1 integrin. (c and d) Immunofluorescent staining of hepatocytes after 14 days of culture on the gel. The images in part c show blue-colored nuclei and green-colored actin filament in cells cultured on the pure collagen gel with an elastic modulus of 14 Pa (i, ii) and collagen-PEG gel with an elastic modulus of 256 Pa (iii). White dashed circles mark hollow lumen formed by the self-organization of hepatocytes. The images in part d show blue-colored nuclei and green-colored β1 integrin in cells cultured on the pure collagen gel with an elastic modulus of 14 Pa (i, ii) and collagen-PEG gel with an elastic modulus of 256 Pa (iii). In each image, white scale bars represent 50 μm.

When observing the β1 integrin expression, which indicates cellular adhesion to the matrix, the softer collagen-PEG hydrogel served to increase the β1 integrin expression of cells than the stiffer, pure collagen hydrogel. Previous studies report that cell clusters formed or placed on a bioactive 2D substrate sense and respond to biophysical properties of the matrix via integrin-ligand bonds and cell−cell junctions.[25,26] As such, we suggest that hepatocytes bound to collagen molecules of the softer gel sense the mechanical signal from the substrate, increase cellular adhesion and growth, and finally form a cell sheet in which cells are interconnected to form the canaliculi-like structure. Cells homogeneously mixed into the hydrogel failed to associate with each other, thus resulting in few clusters with the physiologically relevant ultrastructure. These results indicate that the cells cultured on the 14 Pa collagen-PEG hydrogel were the most physiologically organized even though there was an independency of cell growth on the gel stiffness.

This study demonstrates that the softness of the collagen-PEG hydrogel plays a significant role in regulating the intercellular organization of engineered zebrafish hepatoids. *Ex vivo* cells frequently de-differentiate when cultured on a substrate which has a different modulus from the native tissue. By plating the hepatocytes onto a soft hydrogel with stiffness relatable to the yolk of the zebrafish egg, cells will experience biophysical cues which will result in hepatoids with higher physiological relevance. In particular, mouse hepatocytes cultured on stiffer collagen-polyacrylamide hydrogels exhibited larger cell areas and decreased expression of HNF4α, a transcriptional regulatory factor.[13] Because this factor controls many downstream factors and functions, the culturing of mouse hepatocytes on stiff substrates results in reduced hepatocyte function. Specifically, functional mRNA expression levels of *Baat*, *F7*, and *Gys2* are lowered in addition to that of HNF4α, according to the previous study made with mouse hepatocytes.

Compared with this study, the cells cultured on the softer gel, with an elastic modulus of 14 Pa, formed cohesive sheet-like structures with a canaliculi-like intercellular organization as seen in the actin staining images (Figure 2c). Canaliculi eventually fuse to form bile ducts in the adult zebrafish.[9,27] The bile ducts and blood vessels are jointly responsible for clearing metabolic waste from the hepatocytes.[8,28] In contrast, the hepatocytes on the stiffer collagen hydrogel, with an elastic modulus of 256 Pa, formed separated, small cell clusters. With the introduction of the hepatocytes into a softer microenvironment, the organotypic 3D organization resembled that of a zebrafish liver.

The physiological activity of hepatocytes cultured on the gels was analyzed by examining the ornithine-urea cycle, which is the primary pathway to detoxify ammonia and amino acids in the liver. Cells were analyzed at 27 °C and 37 °C, which represents the zebrafish and human body temperature, respectively (Figure 3). Cellular hepatic cycle activity increased with the cell culture period. After 2 weeks, cells cultured on the collagen-PEG gel

https://dx.doi.org/10.1021/acs.est.0c01988
Environ. Sci. Technol. 2020, 54, 13797−13806

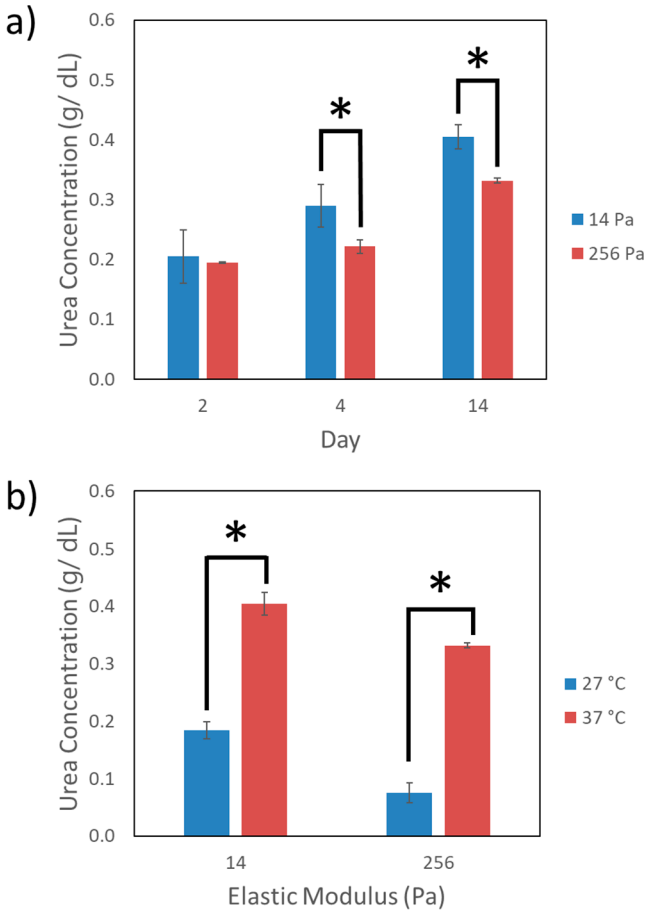

Figure 3. Analysis of urea cycle activity for zebrafish hepatocytes cultured on the gels with different elastic moduli. (a) The urea concentration was measured after 2, 4, and 14 days of culture. (b) Comparison of the urea cycle activity was made between 27 °C and 37 °C to evaluate the effects of environmental temperature. The values and error bars represent the mean and standard deviation of three samples per condition, respectively. The asterisk indicates statistical significance of the values between conditions ($*p < 0.05$).

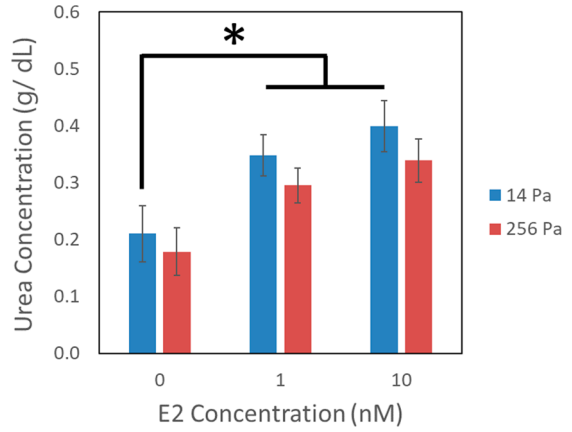

Figure 4. Analysis of hepatic urea cycle activity of zebrafish hepatocytes. Cells were cultured on the collagen gel with an elastic modulus of 14 Pa and the collagen-PEG hydrogel with an elastic modulus of 256 Pa for 2 weeks before exposure to 17β-estradiol (E2). Then, cells were exposed to 0, 1, and 10 nM of E2 for 24 h. The values and error bars represent the mean and standard deviation of three samples per condition, respectively. The asterisk indicates statistical significance of the values between conditions ($*p < 0.05$).

with an elastic modulus of 14 Pa displayed higher hepatic urea activity than those on the pure collagen gel with an elastic modulus of 256 Pa (Figure 3a). The inverse dependency of hepatic urea activity on the elastic modulus was more significant at 37 °C (Figure 3b).

We further assessed the extent to which the elastic modulus of the gel modulates hepatic urea cycle activities at varied concentrations of 17β-estradiol (E2). E2 binds with estrogen receptors to produce vitellogenin (VTG) in the female zebrafish, and its concentration is regulated in the liver through biotransformation.[29] E2 stimulated the hepatic urea cycle activity as displayed, with an increase of the urea concentration with increasing E2 concentration (Figure 4). Interestingly, the dependency of the urea cycle activity on the E2 concentration was more substantial with cells cultured on the collagen-PEG gel with an elastic modulus of 14 Pa than those cultured on the pure collagen gel with an elastic modulus of 256 Pa. Such an inverse dependency of the urea concentration on the elastic modulus of the gel is attributed to the cellular β1 integrin expression increased with the softer gel.

In addition, as shown in Figure 5, bisphenol A (BPA) and E2 were found to have effective VTG responses in the zebrafish hepatocyte clusters formed on collagen and collagen-PEG hydrogels. The hepatocytes cultured in a 2D monolayer on a polystyrene substrate did not markedly induce VTG production in the presence of E2 or BPA (Figure 5a). In contrast, zebrafish hepatocyte clusters formed on collagen-PEG hydrogels with an elastic modulus of 14 Pa resulted in significant increases of VTG activity at a concentration of 10 nM of E2 or 10 μM of BPA. Hepatocyte clusters formed on the collagen gel with an elastic modulus of 256 Pa showed minimal VTG activities after exposure to E2 or BPA, similar to cells cultured on a polystyrene substrate (Figure 5b).

VTG is the serum phospholipoglycoprotein precursor to egg yolk. It is potentially an ideal biomarker for environmental estrogens because estrogen receptors in the fish liver regulate vitellogenesis.[30] VTG is typically found in the blood of female fish, whereas in male fish, the level is very low. However, VTG synthesis can be induced in male fish if they are exposed to exogenous estrogens.[31] Therefore, the presence of VTG in a male fish can be considered a sensitive biomarker of estrogenic chemical exposure.[32] Therefore, E2 is considered to represent EDCs in the environmental system, and the synthesis of VTG in aquatic organisms is a very important marker for assessing endocrine disturbances by natural hormones and EDCs.

A previous study by the US Environmental Protection Agency (EPA) and the US National Toxicology Program (NTP) set 75 μM (17.2 mg/L) as the maximum BPA concentration detected in an environmental sample.[33] In addition, François Brio et al. showed that 10 μM of BPA revealed maximum estrogenic activity of the estrogen receptor and aromatase in zebrafish hepatocytes and larvae.[34] Therefore, zebrafish hepatocytes were exposed to either E2 or BPA. BPA stimulates estrogenic activity of hepatocyte clusters similar to E2. This result suggests that zebrafish hepatoids similarly metabolize both chemicals into VTG. However, the effect is significantly different depending on the substrate on which the zebrafish hepatocytes are cultured. The hepatoids cultured on the pure collagen hydrogel with an elastic modulus of 256 Pa did not respond to the EDCs as the hepatoids on the collagen-PEG hydrogels. From the earlier result, hepatoids on the stiffer hydrogel had disorganized tissue structure in comparison to the hepatoids cultured on the softer

https://dx.doi.org/10.1021/acs.est.0c01988
Environ. Sci. Technol. 2020, 54, 13797−13806

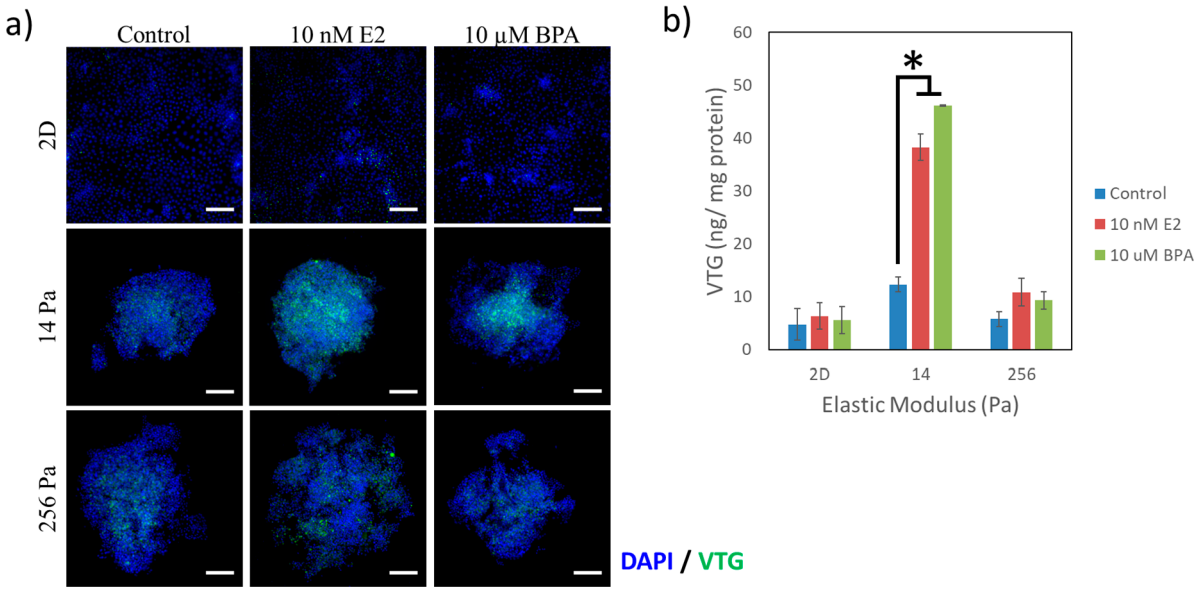

Figure 5. Analysis of the vitellogenin (VTG) in zebrafish hepatocytes after 14 days of culture on a 2D polystyrene substrate, collagen-PEG (elastic modulus ~ 14 Pa), and collagen (elastic modulus ~ 256 Pa) hydrogels. Immunofluorescent staining with DAPI (blue) and VTG (green) of zebrafish hepatocytes exposed to 10 nM of E2 or 10 μM of BPA for 24 h (a). The VTG concentrations as measured with ELISA (b). The white scale bars indicate 100 μm. The asterisk indicates statistical significance of the values between conditions (*$p < 0.01$).

hydrogels (Figure 2c). Therefore, the difference in VTG synthesis levels could be because physiologically similar tissue organization promotes high levels of hepatoid functionality. Thus, the disorganized cells on the 2D plastic substrate and the disorganized hepatoid formed on the pure collagen hydrogel had low responses to EDC exposure. It is likely that the rate of estrogenic activity is altered by the substrate stiffness. This possibility will be examined systematically in future studies.

The combined effects of estrogen concentration and gel softness on the cellular urea production are further related to the change in the ROS-mediated intracellular oxidative stress level. As the liver induces VTG synthesis using the excess E2, cells produce ROS which impacts cells negatively. In particular, we evaluated the general oxidative stress of the cells by monitoring the intracellular ROS level through the oxidation of the CellROX probe via live cell imaging for 16 h. This study discloses that hepatoid-like clusters formed on the softer collagen-PEG hydrogels are able to return the ROS level to a baseline at the elevated 17β-estradiol concentration. In contrast, cell clusters formed on the stiffer collagen hydrogel exhibited a higher ROS level for both elevated 17β-estradiol conditions. In addition, cell clusters showed a drop of ROS level below baseline when exposed to 10 nM 17β-estradiol, indicating that some of the cells likely lost viability and metabolic activities after exposure to excessive 17β-estradiol.

Because 17β-estradiol is localized in the liver for biotransformation into VTG, excessive accumulation from naturally produced and ingested 17β-estradiol will increase the generation of reactive oxygen species (ROS) through mitochondrial and genomic pathways. Live cell imaging was performed to visualize the ROS response of the zebrafish hepatocytes to 17β-estradiol using the positive signal from the CellROX reagent (Figure 6). The fluorescent intensity from the CellROX increases with increasing internal reactive oxygen species. The hepatocytes cultured on the gel with an elastic modulus of 14 Pa displayed consistent clustered cell morphology during the 16 h (Figure 6a). The fluorescent signal from the control conditions demonstrates the homeostatic level of ROS as a byproduct of metabolism and as a signaling molecule. As seen in all three concentrations of 17β-estradiol, the hepatocytes maintained their original morphology. The ROS signal marked by the oxidation of the fluorescent probe of the CellROX reagent was also consistent from 0 to 16 h. However, the morphology of the hepatocytes cultured on the stiffer gel with an elastic modulus of 256 Pa was changed rapidly during the 16 h after exposure to 17β-estradiol (Figure 6b). In particular, the change in morphology from spread to spheroidal was visible after 12 h of exposure to 1 nM 17β-estradiol (Figure 6b-v) and 6 h of exposure to 10 nM 17β-estradiol (Figure 6b-vi). Also, the hepatocytes exposed to 10 nM of 17β-estradiol lost most of the ROS intensity at 16 h.

The live images of ROS signal from the cells were then analyzed with the fluorescence signal intensity (Figure 6c,d). According to the quantitative analysis, even with a 0 nM concentration of 17β-estradiol, the zebrafish hepatocytes cultured on the hydrogel with an elastic modulus of 14 kPa exhibited lower ROS production than the cells cultured in the 256 Pa hydrogel (Figure 5c,d). When the concentration of 17β-estradiol was increased to 1 nM, the hepatocytes on the gel with an elastic modulus of 14 Pa showed an increase of the ROS signal up to 4 to 6 h, followed by the decrease of the intensity. In contrast, cells on the gel with an elastic modulus of 256 Pa displayed a steeper and continuous increase of the ROS signal up to 16 h.

Further increase of the 17β-estradiol concentration to 10 nM resulted in transient increases of ROS signal up to 2 h regardless of an elastic modulus of the gel. However, the hepatocytes cultured on the gel with an elastic modulus of 14 Pa showed a relatively slower increase in the ROS level than those on the gel with an elastic modulus of 256 Pa. In the stiffer hydrogel, ROS generation was decreased after 12 h, indicating that the cells were no longer functioning in metabolic degradation. Taken together, the cells cultured in the collagen-PEG hydrogel with a 14 Pa modulus were better able to metabolize the increased

https://dx.doi.org/10.1021/acs.est.0c01988
Environ. Sci. Technol. 2020, 54, 13797−13806

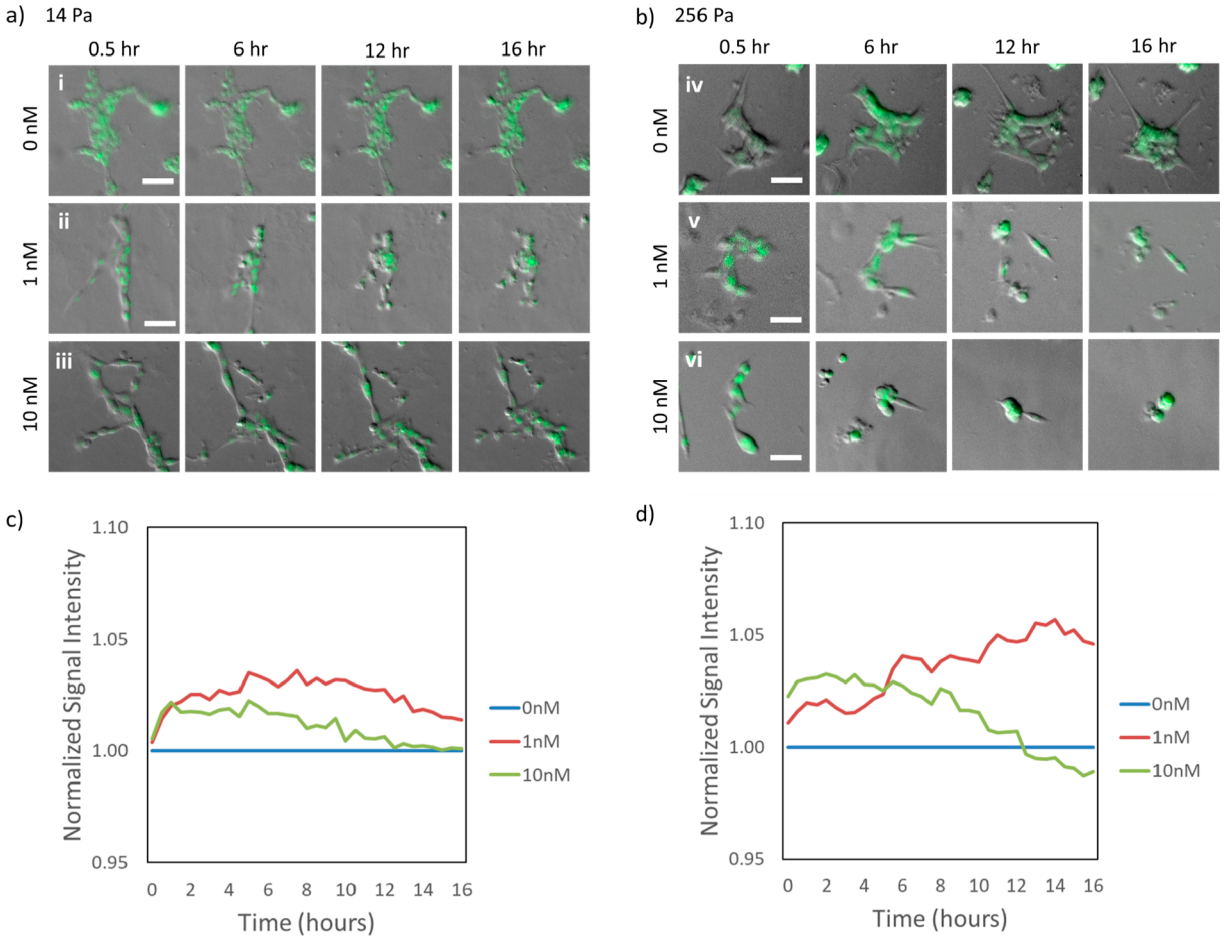

Figure 6. Live cell imaging of reactive oxygen species generation and morphology of zebrafish hepatocyte when exposed to 0 (i, iv), 1 (ii, v), and 10 (iii, vi) nM of 17β-estradiol. Images were taken every 30 min over 24 h after the addition of 17β-estradiol and CellROX reagent (green). The gray scale images are Gradient Light Interference Microscopy (GLIM) images showing the cellular morphology. (a) Zebrafish hepatocytes cultured on the collagen-PEG hydrogel with an elastic modulus of 14 Pa. (b) Zebrafish hepatocytes cultured in a pure collagen hydrogel with an elastic modulus of 256 Pa. The white scalebars indicate 40 μm. (c and d) The normalized signal intensity of CellROX for each hydrogel stiffness, 14 and 256 Pa, comparing their reactive oxygen species generation for increasing concentrations of 17β-estradiol. (c) The reactive oxygen species generation is increased for both 1 and 10 nM concentrations of 17β-estradiol in the 14 Pa hydrogel and the baseline ROS concentration is recovered after 5 h for the 1 nM concentration. (d) For the 256 Pa hydrogel, the ROS levels are increased in both concentrations of 17β-estradiol, but the ROS level drops below the control group after 12 h for the 10 nM concentration.

levels of 17β-estradiol without a significant impact on their morphology. In contrast, the hepatocytes cultured on the 256 Pa hydrogel demonstrated an early loss of functionality from elevated 17β-estradiol concentrations.

These experiments demonstrate an *in vitro* platform for the physiological impacts of endocrine-disrupting factors on zebrafish hepatoids that exhibited similar morphology and functionality as the live zebrafish. These hepatic tissues were engineered by the culturing of cells on the collagen-PEG gel with controlled stiffness while maintaining the pore area and fiber diameter of the hydrogels. The hepatocytes cultured on the collagen-PEG hydrogel with an elastic modulus of 14 Pa formed large sheets with intercellular canaliculi. In contrast, hepatocytes cultured on the pure collagen hydrogel with an elastic modulus of 256 Pa grew slowly without the formation of a cell sheet. Also, the hepatocytes cultured on the softer collagen-PEG hydrogel displayed elevated urea cycle activity and higher sensitivity to external 17β-estradiol than those cultured on the stiffer pure collagen gel. Overall, the cellular response to the gel is attributed to the difference of the gel softness.

Taken together, the results of this study report that the softness of the cell culture substrate plays a significant role in the assembly and physiological function of zebrafish hepatoids. The hepatoids engineered to present a canaliculi-like structure were active to restore intracellular ROS levels to normal by up-regulating detoxification activities upon exposure to 17β-estradiol. Since the zebrafish shares similar embryotic characteristics and homology as humans, the continued study of the zebrafish hepatoid would be beneficial to the understanding of human liver response to endocrine-disrupting chemicals such as 17β-estradiol. In addition, the results of this study will significantly impact current studies that are often plagued by the loss of morphology and functionality of live embryo or primary adult liver cells *in vitro*. Therefore, this study will be broadly useful in the development of an *in vitro* cell or organoid culture platform used for the rapid and precise screening of potentially toxic chemicals.

https://dx.doi.org/10.1021/acs.est.0c01988
Environ. Sci. Technol. 2020, 54, 13797−13806

ENVIRONMENTAL IMPLICATIONS

There are significant ethical and methodological concerns for using zebrafish as model organisms for testing EDCs as well as the aquatic environmental risks from EDC accumulation. The 3Rs, namely, Replacement, Reduction, and Refinement are essential values in legislation and guidelines governing the ethical use of animals in experiments. Hence, there is an ethical obligation to minimize the pain, stress, and suffering of fish, although there is still debate about whether fish can experience pain or have consciousness. Methodological challenges include the de-differentiation of primary zebrafish tissues for *ex vivo* cultures on conventional cell culture substrates. Therefore, the engineered *in vitro* zebrafish liver model not only mimics the natural zebrafish liver but also complements alternatives to animal testing.

Among many challenges faced by researchers in adapting *in vitro* tissue models one is that the cells do not form into physiologically similar units which maintain the structural and functional characteristics of their target organs. This study addresses this challenge by creating a hydrogel system which provides repeatable and consistent hepatoid formation from a singularized cell line. By creating a stable zebrafish liver model *in vitro*, researchers can test EDCs and other water-borne chemicals in a reliable manner.

The limitation of human health relatability is not covered in this study. Although some conclusions can be made about the effects of these EDCs on human health based on the zebrafish liver model, aspects of zebrafish liver analysis, such as the measurement of vitellogenin (VTG), are unrelatable to humans. However, from this study, one can use the hydrogel construct which can regulate phenotypes of human hepatocytes or other cell types and engineer human organoids. Therefore, this study is broadly applicable to toxicology testing where the use of live animal models is costly or ethically prohibitive.

ASSOCIATED CONTENT

Supporting Information

The Supporting Information is available free of charge at https://pubs.acs.org/doi/10.1021/acs.est.0c01988.

Real-time imaging of the ROS response to 17β-estradiol in zebrafish hepatocytes (MP4)

Scheme and figure of zebrafish hepatocytes coated with PEG, cultured on collagen-PEG hydrogel for 14 days (PDF)

AUTHOR INFORMATION

Corresponding Authors

Hyunjoon Kong − *Department of Bioengineering, Institute of Genomic Biology, Department of Chemical and Biomolecular Engineering, and Beckman Institute, University of Illinois at Urbana−Champaign, Urbana, Illinois 61801, United States;* orcid.org/0000-0003-4680-2968; Email: hjkong06@illinois.edu

Young Jun Kim − *Environmental Safety Group, Korea Institute of Science and Technology (KIST) Europe, 66123 Saarbrücken, Germany*; Email: youngjunkim@kist-europe.de

Authors

Kathryn M. Sullivan − *Department of Bioengineering and Institute of Genomic Biology, University of Illinois at Urbana−Champaign, Urbana, Illinois 61801, United States;* orcid.org/0000-0002-7227-396X

Chang Gyun Park − *Environmental Safety Group, Korea Institute of Science and Technology (KIST) Europe, 66123 Saarbrücken, Germany*

John D. Ito − *Department of Chemical and Biomolecular Engineering, University of Illinois at Urbana−Champaign, Urbana, Illinois 61801, United States*

Mikhail Kandel − *Department of Electrical and Computer Engineering and Beckman Institute, University of Illinois at Urbana−Champaign, Urbana, Illinois 61801, United States;* orcid.org/0000-0003-2124-7750

Gabriel Popescu − *Department of Bioengineering, Department of Electrical and Computer Engineering, and Beckman Institute, University of Illinois at Urbana−Champaign, Urbana, Illinois 61801, United States*

Complete contact information is available at: https://pubs.acs.org/10.1021/acs.est.0c01988

Notes

The authors declare no competing financial interest.

ACKNOWLEDGMENTS

This work was supported by a National Research Council of Science & Technology (NST) grant by the Korean Government (CAP-17-01-KIST Europe), partly by the National Science Foundation Research Training Grant (1735252), National Science of Foundation (STC-EBICS Grant CBET-0939511), R01CA238191, and R43GM133280-01. K. Sullivan and M. Kandel are supported by the National Science Foundation Research Training Grant (1735252) Understanding the Brain: Training the Next Generation of Researchers in Engineering and Deciphering of Miniature Brain Machinery. Chang Gyun Park was supported by the KIST Europe signature project (12001). Images presented in this publication were obtained at the core facilities in the Materials Research Laboratory and the Institute of Genomic Biology at the University of Illinois at Urbana-Champaign.

REFERENCES

(1) Thorpe, K. L.; Cummings, R. I.; Hutchinson, T. H.; Scholze, M.; Brighty, G.; Sumpter, J. P.; Tyler, C. R. Relative Potencies and Combination Effects of Steroidal Estrogens in Fish. *Environ. Sci. Technol.* **2003**, *37* (6), 1142−1149.

(2) Pang, Q.; Li, Y.; Meng, L.; Li, G.; Luo, Z.; Fan, R. Neurotoxicity of BPA, BPS, and BPB for the Hippocampal Cell Line (HT-22): An Implication for the Replacement of BPA in Plastics. *Chemosphere* **2019**, *226*, 545−552.

(3) Nagorka, R.; Koschorreck, J. Trends for Plasticizers in German Freshwater Environments − Evidence for the Substitution of DEHP with Emerging Phthalate and Non-Phthalate Alternatives. *Environ. Pollut.* **2020**, *262*, 114237.

(4) Tian, H.; Gao, Z.; Wang, G.; Li, H.; Zheng, J. Estrogen Potentiates Reactive Oxygen Species (ROS) Tolerance to Initiate Carcinogenesis and Promote Cancer Malignant Transformation. *Tumor Biol.* **2016**, *37* (1), 141−150.

(5) Shao, Y.; Xiao, H.; Di Paolo, C.; Deutschmann, B.; Brack, W.; Hollert, H.; Seiler, T. B. Integrated Zebrafish-Based Tests as an Investigation Strategy for Water Quality Assessment. *Water Res.* **2019**, *150*, 252−260.

(6) Bergman, Å.; Heindel, J.; Jobling, S.; Kidd, K.; Zoeller, R. T. *State-of-the-Science of Endocrine Disrupting Chemicals* **2012**, *211*, 2012 DOI: 10.1016/j.toxlet.2012.03.020.

(7) Neale, P. A.; Ait-Aissa, S.; Brack, W.; Creusot, N.; Denison, M. S.; Deutschmann, B.; Hilscherová, K.; Hollert, H.; Krauss, M.; Novák, J.; Schulze, T.; Seiler, T.-B.; Serra, H.; Shao, Y.; Escher, B. I. Linking in Vitro Effects and Detected Organic Micropollutants in Surface Water

Using Mixture-Toxicity Modeling. *Environ. Sci. Technol.* **2015**, *49* (24), 14614−14624.
(8) Wilkins, B. J.; Pack, M. Zebrafish Models of Human Liver Development and Disease. *Compr. Physiol.* **2013**, *3* (3), 1213−1230.
(9) Menke, A. L.; Spitsbergen, J. M.; Wolterbeek, A. P. M.; Woutersen, R. A. Normal Anatomy and Histology of the Adult Zebrafish. *Toxicol. Pathol.* **2011**, *39* (5), 759−775.
(10) Kiamehr, M.; Heiskanen, L.; Laufer, T.; Düsterloh, A.; Kahraman, M.; Käkelä, R.; Laaksonen, R.; Aalto-Setälä, K. Dedifferentiation of Primary Hepatocytes Is Accompanied with Reorganization of Lipid Metabolism Indicated by Altered Molecular Lipid and MiRNA Profiles. *Int. J. Mol. Sci.* **2019**, *20* (12), 2910.
(11) Kim, M.; Lee, J. Y.; Jones, C. N.; Revzin, A.; Tae, G. Heparin-Based Hydrogel as a Matrix for Encapsulation and Cultivation of Primary Hepatocytes. *Biomaterials* **2010**, *31* (13), 3596−3603.
(12) You, J.; Park, S.-A.; Shin, D.-S.; Patel, D.; Raghunathan, V. K.; Kim, M.; Murphy, C. J.; Tae, G.; Revzin, A. Characterizing the Effects of Heparin Gel Stiffness on Function of Primary Hepatocytes. *Tissue Eng., Part A* **2013**, *19* (23−24), 2655−2663.
(13) Desai, S. S.; Tung, J. C.; Zhou, V. X.; Grenert, J. P.; Malato, Y.; Rezvani, M.; Español-Suñer, R.; Willenbring, H.; Weaver, V. M.; Chang, T. T. Physiological Ranges of Matrix Rigidity Modulate Primary Mouse Hepatocyte Function in Part through Hepatocyte Nuclear Factor 4 Alpha. *Hepatology* **2016**, *64* (1), 261−275.
(14) Simonetti, R. B.; Santos Marques, L.; Streit, D. P., Jr; Oberst, R. Zebrafish (Danio Rerio): Ethics in Animal Experimentation. *IOSR J. Agric. Vet. Sci. Ver. I* **2016**, *9* (7), 2319−2372.
(15) Couteau, C.; Coiffard, L. Regulation No 1223/2009 on Cosmetic Products. *Nouv. Dermatologiques* **2010**, *29* ().
(16) Uchea, C.; Owen, S. F.; Chipman, J. K. Functional Xenobiotic Metabolism and Efflux Transporters in Trout Hepatocyte Spheroid Cultures. *Toxicol. Res. (Cambridge, U. K.)* **2015**, *4* (2), 494−507.
(17) Baron, M.; Mintram, K.; Owen, S.; Hetheridge, M.; Moody, A.; Purcell, W.; Jackson, S.; Jha, A. Pharmaceutical Metabolism in Fish: Using a 3- D Hepatic In Vitro Model to Assess Clearance. *PLoS One* **2017**, *12*, No. e0168837.
(18) vom Saal, F. S.; Nagel, S. C.; Coe, B. L.; Angle, B. M.; Taylor, J. A. The Estrogenic Endocrine Disrupting Chemical Bisphenol A (BPA) and Obesity. *Mol. Cell. Endocrinol.* **2012**, *354* (1−2), 74−84.
(19) Nagel, S. C.; Bromfield, J. J. Bisphenol a: A Model Endocrine Disrupting Chemical with a New Potential Mechanism of Action. *Endocrinology* **2013**, *154* (6), 1962−1964.
(20) NCBI, N. C. for B. I. itgb1bp1 integrin beta 1 binding protein 1 [Danio rerio (zebrafish)] https://www.ncbi.nlm.nih.gov/gene/641420.
(21) Kandel, M. E.; Hu, C.; Naseri Kouzehgarani, G.; Min, E.; Sullivan, K. M.; Kong, H.; Li, J. M.; Robson, D. N.; Gillette, M. U.; Best-Popescu, C.; Popescu, G. Epi-Illumination Gradient Light Interference Microscopy for Imaging Opaque Structures. *Nat. Commun.* **2019**, *10* (1), 1−9.
(22) Clay, N. E.; Shin, K.; Ozcelikkale, A.; Lee, M. K.; Rich, M. H.; Kim, D. H.; Han, B.; Kong, H. Modulation of Matrix Softness and Interstitial Flow for 3D Cell Culture Using a Cell-Microenvironment-on-a-Chip System. *ACS Biomater. Sci. Eng.* **2016**, *2* (11), 1968−1975.
(23) Liang, Y.; Jeong, J.; DeVolder, R. J.; Cha, C.; Wang, F.; Tong, Y. W.; Kong, H. A Cell-Instructive Hydrogel to Regulate Malignancy of 3D Tumor Spheroids with Matrix Rigidity. *Biomaterials* **2011**, *32* (35), 9308−9315.
(24) Cha, C.; Kim, S. Y.; Cao, L.; Kong, H. Decoupled Control of Stiffness and Permeability with a Cell-Encapsulating Poly(Ethylene Glycol) Dimethacrylate Hydrogel. *Biomaterials* **2010**, *31* (18), 4864−4871.
(25) Yano, H.; Mazaki, Y.; Kurokawa, K.; Hanks, S. K.; Matsuda, M.; Sabe, H. Roles Played by a Subset of Integrin Signaling Molecules in Cadherin-Based Cell-Cell Adhesion. *J. Cell Biol.* **2004**, *166* (2), 283−295.
(26) Shkumatov, A.; Baek, K.; Kong, H. Matrix Rigidity-Modulated Cardiovascular Organoid Formation from Embryoid Bodies. *PLoS One* **2014**, *9* (4), 1−10.
(27) Yao, Y.; Lin, J.; Yang, P.; Chen, Q.; Chu, X.; Gao, C.; Hu, J. Fine Structure, Enzyme Histochemistry, and Immunohistochemistry of Liver in Zebrafish. *Anat. Rec.* **2012**, *295* (4), 567−576.
(28) Ip, Y. K.; Chew, S. F. Ammonia Production, Excretion, Toxicity, and Defense in Fish: A Review. *Front. Physiol.* **2010**, *1*, 1−20.
(29) Van Der Ven, L. T. M.; Holbech, H.; Fenske, M.; Van Den Brandhof, E. J.; Gielis-Proper, F. K.; Wester, P. W. Vitellogenin Expression in Zebrafish Danio Rerio: Evaluation by Histochemistry, Immunohistochemistry. *Aquat. Toxicol.* **2003**, *65* (1), 1−11.
(30) Cosnefroy, A.; Brion, F.; Maillot-Maréchal, E.; Porcher, J.-M.; Pakdel, F.; Balaguer, P.; Aït-Aïssa, S. Selective Activation of Zebrafish Estrogen Receptor Subtypes by Chemicals by Using Stable Reporter Gene Assay Developed in a Zebrafish Liver Cell Line. *Toxicol. Sci.* **2012**, *125* (2), 439−449.
(31) Mommsen, T. P.; Walsh, P. J. 5 Vitellogenesis and Oocyte Assembly. In *The Physiology of Developing Fish*; Hoar, W. S., Randall, D. J. B. T.-F. P., Eds.; Academic Press, 1988; Vol. *11*, pp 347−406. DOI: 10.1016/S1546-5098(08)60202-2.
(32) Sumpter, J. P.; Jobling, S. Vitellogenesis as a Biomarker for Estrogenic Contamination of the Aquatic Environment. *Environ. Health Perspect.* **1995**, *103*, 173−178.
(33) Crain, D. A.; Eriksen, M.; Iguchi, T.; Jobling, S.; Laufer, H.; LeBlanc, G. A.; Guillette, L. J. An Ecological Assessment of Bisphenol-A: Evidence from Comparative Biology. *Reprod. Toxicol.* **2007**, *24* (2), 225−239.
(34) Le Fol, V.; Aït-Aïssa, S.; Sonavane, M.; Porcher, J.-M.; Balaguer, P.; Cravedi, J.-P.; Zalko, D.; Brion, F. In Vitro and in Vivo Estrogenic Activity of BPA, BPF and BPS in Zebrafish-Specific Assays. *Ecotoxicol. Environ. Saf.* **2017**, *142*, 150−156.

8.4 Original Paper - Hybrid-spheroid culture with nanofiber

NANO · MICRO small
www.small-journal.com

Integration of Bioinspired Fibrous Strands with 3D Spheroids for Environmental Hazard Monitoring

Chang Gyun Park, Indong Jun, Sangmin Lee, Chang Seon Ryu, Sang-Ah Lee, Jaeho Park, Hyung-Seop Han, Honghyun Park, Andreas Manz, Heungsoo Shin, and Young Jun Kim**

Numerous methods have been introduced to produce 3D cell cultures that can reduce the need for animal experimentation. This study presents a unique 3D culture platform that features bioinspired strands of electrospun nanofibers (BSeNs) and aquatic cell lines to compensate for shortcomings in the current cell spheroid generation techniques. The use of BSeNs in 3D zebrafish liver cell cultures is found to improve liver and reproductive functions through spheroid-based in vitro assays such as whole transcriptome sequencing and reproductive toxicity testing, with optimized properties exhibiting results similar to those obtained for fish embryo acute toxicity (FET, OECD TG 236) following exposure to environmental endocrine-disrupting chemicals (17β-Estradiol (E2), 4-hydroxytamoxifen (4-HT), and bisphenol compounds (bisphenol A (BPA) and 9,9-Bis(4-hydroxyphenyl)fluorene (BPFL)). These findings indicate that the beneficial effects of bioinspired materials that closely mimic ECM environments can yield efficient zebrafish cells with intrinsic functions and xenobiotic metabolism similar to those of zebrafish embryos. As a closer analog for the in vivo conditions that are associated with exposure to potentially hazardous chemicals, the straightforward culture model introduced in this study shows promise as an alternative tool that can be used to further eco-environmental assessment.

1. Introduction

The misuse of chemicals can partially explain the increasing incidences of environmental and human health problems.[1–3] The multidisciplinary field termed ecotoxicology investigates how environmental pollutants affect the aquatic and terrestrial environment,[4] and is aimed primarily at understanding undesirable events in the natural environment by performing ecotoxicological testing and risk evaluations of new chemicals that are used, discarded, or reach the environment. Ecotoxicologists also conduct detailed monitoring studies elucidating the physiological and biochemical responses of organisms following pollutant exposure, which often reflect toxic effects.[5] Over the past few decades, government agencies have mandated testing toxicity on live animals to determine the environmental risk of new chemicals or products on the market.[6] However, the use of animals in scientific and medical tests is generally subject to animal welfare protection,[7] and the European Commission (EC) has produced a directive to ban animal testing for cosmetics or household products.[8] The need for alternative approaches to the use of vertebrate animals for hazard assessments of chemicals and pollutants has thus become increasingly important,[9] with the use of vertebrates for environmental risk assessment banned for several regulatory purposes. Therefore, the first consideration when starting a vertebrate ecotoxicity test is to minimize the unnecessary use of vertebrate organisms as far as possible.

C. G. Park, I. Jun, C. S. Ryu, S.-A. Lee, A. Manz, Y. J. Kim
Environmental Safety Group
Korea Institute of Science & Technology Europe (KIST-EUROPE)
66123 Saarbrücken, Germany
E-mail: youngjunkim@kist-europe.de
C. G. Park, A. Manz
Universität des Saarlandes
66123 Saarbrücken, Germany
S. Lee, H. Shin
BK21 Plus Future Biopharmaceutical Human Resources Training and Research Team Hanyang University
Seoul 04763, Republic of Korea
E-mail: hshin@hanyang.ac.kr
The ORCID identification number(s) for the author(s) of this article can be found under https://doi.org/10.1002/smll.202200757.
S. Lee, H. Shin
Department of Bioengineering
Hanyang University
Seoul 04763, Republic of Korea
J. Park, H.-S. Han
Center for Biomaterials
Biomedical Research Institute
Korea Institute of Science and Technology (KIST)
Seoul 02792, Republic of Korea
H. Park
Department of Advanced Biomaterials Research
Ceramics Materials Division
Korea Institute of Materials Science (KIMS)
Changwon 51508, Republic of Korea

DOI: 10.1002/smll.202200757

Fish are ideal sentinels for evaluating aquatic toxicity in vertebrates and have become a popular alternative model system in aquatic ecotoxicology.[10,11] The zebrafish is a particularly convenient model because of its easy maintenance and high numbers of offspring. In particular, fish embryo toxicity (FET) tests using zebrafish have attracted attention as an alternative method for animal experiments.[12,13] Many studies have indicated that fish embryos provide excellent versatility for environmental and biological assessment applications, ranging from acute system toxicity, sub-chronic toxicity, teratogenicity to endocrine disruption.[13–16] Lee et al. comprehensively analyzed acute toxic and thyroid hormone disturbances effect of endocrine-disrupting chemicals (EDCs) in zebrafish embryos.[17] In particular, zebrafish embryos are considered to suffer from no sentinel, minor pain, or discomfort when exposed to chemicals prior to 120 h post-fertilization (hpf).[18] According to EU Directive 2010/63/E.U. on the protection of animals used for scientific purposes, animals in the early life stages are not defined objects for protection.[19] Therefore, zebrafish embryos do not fall within the regulatory framework for animal experiments when still within 120 hpf.

An excellent alternative in vitro ecotoxicity monitoring platform using cells can evaluate acute and subchronic toxicity or mechanistic pathways without any restrictions.[20] Cellular studies are essential in ecotoxicity studies because the primary interaction between hazardous chemicals and environmental species begins at the cellular level.[21] Cytotoxicology, for instance, provides an essential concept for understanding ecotoxicological processes because it plays a crucial role in explaining the mode by which toxins act. Therefore, the relationship between the cytotoxic response and toxicity can be a valuable starting point for ecotoxicological studies. Furthermore, cell culture systems can provide valuable information that can be used better to control cellular functions and processes for in vivo experiments. Even today, most studies are based on experiments using 2D cell cultures as in vitro tests. However, several heterogeneous disparities are associated with 2D cultures in the in vivo environment, such as perturbations in the interaction between cells and the extracellular environment and changes in the cell morphology, polarity, and methods of division.[22] These shortcomings have instigated high demand for new approach methodologies (NAMs) that can more closely mimic in vivo conditions.[23] Thus, over the past few decades, 3D cell cultures have gained increased recognition as a highlighted evaluation tool in biological research. Spheroids are the simplest 3D culture models that are used in studies in which the physiological representation of underlying tissue is compared with other commonly used models such as cells grown in monolayers (2D).[24] Numerous studies have demonstrated the suitability of the 3D spheroid culture system as an in vitro alternative to evaluate chemical toxicity and environmental samples in biological and ecotoxicity studies. Several studies have shown that 3D spheroid models exhibit several in vivo environmental features, such as cell–cell interactions, drug penetration, and resistance.[25,26] For example, Mandon et al. reported that 3D HepaRG spheroids are possible models for genotoxicity assessment to detect carcinogens in vitro.[27] Sirenko et al. reported that human 3D culture models derived from iPSC-differentiated cells could provide valuable systems for analyzing drug-induced toxicity.[33] However, spheroids that are produced by the universal method are subjected to challenges associated with viability, hypoxia, and long-term culture because of the strong cell-to-cell interactions within the spheroids.[28] One significant disadvantage in using conventional spheroid cultures is that nutrients and oxygen are not supplied at sufficient abundance to the core of the spheroids because the diffusion gradient increases alongside the size of a spheroid.[29] In addition, 3D spheroid platforms have been established for in vitro mammalian toxicity studies but have not been actively considered for investigating model aquatic species in environmental applications. Therefore, the overall interspecies response difference between highly simplified 3D rotating ellipsoids and potentially dangerous chemicals in fish models is one of the challenges that researchers must overcome.

Previous studies have revealed that bioinspired materials overcome the limitations posed by the conventional spheroid system and offer advantages such as improved viability, proliferation, and oxygen transport. For example, we previously reported on the use of bioinspired strands of electrospun nanofibers (BSeNs) that were assembled using human cell lines such as fibroblasts, chondrocytes, HUVECs, and stem cells.[30–34] BSeNs are fibrous strands of several micrometers in length with nanoscale diameters that are obtained by electrospinning and mimic the structures of collagen fibrils.[33] BSeN-incorporated spheroids have demonstrated improved viability and reduced hypoxia and apoptosis.[30] Here, we further hypothesized that BSeN would improve the toxicity evaluation of potentially hazardous chemicals and could serve as an in vitro platform for environmental hazard assessment. The objectives of this study were: 1) investigate the effect of using BSeN in 3D spheroids composed of zebrafish liver cells, 2) examine the effect of BSeN in regulating the viability, hypoxia, and functioning of cells in spheroids through spheroid-based in vitro assays, and 3) verify the similarity in using BSeN-incorporated 3D spheroids and fish embryo acute toxicity tests to investigate the correlation between potentially hazardous chemicals and reproductive toxicity (FET, OECD TG 236). We suggest that combining bioinspired materials with cell lines in the aquatic environment may serve as a starting point for an in vitro test method that can be used as a monitoring platform for environmental risk assessment.

2. Results and Discussion

Over the past few decades, the most common method of evaluating the toxicity of a chemical mixture has been through animal testing. However, the use of animals for toxicity testing can raise concerns about animal ethics, and the need for alternative animal testing methods is growing worldwide. In addition, there is growing confidence in the substitution of animal testing as many studies have already demonstrated that the results of alternative animal testing are reproducible and predictable. In this context, different approaches to cell-based platforms should be studied to investigate the effectiveness of alternative tests, even in environmental toxicity assessment. This study uses a combination of aquatic cell lines and bioinspired materials to present high potential as a screening

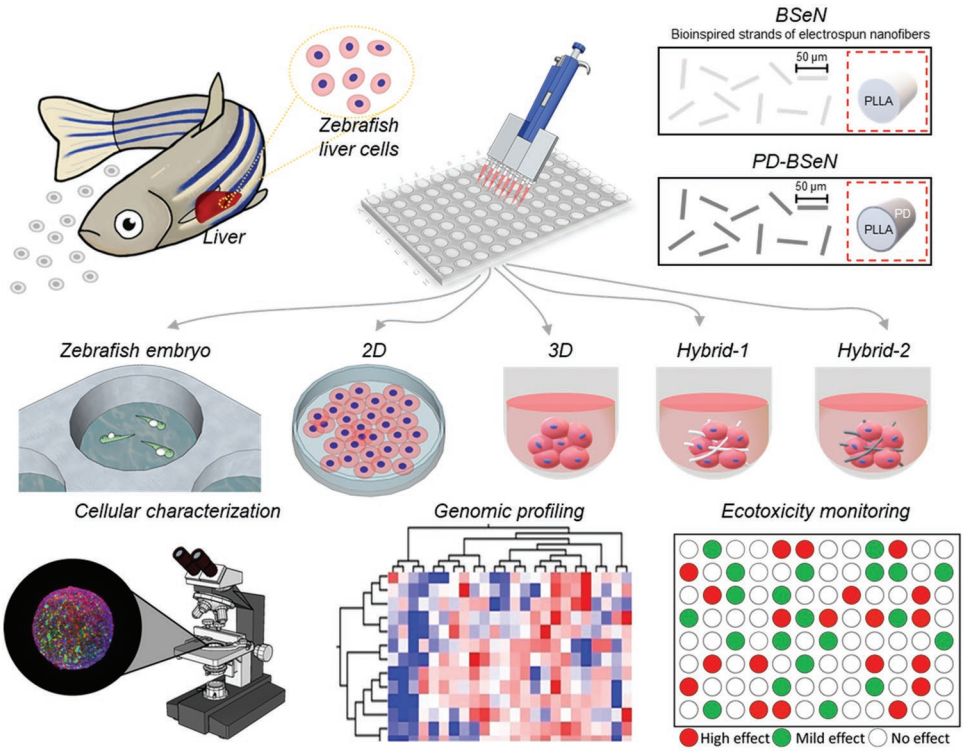

Figure 1. Schematic illustration of this study. Zebrafish liver (ZFL) cells were cultured as monolayers, spheroids, and hybrid-spheroids. BSeN and PD-BSeN were fabricated for use in the hybrid-spheroid cultures. Comparative analyses of the generated groups were conducted using cellular characterization, genomic profiling, and ecotoxicity monitoring techniques depending on culture time.

platform for in vitro environmental hazard assessment. A 3D spheroid-based evaluation platform using bioinspired materials can provide results similar to in vivo experiments and has the advantages of microarrays such as high throughput and simplicity.

2.1. Characterization of BSeNs

Several methods have been used to generate 3D spheroid cultures and extensive reviews of these efforts have been produced elsewhere. One of the most critical issues associated with the most commonly used spheroid cultures is problems with the distribution of oxygen. Increasing the size of a spheroid can lead to oxygen depletion (hypoxia) and causes cell necrosis in the core, and the presence of necrotic cells within a spheroid may render it useless for toxicity screening. Zebrafish liver cells are known to be useful in forming spheroids on non-adhesive plates; however, we previously demonstrated the problem of hypoxia and the changes in the inner structure of the spheroid upon increasing the cell number or prolonging the culture period.[35] Therefore, a multidisciplinary approach is required to overcome the limitations in the existing methods that are used for spheroid generation. Moreover, it is a priority to develop an innovative toxicity assessment platform that can improve the function of a cell while improving the viability of cells inside the spheroid, as this is the main reason for generating spheroids for environmental toxicity assessment using bioinspired materials. In this study, we present a multidisciplinary approach for the production of in vitro toxicological screening platforms using a combination of aquatic cell lines (zebrafish liver cells) and bioinspired materials (**Figure 1**). Our core technique involves the assembly of 3D spheroid cultures of zebrafish cells using BSeNs. We hypothesize that this form of BSeN serves as a physical bridge for the transportation of oxygen and nutrients into the core of spheroids, thereby overcoming the limitations posed by conventional spheroids and providing advantages such as improving viability and increasing proliferation, and supporting the transport of oxygen.

The extracellular matrix (ECM) is a non-cellular 3D macromolecular fibrillar network that can provide a physical platform for cells and stimulate interactive biochemical and biomechanical signals.[36] We previously reported the preparation of ECM-mimicking fibrous strands through the aminolysis-based partial degradation of electrospun nanofibers to produce individual short fibers by cleaving the ester linkage of poly L-lactic acid (PLLA) with ethylenediamine and generating an amide bond with amine functionality (**Figure 2**a; Figure S1, Supporting Information).[30,32] However, substrates that are prepared using PLLA, a synthetic biodegradable material, may not have cell-interactive properties, leading to poor cell interaction. Therefore, we used a mussel-inspired coating method to increase the cell affinity of the BSeN surface. The SEM images showed changes in form from a mesh of aligned nanofibers to well-distributed relatively minor individual short fibers following the fragmentation process (Figure 2b). It was confirmed that aminolysis of partially degraded electrospun nanofibers resulted in the production of individualized fibers with lengths

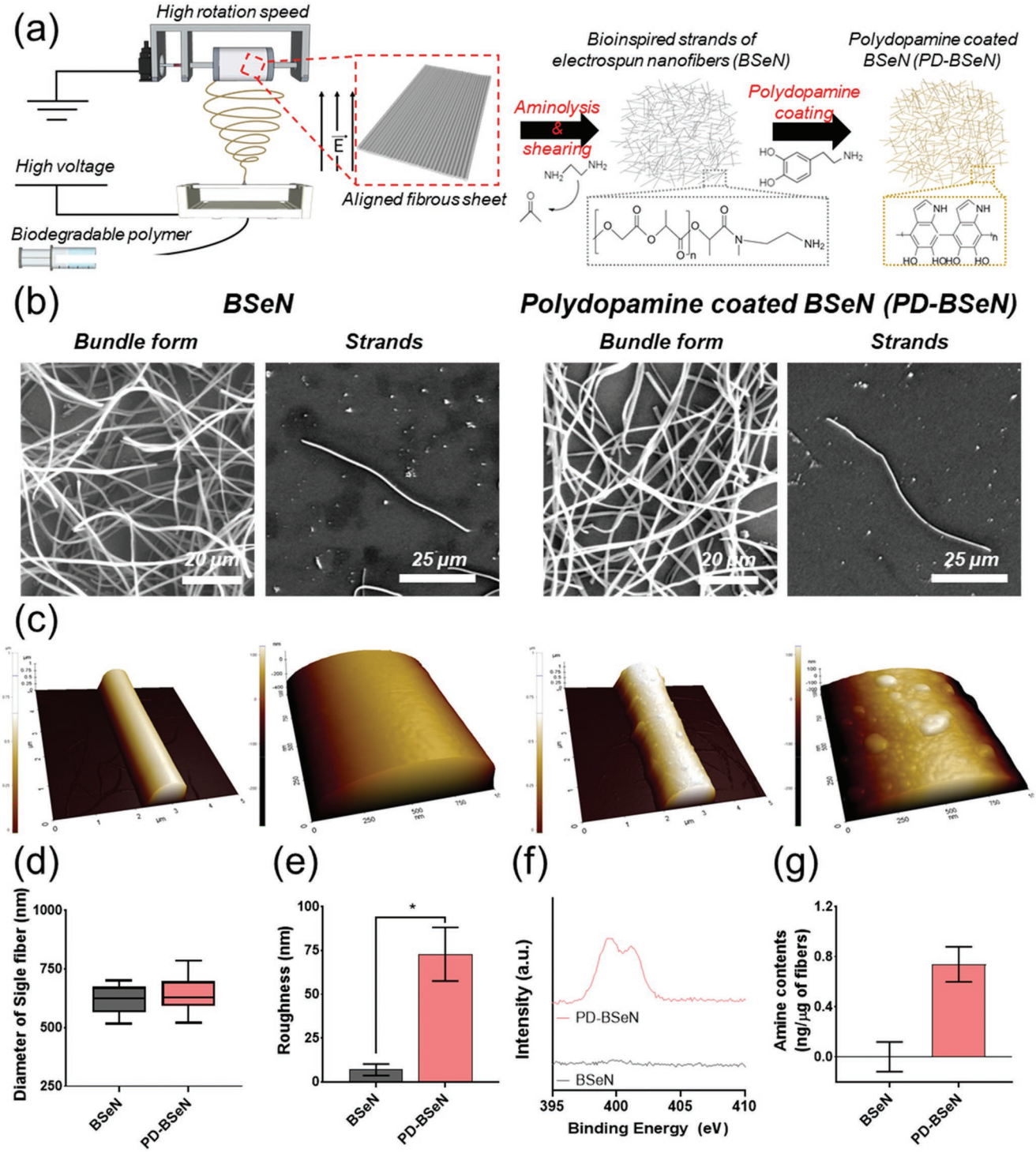

Figure 2. Fabrication and characterizations of nanofibers. a) Schematic representation of BSeN and PD-BSeN generation. b) SEM micrography images and c) 3D AFM images of BSeN and PD-BSeN. d) Diameter of single BSeN and PD-BSeN fibers. The diameter was analyzed by ImageJ software. A total of 50 single fibers were analyzed from SEM images obtained using FEI Quanta 250 FEG Scanning Electron Microscope. Data are expressed as mean ± SD ($n = 50$). e) Surface roughness measurement of BSeN and PD-BSeN. A total of ten single fibers from AFM images were analyzed by ImageJ software. Comparison of the means between two groups was performed using one-way analysis of variance (ANOVA; $^*p < 0.05$, $n = 10$). f) XPS spectrum of nanofibers with and without polydopamine coating. g) Quantification of catecholamine in nanofibers. The quantification was analyzed using Micro-BCA assay ($n = 6$).

of 50–80 μm, regardless of the presence or absence of polydopamine coating on the BSeN. Since BSeN described above has similar dimensions to fibrillar proteins, the major fibrous proteins of the ECM, it will mimic the nanoscale structural aspects of ECM and positively affect the activity of cell–ECM interactions.[37,38] Figure 2c depicts BSeN group surfaces that

have been subjected to polydopamine coating, as confirmed by AFM (atomic force microscopy). The AFM images revealed that PD-BSeN increased the roughness. For example, the roughness value (Ra) of the original BSeN surface was 5.35 ± 2.29 nm, while the roughness of the surface of PD-BSeN increased to 79.42 ± 12.44 nm (Figure 2e). The chemical composition of BSeN was evaluated using XPS, and clear nitrogen peaks (N1s) were observed (Figure 2f; Supporting Information S2). In addition, we provided clear evidence for the presence of catecholamines in the PD-BSeN group using micro-BCA analysis (Figure 2g). Dopamine is considered a small-molecule mimetic of Mytilus edulis foot protein-5 (Mefp-5) in that it contains both catechol and the primary amine functional groups that are present in the side chains of 3,4-dihydroxyphenylalanine (DOPA) and Lys residues.[39,40] Incubation of the target substances in an alkaline dopamine solution (pH 8.0–8.5) leads to the oxidative polymerization of dopamine and the formation of a polymeric coating.[41] It has been proven that various functional coatings can be created on biomaterials via various immobilization reactions using polydopamine coating as a base. Several studies have reported that polydopamine (PD)-coated surfaces become negatively charged because of the deprotonation of one catechol (OH) group, resulting in improved hydrophilicity and biological performance (i.e., cell attachment and proliferation).[42,43]

2.2. Effect of BSeN on 3D Spheroid Formation

We previously investigated and determined the optimal conditions for spheroid formation based on screening under various BSeN conditions (Supporting Information S3a). As a result, the DNA content did not affect the spheroids regardless of the amount of BSeN present. In contrast, the DNA content was significantly reduced in BSeN that was coated with PD for >20 min and showed limitation in spheroid formation (Supporting Information S3b–d and S4). These trends are contrary to the previous results obtained from incorporating BSeN into human cell-based spheroids.[30–32] Human cell lines and fish cell lines were significantly different in size, which is presumed to be one of the reasons why different results can be obtained under the same conditions. Our results suggest that relatively small fish cells are more sensitive to external environmental factors than human cell lines. We plan to focus on studying the fate regulation of fish cells according to the physical parameters of the ECM environment in the future (i.e., topography, stiffness, and roughness). As illustrated in **Figure 3**a, spheroids comprising cells that incorporated BSeN or PD-BSeN were designated Hybrid-1 and Hybrid-2, respectively. 2D and 3D refer to monolayer cells and spheroids, respectively, which were cultured using the generic methods (as a control group).

Figure 3b shows the morphology of the zebrafish liver cell spheroids after incubation for 24 h. The superposed fluorescence images of the actin filament and FITC-coated BSeN showed that the fibrous strands were well distributed throughout the spheroid (Supporting Information S5). SEM images confirmed the distribution of homogenous cells and fibrous strands within the spheroids. High-magnification SEM analysis showed that the cells were firmly attached to the surface of the fibrous strands, resulting in the formation of stable spheroids (Figure 3b; Supporting Information S6). BSeN was found to improve the proliferation of zebrafish liver cells, which can be attributed to the facilitation of mass transport resulting from the formation of spheroids with a loosely arranged structure (Figure 3c–e; Supporting Information S7 and S8). This speculation was partially demonstrated by hypoxic staining. As shown in Figure 3d,e, Hybrid-2 showed reduced hypoxia, while strong hypoxic signals were distributed throughout the spheroids in the 3D group. Although intense cell–cell and cell–material contact within spheroids may be analogous to the physiological environment of natural tissue, the drawbacks of coexisting with materials with low cell affinity limit the proliferation of normal cells in spheroids during long-term culture with a lack of nutrient supply. This phenomenon was clearly observed in Hybrid-1. After culturing for seven days, Hybrid-1 showed a significantly higher proliferation rate than the 3D group (Supporting Information S7). However, under long-term culture conditions, the proliferation capacity of Hybrid-1 was not different from that of the 3D group. (Supporting Information S8). In contrast, the cells in the Hybrid-2 group continued to metabolize, even when cultured for 8 weeks. The antioxidant role of polydopamine[44] may partly explain the differences observed in the Hybrid-1 and Hybrid-2 groups; allowing the cells to improve the cell–material interactions is likely to have improved the problems of apoptosis and necrosis by preventing oxidative stress.

Although spheroids have been widely studied as in vitro analytical assessment tools, concerns about the long-term viability of cells within spheroids have constrained studies evaluating the health effects of long-term exposure to low-level chemicals in the field of environmental toxicity. Nevertheless, the results suggest that applying BSeN to aquatic cells can enable meaningful discovery and provide significant advances in the development of engineering platforms for toxicity assessment and monitoring in ecotoxicology.

2.3. Evaluation of Functions using Spheroid-Based In Vitro Assays

The differential gene expression in spheroids that were cultured for 7 d was also analyzed using whole-transcriptome sequencing analysis (**Figure 4**). A hierarchical clustering heatmap revealed distinct expression profiles between the 2D and 3D spheroids. The 3D spheroids exhibited significant upregulation of 2507 genes and downregulation of 2969 genes compared to the 2D group. This result is consistent with the findings of previous studies, and the trend was consistently observed in the relationship between the 2D and the Hybrid-2 groups. Contrary to our expectations, no distinct differences were observed in the Hybrid-2 group as compared to the 3D group. Both the 3D and Hybrid-2 groups had higher abundances of genes that are related to metabolic pathways than the 2D groups, as shown in Figure 4c. Depending on the cell type and microenvironment, various metabolic adaptations are associated with cell proliferation.[45] It is known that mitochondria produce most of the cellular adenosine triphosphate (ATP) via substrate-level-phosphorylation, primarily through the oxidative phosphorylation system.[46] Studies have suggested that

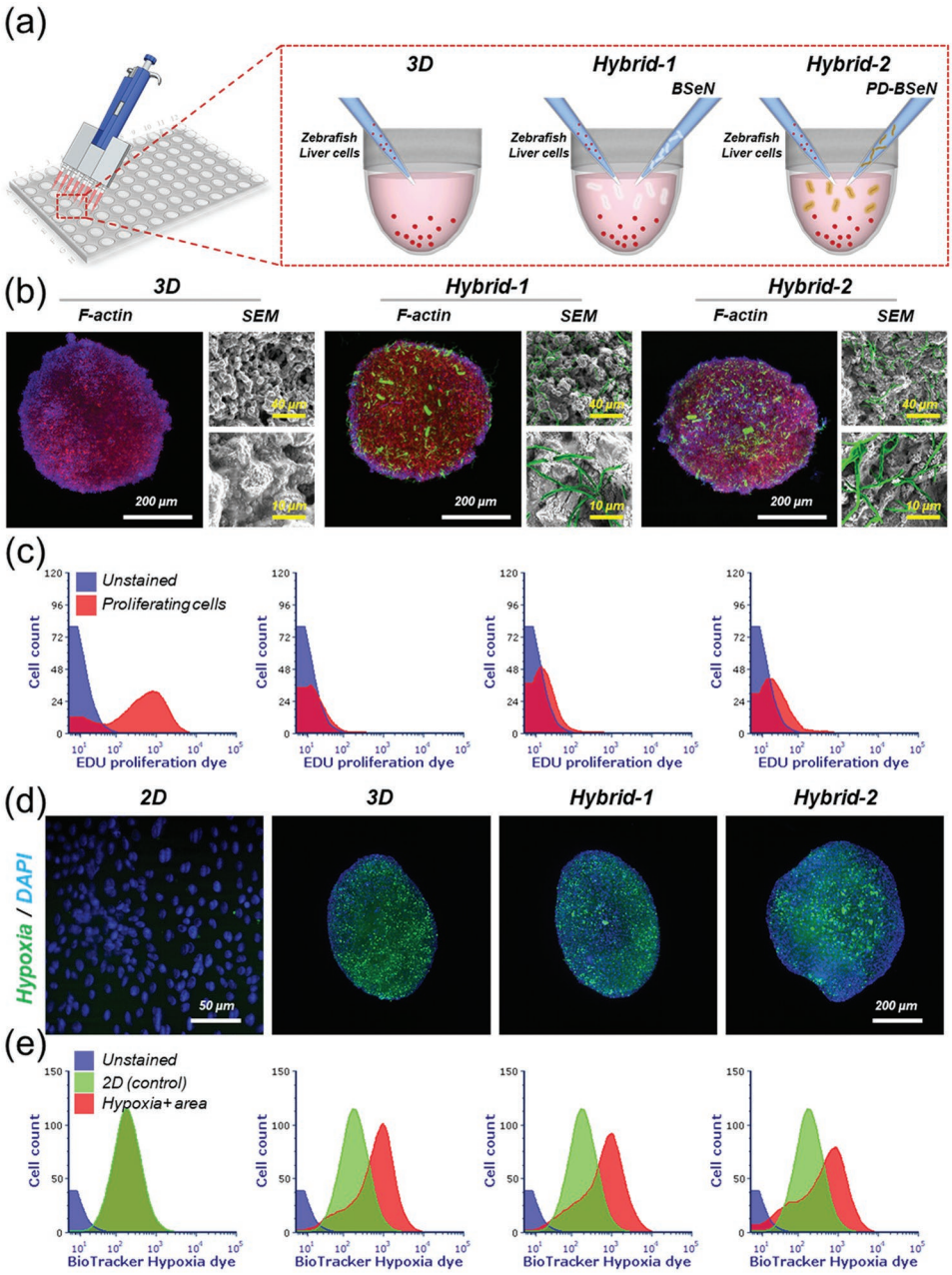

Figure 3. Formation of hybrid-spheroids with BSeN and PD-BSeN and their effects on cell proliferation and hypoxia. a) Schematic illumination of method used to fabricate spheroids (3D), spheroids with BSeN (Hybrid-1), and spheroids with PD-BSeN (Hybrid-2). b) Representative cytoskeletal structure and SEM micrography images of spheroids at day 3. The cytoskeletal structure images were acquired by fluorescence staining for DAPI (nuclei; blue) and F-actin (red), and BSeN and PD-BSeN were also stained by FITC labeling (green). c) FACS results of cell proliferation after 7 days of culture in 2D, 3D, Hybrid-1, and Hybrid-2 groups (2D from left, Hybrid-2 to the right). d) Representative hypoxia images at day 7. Images were acquired by fluorescence staining for DAPI (nuclei; blue) and hypoxia (green). e) FACS results of hypoxia after culturing for 7 days in 2D, 3D, Hybrid-1, and Hybrid-2 groups (2D from left, Hybrid-2 to the right).

oxidative phosphorylation provides the majority of ATP during cell proliferation. As shown in Figure 4c, the oxidative phosphorylation in the Hybrid-2 group differed significantly from that of the 2D group. Although a clear explanation for our results may not be within the scope of this study, we speculate that this is part of an adaptation strategy to hypoxic environments. In other words, these results suggest that cells coexisting with PD-BSeN can maintain their proliferative capacity through oxidative phosphorylation, even under inadequate oxygen levels.

To complement the whole-transcriptome sequencing analysis, we investigated the effect of BSeN on the gene expression levels of spheroids that were cultured for 14 d (**Figure 5**a–d). Zebrafish cell lines that are established from the livers of zebrafish show promise for fundamental studies into estrogen, liver, and reproductive functions. We found that improved

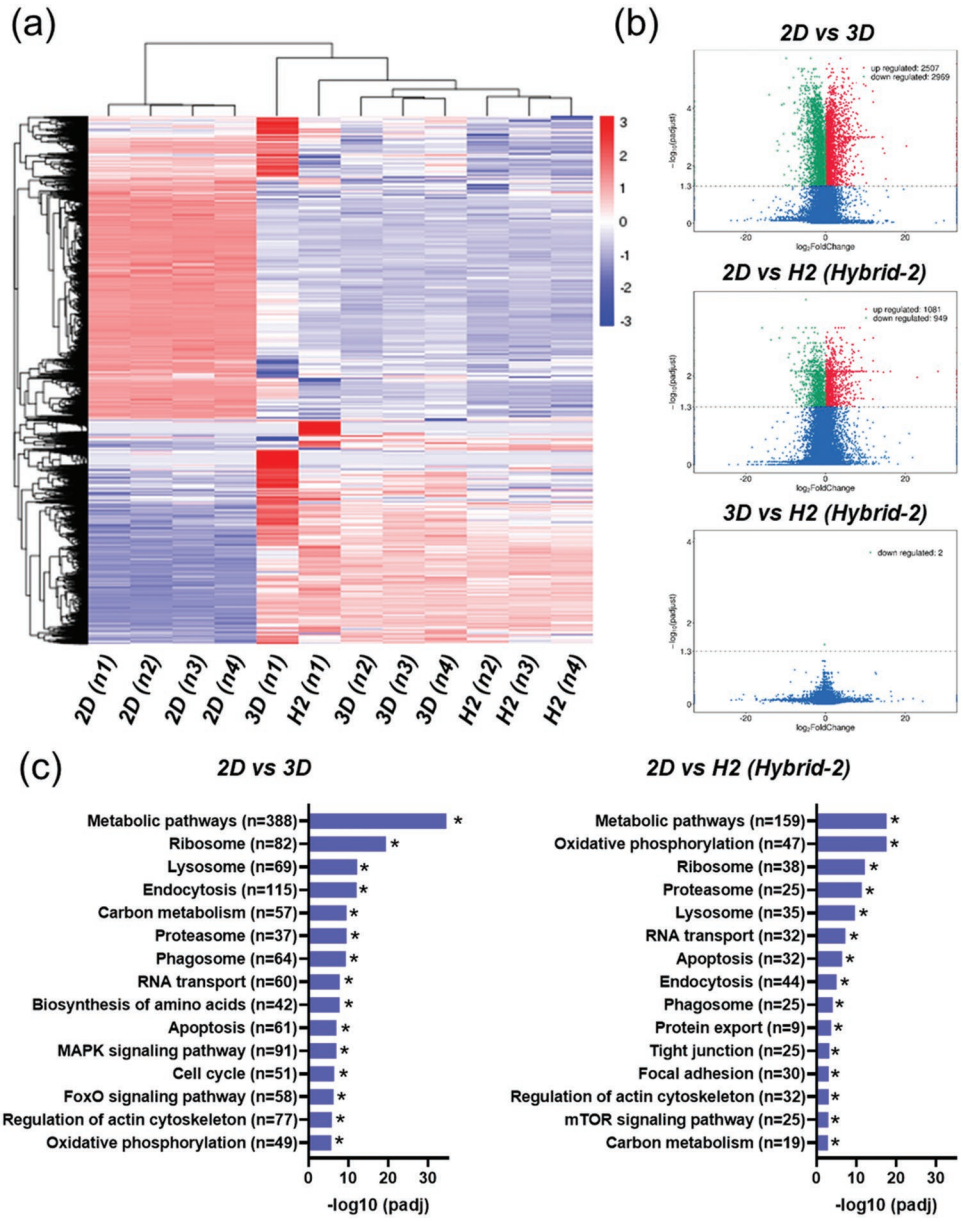

Figure 4. RNA sequencing (RNA-Seq) analysis of 2D, 3D, and Hybrid-2 groups cultured for 7 days ($n = 4$). a) Heatmap hierarchical clustering according to $\log_2$(FPKM+1) indicates differentially expressed genes (DEGs) in the groups. Red and blue indicate genes with high and low expression levels, respectively. b) Volcano plot analysis results. Plots indicate overall DEG distribution. c) KEGG enrichment histogram of transcripts ($^*p_{adj} < 0.05$).

estrogen receptors were achieved in all spheroid groups (3D, Hybrid-1, and Hybrid-2) as compared to the 2D group. For example, the relative gene expression of ESR-1 was 1.27 ± 0.11, 1.15 ± 0.50, and 1.77 ± 0.60 times higher in the 3D, Hybrid-1, and Hybrid-2 groups, respectively, compared with the control (2D). In addition, analysis of the liver-related gene expression showed interesting results. HNFs are a group of transcription factor families whose expression is enriched in the liver compared to other organs.[47] Cells in the 2D group showed similar HNF4A gene expression to the 3D group. However, both Hybrid groups showed more pronounced HNF4A gene expression than the 2D group. Since zebrafish liver cells can perform metabolic functions associated with the liver, they are an excellent cellular tool with which it is possible to determine the effect of exogenous metabolites.[35] We demonstrated that Hybrid-2 incorporated with PD-BSeN had similar or higher expression of drug-metabolizing genes (GSTA1, PXR, and CYP3C1) than the other three groups (1.88 ± 0.16 fold for PXR, 4.02 ± 0.42 fold for GSTA1, and 1.36 ± 0.13 fold CYP3C1) as compared to 2D.

Vitellogenin (VTG) is generally produced in the liver of female vertebrate ovaries in response to circulating endogenous estrogen[48,49] and is a precursor to the turbulence protein. Once produced in the liver, it follows the blood flow to the ovary, where it is absorbed. Many studies have reported that VTG induction can be measured both in vivo and in vitro in fish liver cells (hepatocytes).[35,49] In addition, in vitro VTG assays that use

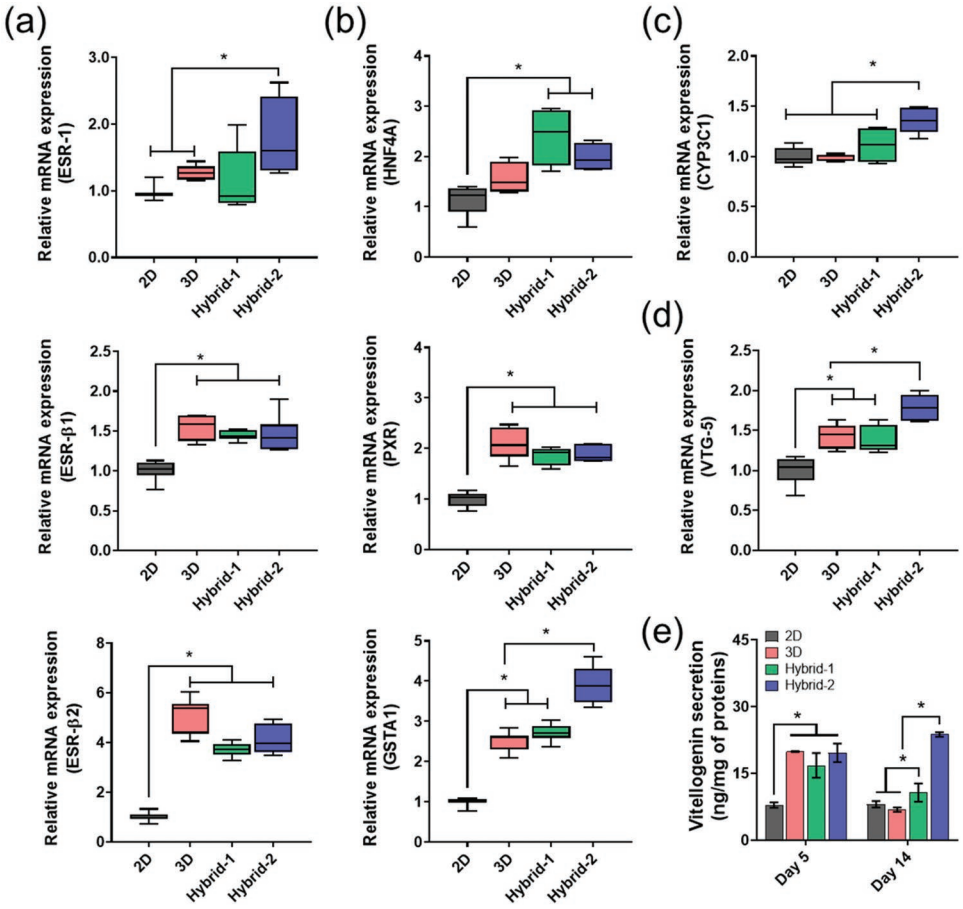

Figure 5. Fold-change in mRNA expression of a) estrogen receptor genes, b) liver-relative genes, c) CYP3C1 gene, d) VTG-5 gene. Each group was cultured for 14 days. Samples were prepared in the same manner as the RNA sequencing analysis. Data are presented as mean ± SD ($n = 8$). e) ELISA quantification of vitellogenin (VTG). The VTG was normalized to total protein concentration, and data are presented as mean ± SD ($n = 5$). a–e) Comparisons of the means between each group were performed using one-way analysis of variance (ANOVA; $*p < 0.05$), followed by Dunnett's T3 test (non-homogeneous variance) or Scheffe's test (homogeneous variance).

cells have been widely recognized as advantageous for detecting the effects of estrogen metabolites because hepatocytes maintain their metabolic state and can detect both estrogenic and antiestrogenic effects. As shown in Figure 5d, the relative gene expression of VTG was higher in the Hybrid-2 group than in the 2D, 3D, and Hybrid-1 groups. Consistent with the trend observed in the gene expression results, the protein detection of VTG in cells cultured for 5 d indicated its overexpression in the spheroid-based groups (3D, Hybrid-1, and Hybrid-2) compared to the 2D groups (Figure 5e; Supporting Information S8). For example, the VTG expression (ng mg^{-1} of proteins) detected after 5 days had dramatically increased from 7.92 ± 0.61 in the 2D group to 19.91 ± 0.09, 16.80 ± 2.77, and 19.63 ± 2.07 in the 3D, Hybrid-1, and Hybrid-2 groups, respectively. We also hypothesized that if the spheroids contain too few cells, the benefit of the enhanced 3D cell-cell adhesion was reduced compared to the 2D culture. In a previous study, we demonstrated that almost negligible levels of VTG were detected in a 2D group with 5000 cells.[35] However, low levels of VTG were also detected in the 2D group with 50 000 cells. We also measured the amount of VTG on day 5 in spheroids with low cell numbers under the same conditions (Supporting Information S10). An average VTG level of 5.69 ± 0.42 ng mg^{-1} of proteins was detected in the spheroid-based groups with or without BSeN. These results indicate that the advantages gained for 3D spheroids containing too few cells may be comparable or even inferior to those using monolayer culture conditions (2D group).

Interestingly, different VTG expression levels were observed after the cells were cultured for 14 days. The results confirmed that the VTG expression was significantly reduced in groups 3D and Hybrid-1 on day 14 as compared to day 5. In contrast, the Hybrid-2 group showed VTG protein expression stability, even when cultured for 14 days. We speculate that these findings may be due to the long-term central hypoxia and necrotic hypoxia in spheroids that occurs under long-term culture. We, therefore, examined the viability of and hypoxia in spheroids at 14 days (Supporting Information S9). The live and dead staining images revealed that the cells in the 3D group were densely distributed throughout the spheroid, and a large number of dead cells were detected on day 14. The overall trend of dead cells was similar to that observed with hypoxia staining. Although some dead cells were observed, the cells observed in the 2D, Hybrid-1, and Hybrid-2 groups were generally living. In addition, hypoxic staining revealed that the hybrid group with

incorporated BSeN showed low fluorescence intensity. These results suggest that the 3D culture method can improve cell functioning but is not valuable as a long-term in vitro evaluation model unless it provides an environment where the cells can live for a long time. The 3D spherical culture methods were found to improve the liver function of the cells, suggesting that the use of BSeN with cell-friendly chemical/structural characteristics positively regulates cell-to-cell interactions with excellent efficacy.

2.4. Comparison of Reproductive Toxicity in In Vitro Cell-Based Platforms and Zebrafish Embryos as a Result of EDC Exposure

Zebrafish embryos have been successfully used for high-throughput toxicity screening.[9] Eleutheroembryos (of <120 hpf) are preferred in vitro testing models because it is thought that embryos in the earliest stages feel less pain than adult fish.[13] Therefore, the eleuthero embryo (developmental stage of 96–120 hpf) has been proposed as a promising toxicity monitoring tool, and international standardized test guidelines have been developed and validated for embryos at his stage (i.e., fish embryo acute toxicity (FET, OECD TG 236).[12,13] VTG assessments are considered one of the primary reproductive indicators for EDCs. This study aimed to compare the acute short-term reproductive toxicity observed in zebrafish embryos with that obtained via cell-based assessment platforms. First, representative EDCs (E2, 4HT, BPA, and BPFL) were selected (Supporting Information S11). The expression of VTG showed little change in the zebrafish embryo with low-dose E2 treatment, but this increased markedly under high-dose E2 concentrations, reaching 1.35 ± 0.10 times the control level. In contrast, exposing zebrafish embryos to 4HT led to a significant reduction of 0.50 ± 0.03 and 0.42 ± 0.05 times that observed in the control at 10×10^{-9} and 1×10^{-6} M, respectively. Compared with the control group, the VTG level increased by 1.36 ± 0.04 times when exposed to BPA and decreased by 0.61 ± 0.02 times when exposed to BPFL.

There is an ongoing debate concerning the extent to which in vitro cell systems are viable for toxicity testing and risk assessment. In general, cell-based assays exhibit lower sensitivity than in vivo experiments when comparing toxic effects. Prior attempts to compare the toxic efficacy of aquatic cell lines with whole fish test systems showed weak correlations.[50] Similarly, we confirmed no difference in the VTG expression as the result of exposure to any substance in the 2D group using zebrafish liver cell lines. In contrast, in the 3D group, high-dose E2 and BPFL produced a similar tendency to that observed using zebrafish embryos, with very low sensitivity to 4HT and BPA substances. These results indicate that the monolayer cell culture platform (2D) exhibits negligible xenobiotic metabolism capacity and that the cell-only 3D culture platform has lower sensitivity to exogenous substances than zebrafish embryos. However, remarkable results were obtained in the Hybrid-2 group. As shown in **Figure 6**, the VTG levels in cells exposed to E2 and BPA increased, while those in cells exposed to 4HT and BPFL decreased compared to the control group. To verify the reliability of the reproductive toxicity data describing the cell-based culture platforms (2D, 3D, Hybrid-1, and Hybrid-2) and the zebrafish embryos, we analyzed the correlation between the expression levels of the groups in a given set of VTG libraries (Figure 6b–e). Consistent with previous results, negligible correlations were obtained between reproductive toxicity and EDC substances in 2D cultured monolayered fish cells and embryos. In the 3D group, although reproductive toxicity endpoints showed a potential correlation with zebrafish embryos, the two groups differed in sensitivity and predictability, with Pearson correlation coefficients of 0.54 and 0.65 as a result of E2 and 4-HT exposure, respectively. Based on the group correlation, it was found that the Hybrid-2 group had a similar response to E2 as the zebrafish embryo (Pearson correlation coefficient of 0.83 (Figure 6b,c)). These results indicate that the toxicity data obtained with the 3D spheroid platform with integrated biomimetic material adequately correlated with the FET results. Therefore, we can conclude that the incorporation of biomimetic materials into 3D spheroid platforms produces an appropriate and preferable in vitro assessment tool for alternative testing. An ideal in vitro toxicological assessment platform should be a 3D co-culture model composed of one or more fish cell lines and should have a system similar to the physiological and morphological properties of the fish model. This study (proof-of-concept stage) proposes that bioinspired materials with aquatic cell lines can be the starting point for in vitro test platforms that can be used as alternative testing. We suggest that a culture platform using bioinspired materials will become more useful in vitro evaluation system, and therefore conducted a follow-up study to investigate the toxic reactivity in vivo fish at the cellular level by studying the fate regulation of fish cells according to parameters (physical/chemical) that can further imitate the cell-matrix environment.

3. Conclusion

Because environmental pollutants adversely affect various molecular mechanisms, cellular models for monitoring and functional studies are needed as an alternative to in vivo exposure studies in ecotoxicology. The present study introduces 3D culture screening platforms that feature BSeNs and aquatic cell lines and investigated the possibility of an alternative animal test method in environmental toxicity evaluation. Our results suggest that the use of BSeN overcomes the limitations posed by conventional spheroid systems and offers advantages such as improved viability, proliferation, and oxygen transport. Furthermore, analysis of the spheroid-based in vitro assays demonstrated that combining BSeN with 3D zebrafish liver cell cultures improved the liver and reproductive functions. Results from the Hybrid-2 group indicated substantial effects on the expression of reproductive proteins such as VTG and showed a high correlation with the reproductive toxicity data of zebrafish embryos that are exposed to EDCs. Our results indicate that the beneficial effects of biomaterials that closely mimic ECM environments can yield efficient zebrafish cells with intrinsic functions and xenobiotic metabolism similar to those of zebrafish embryos. These findings have profound implications for designing in vitro cell culture-based monitoring platforms for alternative testing.

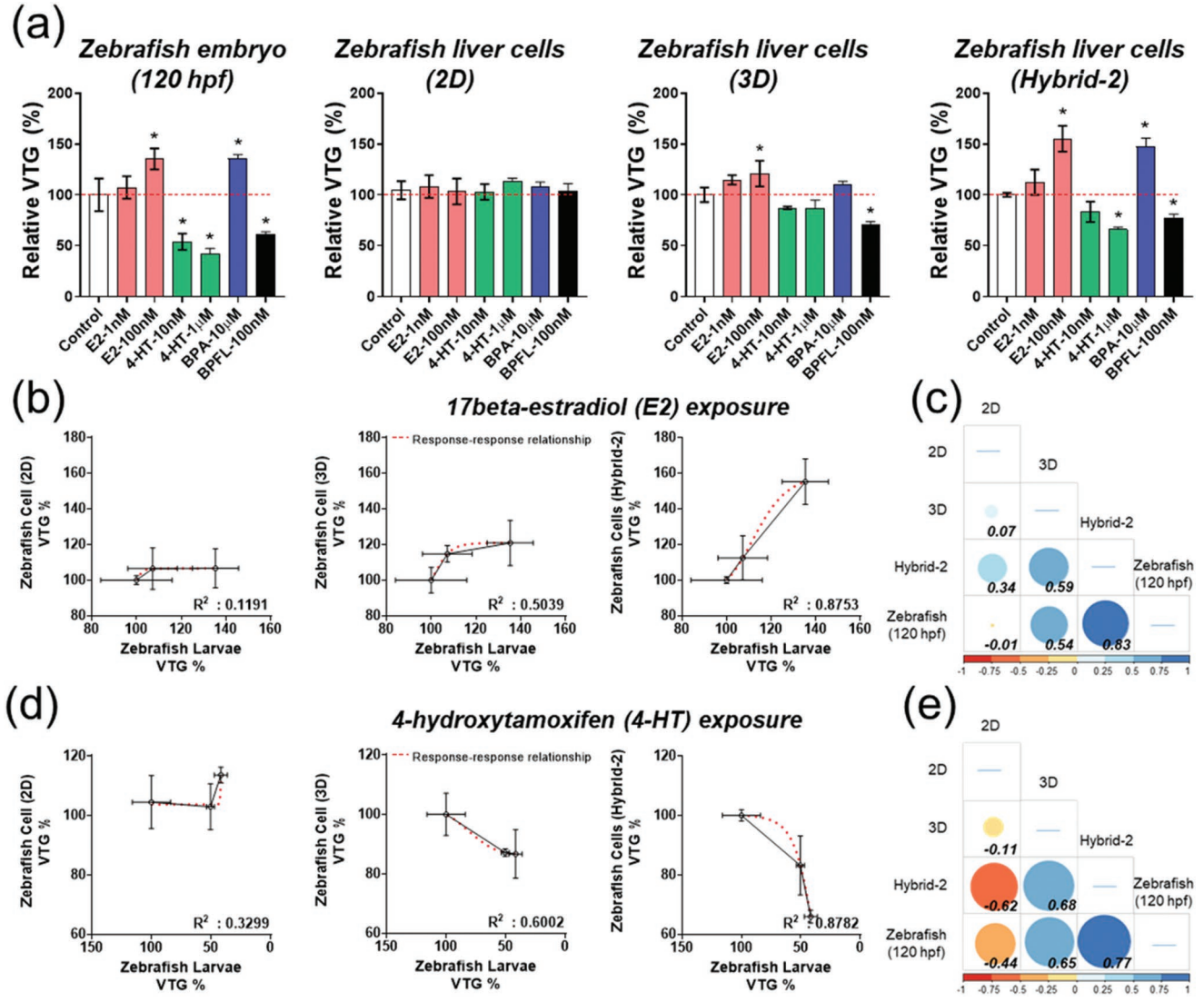

Figure 6. Comparison of vitellogenin levels upon endocrine-disrupting chemicals (EDCs) exposure. a) Relative vitellogenin levels in zebrafish larvae, 2D, 3D, and Hybrid-2 groups. All groups were cultured for 3 days and exposed to each chemical for 48 h. Six replicate samples of each condition were prepared for comparison. Data are presented as mean ± SD ($n = 6$). Comparisons of the means between each group were performed using one-way analysis of variance (ANOVA), followed by Scheffe's test (homogeneous variance). Asterisk means a significant difference compared to the control condition ($p < 0.05$). b–e) Correlation analysis of vitellogenin levels in groups. b) Correlation matrix plot for 17β-estradiol (E2) exposure. Pearson correlation coefficient (r) was calculated between groups. c) Correlation matrix plot for 4-hydroxytamoxifen (HT) exposure. Pearson correlation coefficient (r) was calculated between groups.

4. Experimental Section

A detailed description of all the relevant experimental sections is provided in the Supporting Information. The essential aspects are as follows.

Fabrication and Preparation of BSeN: PLLA electrospun nanofiber sheets were fabricated and prepared as previously described. Briefly, a 4% PLLA solution was prepared in a DCM and trifluoroethanol (TFE) mixture (8:2, v/v), and 10 mL of the solution was ejected by a syringe pump at a rate of 5 mL h^{-1} (KDS200; K.D. Scientific, New Hope, PA, USA) through a 23-gauge needle under 12.8 kV. The solution was then deposited on a rotating mandrel collector (SPG, Incheon, Korea) and the electrospun collected sheet was dried overnight. To fabricate BSeN, PLLA electrospun nanofiber sheets were immersed in 10% (v/v) ethylenediamine solution in isopropyl alcohol (IPA) and incubated for 30 min at 37 °C under vigorous shaking at 200 rpm. The BSeNs were then collected by centrifugation at 4000 rpm for 5 min and washed with IPA (3 times), 70% EtOH (once), and distilled water (DW, 3 times) before they were lyophilized for 24 h. For the polydopamine coating, 50 mg of BSeN was suspended in 70% EtOH and washed with DW. Subsequently, the BSeN was dispersed in dopamine hydrochloride solution dissolved in 10 mM Tris-HCl buffer (2 mg mL^{-1}, pH 8.5) and stirred at 100 rpm for 10 min. Thereafter, the resulting polydopamine-coated BSeN (PD-BSeN) was washed twice with DW and lyophilized overnight.

Cell Culture and Incorporation of ZFL Spheroids with BSeN and PD-BSeN: The zebrafish liver (ZFL) cell line was obtained from ATCC (CRL2643) and cultured in a complete growth medium in T-75 flasks at 28 °C in a cell incubator (Thermo Scientific). The complete growth medium was composed of 50% Leibowitz-15, 35% DMEM, and 15% Ham's F12 supplemented with 15×10^{-3} M HEPES, 0.15 g L^{-1} sodium bicarbonate, 1% penicillin-streptomycin, 0.01 mg mL^{-1} of bovine insulin, 50 ng mL^{-1} mouse epidermal growth factor, 5% heat-inactivated FBS, and 0.5% trout

serum. For comparative experiments, cells from the same batch were used, and the density was fixed at 50000 cells per well. ZFL cells in T-75 flasks were washed with PBS and treated with 0.25% trypsin–EDTA. The cells were then suspended in a complete growth medium and centrifuged at 125 × *g* for 5 min. The pelleted cells were resuspended in the medium and counted using a cell counter (TC20 automated cell counter (Bio-Rad Laboratories, Feldkirchen, Germany). After counting, the cells were seeded in a six-well flat-bottom plate (Thermo Scientific) to produce the monolayer culture. The cells were seeded in BIOFLOAT 96-well U-bottom plates (faCellitate, Mannheim, Germany) and centrifuged at 125 × *g* for 5 min for the spheroid culture. To fabricate hybrid spheroids, BSeN and PD-BSeN were sterilized using 70% ethanol under UV exposure for 30 min and then washed twice with distilled water. Then, ≈50000 cells were combined with 1 µg of BSeN or PD-BSeN and seeded into each well of BIOFLOATTM 96-well U-bottom plates. The mixture was centrifuged at 125 × *g* for 5 min and cultured in an incubator at 28 °C. The complete growth medium was replaced at a half-ratio every 2–3 days.

Zebrafish and Fish Embryo Acute Toxicity (FET): Adult wild-type zebrafish were obtained from the European Zebrafish Resource Center (EZRC; Karlsruhe, Germany). Fish maintenance, breeding conditions, and egg production were performed under internationally accepted standards (temperature 26.0 ± 1.0 °C and 10/14 h dark/light cycle). The zebrafish were fed twice daily with freshly hatched brine shrimp. The embryo acute toxicity test was conducted according to OECD TG 236 with slight modifications. Briefly, freshly laid eggs were transferred to sterilized dishes filled with clean fish water (E3 medium). After controlling fertilization, eleuthero embryos were transferred to multiple wells (6 well, Corning) at 72 hpf with 6 mL of test solution added per well. The exposure concentrations of E2, 4-HT, BPA, and BPFL used in the toxicity assessment were selected through a preliminary range-finding test (Supporting Information S11). For the FET, stock solutions of E2, 4-HT, BPA, and BPFL were prepared by dissolving each chemical in dimethyl sulfoxide (DMSO). Diluted solutions were prepared by diluting these stocks at least 100-fold using culture media. The chemicals were exposed to eleutheroembryos for 48 h, and the embryos were employed for VTG measurement. The detail of VTG measurement is indicated in the experimental section of Supporting Information.

Supporting Information

Supporting Information is available from the Wiley Online Library or from the author.

Acknowledgements

I.J. and C.G.P. contributed equally to this work. This research was supported by a National Research Council of Science & Technology (NST) grant by the Korean Government (MSIP, No. CAP-17-01-KIST Europe) and theKorea Institute of Science and Technology Europe Basic Research Program (12201). This research was supported by a National Research Foundation of Korea (NRF) grant funded by the Korean government (MEST) (Grant No. NRF-2020R1A4A3078645 and NRF-2019R1A2C2084965).

Conflict of Interest

The authors declare no conflict of interest.

Data Availability Statement

The data that support the findings of this study are available on request from the corresponding author. The data are not publicly available due to privacy or ethical restrictions.

Keywords

biomimetics, environmental hazard assessment, fibrous strands, spheroids

Received: February 4, 2022
Revised: March 22, 2022
Published online: May 5, 2022

[1] F. O. Adeola, Global Impact of Chemicals and Toxic Substances on Human Health and the Environment, in *Handbook of Global Health* (Eds: I. Kickbusch, D. Ganten, M. Moeti), Springer International Publishing, Cham **2021**, p. 2227.
[2] L. S. Birnbaum, *Fertil. Steril.* **2008**, *89*, e31.
[3] A. C. Tweedale, *J. Appl. Toxicol.* **2017**, *37*, 92.
[4] A. T. Ford, M. Agerstrand, B. W. Brooks, J. Allen, M. G. Bertram, T. Brodin, Z. Dang, S. Duquesne, R. Sahm, F. Hoffmann, H. Hollert, S. Jacob, N. Kluver, J. M. Lazorchak, M. Ledesma, S. D. Melvin, S. Mohr, S. Padilla, G. G. Pyle, S. Scholz, M. Saaristo, E. Smit, J. A. Steevens, S. van den Berg, W. Kloas, B. B. M. Wong, M. Ziegler, G. Maack, *Environ. Sci. Technol.* **2021**, *55*, 5620.
[5] L. M. Schuijt, F. J. Peng, S. J. P. van den Berg, M. M. L. Dingemans, P. J. Van den Brink, *Sci. Total Environ.* **2021**, *795*, 148776.
[6] D. Krewski, D. Acosta, Jr., M. Andersen, H. Anderson, J. C. Bailar, 3rd, K. Boekelheide, R. Brent, G. Charnley, V. G. Cheung, S. Green, Jr., K. T. Kelsey, N. I. Kerkvliet, A. A. Li, L. McCray, O. Meyer, R. D. Patterson, W. Pennie, R. A. Scala, G. M. Solomon, M. Stephens, J. Yager, L. Zeise, *J. Toxicol. Environ. Health, Part B* **2010**, *13*, 51.
[7] B. Grune, A. Hensel, G. Schonfelder, *Nature* **2014**, *512*, 28.
[8] J. Knight, C. Rovida, R. Kreiling, C. Zhu, M. Knudsen, T. Hartung, *ALTEX* **2021**, *38*, 653.
[9] A. Lillicrap, S. Belanger, N. Burden, D. D. Pasquier, M. R. Embry, M. Halder, M. A. Lampi, L. Lee, T. Norberg-King, B. A. Rattner, K. Schirmer, P. Thomas, *Environ. Toxicol. Chem.* **2016**, *35*, 2637.
[10] OECD, *Test No. 203: Fish, Acute Toxicity Test.* **2019**.
[11] K. Bambino, J. Chu, *Curr. Top. Dev. Biol.* **2017**, *124*, 331.
[12] OECD, *Test No. 236: Fish Embryo Acute Toxicity (FET) Test.* **2013**.
[13] M. Sobanska, S. Scholz, A. M. Nyman, R. Cesnaitis, S. Gutierrez Alonso, N. Kluver, R. Kuhne, H. Tyle, J. de Knecht, Z. Dang, I. Lundbergh, C. Carlon, W. De Coen, *Environ. Toxicol. Chem.* **2018**, *37*, 657.
[14] E. Ortiz-Villanueva, J. Jaumot, R. Martinez, L. Navarro-Martin, B. Pina, R. Tauler, *Sci. Total Environ.* **2018**, *635*, 156.
[15] M. A. Ibrahim, S. Z. Zulkifli, M. N. A. Azmai, F. Mohamat-Yusuff, A. Ismail, *Toxicol. Rep.* **2020**, *7*, 1039.
[16] S. Jarque, M. Rubio-Brotons, J. Ibarra, V. Ordonez, S. Dyballa, R. Minana, J. Terriente, *Reprod. Toxicol.* **2020**, *96*, 337.
[17] J. Lee, S. Kim, Y. J. Park, H. B. Moon, K. Choi, *Environ. Sci. Technol.* **2018**, *52*, 8858.
[18] S. Scholz, *Arch. Toxicol.* **2013**, *87*, 767.
[19] F. Busquet, A. Kleensang, C. Rovida, K. Herrmann, M. Leist, T. Hartung, *ALTEX* **2020**, *37*, 167.
[20] P. Macko, T. Palosaari, M. Whelan, *Toxicol. In Vitro* **2021**, *76*, 105206.
[21] N. Prinz, Š. Korez, Understanding How Microplastics Affect Marine Biota on the Cellular Level Is Important for Assessing Ecosystem Function: A Review, in *YOUMARES 9 - The Oceans: Our Research, Our Future: Proceedings of the 2018 conference for YOUng MArine RESearcher in Oldenburg, Germany* (Eds: S. Jungblut, V. Liebich, M. Bode-Dalby), Springer International Publishing, Cham **2020**, p. 101.
[22] R. Edmondson, J. J. Broglie, A. F. Adcock, L. Yang, *Assay Drug Dev. Technol.* **2014**, *12*, 207.

[23] A. Punt, H. Bouwmeester, B. J. Blaauboer, S. Coecke, B. Hakkert, D. F. G. Hendriks, P. Jennings, N. I. Kramer, S. Neuhoff, R. Masereeuw, A. Paini, A. Peijnenburg, M. Rooseboom, M. L. Shuler, I. Sorrell, B. Spee, M. Strikwold, A. D. Van der Meer, M. Van der Zande, M. Vinken, H. Yang, P. M. J. Bos, M. B. Heringa, *ALTEX* **2020**, *37*, 607.
[24] M. W. Laschke, M. D. Menger, *Trends Biotechnol.* **2017**, *35*, 133.
[25] E. L. Fong, S. E. Lamhamedi-Cherradi, E. Burdett, V. Ramamoorthy, A. J. Lazar, F. K. Kasper, M. C. Farach-Carson, D. Vishwamitra, E. G. Demicco, B. A. Menegaz, H. M. Amin, A. G. Mikos, J. A. Ludwig, *Proc. Natl. Acad. Sci. U. S. A.* **2013**, *110*, 6500.
[26] S. A. Langhans, *Front. Pharmacol.* **2018**, *9*, 6.
[27] M. Mandon, S. Huet, E. Dubreil, V. Fessard, L. Le Hegarat, *Sci. Rep.* **2019**, *9*, 10548.
[28] O. Sirenko, M. K. Hancock, J. Hesley, D. Hong, A. Cohen, J. Gentry, C. B. Carlson, D. A. Mann, *Assay Drug Dev. Technol.* **2016**, *14*, 381.
[29] H. M. Tse, G. Gardner, J. Dominguez-Bendala, C. A. Fraker, *Front. Bioeng. Biotechnol.* **2021**, *9*, 634403.
[30] T. Ahmad, J. Lee, Y. M. Shin, H. J. Shin, S. K. Madhurakat Perikamana, S. H. Park, S. W. Kim, H. Shin, *Acta Biomater.* **2017**, *64*, 161.
[31] T. Ahmad, H. J. Shin, J. Lee, Y. M. Shin, S. K. M. Perikamana, S. Y. Park, H. S. Jung, H. Shin, *Acta Biomater.* **2018**, *74*, 464.
[32] J. Lee, S. Lee, T. Ahmad, S. K. Madhurakkat Perikamana, J. Lee, E. M. Kim, H. Shin, *Biomaterials* **2020**, *255*, 120192.
[33] J. Lee, S. Lee, S. J. Huh, B.-J. Kang, H. Shin, *Adv. Sci.* **2022**, *9*, 2103525.
[34] J. Lee, S. Lee, S. M. Kim, H. Shin, *Biomater. Res.* **2021**, *25*, 14.
[35] C. G. Park, C. S. Ryu, B. Sung, A. Manz, H. Kong, Y. J. Kim, *Aquat. Toxicol.* **2022**, *245*, 106105.
[36] F. Gattazzo, A. Urciuolo, P. Bonaldo, *Biochim. Biophys. Acta* **2014**, *1840*, 2506.
[37] J. Nicolas, S. Magli, L. Rabbachin, S. Sampaolesi, F. Nicotra, L. Russo, *Biomacromolecules* **2020**, *21*, 1968.
[38] B. Sun, *Cell Rep. Phys. Sci.* **2021**, *2*,
[39] Y. Li, J. Cheng, P. Delparastan, H. Wang, S. J. Sigg, K. G. DeFrates, Y. Cao, P. B. Messersmith, *Nat. Commun.* **2020**, *11*, 3895.
[40] H. Lee, S. M. Dellatore, W. M. Miller, P. B. Messersmith, *Science* **2007**, *318*, 426.
[41] J. Park, T. F. Brust, H. J. Lee, S. C. Lee, V. J. Watts, Y. Yeo, *ACS Nano* **2014**, *8*, 3347.
[42] T. G. Barclay, H. M. Hegab, S. R. Clarke, M. Ginic-Markovic, *Adv. Mater. Interfaces* **2017**, *4*, 1601192.
[43] M. Xue, D. Zhou, Y. Ji, Y. Xie, C. Li, J. Zhao, *RSC Adv.* **2020**, *10*, 1639.
[44] F. Mollica, R. Lucernati, R. Amorati, *J. Mater. Chem. B* **2021**, *9*, 9980.
[45] A. Giralt, L. Fajas, *Front. Endocrinol.* **2017**, *8*, 362.
[46] D. F. Wilson, *J. Physiol.* **2017**, *595*, 7023.
[47] Z. Zhou, M. J. Xu, B. Gao, *Cell Mol. Immunol.* **2016**, *13*, 301.
[48] J. Robitaille, N. D. Denslow, B. I. Escher, H. G. Kurita-Oyamada, V. Marlatt, C. J. Martyniuk, L. Navarro-Martin, R. Prosser, T. Sanderson, V. Yargeau, V. S. Langlois, *Environ. Res.* **2022**, *205*, 112483.
[49] Z. Dang, *Environ. Int.* **2016**, *92-93*, 422.
[50] E. T. Rodrigues, A. T. Varela, M. A. Pardal, P. J. Oliveira, *Environ. Pollut.* **2019**, *252*, 476.